FUNCTIONALIZED GEOPOLYMERS DERIVED FROM CLAY AND RICE HUSK FOR REMOVAL OF SELECTED HEAVY METALS AND METHYLENE BLUE FROM AQUEOUS SOLUTION

MAINGI MUKORA FRANCIS

B.Ed. SC., MSc.

184/33102/2015

A Thesis Submitted in Partial Fulfillment of the Requirements for the Award of the Degree of Doctor of Philosophy (Chemistry) in the School of Pure and Applied Science of Kenyatta University

October, 2018

DECLARATION

I certify that besides where due acknowledgement has been made, this work is my own and has not been submitted formerly to qualify for any other academic award.

Maingi Mukora Francis

Signature ..... Date 31/10/2018

Department of Chemistry

Kenyatta University

This thesis has been submitted with our approval as university supervisors

Dr Harun Mbatha Mbuvi

Department of Chemistry

Kenyatta University

Sign..... Date 31/10/18

Dr. Margaret Mwihaki Ng'ang'a

Department of Chemistry

Kenyatta University

Sign..... Date 31/10/2018

Dr. Henry Mwangi

Department of Chemistry

Kenyatta University

Sign..... Date 31/10/2018

DEDICATION

With great joy, happiness, and appreciation, I would like to dedicate this work to my entire family for their encouragement and support towards my studies. My wife Grace Nduta for her steadfastness love and prayers. My children namely; Moureen Wambui, Doreen Njanju and Allan Maingi for their patience and perseverance. Without their support, help, encouragement and prayers, I would not have completed the programme.

ACKNOWLEDGEMENTS

My gratitude goes to my Heavenly Father, the giver and keeper of life. I will endlessly be indebted to my supervisors; Dr. Harun Mbuvi, Dr. Margaret Ng'ang'a and Dr. Henry Mwangi of Department of Chemistry, Kenyatta University for their wise counsel which has been so instrumental to my success. Without their constant and tremendous support, encouragement, and guidance throughout these years, I would not have been able to achieve my ultimate goal.

I am grateful to Kenya Industrial Research Development Institute for providing services of atomic absorption spectrometer. Department of Chemistry in the Ministry of Roads and Infrastructure, Material Testing and Research for allowing me to use your energy dispersive X-ray spectrometer, International Center for Research on Agro Forestry for providing X-Ray diffraction services, University of KwaZulu-Natal for providing scanning electron microscope (SEM) services and more so Dr. Alloice Ogweno for his assistance.

I am indebted to the technical staff in the Department of Chemistry, Kenyatta University, for their patience, time and selflessness that they exhibited towards me. Special thanks go to all my friends and fellow graduate students for their encouragement and support throughout my studies, which made my long PhD journey easier.

TABLE OF CONTENTS

LIST OF FIGURES

LIST OF TABLES

LIST OF ABBREVIATIONS AND ACRONYMS

CC	Calcined clay
CCD	Charge-coupled device
DLaTGS	Deuterated L-alanine doped Triglycine Sulfate
DNA	Deoxy Ribonucleic Acid
DOC	Dissolved Organic Carbon
ED	Electro Dialysis
EDS	Energy Dispersive Spectroscopy
FAAS	Flame Atomic Absorption Spectroscopy
FAO	Food and Agriculture Organization
FT-IR	Fourier Transform Infra-Red
GSH	Glutathione
ICDD	International Centre for Diffraction Data
MB	Methylene Blue
MCA	Multichannel Analysis
MCL	Maximum Permissible Limit
MK	Metakaolin
PDF	Powder Diffraction File
RHA	Rice Husk Ash
SEM	Scanning Electron Microscope
TMP	Trans Membrane Pressure
UF	Ultra Filtration
UNESCO	United Nation Educational, Scientific and Cultural Organization
WHO	World Health Organization
XRD	X-Ray Diffraction
XRF	X-Ray Fluorescence

ABSTRACT

With the onset of industrialization, humanity has witnessed various ecological issues in the society and disturbance of ecosystem. Heavy metals and methylene blue are very toxic substances known to cause detrimental effects to human health when ingested even at low concentrations. Several techniques are available for removal of heavy metals, and dyes from the wastewater such as chemical precipitation, ion exchange, adsorption, membrane among others. Among these technologies adsorption is preferable for wastewater treatment due to its simplicity in design, high efficiency and availability of materials involved. Geopolymers are inorganic polymers and have been in use in construction industries as alternatives to ordinary portland cement but very little information is available on their use in environmental pollution management. This study aimed at synthesizing and functionalizing amorphous geopolymers from common clay and rice husk ash for use as adsorbents in removal of heavy metal ions and methylene blue from contaminated water. There is adequate literature indicating that clay minerals contain both silicates and alumina while rice husk ash contains substantial amounts of silica. This work therefore reports synthesis of geopolymers GP-1, GP-2 and GP-3 using clays and rice husk ash that were functionalized using citric acid and EDTA for use in adsorption of heavy metals and colour. Characterization of the geopolymers was done using FT-IR, EDS, XRD and SEM. Batch experiments using Pb (II), Cd (II), Zn (II) ions and methylene blue (MB) were done. FT-IR indicated presence of Al-O and Si-O bonds which are the finger prints of geopolymers. XRD analysis showed presence of amorphous phase between 18-36° (2θ) an indication that geopolymerization occurred. SEM analysis revealed the formation of a heterogeneous matrix which consists of a dense continuous gel with microcracks and voids on geopolymer adsorbents. The mean percentage uptakes of 99.32 ± 0.04, 99.74 ± 0.01, 91.33 ± 0.06 and 91.99 ± 0.57 of Pb (II), Cd (II), Zn (II) and MB were achieved respectively. Various equilibrium models were employed and from the correlation coefficients ($R^2 > 0.94$), the data was found to fit best in Langmuir Freundlich model (Sips). The highest adsorption capacities of Pb (II), Cd (II), Zn (II) and MB were 326.5, 175.5, 169.9 and 20.74 mg/g respectively, attained using GP-3E. Increased adsorption of Pb (II), Cd (II), Zn (II) ions and MB was observed upon functionalization as well as when Si/Al ratio increased. Kinetic studies showed that a pseudo- second order model was more suitable than the first order in explaining the adsorption mechanism. This indicated that the adsorption transient behaviour used valence forces or exchangeable electrons and that chemisorption was more pronounced in the rate determining step. Thermodynamic studies revealed that the adsorption process was endothermic and physisorption since values of ΔH° obtained were < 40 kJ/mol. From the adsorption data, it's evident that synthesized geopolymers are potential adsorbents for removal of heavy metals and MB and may be employed in wastewater management.

CHAPTER ONE

INTRODUCTION

1.1 Background information

Water is an essential resource for life which greatly influences our public and environmental health as well as provides the pedestal for most of our economic activities. Unsustainable use of fresh water resources, population increase, and the trend in industrial revolution have led to environmental degradation especially by the release of partially treated or untreated wastewater into aquatic systems. Thus, the global freshwater resource is at risk and majority of the problems that humanity faces in the twenty-first century are related to water quantity and/or water quality issues (UNESCO, 2009).

The importance of water for sustenance of life cannot be overemphasized and its depletion either through contamination, or careless use results in serious consequences (Owa, 2013). About 70 % of the earth is covered with water, but hardly 2 % of it is suitable for drinking (Mann *et al*., 2014). The relative importance of water quality versus water quantity, sanitation and hygiene education interventions for cushioning the human well-being has been the subject of substantial debate (Esrey *et al.*, 1985; 1991). Nevertheless, there is broad agreement that good water quality, free of pathogens, colour and heavy metals is important to human health.

Water is regarded polluted if some components or condition exists in such a magnitude that the water cannot be used for a particular purpose. Water pollution affects flora and organisms dwelling in the water bodies. Water quality is affected by human activities and is declining due to the rise of urbanization, population growth, industrial production,

climate change and other factors. The resulting water pollution is a serious threat to the well-being of both the earth and its population (Halder and Islam, 2015). Moreover the discharge of toxic heavy metals into water bodies is a serious pollution problem affecting quality especially in wetlands and other masses due to their toxicity and bio accumulative effect, creating a direct hazard to human health (Ogoyi *et al*., 2011).

A group of metals and metalloids with atomic density greater than 4 g/cm^3 are collectively termed as heavy metals (Hutton and Symon, 1986; Nriagu and Pacyna, 1988). They enter into the ecosystem through natural and anthropogenic means such as natural weathering of the earth's crust, mining, soil erosion, industrial discharge, urban runoff, sewage effluents, pest or disease control agents applied to plants, air pollution and a number of other sources (Yu, 2005). Some heavy metals like Fe, Zn, Ca and Mg have been reported to be of bio-importance to man and their daily medicinal and dietary allowances have been recommended (Duruibe *et al.,* 2007). However, some others like As, Cd, Pb, and methylated forms of Hg have no known biological importance in human physiology hence consumption even at very low concentrations can be toxic (Fosmire, 1990; European Commission, 2002).

Although heavy metal poisoning ought to be clinically diagnosed and medically treated, the first remedy is to stop heavy metal pollution and the subsequent human poisoning (Duruibe *et al*., 2007). Contamination of food by heavy metals is a serious hazard depending on the relative level of the metals. Cd and Pb are some of these metals that may injure the kidneys and cause symptoms of persistent toxicity, along with impaired organ functions, poor reproductive capacity, hypertension, tumors and hepatic dysfunction (Abou-Arab *et al.*, 1996).

Dyes used in a lot of industries including textile, paper, plastics, leather-based, food and cosmetics, represent a large group of chemicals that get jumbled together in wastewater among many that contribute to water pollution (Bulut and Aydin, 2006). Recently, there has been dramatic increase in the annual production of various artificial dyes representing more than 10,000 dyes (Alzaydien, 2009). Many azo dyes and their intermediates have poisonous consequences on the surroundings and human health because of their carcinogenicity and visibility (Gong *et al*., 2005). According to literature, incomplete degradation of dyes by microorganisms inside the sediment leads to manufacturing of some carcinogenic and dangerous amines (Vandevivere *et al*., 1998).

Further, presence of colouration materials in water bodies can also decrease the light transmission which decreases photosynthetic activities, leading to decreased growth of microorganisms and subsequently lowering the biodegradation of impurities in water (Santhi *et al*., 2009). Methylene blue (MB) dye is a fundamental dye that has drastically been utilized in textiles and printing enterprises and it has been determined to be non-biodegradable dye. Consequently, it is vital that wastewater contaminated with MB dye be sufficiently treated before discharge (Elmorsi *et al*., 2014).

Several techniques are available for treatment and removal of heavy metals, turbidity and dyes from the wastewater such as chemical precipitation, ion exchange, adsorption, membrane filtration, coagulation and flocculation, floatation and electrochemical treatment (Fu and Wang, 2011). Chemical precipitation is not economical and produces large amounts of sludge. Ion exchange is costly, especially when treating a large amount of wastewater containing heavy metals in low concentrations, so it cannot be used on a large scale. The use of coagulation and flocculation of heavy metal wastewater treatment

technique involves chemical consumption and increased sludge volume generation. Floatation and electrochemical heavy metal wastewater treatment techniques involve high initial capital, maintenance and operation costs (Fu and Wang, 2011). Adsorption has a proven efficiency in the removal of organic and mineral pollutants and therefore appears to be the most plausible for future use in industrial wastewater treatment and for economic considerations (Garg *et al*., 2003; Abdelghani *et al*., 2007).

In 1979, Davidovits coined the term *geopolymer* to represent an inorganic polymer consisting of SiO_4^{4-} and AlO_4^{5-} as the structural units (Davidovits, 1989). These inorganic polymers are formed by polycondensation reaction between an alkaline solution like sodium hydroxide and sodium silicate with an aluminosilicate source such as metakaolin (MK), fly ash, rice husk ash (RHA). Geopolymer chemistry is associated with that of zeolites, since they have comparable chemical composition (Provis *et al*., 2005). Similar to zeolite, geopolymer, an inorganic polymer, has a three-dimensional polymeric structure and pores formed by the condensation of aluminosilicate mineral powder in addition to an alkali solution at a temperature below 100 $^{\circ}$C, which Davidovits developed in 1978 (Davidovits *et al*., 1990).

Several researchers used metakaolin as an ideal raw material for the manufacture of geopolymers (Duxson *et al*., 2007; Goretta *et al*., 2007) because of its high reactivity and purity compared to other clays (Yip *et al*., 2003; Kong *et al*., 2007; Cheng *et al*., 2012). This work focuses on a new and green developing field that utilizes available and plentiful raw materials such as common clay that has not been used and rice husk waste for wastewater management. Therefore, wastewater treatment using a geopolymer as an adsorbent should be more feasible, and thus merits further examination.

Common clay is made of layered sheets composed of polymeric sheets of SiO_4 tetrahedral linked into (Al, Mg, Fe)$(O,OH)_6$ octahedral sheets belonging to the family of phyllosilicate (Sposito, 2008). Presence of aluminosilicate in clay makes it useful for synthesis of geopolymers. They are very important industrial minerals and have been used as starting materials for many industrial applications due to their abundances and low cost (Suryadi *et al*., 2015). Clays are utilized in agricultural, engineering, construction, environmental remediation, geology, pharmaceuticals, food processing, and many other industrial applications (Murray, 2006).

Rice husk is a derivative of the rice milling process. It is a unique crop residue with a high content of ash. Rice husk ash (RHA) contains as high as 90–98 % silica (Adam *et al*., 2006). This husk can be used as a fertilizer in agriculture or as an additive for cement and concrete fabrication. In the preparation of elementary silicon and a range of silicon compounds rice husk has become a source of silica (Della *et al*., 2002). In this study, rice husk ash was used as a source of extra silica in the synthesis of geopolymers.

1.2 Statement of the problem

Increase in pollution of water bodies is directly or indirectly related to increasing urbanization and indiscriminate disposal of agrochemical and industrial effluents into aquatic systems (Dua and Gupta, 2005). Essential, non-essential heavy metals and methylene blue are of important environmental and health concern. This is due to the toxicity they exhibit at increased levels of bioavailability due to the excessive accumulation and circulation in the biosphere (Nriagu and Pacyna, 1988). The most widely used methods for their removal are chemical or electrochemical precipitation, both of which pose a significant problem in terms of disposal of the precipitated wastes

(Ozdemir *et al*., 2005), and ion-exchange treatments, which do not appear to be economical (Pehlivan and Altun, 2006).

Adsorption could be an alternative method to clean up industrial wastewaters containing heavy metals. The adsorption process is a captivating alternative for the removal of heavy metals ions from effluents since it is effective and easily attainable (Pamukoglu and Kargi, 2008). Apparently not much is known on the use of geopolymers in wastewater treatment despite their desirable properties and other advantages such as high strength, acid/alkaline resistance, heat resistance, and effective solidification of toxic waste (Van Jaarsveld *et al*., 1998; Duxson *et al.*, 2007). The focus of this work was to develop a new wastewater treatment method using geopolymers and functionalized geopolymers synthesized from common clay and rice husk waste, which are available and abundant, that would supplement the adsorption treatment method. The new process is technically feasible, economically achievable and environmentally safe.

1.3 Justification and significance of the study

It has been observed that pollutants originating from anthropogenic activities dramatically alter the quality of water. To eliminate impacts on water due to heavy metal pollution, it is necessary to have appropriate wastewater management strategies and efficient treatment designs. However, the effectiveness of such strategies and treatment designs will strongly depend on the cost of production. Many industries in Kenya are located in urban centers. These include metal, textile, paper, dairy processing, pharmaceutical, soft drinks, bakeries, and power. Each of these disposes high levels of different metals, which on aggregate and in combination, pollutes the water bodies. Various conventional treatment strategies such as chemical precipitation, ion exchange, filtration and electrochemical treatment have been applied for removing these heavy metals, but most

of them are only suitable for large scale treatments and are costly to operate (Aeisyah *et al*., 2014). All these techniques also lead to certain disadvantages like removal of heavy metals to a lesser extent, high-energy requirements and production of toxic sludge (Eccles, 1999).

There is a perceived necessity and growing interest in finding adsorbents that are more cost-effective and produce fewer limitations. Therefore, finding suitable materials and operating conditions are essential to addressing the concerns of heavy metal pollution. Common clay is abundant; rice husk is an industrial waste, both of which are locally available and rich in aluminosilicate and silica respectively which were used in the synthesis of geopolymer adsorbents. Surface functionalization of the geopolymer material enhanced selectivity and efficiency of the adsorbent. This study is of value to the wastewater treatment plants and also acts as a source of baseline data for future researchers who may want to engage in similar studies.

1.4 Hypotheses

i. Common clay and ash from waste rice husk can be used as raw materials in the synthesis of geopolymer adsorbents for removal of selected heavy metals and methylene blue from contaminated waters.
ii. Functionalizing the geopolymers enhances efficiency and capacity to remove selected heavy metals and methylene blue from contaminated water.

1.5 General objective

To synthesize and functionalize amorphous geopolymers from common clay and rice husk ash for use as adsorbents in removal of selected heavy metal ions and methylene blue from contaminated water.

1.5.1 Specific objectives

i. To determine the chemical composition of rice husk ash and common clay minerals using energy dispersive spectrometry (EDS).

ii. To synthesize and characterize geopolymer adsorbents derived from rice husk ash and common clay using x-ray diffraction (XRD), fourier transform infra-red (FT-IR), scanning electron microscope (SEM) and EDS.

iii. To functionalize and characterize the geopolymer adsorbents using citric acid and ethylene diamine tetra acetic acid (EDTA) for adsorption of Cd (II), Pb (II), Zn (II) ions and methylene blue respectively using XRD, FT-IR, SEM and EDS.

iv. To determine the percentage removal of Cd (II), Pb (II), Zn (II) ions and methylene blue at varying pH, contact time, shaking speed, temperature sorbent dose, initial adsorbate concentration and Si/Al ratio in the geopolymers.

v. To determine the adsorption capacities and percentage regeneration of the geopolymers after the adsorption/desorption process.

vi. To determine the transient behaviour of adsorption of Pb (II), Zn (II), Cd (II) ions and methylene blue using kinetic and thermodynamic models.

1.6 Scope and limitation

i. The study was restricted to clay from Kakamega, Kuresoi and Molo and not from the whole country.

ii. Only rice husk from Mwea was used

iii. Clay and rice husk was used as a source of aluminosilicate and silica respectively.

iv. This research focused on three heavy metal ions; Cd (II), Pb (II), Zn (II) ions and methylene blue. Other heavy metals and pollutants were not considered.

CHAPTER TWO

LITERATURE REVIEW

2.1 Heavy metals and their toxicities in human beings

The most common toxic heavy metals in wastewater include; lead (Pb), cadmium (Cd), zinc (Zn), mercury (Hg), arsenic (As), silver (Ag) chromium (Cr), copper (Cu) iron (Fe), and the platinum group elements (Duruibe *et al*., 2007). Serious health and environmental problems and an upsurge in wastewater treatment costs may occur due to the release of high amounts of heavy metals into water bodies (Akpor, 2014) . They also occur in small amounts naturally and may enter into aquatic system through leaching from rocks, airborne dust, forest fires and vegetation (Fernandez-Leborans and Herrero, 2000; Ogoyi *et al*., 2011).

Copper, selenium and zinc are essential in maintaining the metabolism of the human body (Fraga, 2005). However, their presence at high concentrations in the environment is of major apprehension because of their toxicity, bioaccumulation, and threatens the environment. According to Jarup (2003), prolonged exposure to heavy metals such as cadmium, copper, lead, nickel and zinc can cause deleterious health effects in humans. The primary sources of heavy metal pollution are industries and mining sites (Duruibe *et al*., 2007). Lead and cadmium are among the most widely distributed in the environment (Goyer *et al*., 1995). They have no important role in biochemical reactions and are poisonous to cells in both low and high concentrations (Cols *et al*., 2001). Valls *et al*. (2000) found out that unlike organic contaminants which can be converted into non-toxic derivatives, metals are intrinsically persistent in nature.

Most of the industries which use raw materials containing heavy metals end up disposing their waste in rivers thus polluting them (Chen and Burns, 2006). Such industries include smelting industries, hides and skins processing industries, soaps, detergents and perfume producing industries. Some health effects of heavy metals include diarrhea, stomatitis, tremor, hemoglobinuria, rust– red colour to stool, paralysis, vomiting and convulsion, depression, renal dysfunction, cancer and Alzheimer's disease (Verma and Dwivedi, 2013). Table 2.1 shows a summary of toxicity and maximum contaminant levels of common hazardous heavy metals established by USEPA.

Table 2.1: The MCL standards for the most hazardous heavy metals (USEPA)

Heavy metal	**Toxicity**	**MCL (mg / L)**
Arsenic	Skin manifestations, visceral cancers, vascular disease	0.05
Cadmium	Kidney damage, renal disorder, human carcinogen	0.01
Chromium	Headache, diarrhea, nausea, vomiting, carcinogen	0.05
Copper	Liver damage, Wilson disease, insomnia	0.25
Nickel	Dermatitis, nausea, chronic asthma, coughing, human carcinogen	0.2
Zinc	Depression, lethargy, neurological signs and nervous system	0.8
Lead	Damage to the fetal brain, diseases of the kidneys, circulatory system and nervous system	0.006
Mercury	Rheumatoid arthritis, and diseases of the kidneys, circulatory system and nervous system	0.00003

MCL- Maximum Contaminant Limit
Source: (Babel and Kurniawan, 2003)

2.1.1 Occurrence and toxicity of lead

Lead is an ubiquitous environmental and industrial pollutant that has been detected in every facet of environmental and biological systems (Juberg *et al*., 1997). Reproductive dysfunction by lead (Pb) has distinct morphological and biochemical features such as

disorganized epithelia, decreased sperm quality, altered sperm morphology, and low androgen levels (Alexander *et al*., 1996; Hsu *et al*., 1997). It has a primary toxic effect on the hypothalamic pituitary unit, a primary effect on the testes, and acts at all levels of the human reproductive system (Sokol *et al*., 2002). It has a negative influence on the somatic development and decreases the visual acuity and auditive thresholds (Simeonov *et al*., 2011). Its acute exposure causes brain damage, neurological symptoms, brain damage and could lead to death (Simeonov *et al*., 2011).

2.1.2 Occurrence and toxicity of cadmium

Cadmium (Cd), a pervasive heavy metal and an environmental pollutant, is found in soil, water and air (Fahim *et al.*, 2012). It is one of the components abundantly existing in nickel cadmium (Ni-Cd) battery wastes, cigarette smoke, blue paint pigments, copper smelters among others (Svoboda *et al*., 2000). Cadmium (Cd) is a carcinogenic metal to which humans are exposed through contaminated foods, water or air. Chronic cadmium poisoning can result in nephrotoxicity, osteoporosis, cardiovascular diseases, testicular necrosis, prostatic and testicular cancers, renal failure and neurodegenerative conditions (Yu *et al.*, 2007). Moreover, it was reported that spermatogenesis is disturbed by free radical toxicity (Aruldhas *et al*., 2005) . It depletes many essential metal antioxidants including selenium in the body (Sato and Takizawa, 1982).

Apparently, its exposure results in decreased glutathione (GSH) levels, which causes an increase in reactive oxygen species leading to increase in lipid peroxidation, change in intercellular stability, damage to deoxyribonucleic acid (DNA) and cell membranes and consequently inducing cell death (Stohs *et al*., 2000). The metal accumulates in the human body affecting negatively several organs: liver, kidney, lungs, bones, placenta, and

brain (Castro-González and Méndez-Armenta, 2008). Therefore, the maximum concentration limit for cadmium (II) ions in drinking water must be strictly regulated. The World Health Organization (WHO), set a maximum guideline concentration of 0.003 mg/L for cadmium (II) in drinking water (WHO, 2008). Hence, there is great interest regarding the removal of cadmium from wastewater streams.

2.1.3 Occurrence and toxicity of zinc

Zinc is considered relatively nontoxic, especially if taken orally. However, excess amount can cause system dysfunctions that result in impairment of growth and reproduction (Peter and Olalekan, 2014). The metal is an essential element for life and acts as a micronutrient when present in trace amounts (Arias and Sen, 2009). However, clinical signs of its toxicities include vomiting, diarrhea, bloody urine, liver failure, kidney failure and anemia (Fosmire, 1990). Release of zinc into groundwater resources occurs largely via anthropogenic activities such as mining or through industrial production. The main sources in the environment are from manufacturing of brass, bronze alloys and galvanization (Weng and Huang, 2004). Further, it is also utilized in paints, rubber, plastics, cosmetics and pharmaceuticals (Weng and Huang, 2004). The main symptoms of zinc poisoning are dehydration, electrolyte imbalance, stomachache, nausea, dizziness and neuropathy (Sen and Khoo, 2013). WHO recommended maximum acceptable concentration of zinc in drinking water as 5.0 mg/L (Mohan and Singh, 2002). Beyond the permissible limits, Zn (II) is toxic (Bhattacharya *et al*., 2006).

2.2 Methylene blue and its toxicity in human beings

Dyes are mixtures that have been utilized as a part of numerous ventures for various purposes, for example, in nourishment preparation, materials, paper, cosmetics and other enterprises. The effluents from these businesses are the principle wellsprings of

ecological colour contamination (Sarioglu and Atay, 2006). Because of the wasteful aspects of the modern colouring process, a portion of the utilized dyes are lost in the effluents of textile units, rendering them exceedingly coloured (Maleki *et al*., 2010). Direct release of these effluents causes an increase in dangerous materials in wastewater which leads to their expansion in visual impacts (Dehghani *et al*., 2008). The structure of methylene blue (Methylthioninium chloride) is as shown in figure 2.1.

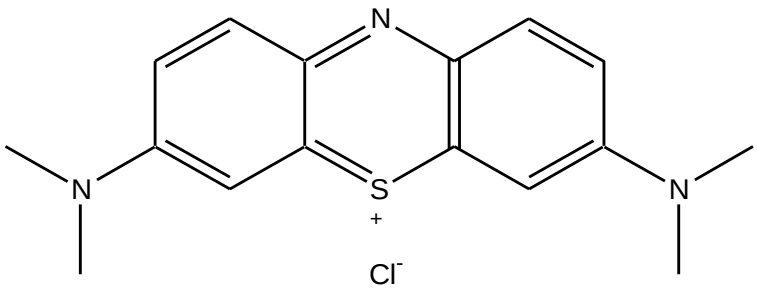

Methylthioninium chloride,

Figure 2.1: Structure of Methylene blue
Source: (Derakhshan and Baghapour, 2013)

Methylene blue (MB) is the most utilized material for dyeing cotton, wood, and silk with MB hydrochlorine sub-atomic weight 373.9 with three water molecules. Methylene blue induces hemolytic anemia in individuals with glucose-6-phosphate dehydrogenase (G-6-PD) enzyme deficiency (Thienes and Haley, 1972). Methylene blue is a severe eye irritant (Lenga, 1988). High concentrations of methylene blue have been found to induce corneal and conjunctiva injury (Grant, 1986). In order to lessen the cost of wastewater treatment, endeavors have been made to discover low cost alternative adsorbents. Various approaches have been made to create less expensive and successful adsorbents to expel dyes from an assortment of starting materials derived from waste (Annadurai *et al*., 2002; Özer *et al*., 2007).

2.3 Existing wastewater treatment technologies for heavy metals and MB removal

Heavy metals are environmental priority pollutants and are becoming one of the most serious environmental problems (Fu and Wang, 2011). Therefore toxic heavy metals should be removed from the wastewater to protect the people and the environment. Many methods are being used to remove heavy metal ions as mentioned earlier (Fu and Wang, 2011). Currently the common methods available for removal of metal ions from wastewater are coagulation, chemical precipitation, ion-exchange, reverse osmosis among others (Hui *et al*., 2005). However, most of these methods suffer from some drawbacks, such as high capital and operational costs or the disposal of the residual metal sludge (Kobya *et al*., 2005).

2.3.1 Chemical precipitation

According to Parmar and Thakur (2013), this process is effective and most widely used in industries since it is simple and inexpensive to operate. In the precipitation processes, chemicals react with heavy metal ions to form insoluble precipitates. Treated water is then decanted and appropriately discharged or reused. The conventional chemical precipitation processes include hydroxide precipitation and sulfide precipitation (Ku and Jung, 2001). The conceptual mechanism of heavy metal removal by chemical precipitation is presented in equation 2.1 (Wang *et al*., 2004).

$$M^{n+}_{(aq)} + n\,(OH)^{-}_{(aq)} \rightleftharpoons M(OH)_{n(s)} \quad \text{..... 2.1}$$

Where M^{n+} and OH^- represent the dissolved metal ions and the precipitant respectively, while $M(OH)_n$ is the insoluble metal hydroxide.

These conventional chemical precipitation processes produces insoluble precipitates of heavy metals as hydroxide, sulfide, carbonate or phosphate. Very high-quality debris is generated in the precipitation process and chemical precipitants, coagulation, and flocculation processes are used to grow its size and remove it as sludge (Ku and Jung, 2001; Fu and Wang, 2011). However, one of the drawbacks of this method is that it requires large amounts of chemical to reduce metals to acceptable levels for discharge. Other drawbacks are excessive sludge production that requires further treatment, slow metal precipitation, poor settling, aggregation of metal precipitates, and long term environmental impacts of sludge disposal (Aziz *et al*.,2008).

2.3.2 Ion exchange

These processes have been used widely in the removal of heavy metals from wastewater due to their many advantages, such as high treatment capacity, high removal efficiency and fast kinetics (Kang *et al*., 2004). They, have specific abilities to exchange their cations with the metals present in the wastewater (Moosavirad *et al*., 2015). Among the materials used in ion-exchange processes, synthetic resins are commonly preferred as they effectively remove the heavy metals from the solution (Alyüz and Veli, 2009). A notable disadvantage is that corrosion is a significant limiting factor, where electrodes must be frequently replaced (Kurniawan *et al*., 2006).

2.3.3 Physico-chemical methods

Physical separation techniques are primarily applicable to particulate forms of metals, discrete particles or metal-bearing particles (Dermont *et al*., 2008). The methods consists of mechanical screening, hydrodynamic classification, gravity concentration, flotation, magnetic separation, electrostatic separation, and attrition scrubbing (Dermont *et al*., 2008). Factors that may limit the applicability and effectiveness of the physical chemical

processes are the high content of clay/silt, humus, calcite, Fe and Ca, heavy metals, anions, or high buffering capacity (Fu and Wang, 2011).

2.3.4 Membrane filtration

This method has received considerable attention in treatment of inorganic effluents. The technique is able to cast off suspended solids, organic compounds and inorganic contaminants together with heavy metals (Gunatilake, 2015). Depending on the size of the particle that can be retained, various types of membrane filtration such as ultrafiltration, Nano filtration and reverse osmosis can be employed for heavy metal removal from wastewater (Gunatilake, 2015). Ultrafiltration (UF) makes use of a permeable membrane to split heavy metals, macromolecules and suspended solids from inorganic solution on the premise of the pore size and molecular weight of the separating compounds (Vigneswaran *et al*., 2004).

Ultra-filtration has the ability to achieve more than 90% uptake efficiency with a metal ion concentration in the range of 10 to 112 mg/L at pH ranging from 5 to 9.5 depending on the membrane traits (Barakat, 2011). UF performance due to membrane fouling has hindered it from a wider application in wastewater treatment. Fouling has many adverse effects on the membrane system such as flux decline, an increase in trans membrane pressure (TMP) and the biodegradation of the membrane materials (Kurniawan *et al*., 2006). These effects result in high operational costs for the membrane system (Barakat, 2011).

2.3.5 Electro dialysis

A process where ionized species in the solution are passed through an ion exchange membrane by applying an electric current is known as electro dialysis (ED) (Gunatilake,

2015). When a solution containing ionic species passes through the cell compartments, the anions migrate towards the anode and the cations toward the cathode, crossing the anion exchange and cation-exchange membranes (Chen, 2004). A notable disadvantage is membrane replacement and the corrosion process (Kurniawan *et al*., 2006). Since ED is a membrane process, it requires clean feed, careful operation and periodic maintenance to prevent any stack damages making the technique expensive (Barakat, 2011).

2.3.6 Adsorption

Physical and/ or chemical interactions that occur when a substance is transferred from the liquid phase to the solid surface, and becomes bound is termed as adsorption (Babel and Kurniawan, 2003). In the recent past, a number of approaches have been investigated for safe and economical treatment of heavy metal laden wastewater (Tripathi and Rawat Ranjan, 2015). Adsorption has emerged to be a better alternative treatment out of all the methods. It is said to be effective and economical because of its relatively low cost (Shah *et al*., 2009). The key benefits of the adsorption method for heavy metal removal are lower operational costs, unproblematic design and easy operation (Acar and Eren, 2006).

Generally, the heavy metals are present in the wastewater at low concentrations and adsorption becomes suitable where the ions are present at concentrations of as low as 1 mg/L. This makes adsorption an economical and favourable technology for their removal. The adsorbent origin can be of mineral, organic or biological such as zeolites, commercial byproducts, agricultural waste, biomass and polymeric material (Tripathi and Rawat Ranjan, 2015). Activated carbon is one of the conventional adsorbent that has been used extensively in many applications. Table 2.2 shows reported removal percentages of Pb (II), Cd (II) and Zn (II) using activated carbon (Mona *et al*., 2014).

Table 2.2: Removal efficiencies of Pb (II), Cd (II) with 100 mg/L initial concentrations using activated carbon

Heavy metal ions	Initial conc^{n}(C_o) (mg/L)	Residual conc^{n} (mg/L)	Removal efficiency (%)
Cd(II)	100	30.20	70
Pb(II)	100	27.00	73

Source: (Mona *et al*., 2014).

However, the high cost of the activation limits its usage in wastewater treatment processes. In the approach to replace the conventional adsorbents, geopolymers similar to zeolite materials are a new approach for removal of metal ions from wastewater (Xu and van Deventer, 2000; Barbosa and MacKenzie, 2003; Buchwald *et al*., 2011). This study aims at contributing in the search for cost effective or low cost adsorbents of natural origin. It also aims at applicability of the adsorbents in recovery as well as removal of heavy metals and colour from the industrial wastewater.

2.4 Clay as a source of alumina

Chemically, clays are aluminosilicate minerals (Grimshaw, 1971) which have many industrial applications. Clays have become an important source of aluminium and its compounds (Grim, 1981). Clay is available locally in millions of tonnes especially in the rice-growing areas such as the Kano plains in Lake Victoria basin or Mwea in Kirinyaga County (Muriithi *et al*., 2012). Clay minerals are determined by their chemical composition, layered structure and size. They can be categorized into four subgroups; kaolinite, smectite, mica, and chlorite (Shichi and Takagi, 2000; Nayak and Singh, 2007). Kaolin is one of the most valuable, versatile, and widely used industrial minerals. It is used extensively in ceramics, rubber, paint, plastics, and pharmaceutical industries

(Murray, 1991; Bundy, 1993). Presence of aluminosilicate in clay makes it a good raw material for the synthesis of geopolymers.

2.5 Rice husk as a source of silica

Presently, the world production of rice is approximately 500 million tonnes a year containing 50-100 million tonnes of rice husks (Andreoli *et al*., 2000). Rice husk is a by-result of the rice processing industry. The silica content in the rice husk ash (RHA) can be as high as 90–98% (Adam *et al*., 2006). The percentage of rice husk in paddy rice varies across different countries and this is influenced by various factors such as species, cultivation area, soil fertility, weather, irrigation efficiency and farming practices (Bhattacharya *et al*., 1999). However, 20 percent is generally considered as a fair average for general rice husk (Beagle, 1978).

It is reported that approximately 0.23 tonnes of rice husk (rice hull) are formed from every tone of rice produced (Jain *et al*., 1996). When RH is burnt in air, it leads to the formation of silica ash, which varies from gray to black depending on the inorganic impurities and unburnt carbon amounts (Krishnarao *et al*., 2001). Table 2.3 shows properties of rice husk ash produced by different burning conditions.

Table 2.3: Rice husk ash properties produced from different burning conditions

Burning temperature	Hold time	Furnace environment	Properties of rice husk ash	
			Silica form	Surface area (m^2/g)
500-600 °C	1 min	Moderately	Amorphous	122
	30 min	oxidizing		97
	2 hrs			76
700-800 °C	15 min-1 hr			100
	>1 hr	Highly	Partially crystalline	6-10
>800 °C	>1 hr	oxidizing	crystalline	< 5

Source: (Singh and Singh, 2015) *Note:* Moderately oxidizing = CO_2 environment
Highly oxidizing = O_2 environment

The husk, if burned at high temperatures in the presence of oxygen, yields ash with a high content of silica (more than 90 percent by weight), which is seen as the most advantageous property of rice husk ash compared to ash obtained from burning other solid fuels (Muthadhi *et al*., 2007). However, the burning conditions of rice husk result in different forms of rice husk ash, the crystalline and amorphous forms, and these different forms benefit different applications. While amorphous silica had been proven to be useful in the cement, construction, and rubber industries (Mehta and Pitt, 1976), crystalline silica has been found to be useful for products such as steel, ceramics and refractory bricks. Because of its high silicon content, rice husk has turned into a good source of basic silicon and various silicon compounds particularly silica, silicon carbide and silicon nitride (Della *et al.*, 2002). Rice husk ash has been used in the geopolymer synthesis (Lopez *et al*., 2014a).

2.6 Geopolymers

Geopolymers are inorganic polymeric materials formed when solid aluminosilicate is reacted with concentrated alkali hydroxide solution (Davidovits, 1991). The chemical

composition of geopolymer is similar to natural zeolitic materials in terms of chemical composition, but their microstructure is amorphous instead of crystalline (Palomo *et al*., 1999; Xu and van Deventer, 2000). Reaction mechanisms have been proposed for this geopolymerization involving the breakdown of the solid aluminosilicate into smaller "monomers" where aluminium is already tetrahedrally coordinated. The second step is the polycondensation of these monomers into the geopolymer (Duxson *et al*., 2007; Rahier *et al*., 2007). As a result of these reactions, solid, hard, and stable materials with hydroxysodalite, feldspathoid, or zeolite like structures are formed (Davidovits, 1998).

The volume of data available in the field of aluminosilicate dissolution and weathering represents a whole field of scientific endeavor in itself (Blum and Lasaga, 1988; Oelkers, 2001). Dissolution of amorphous aluminosilicate is rapid at high pH, and this quickly creates a supersaturated aluminosilicate solution. In concentrated solutions this results in the formation of a gel, with the oligomers in the aqueous phase forming large networks by condensation. This process releases water that was nominally consumed during dissolution (Duxson *et al*., 2007).

As such, water plays the role of a reaction medium, but resides within pores in the gel. This type of gel structure is commonly referred to as bi-phasic, with the aluminosilicate binder and water forming the two phases (Duxson *et al*., 2007). The time for the supersaturated aluminosilicate solution to form a continuous gel varies considerably with raw material, processing conditions and solution composition and synthesis conditions (Crea *et al*., 1991; Ivanova *et al*., 1994). These are typically dilute, and the concentration of dissolved silicon and aluminum is observed to oscillate due to the slow response of the system far from equilibrium (Faimon, 1996). After gel formation, the system continues to

rearrange and reorganize, resulting in formation of the three-dimensional aluminosilicate network. Figure 2.2 shows the structure of geopolymer.

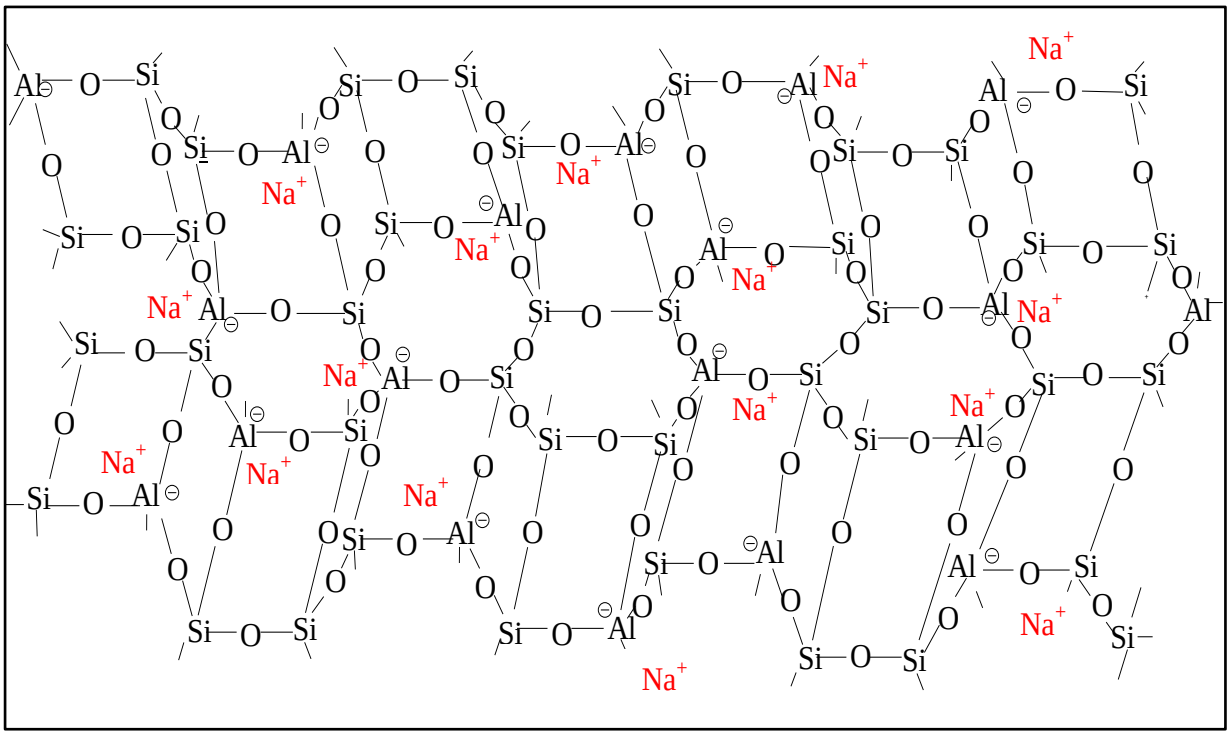

Figure 2.2: Structure of geopolymer
(Source: Davidovits, 1991)

Nucleation, or the dissolution of the aluminosilicate material and formation of polymeric species, is highly dependent on thermodynamic and kinetic parameters and encompasses the two first steps proposed by Glukhovsky (1959). Growth is the stage during which the nuclei reach critical size and crystals begin to develop. These processes of structural reorganization determine the microstructure and pore distribution of the material, which are critical in determining many physical properties (Duxson *et al.*, 2005; Duxson *et al.*, 2007). Geopolymers derived from different combinations of raw materials can easily be synthesized containing multivalent cations (Alonso and Palomo, 2001; Granizo *et al.*, 2002; Lee and Van Deventer, 2002a; Yip and Van Deventer, 2003). Therefore during the course of alkali-mediated reaction, Al (IV) and Si (IV) are converted to tetrahedral sites

with an associated alkali cation to maintain electro neutrality (Davidovits, 1991). The speciation of aluminum in alkaline solutions is restricted to $Al(OH)_{4\ (aq)}^{-}$ in all but the most concentrated aluminate solutions, where some dimerization is observed (Swaddle *et al*., 1994). These geopolymers are expected to have unique properties such as zeolite adsorbents. However, the details about geopolymer adsorbents still are not well known at this time (López *et al*., 2014a). If geopolymers can actually remove metal ions from waste water via adsorption, the matrix could become new approach for several industries (López *et al*., 2014a).

2.6.1 Functionalization of geopolymers

Functionalization of the surface of geopolymers changes the material in ways determined by the functional group (Ali *et al*., 2016). Properties that can be varied include surface charge, hydrophobicity, molecular binding and reactivity. Methods used for functionalization of silanol groups in silica based materials, such as mesoporous silica can be readily adapted for geopolymers since they are zeolite analogues (Richer, 1998). Aluminium is hexa, penta and tetra-coordinated in the precursor and after geopolymerization tetra-coordinated aluminium provides negative charges to the surface of the aluminosilicate framework. This extra negative charges are neutralized by cations such as sodium and potassium (Van Jaarsveld *et al*., 1998). This shows that geopolymer or clay has a potential to be functionalized at the surface (Yan *et al*., 2007). This information forms the basis of one of our objectives of studying the surface functionalization of geopolymer.

2.6.2 Compositional and microstructural analyses of geopolymers and source materials

The geopolymers like other molecular sieves are characterized using FT-IR, SEM, EDS, XRD among other methods. Characterization using FT-IR spectroscopy is for determination of molecular vibration of the geopolymers, X-ray diffractometer (XRD) for crystal structure determination, X-ray fluorescence (XRF) or EDS to qualitatively and quantitatively identify the chemical composition of principal components (López *et al*., 2014b).

2.7 Adsorption isotherms

The adsorption isotherm is the relationship between the amount of sorbate adsorbed by an adsorbent (solid) and its equilibrium concentration at constant temperature (Theodore and Ricci, 2010). An equilibrium is arrived at where a number of molecules arriving on the surface of an adsorbent equals the number of molecules that are leaving (Thajeel, 2013). Equilibrium data is analyzed using commonly known adsorption isotherms (Rahimi and Vadi, 2014). The earliest and simplest known relationships describing the adsorption process are the Freundlich and the Langmuir isotherms (Jalali *et al*., 2002). Modified Langmuir Freundlich isotherm is a versatile isotherm expression that simulate both Langmuir and Freundlich behaviors (Sips, 1948; Nahm *et al*., 1977). Both the Langmuir-type and Freundlich-type adsorption behavior in linearized forms have been used for modeling pH-dependent sorption effects of adsorption of arsenic ions (Jeppu and Clement, 2012). Equations 2.2, 2.3, 2.4 and 2.5 represent Langmuir, Freundlich, Langmuir Freundlich and Temkin isotherms respectively.

$$\frac{C_e}{q_e} = \frac{C_e}{q_m} + \frac{1}{K_L q_m} \quad \text{..... 2.2}$$

(Langmuir, 1916)

Where c_e is equilibrium concentration, q_e is adsorption at equilibrium K_L is Langmuir constant and q_m is adsorption capacity.

$$\text{Ln } q_e = \text{Ln } K_F + \frac{1}{n} \text{Ln } C_e \quad \text{..... 2.3}$$

(Freundlich, 1906)

Where c_e is equilibrium concentration, q_e is adsorption at equilibrium K_F is Freundlich constant and 1/n is heterogeneity index.

$$q_e = \frac{Q_m (K_a C_{eq})^n}{(K_a C_{eq})^n + 1} \quad \text{..... 2.4}$$

(Turiel *et al*., 2003)

Where c_{eq} is equilibrium concentration, q_e is adsorption at equilibrium K_a is Langmuir Freundlich constant, n is heterogeneity index and Q_m is adsorption capacity.

The Temkin isotherm assumes that the heat of adsorption of all the molecules in the layer would reduce linearly with coverage due to the impact of indirect sorbent-sorbate interactions (Temkin *et al*., 1940). This model also assumes that adsorption is characterized by a uniform distribution of binding energies, up to some maximum binding energy. Derivation of the Temkin isotherm is achieved using equation 2.5.

$$q_e = B_1 \text{ In } k_T + B_1 \text{In } C_e \text{……..……2.5}$$

Where B_1 is the Temkin constant related to the heat of adsorption and k_T is the equilibrium binding constant (Lmg^{-1}). A plot of q_e versus ln C_e enables the determination of the isotherm constants B_1 and k_T from the slope and intercept of the straight line plot.

2.8 Kinetic studies

Information about the system dynamics, that is, the adsorption rate, residence time and mass transfer parameters such as external mass transfer coefficients and intra-particle diffusivity are supplied in kinetic studies (Zendelska *et al*., 2014). These parameters are essential in the design and operation of any adsorption column in wastewater treatment plants. Therefore, kinetic studies help to evaluate the suitability of any material as a possible adsorbent in removing pollutants from aqueous solutions (Connors, 1990). Laxmipriya *et al*. (2018) reported on understanding of the kinetics and mechanism of heavy metal adsorption onto a pyrophyllite mine waste based geopolymer.

2.9 Desorption studies

For wastewater treatment, reusability of geopolymer adsorbent materials is of importance in economic development, since it helps to protect the environment by recycling of the adsorbate ions and adsorbent. The successful application of this technique also reduces the dependence on thermal activation, incineration, and land disposal, which directly or indirectly increases environmental pollution (Kumar, 2013).

CHAPTER THREE

MATERIALS AND METHODS

3.1 Research design and validation

These studies utilized an experimental design where experimental data obtained in the research was used to measure and describe the relationship or association between variables (Baker, 2017). The instruments used were validated by means of inter laboratory comparison as a means of method validation. In this case similar analytical instruments in different laboratories were subjected to same written protocols and analysed the same samples (IUPAC, 2000). Reference material activated carbon (AC) was used in studying the effect of initial concentration on adsorption process. All instruments used were calibrated before use and adsorption studies used procedures validated in literature.

3.2 Apparatus and instrumentations

The equipment used were FAAS (AA 6300 Shimadzu), XRD (D2 Phaser- Bruker), centrifuge (Eppendorf 5810), Fisher brand test sieve aperture 250 microns (ISO3310/ 1.mill), XRD mccrone micronizing mill (Glen creston company), EDX spectrometer (800HS), XRF (S1 titan), electric shaker (SHR-2D and D-3162), electric weighing balance (ATY224 Shimadzu), muffle furnace (Eisklo LN 120), aspirator pump (7049-05), water still (model WSB/4), grinding mill (Reutsch SR 200), FTIR (IRTracer-100), fabricated ball mill, UV-VIS (Specord 200 plus), pH meter (Starter 2000) and scanning electron microscope (SEM) (Zeiss Evo LS 15).

3.3 Chemicals

Chemicals used in this study were of analytical grade manufactured by Sigma Aldrich Company. They included, Pb $(NO_3)_2$, HNO_3, Cd $(NO_3)_2$ H_2O, Zn $(NO_3)_2$ $6H_2O$, Citric

acid, Disodium EDTA, KBr, Methylene blue ($C_{16}H_{18}ClN_3S$) and NaOH used in adsorption experiments.

3.4 Collection and pretreatment of clay and rice husk materials

The clays used were obtained from Kakamega, Kuresoi and Molo areas of Kenya. They were transported to Kenyatta University laboratory, washed with distilled water and then air dried for two weeks. Calcination was done at 700 $^{\circ}$C in a furnace (Eisklo LN 120) and the clay later ground to a fine powder using a grinder (Reutsch SR 200). The calcined clays were used as a source of Al_2O_3. Rice husk obtained from a rice processor at Mwea in Kenya was washed with distilled water using a liquid/solid ratio of 15 L: 1kg. The solids were allowed to settle, filtered and dried at 60 $^{\circ}$C in an oven for 12 hours. Leaching was then carried out with 3 % HCl solutions using reflux boiling apparatus, for 2 hours. The solids were washed with distilled water to remove the acid retained, and then dried at 60 $^{\circ}$C for 12 hours. Calcination was done at 600 $^{\circ}$C for 2 hours using a muffle furnace to obtain ash which was used as a source of silica (Nogueira and Margarido, 2012).

3.5 Elemental analysis of calcined clay and rice husk ash

The chemical composition of the calcined clay and rice husk ash were analysed using energy dispersive X- ray spectrometry. Alumina, silica and other constituent components in the ashes were analysed in situ using the method described by Küpper *et al*. (2000).

3.6 Synthesis of geopolymer samples

The procedure was adopted from López *et al*. (2014a) but with slight modifications. 20 g of rice husk ash (RHA) was weighed and placed in three different 250 mL Erlenmeyer conical flasks. Alkaline activating solution of sodium hydroxide was prepared 24 hours prior to mixing with calcined clays (Ferone *et al*., 2013). 100 mL of 8.0 M NaOH was

added to each conical flask and the mixture stirred using a magnetic stirrer for 15 minutes. 50 g of calcined clays (CC) was weighed and added to each of the three Erlenmeyer conical flasks labeled GP-1, GP-2 and GP-3 respectively. The mixtures were then transferred to 250 mL plastic bottles and shaken in a ball mill for 5 hours (López *et al*., 2014a). The fluid matrix was then poured into ceramic crucibles and cured in an oven at a temperature of 80 $^{\circ}$C for 12 hours. The temperature conditions were then adjusted to 200 $^{\circ}$C for another 12 hours to facilitate complete polycondensation (López *et al*., 2014a). The ultimate geopolymer materials obtained were washed with distilled water severally to a pH of 7.0 ± 0.5. Filtration was then done using aspirator pump model 7049 and residues dried in an oven at 100 $^{\circ}$C for 12 hours to get rid of all water present. Grinding to fine powder was done using a grinding mill (model SR 200). The geopolymer materials GP-1, GP-2 and GP-3 were preserved for functionalization and characterization, and then preserved for use as adsorbents.

3.7 Functionalization of geopolymers

The geopolymer samples were functionalized using the procedure adopted from Beyer (2002) with modification to allow attachments of citric acid and EDTA through silanol functional groups by condensation. 100 mL of 0.3 M citric acid and EDTA was added separately to 50 g of the geopolymer samples GP-1, GP-2 and GP-3 in 250 mL Erlenmeyer volumetric flasks respectively. The mixtures were then shaken in an electric water bath shaker model D-3162 at 80 $^{\circ}$C with a shaking speed of 160 rpm for 4 hours. The samples were latter washed several times with distilled water to a pH of 7.0 ± 0.5 and then dried at 100 $^{\circ}$C in an oven for 12 hours (Xu *et al*., 2013).

3.8 Analysis and characterization of geopolymers

3.8.1 Analysis of the chemical composition of geopolymers using XRF

An automated Bruker model S1 Titan hand held XRF analyzer was used for chemical characterization of the geopolymer samples. Energy calibration was carried out first to ensure that peak energies were accurately tied to specific elements. The powdered samples were loaded into the sample cups with care on a laminar flow clean bench with no use of rubber gloves to prevent zinc contamination. A scan time of 60 seconds per sample was performed and reports generated from computer coupled to the XRF.

3.8.2 XRD characterization of geopolymers

The geopolymers were analyzed using XRD with Cu Kα radiation at 40 kV and 40 mA using a graphite monochromator (λ=1.5418 À) at a scanning speed of 3° 2θ/min. 10 g of each sample were dispersed in ethanol and milled for 12 minutes using an XRD Mccrone micronizing mill after which the mixture was centrifuged at a rate of 400 rpm using a centrifuge (Eppendorf 5810) for 10 minutes to allow separation. Hexane was then added and vibrated to reduce preferred orientations. The treated samples were then heated in an oven at 70 $^{\circ}$C for six hours to dry. Sieving was performed using a sieve fisher brand of aperture 250 μm. Subsequently, each was placed in a sample disk and mounted on an aluminum rod perpendicular to the bedding plane and parallel to the horizontal axis of a goniometer (Ischia *et al*., 2005) in XRD for analysis.

Data integration and evaluation was done using EVA software. The intensity of the diffraction of a sample under investigation was continuously recorded as the sample and detector rotated through their respective angles. This was to ensure high peak / foundation proportions, low sensitivity to sample density variations and decent counting insights. The strongest peaks stayed within the linearity range of the counter and the beam stayed

within preparation for the lowest 2θ angle diffraction, from which the examination was performed. Counting time was 450 seconds for each spot. The powder diffraction file (PDF) database and international table for crystallography from the international center for diffraction data (ICDD) present in coupled computer library were used in the phase's identification (Treacy and Higgins, 2001). The position and relative intensities of a series of peaks were used to match experimental data from diffractograms to reference patterns in the database (Treacy and Higgins, 2001).

3.8.3 FT-IR characterization of geopolymers

A spatula full of KBr was added into an agate mortar and ground into a fine powder until crystallites were no longer present and it turned "pasty" and stuck to the mortar. A small amount of powder sample was taken (about 0.1 g of the KBr, or just enough to cover the tip of spatula) and mixed with the geopolymer powder. The powder mixture was added to the 7 mm collar and then put into the hand press. The powder was pressed for approximately 2 minutes to form a good thin and transparent KBr pellet. The die set and 7 mm collar were later disassembled and taken out and then put onto the sample holder for FT-IR analysis (Cullum and Vo-dinh, 2014).

3.8.4 SEM characterization of geopolymers

Scanning electron microscopy (SEM) was used to record micrographs while energy dispersive X-ray spectroscopy (EDX) was used as an additional tool for the semi-quantitative analysis (Heath, 2015). The computer-assisted SEM analyses were conducted on the geopolymer samples. Samples were thoroughly degreased, cleaned ultrasonically using methanol and dried to eliminate any outgassing from organic contamination and water. After cleaning the samples with methanol, they were blown with compressed gas to get rid of the volatile solvent. 10.0 g of powdered samples (GP-1 to GP-3E) were

securely mounted on a SEM stub using conductive carbon tape after which they were coated (3 coats) with gold to enhance their conductivity. They were then loaded onto a sample holder and the areas of interest scanned. The EDX analyses were also carried out on the areas of interests. The carbon tapes used were vacuum compatible.

3.9 Preparation of solutions

Stock solutions were prepared using lead (II) nitrate, cadmium (II) nitrate, zinc (II) nitrate and methylene blue which were all of analytical grade supplied by Sigma Aldrich (Kenya). Lead (II) ions solution was prepared by dissolving an accurate quantity of 1.559 g of lead (II) nitrate in 700 mL of distilled water and diluting to 1000 mL. Exactly 2.74 g of cadmium (II) nitrate and 4.55 g of zinc (II) nitrate were prepared in the same way. 1.000 g of methylene blue ($C_{16}H_{18}ClN_3S$) was dissolved in distilled water to make 1000 mg/L. Working solutions obtained by serial dilution of the stock solution.

3.10 Optimization of pH

3.10.1 Optimization of pH for adsorption of Pb (II), Cd (II) and Zn (II) ions onto geopolymers

Experiments were conducted by varying pH from 2 to 6 while maintaining all other experimental conditions constant for Pb (II), Cd (II) and Zn (II). The pH adjustments were done using the procedure given by Moreno-piraján and Giraldo (2012). 50 mL pH adjusted solutions containing 100 mg/L of each one of the Pb (II), Cd (II) and Zn (II) ions in monocomponent systems were placed in 100 mL stoppered plastic bottles. 0.10 g (weight with analytical precision) of geopolymer materials was put into each of the stoppered bottles. The bottles were placed in a thermostatic electric shaker (SHR-2D) at 120 rpm, maintained at 25 $^{\circ}$C ± 1 and shaken continuously for one hour. All experiments were carried out in triplicates and mean average values were used for further calculations.

The reagent bottles were successively withdrawn after shaking and the supernatant solutions filtered using whatman no 41 filter papers. The residual metal ions was analyzed by means of FAAS using the procedure adopted from Ryan *et al*. (2001).

3.10.2 Studies on point of zero charge (pH pzc)

The pH pzc for the adsorbent was determined according to the method of El-Sayed (2011). 0.10 g of the polymer was placed in a 250 mL Erlenmeyer flask and 50 mL of deionized water added. The initial pH values of the solution were roughly adjusted to 4.0–12 by adding either 0.1 M HCl or 0.1 M NaOH. The mixtures were shaken in an electric shaker (SHR 2D) and allowed to equilibrate for 12 hours with periodic shaking at a speed of 120 rpm. The pH values of the supernatant liquids were noted and the relation between the initial and final pH values was deduced and evaluated to obtain the pH pzc.

3.10.3 Optimization of pH of adsorption of MB onto geopolymers

The effect of pH on the methylene blue (MB) adsorption process was studied by varying the initial pH of the solution from 4 to 12. The pH was adjusted using 0.1 M HCl and / or 0.1 M sodium hydroxide (NaOH), and measured using a pH meter (Model starter 2000). The MB initial concentration was fixed at 25 mg/L with adsorbent dose of 0.1 g/25 mL at 298 K. The mixture was agitated at 120 rpm for a period of one hour to achieve equilibrium and then filtered. The filtrate was analysed for residual MB concentration using a UV-Vis spectrophotometer (Specord 200 plus). This procedure was adopted from Mohd and Zainal (2011).

3.11 Optimization of contact time on adsorption of Pb (II), Cd (II), Zn (II) and MB

The impacts of residence time were investigated by varying time from 20 to 100 minutes. 0.10 g of geopolymer material was added to 50 mL of 100 mg/L metal ion solutions and

25 mL of 25 mg/L of MB in each of a series of adsorption bottles. The bottles were placed in a thermostatic electric shaker at 120 rpm, maintained at 25°C ± 1 at a pH of 4.0 for Pb (II) and 5.0 for both Cd (II) and Zn (II). After 20 minutes of adsorption time was completed, the adsorbents were removed from the solution by filtration and the concentration of residual metal ion and MB in each solution determined using FAAS and UV/Vis spectrophotometry respectively. Subsequently, the same procedure was repeated by adjusting time to 40, 60, 80 and 100 minutes respectively.

3.12 Optimization of shaking speed on adsorption of Pb (II), Cd (II), Zn (II) and MB

To determine the effect of shaking speed, 0.10 g of synthesized material was put in each of the bottles containing 50 mL of metal ions and 25 mL of MB working solutions. The bottles were placed in a thermostatic electric shaker at room temperature of 25°C ± 1 and were shaken continuously for one hour at shaking speed of 120 rpm and optimum pH of Pb (II), Cd (II), Zn (II) and MB. Filtration was done and metal ions present analyzed. The procedure was repeated with shaking speeds of 150, 180, 210 and 240 rpm.

3.13 Optimization of temperatures on adsorption of Pb (II), Cd (II), Zn (II) and MB

The temperature range of 293 K to 328 K was used for 100 mg/L monocomponent system of Pb (II), Cd (II) and Zn (II) ions adsorption to determine the equilibrium temperature. For each experimental run, 50 mL aqueous solution of the known concentration at optimum pH of adsorbate ions was put in a 100 mL stoppered plastic bottles containing 0.10 g of the adsorbent. The bottles were placed in a thermostatic electric shaker at a constant shaking speed of 120 rpm at the specified temperature and withdrawn after shaking for one hour. Filtration was done and residual metal ions present analyzed. For MB, 25 mL of 25 mg/L of working solution was put in stoppered plastic bottles. 0.10 g of

adsorbent was added to each of the bottles and shaken in an electric shaker at a constant speed of 120 rpm in a temperature range of 298 – 328 K. After filtration, the filtrate was analysed for residual MB concentration using UV-Vis spectrophotometry.

3.14 Optimization of adsorbent dose on adsorption of Pb (II), Cd (II), Zn (II) and MB

Weighed amounts of geopolymer materials of mass (0.1 - 0.5 g) were introduced into stoppered reagent bottles containing 50 mL of 100 mg/L metal ions solutions and 25 mL of 25 mg/L of MB. The suspensions were shaken at room temperature ($25^{\circ}C \pm 1$) using an electric shaker for a prescribed time of one hour at 120 rpm. Aqueous samples were taken from the solution and analyzed. All samples were filtered prior to the analysis in order to minimize the interference of the geopolymer fines with the analysis. The concentrations of metal ions in the solutions after adsorption were determined using flame atomic absorption spectrophotometry at a wavelength of 283.3 nm for lead, 228.8 nm for cadmium and 213.8 nm for zinc while the MB concentration was determined using UV-Vis spectrophotometry at a wavelength of 665nm.

3.15 Optimization of initial concentration on adsorption of Pb (II), Cd (II), Zn (II) and MB

The adsorption of metal ions by the geopolymer adsorbents was investigated by varying their initial concentrations from 20 to 200 mg/L and from 25 to 50 mg/L for MB, while maintaining all other experimental conditions constant. 0.10 g of geopolymer material was placed in each of the bottles. 50 mL of concentrations 20, 50, 100 and 200 mg/L of metal ions and 25 mL of concentrations 25, 30, 40 and 50 mg/L of MB were put in plastic bottles and placed in an electric shaker at 120 rpm for one hour. The reproducibility during concentration measurements was ensured by repeating the experiments three times under identical conditions.

3.16 Column studies for Pb (II), Cd (II) and Zn (II) ions using geopolymers

The column procedure was adopted from Biswas and Mishra (2015) with slight adjustments. A glass column made of Pyrex tube with an internal diameter of 1 cm and height of 60 cm was fitted with cotton wool and held firmly in a vertical position with the aid of a retort stand. To assist in a uniform flow of the wastewater into the column, glass beads were placed to attain 3 cm in height. 0.50 g of the prepared geopolymer was packed in the column, and then cotton wool placed on top of the bed and firmly secured in place by layer of glass beads in order to provide a uniform flow of the solution through the column. Distilled water was poured to wet the column and ensure that all air between and within the geopolymer particles was expelled before the experiment began. Adsorption experiments were done for 50 mL of 100 mg/L of synthetic wastewater samples of Pb (II), Cd (II) and Zn (II) ions. Elusion was by gravity through the geopolymer materials. The eluents were then analysed for residual metal ions concentration using FAAS (Agbozu and Emoruwa, 2014).

3.17 Adsorption isotherms

Adsorption and desorption quantitative data of metal ions and MB obtained in section 3.14 was treated using Freundlich, Langmuir, modified Langmuir Freundlich (Sips isotherms) and Temkin isotherms. The models were used to determine adsorption capacities of the geopolymers synthesized using different clays and rice husk ash (RHA). FAAS was used to determine both the initial metal ion concentration before adsorption (C_o) and the residual metal ion concentration (C_e) obtained after the adsorption process. The amount of adsorption at equilibrium, q_e (mg/g), was calculated by equation 3.1.

$$q_e = \left[\frac{C_o - C_e}{W}\right] V \quad \text{.....3.1}$$

Where; C_o and C_e (mg/L) are concentrations of the respective metal ions at initial and equilibrium conditions respectively. V is the volume of the solution (L) and W is the mass of dry adsorbent used (g) (Vijayakumar *et al*., 2012). For the Freundlich isotherm, the plot of log q_e against log C_e will give a straight line with a slope of 1/n and intercept of log K_F. For Langmuir isotherm, the plot of C_e/q_e against C_e gives a straight line with a slope of $1/Q_{max}$ and intercepts $1/Q_{max} K_L$ (Tan and Hameed, 2010).

The essential features of the Langmuir isotherm were expressed in terms of equilibrium parameter R_L, which is a dimensionless constant referred to as separation factor or equilibrium parameter (Weber and Chakravorti, 1974). For Temkin isotherm q_e was plotted against Log C_e and its parameters calculated using equation 2.5. For modified Sips isotherm C_e was plotted against q_e and the model fitting was accomplished using the generalized reduced gradient algorithm available in Microsoft Excel solver.

3.18 Thermodynamic studies of the adsorption process

Adsorption standard free energy changes (ΔG°), the standard enthalpy change (ΔH°) and the standard entropy change (ΔS°) were obtained using data obtained from experiments described in section 3.12. Thermodynamic parameters were calculated at using equations 3.2 and 3.3 (Yao *et al*., 2010).

$$\Delta G^\circ = -RT \ln k_c \quad \text{.....3.2}$$

$$\text{Ln } k_c = \Delta S^\circ/R - \Delta H^\circ/RT \quad \text{.....3.3}$$

where R (8.3145 J mol^{-1} K^{-1}) is the gas constant, k_c (L g^{-1}) is the Langmuir constant and T (K) is the absolute temperature (Yao *et al*., 2010).

3.19 Kinetic studies of the adsorption process

The experiment described under section 3.10 provided C_t data. Equation (3.4) was used in calculating of q_t.

$$qt = (C_0 - C_t)\frac{V}{W} \quad \text{..... 3.4}$$

Where V is the volume of adsorbate solution in (L), and W is the mass of the adsorbent in (g). The data obtained was used to plot graphs of log (q_e - q_t) against t for pseudo- first order and t/q_t against t for pseudo- second order and determine kinetic parameters as per equations 3.5 and 3.6 respectively.

$$\text{Log}\,(q_e - q_t) = \text{Log}\,qe - \frac{K\,t}{2.303} \quad \text{..... 3.5}$$

$$\frac{t}{q_t} = \frac{1}{K_2 q_e^2} + \frac{1}{q_t}\,t \quad \text{..... 3.6}$$

Where q_e is amount adsorbed at equilibrium, q_t is amount adsorbed at a given time, t is residence time in minutes, k is the Lagergren rate constant and k_2 is the rate constant for pseudo -second order (Lagergren, 1898). The data obtained was also used to plot the intraparticle diffusion models. The intraparticle diffusion equation is presented in 3.7.

$R = K_{id}(t)^a$ 3.7

The linearized form of the equation is given in 3.8

$\text{Log } R = \text{Log } K_{id} + a \text{ Log } (t)$ 3.8

Where R = percent of MB adsorbed, t = contact time (minutes), 'a' = gradient of linear plot and k_{id} is the rate constant (Weber and Morris, 1963).

3.20 Desorption studies

The desorption procedure was adopted from Edokpayi *et al*. (2015) with slight adjustment. For the desorption studies, contact was made between 1.0 g of geopolymer materials and 200 mL Pb (II), Cd (II) and Zn (II) ions solutions for a residential time of 24 hours. After metal ion sorption, the geopolymers were filtered, washed three times with distilled water to remove residual metal ions on the surface, and kept in contact with the 200 mL of 0.1 M NaCl desorbent solution. The mixtures were shaken in an electric shaker (model SHR-2D). One mL aliquots were sequentially removed using a 1.0 mL dropper at predetermined times (15, 30, 60, 120, 240 and 600 minutes) and analyzed using AAS to determine the concentration of metal ions after desorption (Moyo *et al*., 2013). The percentage of metal ions desorbed was calculated by the following equation 3.9.

$\%\ \text{Desorption} = 100\ [C_D V_D] / q_e m$ …… 3.9

where C_D (mg/L) is the concentration of metal ions in the desorbed solution, V_D (L) is the volume of desorbed solution, m (g) is the mass of adsorbent used for desorption studies

and q_e (mg/g) is the adsorption capacity of the adsorbent for metal ions (Akpomie *et al*., 2015). The desorption studies of MB was not done due to its decomposition with time.

3.21. Analysis of Pb (II), Cd (II), Zn (II) and MB

The standard solutions were aspirated into the atomic absorption spectrophotometer and their respective concentrations recorded. The sample solutions were also aspirated into the FAAS (AA 6300 Shimadzu) and their respective concentrations recorded as well. The operating conditions used during analysis of the metal ions were as presented in table 3.1.

Table 3.1: Operating conditions used for the FAAS (AA6300 Shimadzu) instrument

Metal ions	Wavelengths (nm)	Slit width (nm)	Atomization	Lamp mode
Pb (II)	283.3	0.7	Furnace	BGC- D_2 (mA)
Cd (II)	228.85	1.0	Flame	BGC- D_2 (mA)
Zn (II)	213.8	0.7	Flame	BGC- D_2 (mA)

Source: operating manual of AAS (AA6300 Shimadzu)

Concentrations of MB were analysed using UV-Vis spectrophotometry at wavelength of 665nm.

3.22 Statistical analysis

Sorption and desorption data were collected as an average of three replicates and the standard deviation was calculated and used as error bars to discriminate differences among isotherms. Variances among parameters treatment were analyzed by calculating *P*-values associated with one-way ANOVA test with *post hoc* comparison (Tukey HSD test). The results were considered statistically significant at $P < 0.05$ (Taylor *et al*., 2012). The data was analyzed using software Minitab 17 statistical software package and excel.

CHAPTER FOUR

RESULTS AND DISCUSSION

4.1 Chemical composition of calcined clays and rice husk ash

Energy dispersive X-ray fluorescence spectrometer (EDX) was used to determine the chemical compositions of raw materials. Table 4.1 shows that the main oxide components of the raw materials from Kakamega clay (KK), Kuresoi (KR), Molo (ML) and ash from rice husk (RHA) from Mwea were silica and alumina.

Table 4.1: Mean percentage chemical composition of calcined clays and rice husk ash

Oxides (%)	KK	KR	ML	RHA
	Mean± SD	Mean± SD	Mean± SD	Mean± SD
SiO_2	40.94 ± 0.36	36.16 ± 0.37	37.17 ± 0.43	71.54 ± 0.50
Al_2O_3	36.25 ± 1.21	32.54 ± 1.34	30.03 ± 1.50	11.53 ± 0.99
Fe_2O_3	6.96 ± 0.04	11.34 ± 0.05	17.84 ± 0.06	10.43 ± 0.04
CaO	0.76 ± 0.01	0.16 ± 0.03	0.52 ± 0.01	1.32 ± 0.01
MnO	nd	0.08 ± 0.01	0.14 ± 0.01	0.48 ± 0.01
K_2O	13.86 ± 0.10	18.23 ± 0.12	12.05 ± 0.11	3.32 ± 0.06
TiO_2	0.92 ± 0.02	0.82 ± 0.02	1.50 ± 0.03	1.16 ± 0.02
SO_3	0.05 ± 0.00	0.06 ± 0.00	0.07 ± 0.00	0.09 ± 0.01
ZrO_2	0.18 ± 0.00	0.11 ± 0.00	0.48 ± 0.00	0.07 ± 0.00
V_2O_5	0.07 ± 0.01	nd	nd	nd
SrO	0.05 ± 0.00	0.05 ± 0.00	nd	0.02 ± 0.00
NbO	nd	nd	0.11 ± 0.00	0.02 ± 0.00
Rb_2O	0.03 ± 0.00	0.03 ± 0.00	0.03 ± 0.00	nd

KK- Kakamega clay, KR- Kuresoi clay, ML- Molo clay, RHA- rice husk ash, nd- not detected and SD- standard deviation

The percentage of SiO_2 was 40.94, 36.16, 37.17 and 71.54 %, Al_2O_3 was 36.25, 32.54, 30.03 and 11.53 %, Fe_2O_3 was 6.96, 11.34, 17.84 and 10.43, and K_2O was 13.86, 18.23, 12.05 and 3.31 % for KK, KR, ML and RHA respectively. All the other oxides were below 1 % in all parent materials with the exception of TiO_2 in ML and RHA which was at 1.50 and 1.16 % respectively. These results are in tandem with data reported by Nmiri *et al*. (2017) on oxide analysis of kaolinite clay.

4.2 Chemical composition of geopolymers

Table 4.2 shows the X-ray fluorescence spectrometry data on elemental composition of the geopolymers as obtained from XRF (SI Titan).

Table 4.2: Mean percentage of chemical composition of geopolymers

Oxides (%)	GP-1	GP-2	GP-3
	Mean ± SD	Mean± SD	Mean± SD
SiO_2	66.84 ± 0.44	66.21 ± 0.49	73.99 ± 0.45
Al_2O_3	16.05 ± 0.39	15.83 ± 0.43	8.93 ± 0.32
Fe	6.42 ± 0.03	5.65 ± 0.03	9.05 ± 0.04
CaO	1.88 ± 0.02	1.43 ± 0.02	0.92 ± 0.02
MgO	nd	1.21 ± 1.52	nd
Mn	0.11 ± 0.01	0.09 ± 0.01	0.07 ± 0.01
K_2O	4.43 ± 0.03	6.08 ± 0.04	2.89 ± 0.02
P_2O_5	nd	0.64 ± 0.05	0.61 ± 0.05
Ti	1.38 ± 0.01	1.12 ± 0.01	1.85 ± 0.01
Cr	0.28 ± 0.01	0.19 ± 0.00	0.12 ± 0.00
Ni	0.13 ± 0.00	0.08 ± 0.00	nd
S	0.89 ± 0.03	0.72 ± 0.03	0.92 ± 0.03
Cl	0.36 ± 0.01	0.42 ± 0.02	0.21 ± 0.01
Zr	0.07 ± 0.00	0.06 ± 0.00	0.17 ± 0.00
Sr	0.05 ± 0.00	0.05 ± 0.00	0.01 ± 0.00
Mo	0.05 ± 0.00	0.03 ± 0.00	0.02 ± 0.00
Rb	0.02 ± 0.00	0.03 ± 0.00	0.02 ± 0.00
LOI	1.09	0.14	0.04

GP-1= geopolymer from Kakamega clay, GP- 2= geopolymer from Kuresoi clay, GP- 3= geopolymer from Molo clay, SD = standard deviation, nd= not detected and LOI= loss on ignition

The main components of the geopolymer materials GP-1, GP-2 and GP-3 were silica and alumina. The percentage of SiO_2 was 66.84, 66.21 and 73.99 % and that of Al_2O_3 was 16.05, 15.83 and 8.93 % for GP-1, GP-2 and GP-3 respectively. Other elements and oxides found included Fe at 6.42, 5.65 and 9.05 %, K_2O at 4.43, 6.08 and 2.89 %, CaO at 1.88, 1.43 and 0.92 % and Ti at 1.38, 1.12 and 1.85 % for GP-1, GP-2 and GP-3 respectively. All the other elements were below 1 % in all geopolymers with the exception of MgO in GP-2 which was at 1.21 %. The loss of ignition, LOI was 1.09, 0.14 and 0.04 for GP-1, GP-2 and GP-3 respectively. The powder sample of geopolymers GP-1, GP-2 and GP-3 showed increase in the content of SiO_2. This was due to the reaction

between calcined clay and the alkaline activator (mixture of RHA and NaOH), which is known as geopolymerization (Al bakri Abdullah *et al*., 2012). The results on composition of geopolymers are in agreement with results obtained by López *et al*. (2014a) showing that the main components of geopolymer are silica and alumina.

4.3 Characterization of geopolymers by FT-IR

Spectroscopic analysis was carried out by using Fourier Transform Infra-Red Analysis (FT-IR). FT-IR absorption spectra were recorded in the 4000–400 cm^{-1} range using a Nicolet system, IRTracer 100 model Shimadzu, equipped with a DLaTGS (deuterated, L-alanine doped triglycine sulfate with potassium bromide windows) detector. The spectrum of each sample represents an average of 32 scans. Figure 4.1 shows the spectra obtained before adsorption process was carried out.

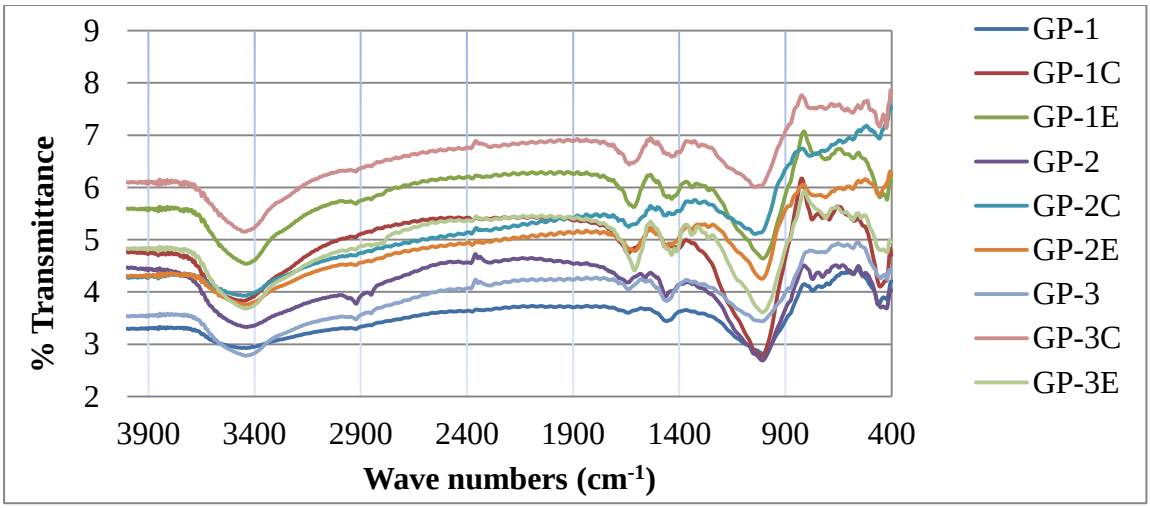

Figure 4.1: FT-IR spectra for geopolymers before adsorption process
C- Citric acid functionalized geopolymer
E- EDTA functionalized geopolymer

In all geopolymeric materials, spectra bands were observed around~1600 cm^{-1} and~3450 cm^{-1} that were attributed to (H–O–H) and (–OH, H–O–H) bending and stretching vibrations respectively. Water was needed for the process of geopolymerization as it

implicated the destruction of solid particles and hydrolysis of dissolved Al^{3+} and Si^{4+} ions as reported by Mu *et al*. (2012). Another spectral band at around 1400 cm^{-1} appeared in all the geopolymer as shown in both figure 4.1 and 4.2. Figure 4.2 presents the spectra of geopolymers after adsorption process.

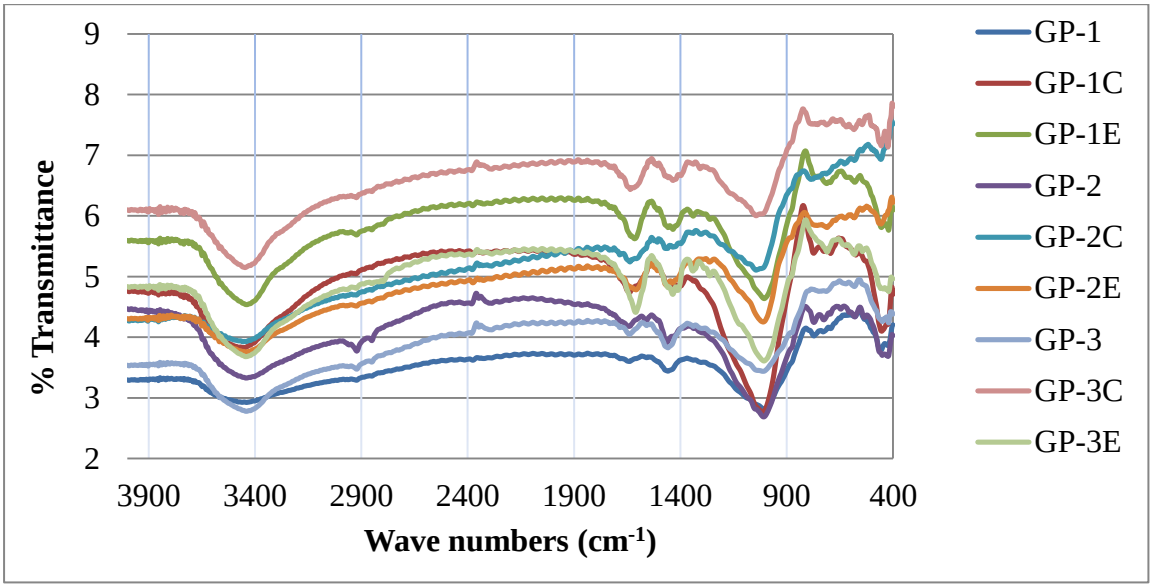

Figure 4.2: FT-IR Spectra of geopolymers after adsorption process
C- Citric acid functionalized geopolymer
E- EDTA functionalized geopolymer

This band is characteristic of the asymmetric O-C-O bonds of CO_3^{2-} stretching mode, indicating the presence of sodium bicarbonate that is suggested to occur due to the atmospheric carbonation of a high alkaline NaOH aqueous phase, which is diffused on the geopolymeric materials surface (Lee and Van Deventer, 2002b; Swanepoel and Strydom, 2002; Fernández-Jiménez and Palomo, 2005). Excess sodium content can form sodium carbonate by atmospheric carbonation and may disrupt the polymerization process (Barbosa and MacKenzie, 2003). The strong peak at~1000 cm^{-1} is associated with Al-O and Si-O asymmetric stretching vibrations and is the fingerprint of the geopolymerization according to Phair and Van Deventer (2002). In the region of 775 - 650 cm^{-1}, the bands are due to symmetrical vibrations of tetrahedral groups (TO_4). The peak at~460 cm^{-1} is

assigned to in-plane bending of Al-O and Si-O linkages (Phair and Van Deventer, 2002) and appears in all spectra's of geopolymers shown in figures 4.1 and 4.2.

Functionalizing with citric acid and EDTA, the shoulder band at~1700 cm^{-1} was observed corresponding to the asymmetric stretching vibration of COOH group (Baranauskas *et al*., 2002; Peleckis *et al.*, 2002) and a respective symmetric vibration was also observed at~1396 cm^{-1}. The peak observed at~1595 crn^{-1} region, for all the citric acid and EDTA functionalized geopolymers was due to the asymmetric stretching vibration of -COO- groups (Rama *et al*., 1995; Hon *et al*., 2002). These vibration peaks are missing in geopolymers that are not functionalized and therefore gives an inference that citric acid and EDTA were tethered onto the geopolymers. Functionalization using EDTA and citric acid led to an increase in absorbance at the wavenumber 3450 cm^{-1}. This represents an increase in the amount of -OH functional group in the sample (Chiem *et al*., 2006).

The strong peak at~1000 cm^{-1} for all geopolymer materials is associated with Al-O and Si-O asymmetric stretching vibrations. After adsorption, Al-O and Si-O asymmetric stretching vibrations which are the confirmation of the geopolymerization reduced as displayed by the FTIR spectra. This could be attributed to the fact that the two groups were used in adsorption process.

4.4 Microstructure analysis of geopolymers by scanning electron microscope

The particle morphology and the microstructure of the cured geopolymers were examined using a scanning electron microscope (SEM) (Zeiss Evo LS 15) at an accelerating voltage of 5 kV. Figure 4.3 and 4.4 shows the microstructure of the GP-1 and GP-1C respectively.

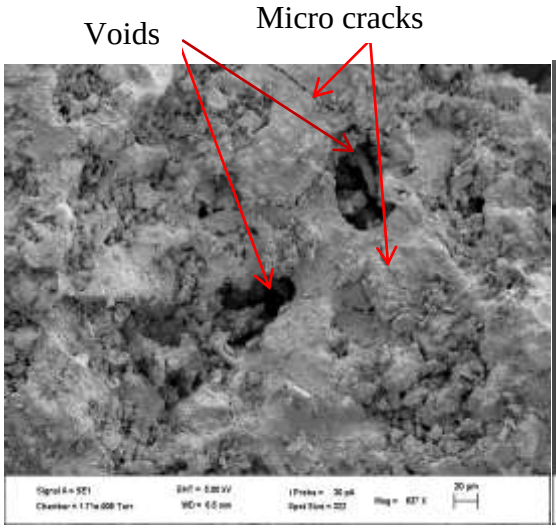

Figure 4.3: SEM image of GP-1

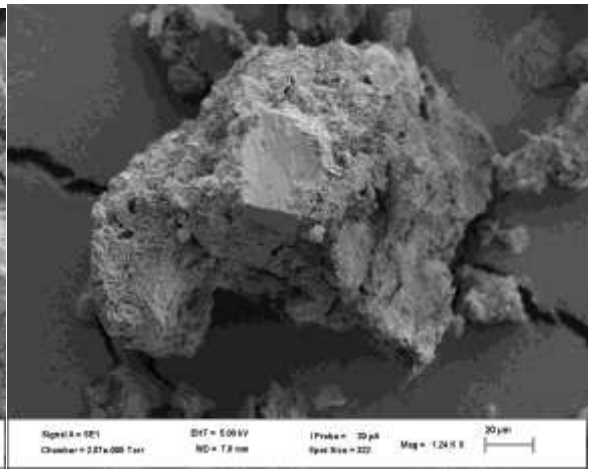

Figure 4.4: SEM image of GP-1C

A more porous microstructure with voids is clearly observed in these SEM micrographs. All figures (Fig 4.3 to 4.9) reveal that the particles of geopolymer concrete were irregularly shaped but very compact. In this geopolymer concrete, the continuity of the mass of reaction product appears like a layer of viscous fluid, suddenly frozen indicating complete polymerization process. Cracks present in the geopolymer gel were believed to occur when the sample was placed in vacuum for SEM coating (Li *et al*., 2013). SEM images in all figures disclosed that paste and mortar formed a relatively dense reacted product.

There were few micro cracks recorded in the geopolymers. These microcracks may be caused by the loading process during SEM analysis and also may be introduced by shrinkage during geopolymer curing where water evaporated (He, 2012). A small group of bright particles which are believed to be zeolites crystals were observed in all geopolymers. SEM micrographs show that microstructures of geopolymers changed with Si: Al ratio and this was in tandem with what was observed by Duxson *et al*. (2005). Figure 4.5 and 4.6 shows the SEM micrographs of GP-1E and GP-2.

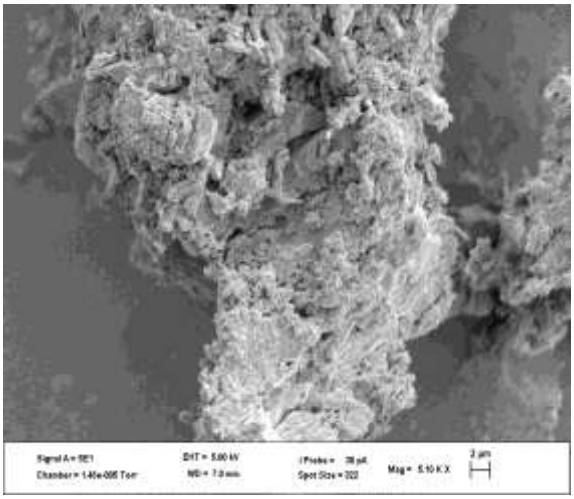

Figure 4.5: SEM image of GP-1E

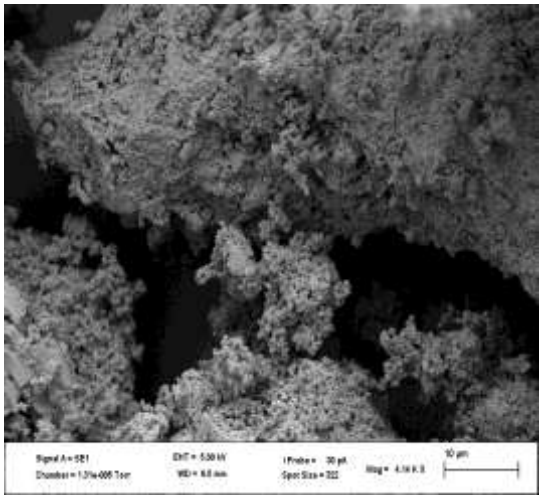

Figure 4.6: SEM image of GP-2

It has been recognized that the SiO_2/Al_2O_3 ratio has a very significant effect on geopolymer characteristics, particularly the microstructural evolution and final geopolymer pore structure (Duxson *et al*., 2005; Sindhunata *et al*., 2006). SEM micrographs exhibited significant change in microstructure with functionalization as shown in figures 4.4, 4.6 and 4.8. Cavities surroundings in figures 4.6 and 4.8 consist of tubular vitreous network (Mu *et al*., 2012). The considerable number of unreacted spheres, as well as the presence of pores (Fig. 4.6) in the geopolymer matrix indicates an incomplete reaction.

Figures 4.3, 4.5, 4.7, 4.10 and 4.11 consisted of two parts, one showing patches of porous, discrete, shaped particles, while the other presenting a dense and continuous gel-like matrix without explicit particles or particle boundaries. Therefore, it is reasonable to conclude that the continuous, gel-like area with no voids is made of geopolymer binder, and the porous-like particles in the porous area are not geopolymer rather NaOH or Na_2CO_3 microcrystals as was suggested by He (2012). Figure 4.7 and 4.8 shows the micrographs of GP-2E and GP-2C.

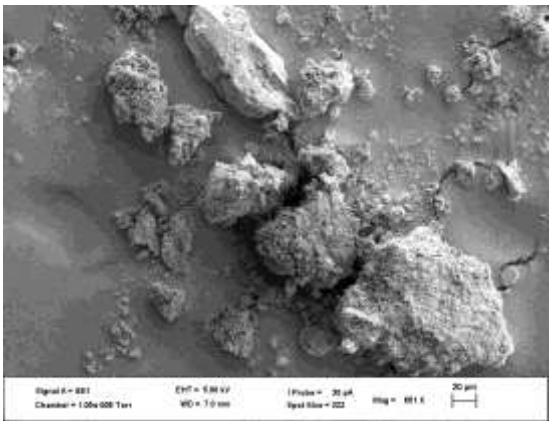

Figure 4.7: SEM image of GP-2E

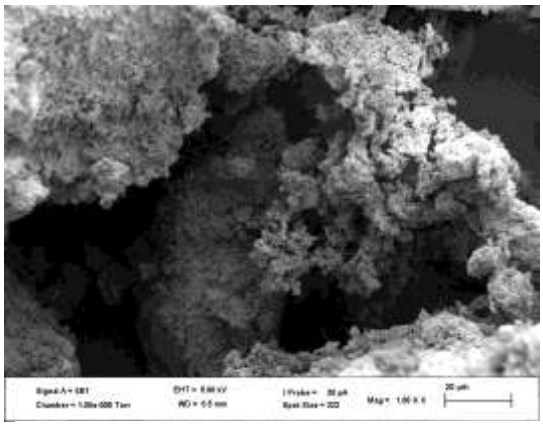

Figure 4.8: SEM image of GP-2C

EDXRF analysis of gel presented in appendix 9 shows that gel mostly consisted of the phases containing Na-Si-Al in the bulk region suggesting the formation of silicate-activated gel by polymerization throughout the inter particles volume (Silva *et al*., 2007; Lloyd *et al*., 2009). This correlates with the published works of Lee and Van Deventer (2002a). Some needle or lathe-shaped particles were formed in the pores or the fractured surfaces (Fig 4.9). It appears that some of these needles were formed after the compression during SEM analysis, as evidenced by the newly grown needles around fractured particles (Fig. 4.9).

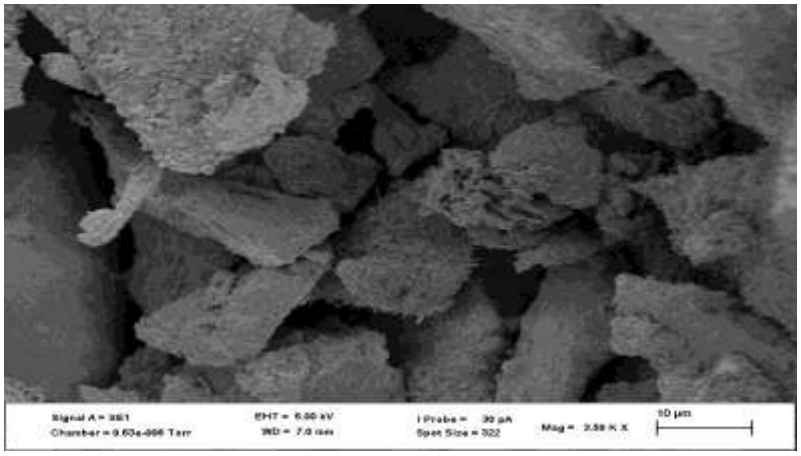

Figure 4.9: SEM image of GP-3E

It is noteworthy that similar particles were observed in a fly ash-based geopolymer (Guo *et al*. 2010). Bulky and dense, gel-like substances were also present (Fig. 4.11), which are

most likely the geopolymer binder with inactive fillers. This is further supported by the EDXRF analyses shown in the spectrum in appendix 9. The major elements (Na, Al, Si, and O) make up geopolymers while, Ca, Mg and Fe are also present and influence the geopolymerization process according to Duxson *et al*. (2007). These remnants (Fe, Ca, K, Mg) obviously represent calcined clay and rice husk ash phases, which for various reasons, did not dissolve during alkali activation (Mu *et al.*, 2012). Lloyd *et al.* (2009) suggested that during alkaline activation, these remnants may have been dispersed throughout the gel. Figure 4.10 and 4.11 shows the images of GP-3 and GP-3C.

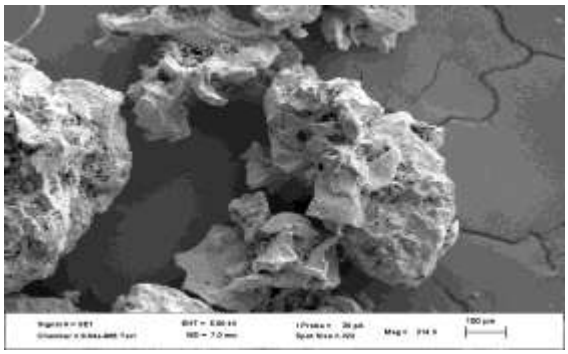

Figure 4.10: SEM image of GP-3

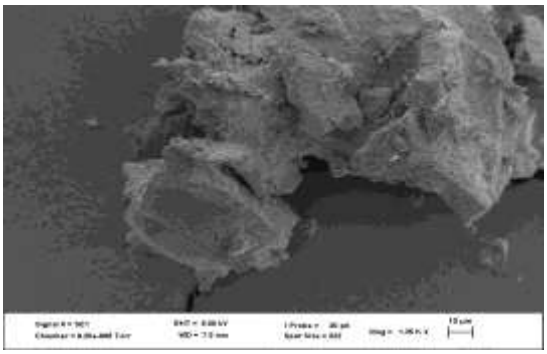

Figure 4.11: SEM image of GP-3C

4.5 XRD characterization of geopolymers

Figures 4.12 to 4.20 present the X-ray diffraction pattern of geopolymers. In the diffraction patterns, the 2θ angle is on abscissa and the intensity of mineral is plotted along ordinate. The intensity is represented in counts. The X-ray diffraction (XRD) analysis was conducted to determine the crystalline phases of the geopolymers. Figure 4.12 shows the powdered diffraction pattern of GP-1.

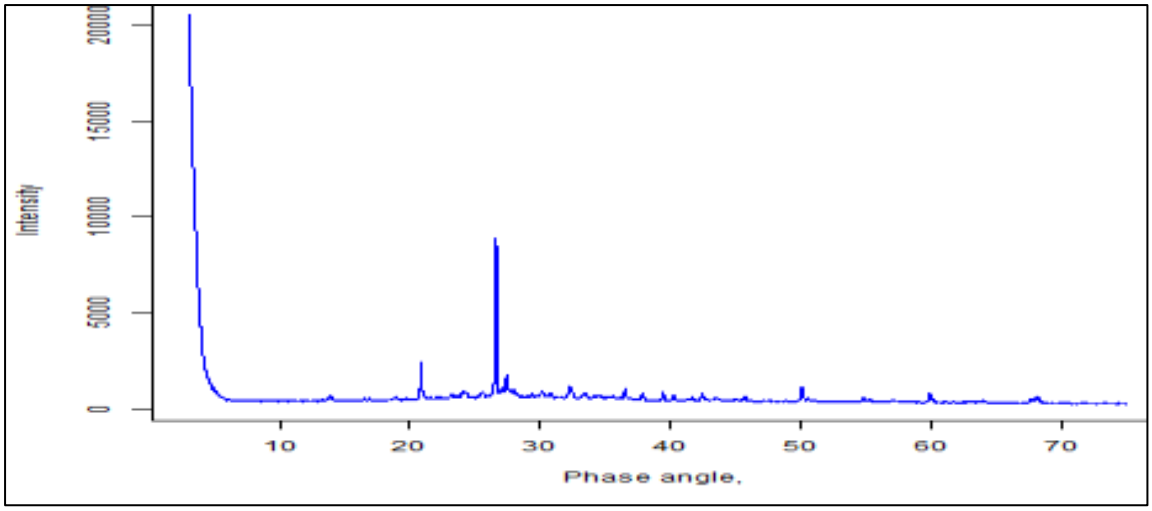

Figure 4.12: Powder diffraction pattern of GP-1

Figures (4.12, 4.13 and 4.14) show the XRD data obtained for the three geopolymer materials (GP-1, GP-2 and GP-3) with different SiO_2: Al_2O_3 ratios respectively. Various crystalline phases were identified which included quartz (SiO_2), albite ($NaAlSi_3O_8$), vermiculite (Mg, Fe, Al) $_3$ (Al, Si)$_4O_{10}$)$(OH)_2.4H_2O$), microcline ($KAlSi_3O_8$), analcime ($NaAlSi_2O_6 \cdot H_2O$) and natrite (Na_2CO_3). The formation of carbonates was attributed to improper sealing of the samples, which allowed atmospheric CO_2 to react with the sodium-rich pore solutions (Hajimohammadi *et al.*, 2011). Figure 4.13 represents diffraction pattern of GP-2

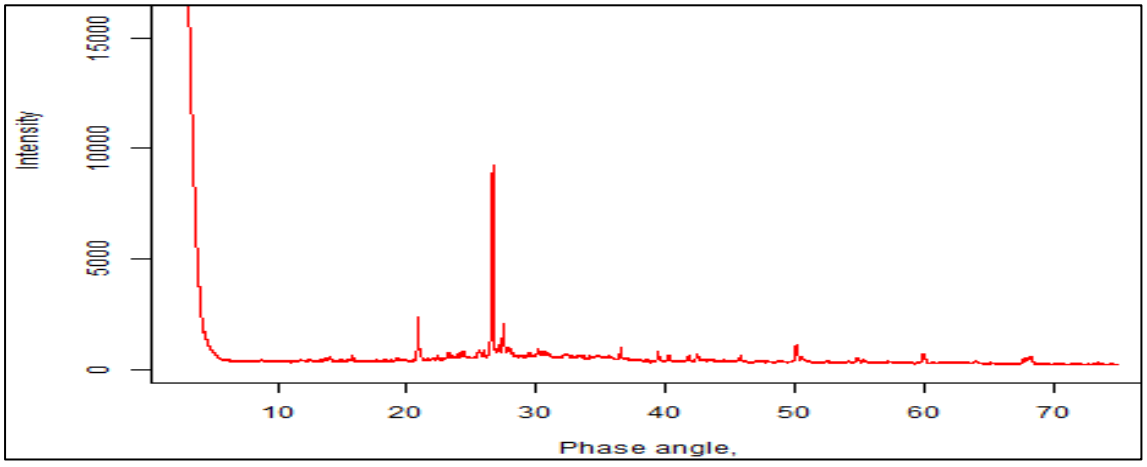

Figure 4.13: Powder diffraction pattern of GP-2

The degree of crystallinity calculated as per procedures given by Murthy (2004) was 64.28 % wt. crystallinity and 35.72 % wt. amorphous for GP-1. Quartz, which was recognizable in all samples and in large percentages after geopolymerization, was the main crystalline phase present in calcined clay, and the rice husk ash. There was formation of 1.8 % analcime in GP-2, which was absent in GP-1 and GP-3. Analcime is a relatively high-silica crystalline phase, and the formation of higher amounts of this phase indicates that there was most likely a high-silica environment in the regions of the gel in which it was formed.

A similar report has been discussed previously for geopolymer-forming systems (Silva *et al*., 2007) and for zeolite synthesis by hydrothermal transformation of gels and clays (Barrer and Mainwaring, 1972). It is worth noting that, although the calcined clay contained alumina (Al_2O_3) as indicated by the chemical composition analysis (Table 4.1), no alumina peaks were identified in the XRD patterns of geopolymers. This suggests that the alumina in the calcined clay was mainly present in amorphous form and hence could not have been detected by XRD. Figure 4.14 shows the diffraction pattern of GP-3.

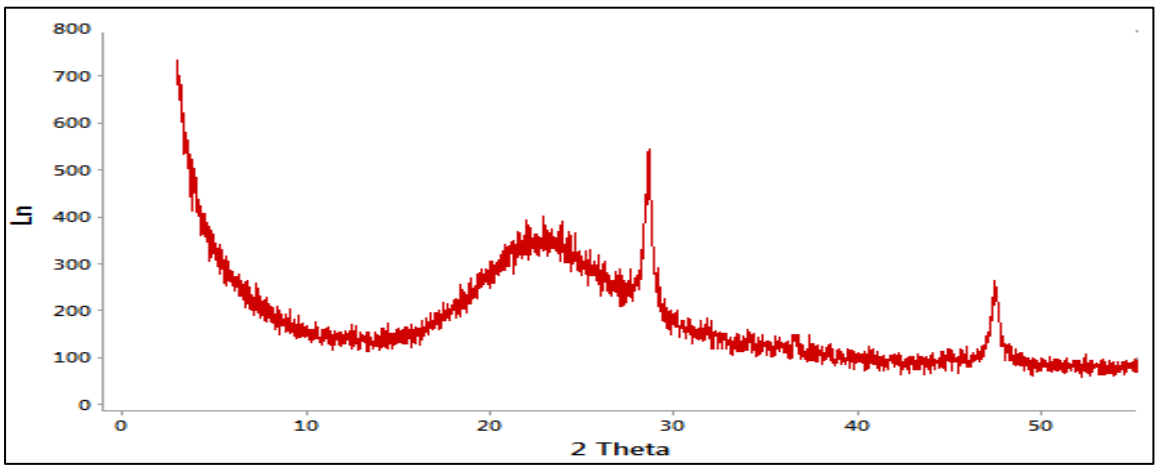

Figure 4.14: Powder diffraction pattern of GP-3

The fact that analcime was not observed in GP-1 and GP-3 may be due to the heterogeneity of the geopolymers, leading to the growth of different phases in local areas, or also it could be a sign of a higher degree of Si contribution to the final geopolymer binder due to the favourable activating energy of the transformation of such regions (compared to less Si-rich regions) to higher Si- crystallites (Hajimohammadi *et al*., 2011).

In the three types of geopolymers, there was a broad hump between 18 - 36° (2θ). The amorphous hump conforms to Li and Liu (2007) and Guo *et al*. (2010) stipulation that the hump is a characteristic reflection of amorphous geopolymers. Apparently, this broad reflection was more pronounced in the GP-3, but not so elaborate for the GP-1 and GP-2, suggesting a higher degree of geopolymerization and more pure geopolymer binder in the GP-3 than in the GP-1 and GP-2 (He, 2012).

Hydrothermal treatments of the paste during geopolymerization lead to formation of 2.2 % vermiculite ($(Mg, Fe^{2+}, Fe^{3+})_3[(Al, Si)_4O_{10}](OH)_2 \cdot 4H_2O$) detected in GP-2 and was absent in GP-1 and GP-3. This phenomenon could be attributed to the presence of MgO detected in GP-2. 2.1 and 3.1 % of heulandite $(Ca, Na)_{2-3}Al_3(Al, Si)_2Si_{13}O_{36} \cdot 12H_2O$) was identified in GP-1 and GP-3 respectively. This could have been caused by the presence of high % of calcium oxide in both Kakamega and Molo clays as detected in EDXRF analysis. 6 % of ilmenite ($FeTiO_3$) was found to be present in GP-3 but was missing in GP-1 and GP-2. Presence of high % of iron and titanium in Molo clay than in Kakamega and Kuresoi clay could have been the probable cause of the presence of ilmenite in GP-3. High silicate due to high Si: Al ratio in GP-3 led to geopolymers gel in the system that were thought to be predominantly amorphous (Rees *et al*., 2007). Similarity experienced in diffraction patterns of GP-1 and GP-2 could have been

attributed to closeness in their Si: Al ratio (4.16 and 4.18 respectively) and their crystalline phases. Figure 4.15 shows the diffraction pattern of GP-1E.

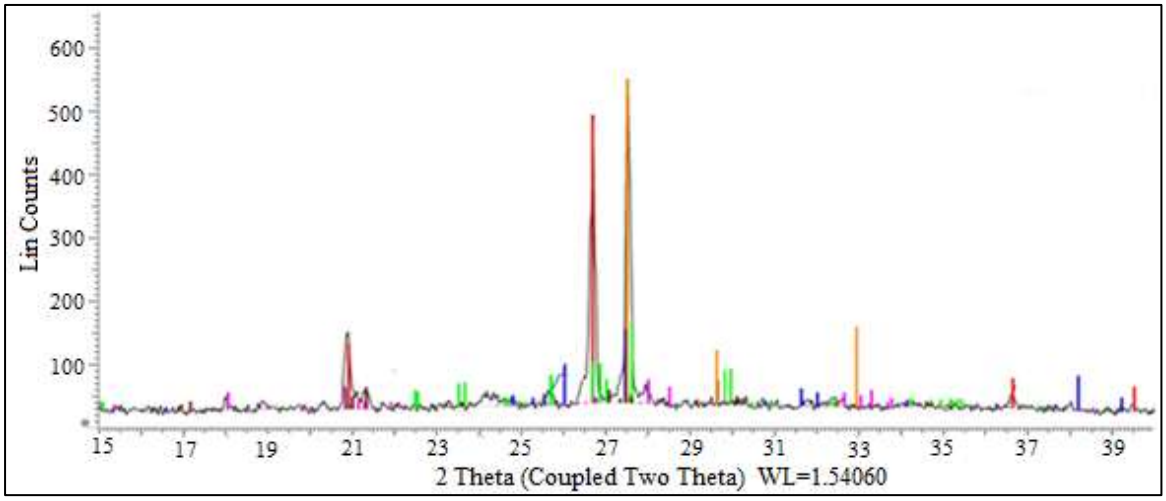

Figure 4.15: Powder diffraction pattern of GP-1E

The most noticeable difference between the samples GP-1 and GP-1E was the bigger relative size of the crystalline peaks for the samples functionalized with EDTA, compared to those of unfunctionalized samples. The degree of crystallinity increased slightly to 65.32 % wt. crystallinity and 34.68 % wt. amorphous when calculated using the procedures adopted from Murthy (2004). This led to inferring that tethering the geopolymer with EDTA could have caused a reaction between the amorphous phases of geopolymer hence increasing its degree of crystallinity. The main sharp peaks were of quartz and albite ($NaAlSi_3O_8$). Diffraction pattern of GP-1C is shown in figure 4.16.

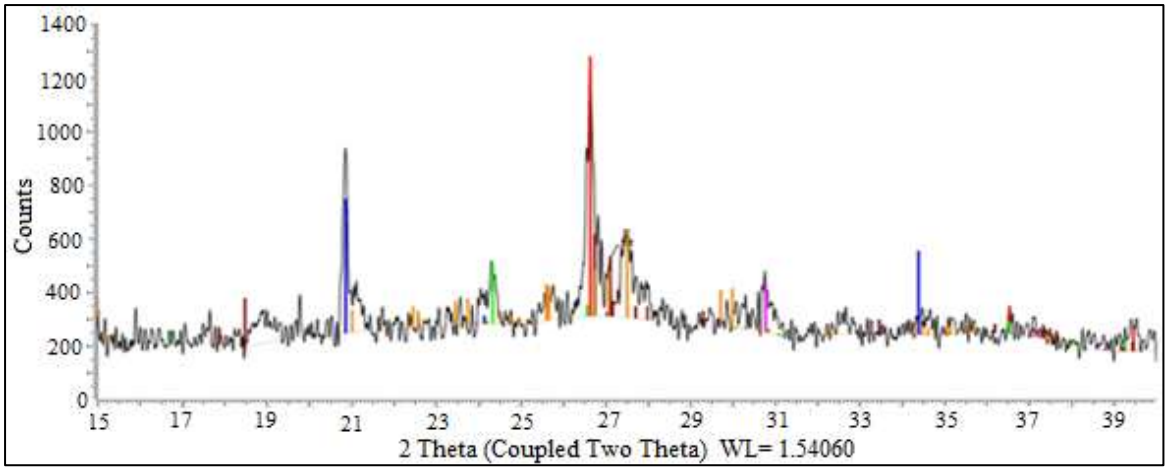

Figure 4.16: Powder diffraction pattern of geopolymer GP-1C

The main crystalline phases identified in diffraction pattern (Figure 4.16) were quartz (SiO_2) occurring at 20.6° (2θ), carnegiete ($AlNaSiO_4$) at 20.85° (2θ), columbite at 24.29 (2θ), and microcline ($Al_{0.93}KO_8Si_{3.07}$) at 27.52°(2θ). An amorphous hump was observed between 18 and 31° (2θ). The presence of quartz was an indication that calcined clay from Kakamega and rice husk ash contained both amorphous and crystalline phases. The amorphous form being reactive took part in geopolymerization while the crystalline form was detected by XRD since it is unreactive form. These crystalline phases which are zeolitic in nature were formed due to presence of sodium and potassium in the clay minerals used. Figure 4.17 shows the diffraction pattern of GP-2C.

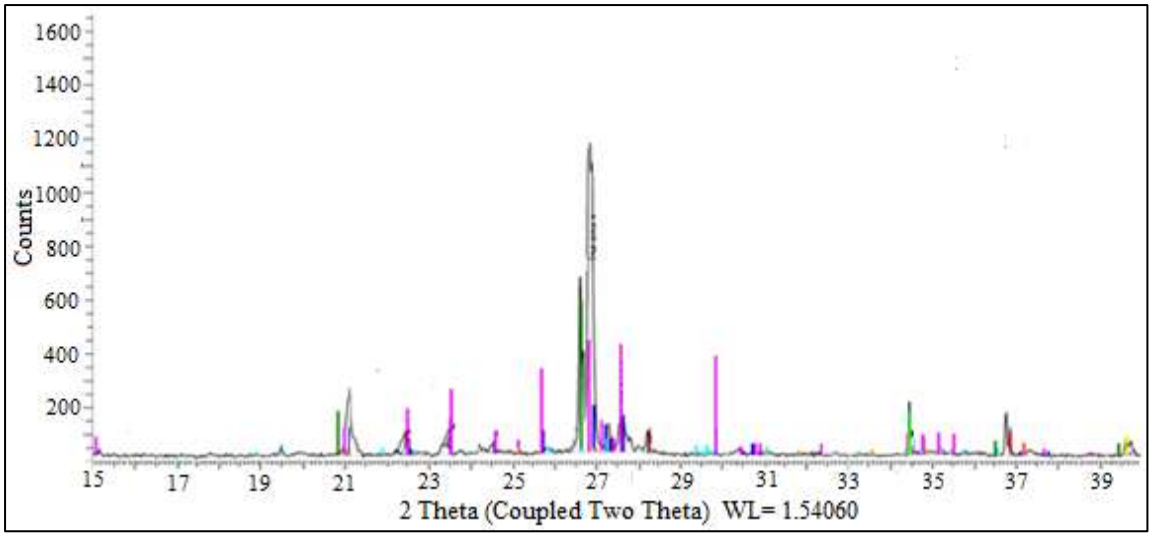

Figure 4.17: Diffraction pattern of GP-2C

The figure displays the diffraction pattern of GP-2C showing that the degree of crystallinity changed from 73.68 to 74.32 % wt. upon citric acid functionalization. A few crystalline phases identified in the geopolymer were analcime, quartz and microcline but their percentage phase composition dropped from 1.8, 30.3 and 49.5 % to 0.6, 25.3 and 41.2 % respectively after citric acid tethering. This could mean that some of these phases in the geopolymer reacted with the citric acid used. However, for all geopolymers, a very weak, broad hump between 18 - 36° (2θ) was observed (it becomes less clear due to the large vertical axis scale), which is regarded as the characteristic peak of geopolymers (Davidovits, 1991; Duxson *et al*., 2007). Figure 4.18 shows the diffraction pattern of GP-2E.

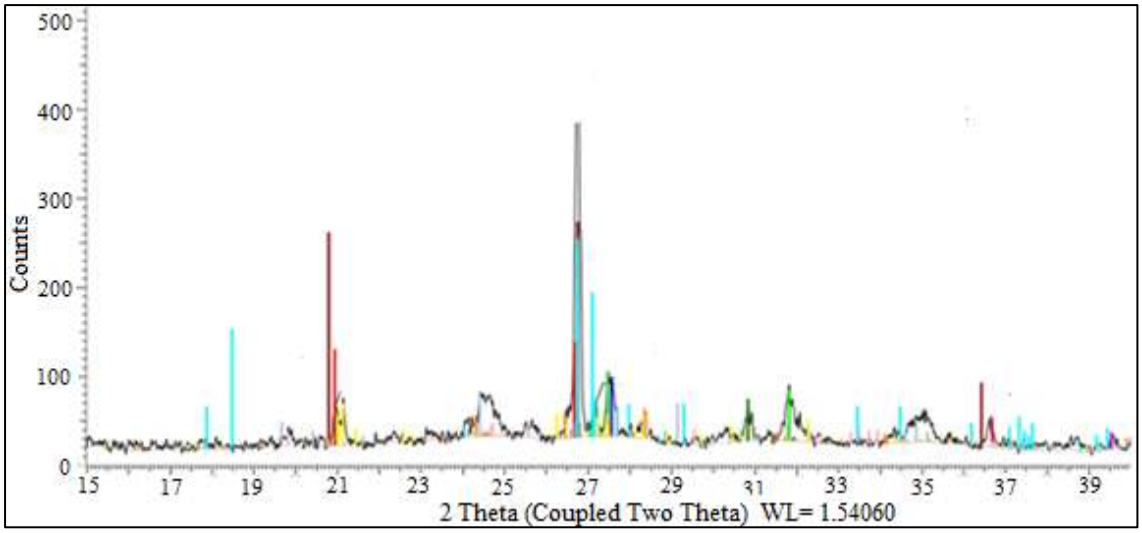

Figure 4.18: Powder diffraction pattern of GP-2E

Few crystalline phases were identified and were quartz (SiO_2), albite ($NaAlSi_3O_8$) and microcline ($KAlSi_3O_8$). The phases appeared in the geopolymer due to hydrothermal reactions. The percentage composition of these phases changed from 30.3, 26.4 and 49.5 % before functionalization to 6.9, 11.0 and 37.5 % upon functionalization. Degree of crystallinity also increased from 73.68 to 73.89 % wt. This may be as a result of the reaction between EDTA and the metal impurities dispersed in the geopolymeric gel to form M $(EDTA)^{n-}$ (Zhao *et al*., 2004) resulting in introduction of more crystalline phases. Figure 4.19 and 4.20 represents diffraction patterns of GP-3C and GP-3E respectively.

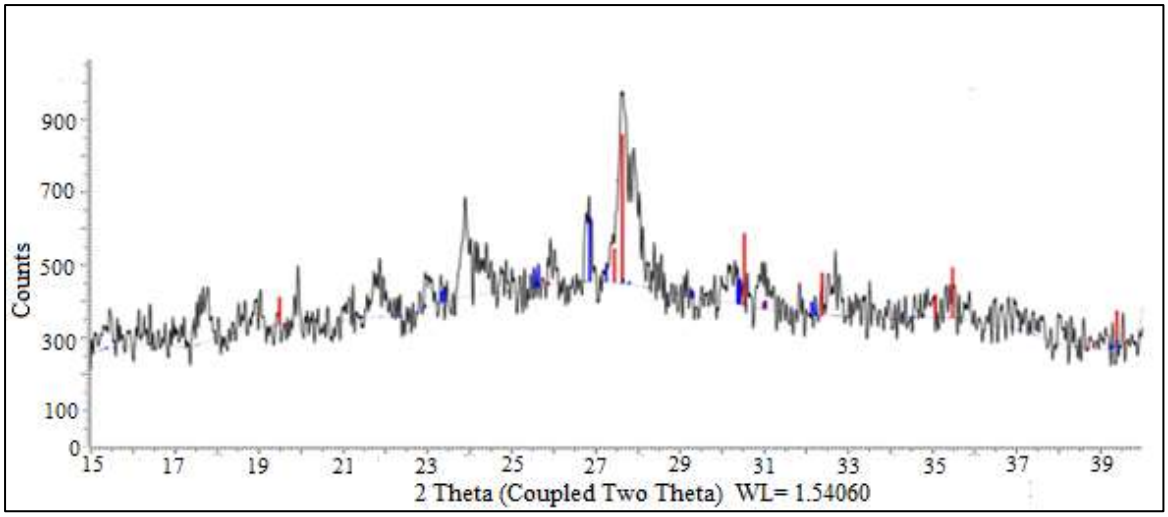

Figure 4.19: Powder diffraction pattern of GP-3C

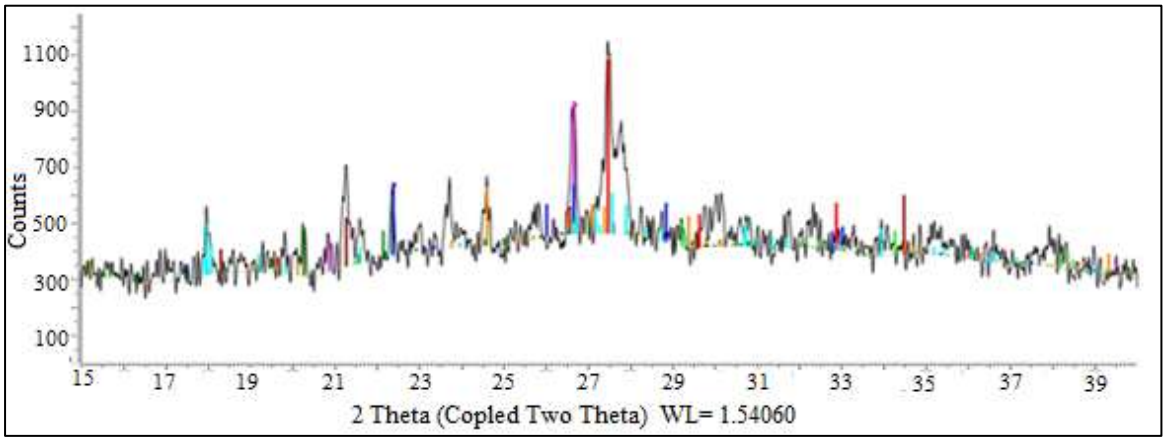

Figure 4.20: Powder diffraction pattern of GP-3E

Powdered x-ray diffraction analysis of these geopolymers showed they contained quartz (SiO_2), albite ($NaAlSi_3O_8$), dolomite ($CaMg\ (CO_3)_2$, microcline ($KAlSi_3O_8$) and muscovite ($KAl_2\ (AlSi_3O_{10})\ (F, OH)_2$) as the main crystalline phases. A broad hump between 18-36° 2θ was observed in both geopolymers.

4.6 Adsorption experiments of heavy metals using geopolymers

4.6.1. Effect of pH on adsorption of Pb (II), Cd (II) and Zn (II) ions

pH is one of the most important controlling parameters in all adsorption processes (Fatiha and Belkacem, 2016). It affects both the surface charge of adsorbent and degree of

ionization of the heavy metal ions in solution (Rao *et al*., 2010). The initial pH of a solution may also affect the extent of dissociation of the functional groups on the adsorbent (Nandi *et al*., 2009). pH influences the chemical structure of the metal ions in aqueous solution, hence influencing its bioavailability (Ozacar and Sengil, 2005). To study the pH effect on adsorption of metal ions using geopolymer, the pH was varied from 2.0 to 6.0. Appendices 11, 12 and 13 show the calibration curves of Pb (II), Cd (II) and Zn (II) respectively.

4.6.1.1 Effect of initial pH on adsorption of Pb (II) ions

The adsorption of Pb (II) ions was found to be strongly dependent on the pH of the solution. Figure 4.21 shows the effect of varying pH on adsorption of Pb (II) ions.

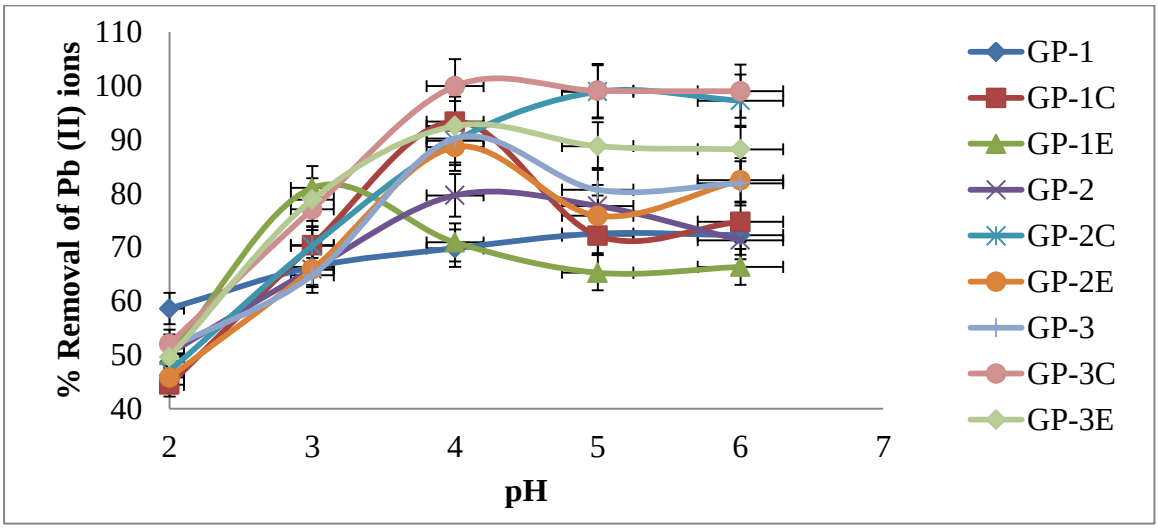

Figure.4.21: Effect of pH on Pb (II) ions removal onto geopolymer materials (Pb (II) ions concentration = 100 mg/L, adsorbent dose = 0.1 g/50 mL, shaking speed = 120 rpm, temperature = 25 °C ± 1 and error bars indicate the average deviation from the mean).

The figure demonstrates that the optimum pH for the adsorption of Pb (II) ions was about 4.0 on both geopolymers and their functionalized counterparts which were rather acidic. Adsorption of Pb (II) ions on geopolymer material increased to optimum mean percentages of 72.54± 0.43, 79.65 ± 0.27 and 90.23 ± 0.04 for GP-1, GP-2 and GP-3

respectively at a pH of 4.0 as shown in appendices 1A, 1B and 1C. GP-3 gave higher adsorption of Pb (II) than GP-1 and GP-2 and this could be associated with the high SiO_2: Al_2O_3 ratio that led to increase in the silica content in the framework causing increased negatively charged groups of O-Si-O- in the geopolymers (Aranberri and Bismarck, 2007).

Citric acid and EDTA functionalized geopolymers recorded an increase in mean percentage adsorption from between 40 – 50 % at pH of 2 to 93.34 ± 0.06, 98.90 ± 0.06, 88.61 ± 0.07, 99.32 ± 0.04 and 92.53 % ± 0.08 for GP-1C, GP-2C, GP-2E, GP-3C and GP-3E at a pH of 4. This might be due to the stronger chelating properties of EDTA and citric acid in functionalized geopolymers on the heavy metal ions. The low adsorption percentage of Pb (II) at lower pH values could be explained by the competition between H^+ and Pb (II) ions on the available exchange sites of the adsorbents (Sari *et al.*, 2007). However, the experiments on adsorption of Pb (II) ions could not be performed beyond pH of 6.0 due to the low solubility of lead (II) hydroxide, which could be formed as white precipitate in water at that pH (Sen Gupta and Bhattacharyya, 2008). A similar trend of effect of pH on adsorption of Pb (II) ions was reported by Amer *et al*. (2010) on adsorption of Pb (II), Zn (II) and Cd (II) ions onto polyphosphate-modified kaolinite clay.

4.6.1.2 Effect of initial pH on adsorption of Cd (II) ions

Figure.4.22 expresses the effect of initial pH of the solution on the adsorption of Cd (II) ions onto geopolymers.

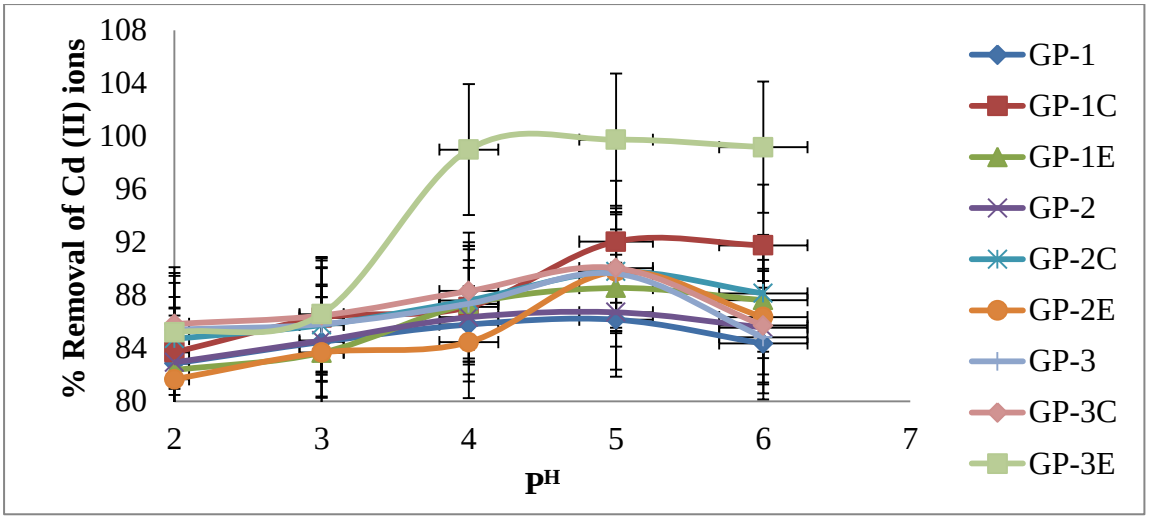

Figure.4.22: Effect of pH on Cd (II) ions removal onto geopolymer materials (Cd (II) concentration=100 mg/L, adsorbent dose = 0.1 g/50 mL, shaking speed = 120 rpm, temperature = 25 °C ± 1 and error bars indicate the average deviation from the mean).

The mean percentage removal increased from 82.85 ± 0.20, 82.93 ± 0.13 and 85.41 ± 0.11 to 86.16 ± 0.31, 86.71 ± 0.26 and 89.63 % ± 0.18 when the pH was varied from pH 2 to 5, for geopolymer materials GP-1, GP-2 and GP-3 respectively. Functionalized geopolymers GP-1C, GP-1E, GP-2C, GP-2E, GP-3C and GP-3E registered optimum mean adsorption of 92.05 ± 0.10, 88.55 ± 0.19, 89.79 ± 0.05, 89.78 ± 0.07, 90.05 ± 0.05 and 99.74 % ± 0.01 at pH of 5 respectively as shown in appendices 2A, 2B and 2C.

Low adsorption was registered at low pH and this could have been caused by electrostatic repulsion between the positively charged geopolymer surface and the metal ions (Malferrari *et al*., 2007). The optimum adsorption pH was between 4 and 5 for geopolymers (GP-1, GP-2 and GP- 3) and functionalized geopolymers (GP-1C and 1E, GP-2C and 2E, GP-3C and 3E) as per figure 4.22. The working pH value for cadmium removal onto geopolymer materials was then chosen as 5.0. Similar results on effect of pH on adsorption of cadmium has been reported in literature (Kounou *et al*., 2015).

4.6.1.3 Effect of initial pH on adsorption of Zn (II) ions

Zn (II) ions uptake by geopolymer materials increased with increase in pH. Maximum mean equilibrium uptake was 80.26 ± 0.10, 93.56 ± 0.07, 81.19 ± 0.06, 79.29 ± 0.13, 81.39 ± 0.16, 81.16 ± 0.08, 80.07 ± 0.13, 91.33 ± 0.06 and 81.83 % ± 0.05 as shown in appendices 3A, 3B and 3C using GP-1, 1C, 1E, 2, 2C, 2E, 3, 3C and 3E at pH of 5.0 respectively. At low pH, adsorption was low due to large quantities of protons competing with Zn (II) ions for adsorption sites. The pH dependent adsorption onto geopolymer materials is shown in figure 4.23.

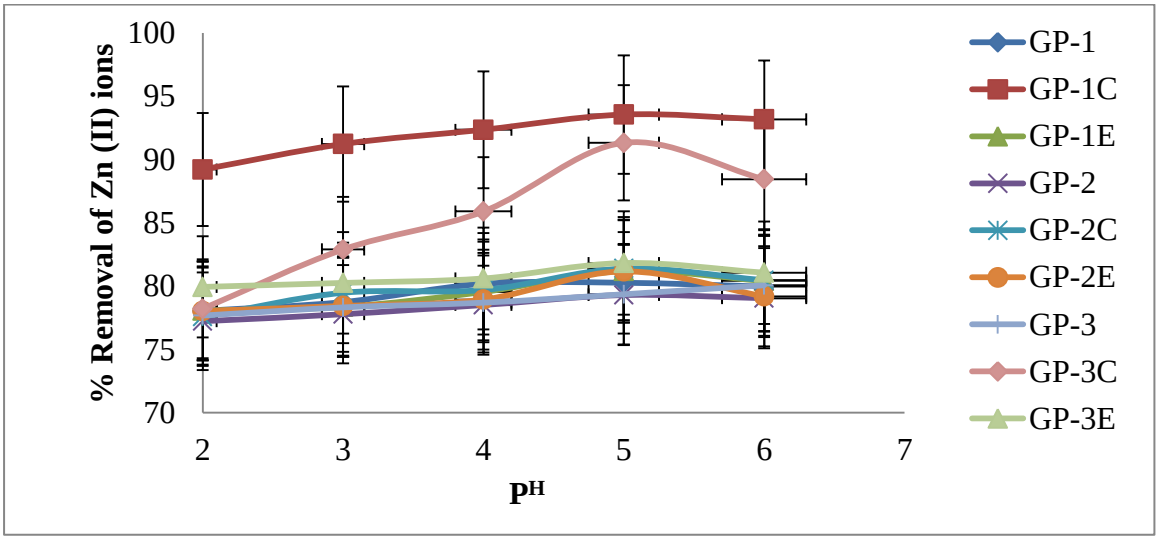

Figure.4.23: Effect of pH on Zn (II) ions removal onto geopolymer materials (Zn (II) concentration = 100 mg/L, adsorbent dose = 0.1 g/50 mL, shaking speed = 120 rpm, temperature = 25 °C and error bars indicate the average deviation from the mean).

The mean percentage removal reached plateau at pH 5. It is known that Zn species are present in deionized water in the forms of Zn^{2+}, $ZnOH^{+}$, ZnO and $Zn(OH)_2$ (Reichle *et al*., 1975). Within the pH range of 1.0 - 5.0, the solubility of the $Zn(OH)_2$ is high and therefore, the Zn (II) ions were the main species in the solution. Similar results were reported by Abdelghani and Elchaghaby (2007) on adsorption of Cu (II), Zn (II), Cd (II) and Pb (II) using Nile rose plant.

4.6.2 Effect of contact time on adsorption of Pb (II), Cd (II) and Zn (II) ions

The importance of contact time comes from the need for characterization of the feasible rapidness of binding and removal processes of the heavy metal ions by the new geopolymers and obtaining the optimum time for complete removal of the target metal ions (Arshadi *et al*., 2014). In an adsorption system, the contact time plays a vital role irrespective of the other experimental parameters affecting the adsorption kinetics (Vaishnav *et al*., 2011). The adsorption experiments were carried out at different time intervals (20 - 100 minutes).

4.6.2.1 Effect of contact time on adsorption of Pb (II) ions

The relationship between contact time and the percentage removal of Pb (II) ions from wastewater with geopolymer and functionalized geopolymers is shown in figure 4.24.

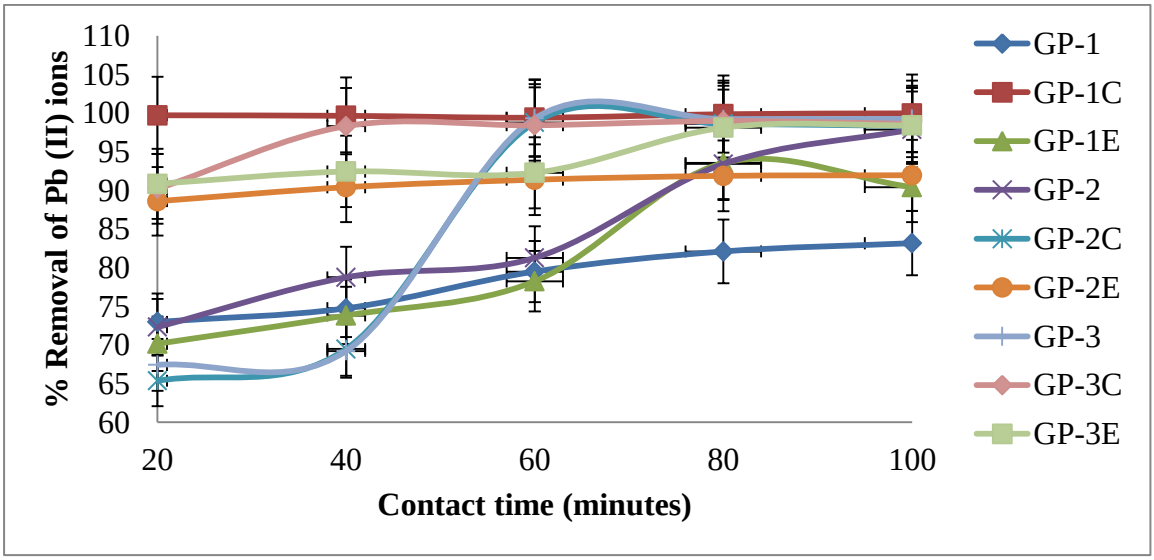

Figure.4.24: Effect of contact time on Pb (II) ions removal onto geopolymer materials (Pb (II) ions concentration = 100 mg/L, adsorbent dose = 0.1 g/50 mL, shaking speed = 120 rpm, pH = 4.0 temperature = 25 °C and error bars indicate the average deviation from the mean).

The effect of contact time was studied at a room temperature of 25 °C ± 1. The highest percentage metal ions removal achieved were 83.18 ± 0.08, 99.97 ± 0.01, 93.54 ± 0.12,

97.88 ± 0.07, 98.79 ± 0.05, 91.88 ± 0.10, 98.98 ± 0.07, 99.32 ± 0.03 and 98.42 % ± 0.21 for GP-1, 1C, 1E, 2, 2C, 2E 3, 3C and 3E respectively. Citric acid and EDTA functionalized geopolymers recorded higher metal ion removal than their corresponding geopolymer analogues as shown in appendices 1G, 1H and 1I.

The results showed that adsorption efficiency increased with increase in contact time. This may be due to the fact that the number of active adsorption sites on the surface of adsorbent were more initially (Dubey and Shiwani, 2012). The fast adsorbate adsorption at the initial stage was probably due to the initial concentration gradient between the adsorbate in solution and the number of vacant sites available on the adsorbent surface. Adsorption rate slowed down after 80 minutes and this could have been due to the electrostatic hindrance caused by already sorbed positively charged adsorbate species and the slow pore diffusion of the ions. The slow rate could also be due to lesser number of available active sites and slow rate of conveying adsorbates from the outer surface to the inner surface of the adsorbent (Dubey and Shiwani, 2012). Similar results have been reported in literature (Al-Anber and Matouq, 2008; El-Ashtoukhy *et al*., 2008).

4.6.2.2 Effect of contact time on adsorption of Cd (II) ions

The effect of contact time between the Cd (II) ions and the geopolymers is shown by figure 4.25.

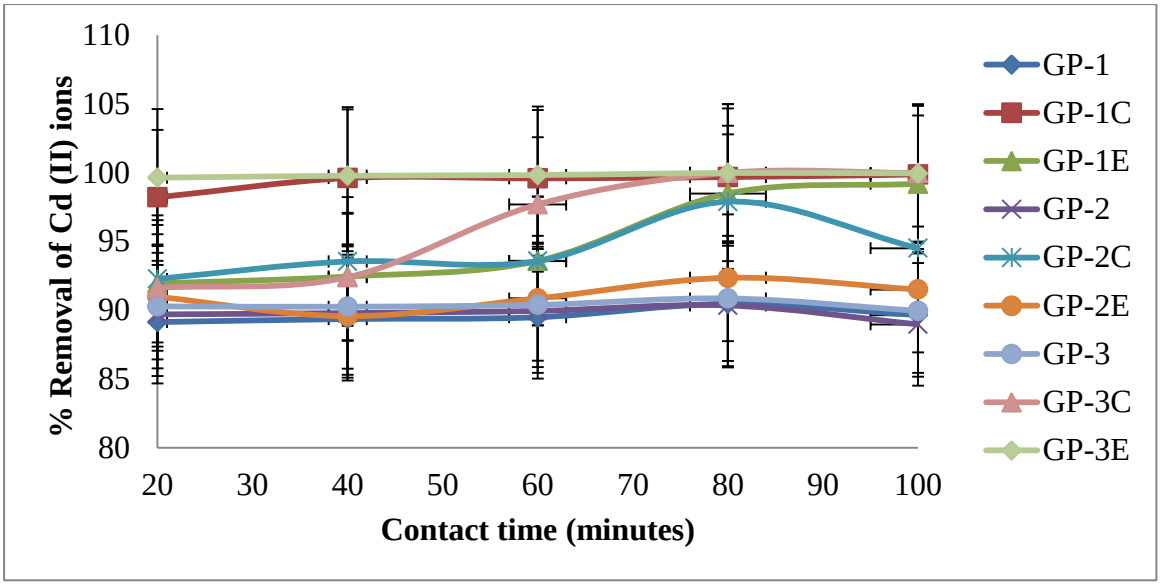

Figure.4.25: Effect of contact time on Cd (II) ions removal onto geopolymer materials (Cd (II) concentration = 100 mg/L, adsorbent dose=0.1 g/50 mL, shaking speed = 120 rpm, pH = 5.0 temperature = 25 °C and error bars indicate the average deviation from the mean).

The removal efficiency increased with increasing contact time and then became constant or dropped with most of the geopolymers. The optimum mean percentage uptake attained were 90.46 ± 0.48, 99.87 ± 0.00, 99.20 ± 0.01, 90.34 ± 0.12, 97.89 ± 0.07, 92.35 ± 0.08, 90.85 ± 0.06, 99.99 ± 0.00 and 99.98 % ± 0.00 for GP-1, GP-1C, GP-1E, GP-2, GP-2C, GP-2E, GP-3, GP-3C and GP-3E respectively as shown in appendices 2G, 2H and 2I. Equilibrium was reached within 40 minutes for GP-1C and 80 minutes for all the other geopolymers. The extent of sorption increased expeditiously during the initial stage and then became slower at later stages till the equilibrium was attained (Krika *et al*.,2016). Similar results were reported by Zhang *et al*. (2008).

4.6.2.3 Effect of contact time on adsorption of Zn (II) ions

The results of the effect of contact time on removal efficiency for Zn (II) using 0.10 g of geopolymers at room temperature (25 °C ± 1) are illustrated in figure 4.26.

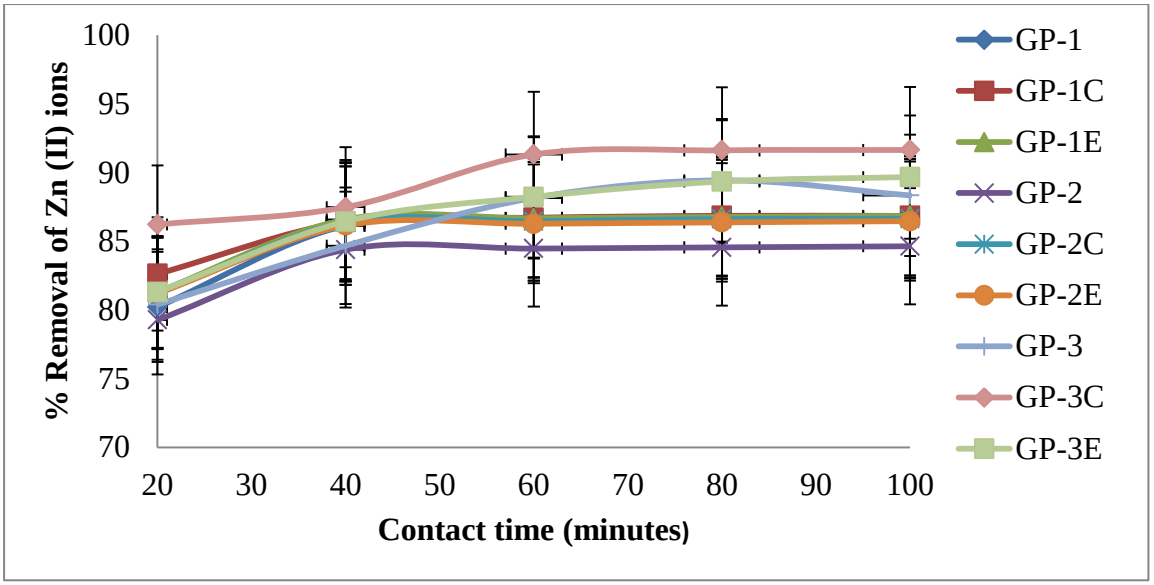

Figure.4.26: Effect of contact time on Zn (II) ions removal onto geopolymer materials (Zn (II) concentration = 100 mg/L, adsorbent dose = 0.1 g/50 mL, shaking speed = 120 rpm, pH = 5.0, temperature = 25 °C and error bars indicate the average deviation from the mean).

The mean percentage uptake obtained was 86.67 ± 0.11, 86.85 ± 0.07, 86.85 ± 0.08, 84.64 ± 0.12, 86.63 ± 0.12, 86.47 ± 0.03, 89.44 ± 0.12, 91.64 ± 0.01 and 89.67 % ± 0.05 for GP-1, GP-1C, GP-1E, GP-2, GP-2C, GP-2E, GP-3, GP-3C and GP-3E respectively as also shown in appendices 3G, 3H and 3I. The adsorption rate was observed as rapid in the first 20 minutes, followed by a gradual increase with time until equilibrium adsorption was recorded at 40 minutes for GP-1, 1C, 1E, 2, 2C, 2E and 80 minutes for GP-3 and 3E. The attainment of equilibrium adsorption might have been due to reduction in the available active sites on the adsorbent with time resulting in limited mass transfer of the adsorbate molecules from the bulk liquid to the external surface of adsorbent. A similar trend on effect of time on adsorption has been reported by other researchers (Ii *et al*., 2011; Mehdizadeh *et al*., 2014).

4.6.3 Effect of initial concentration of metal ions on the adsorption process

Initial concentration of metal ions is an important factor for practical application (Sobhanardakani *et al*., 2016). In order to determine maximum capacity of Pb (II), Cd (II)

and Zn (II) ions adsorbed by geopolymers, it is necessary that adsorption equilibrium data be studied at different concentrations of ions (Malakootian *et al*., 2016). The effect of concentration on the sorption by the geopolymers was investigated by varying it from 20 to 200 mg/L at a pH of 4.0 for Pb (II) and Cd (II) and 5.0 for Zn (II) for 60 minutes equilibration time.

4.6.3.1 Effect of initial concentration of Pb (II) ions on adsorption

Results of the study on the influence of initial Pb (II) ions concentration on the removal efficiency of the geopolymers are depicted in figure 4.27 and the results obtained indicated that the adsorption efficiency decreased with increase in initial Pb (II) ions concentration.

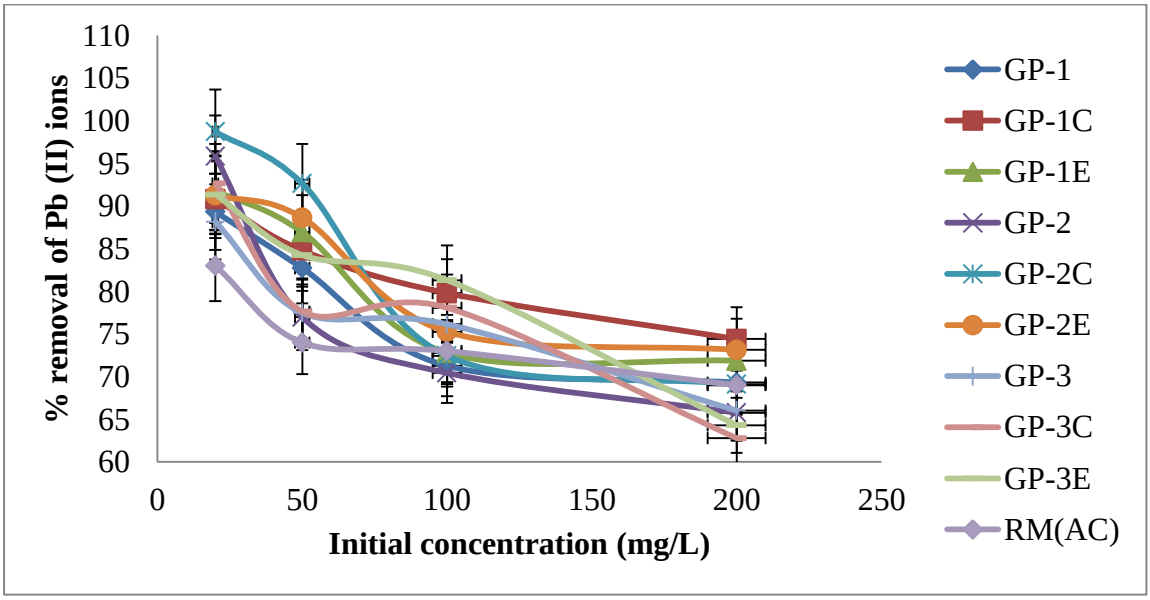

Figure.4.27: Effect of metal ion concentration on Pb (II) ions removal onto geopolymer materials (Contact time = 60 minutes, adsorbent dose = 0.1 g/50 mL, shaking speed = 120 rpm, pH = 4.0, temperature = 25 ^{o}C, RM (AC) = reference material activated carbon and error bars indicate the average deviation from the mean).

The results trend obtained are in agreement with the results of reference material (AC). However the removal efficiency of the geopolymers at low concentration were higher than those of reference an indication the adsorbent are better than activated carbon for low concentration of Pb (II) ions.

Mean percentage removal decreased from 89.33 ± 1.12, 90.79 ± 0.03, 91.81 ± 0.24, 95.82 ± 0.05, 98.72 ± 0.09, 91.26 ± 0.61, 88.15 ± 2.44, 92.64 ± 0.32 and 91.35 % ± 0.92 to 69.31 ± 0.04, 74.87 ± 0.10, 71.87 ± 0.29, 65.77 ± 0.04, 69.10 ± 0.08, 73.14 ± 0.03, 66.02 ± 0.04, 62.79 ± 0.11 and 64.30 % ± 0.00 when concentration was varied from 20 – 200 mg/L for GP-1, GP-1C, GP-1E, GP-2, GP-2C, GP-2E, GP-3, GP-3C and GP-3E respectively as shown in appendices 1N, 1O and 1P. Adsorption decreased with increase of initial concentration and any increase of metal ion led to increase of the residual ion in solution. It is probable that along with increase of surface load (adsorbed substances) on the adsorbent, upper surface adsorption sites are saturated and the efficiency of removal decreases rapidly (Banat *et al.*, 2000).

At lower concentrations, the number of moles of Pb (II) ions are small relative to the available adsorption sites on the adsorbent hence high rate of adsorption (Jnr and Spiff, 2005). However, at higher concentrations, most of the adsorption sites are occupied by Pb (II) ions and the available sites of adsorption become fewer (Berhe *et al.*, 2015). Rezaei (2016) reported that with increase of metal ion concentration, adsorption decreases. This behaviour is connected with the competitive diffusion process of the metal ions through the micro channel and pores in geopolymers (Al-Anber and Al-Anber, 2008). This competition locks the inlet channel on the surface and prevents the metal ions from passing deep inside the geopolymer, hence adsorption occurs on the surface only (Al-

Anber and Al-Anber, 2008). A similar trend of decrease in adsorption of Pb (II) ions with increase in metal ion concentration was reported by Senthil Kumar and Gayathri (2009).

4.6.3.2 Effect of initial concentration on adsorption of Cd (II) ions

The experimental results for the adsorption of Cd (II) ions on the geopolymers at various concentrations with contact time of one hour are portrayed in figure 4.28.

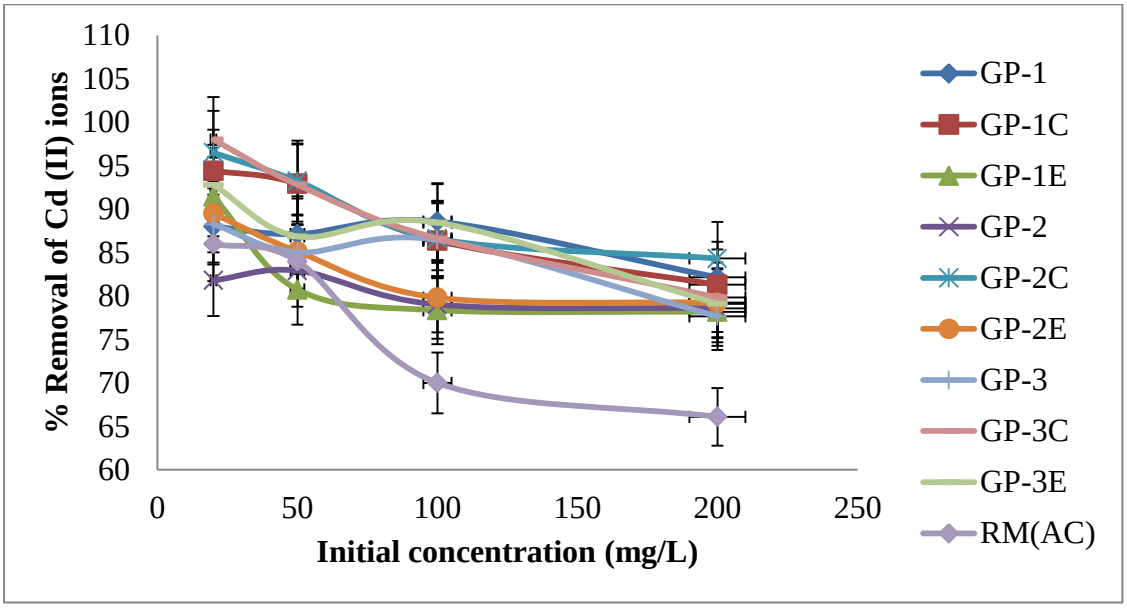

Figure.4.28: Effect of metal ion concentration on Cd (II) ions removal onto geopolymer materials (Contact time = 60 minutes, adsorbent dose = 0.1 g/50 mL, shaking speed = 120 rpm, pH = 5.0, temperature = 25 $^{\circ}$C, RM (AC) = reference material activated carbon and error bars indicate the average deviation from the mean).

The removal efficiency of the reference material (AC) used decreased significantly as compared to the geopolymers at low concentrations but maintained the experimental trend. The mean percent adsorption decreased with increase in initial metal ion concentration. Mean percentage uptake dropped from 88.01 ± 0.82, 94.42 ± 0.31, 91.44 ± 0.81, 81.80 ± 2.64, 96.49 ± 0.09, 89.49 ± 0.15, 88.26 ± 2.25, 98.00 ± 0.03 and 92.77 % ± 0.55 to 82.14 ± 0.21, 81.30 ± 0.01, 78.19 ± 0.04, 78.59 ± 0.06, 84.32 ± 0.05, 779.29 ± 0.05, 77.66 ± 0.41, 79.85 ± 0.07 and 79.11 % ± 0.06 when the concentration was varied

from 20 - 200 mg/L, for GP-1, GP-1C, GP-1E, GP-2, GP-2C, GP-2E, GP-3, GP-3C and GP-3E respectively as shown in appendices 2M, 2N and 2O.

The trend shows clearly that the adsorption is highly dependent on the initial concentration of cadmium ions. This could be attributed to the fact that at lower concentration, the ratio of the initial number of metal ions to the available surface area is low; subsequently the fractional adsorption becomes independent of initial concentration (Vijayakumaran *et al*., 2009). Percentage removal of metal ions is dependent upon its initial concentration since at high concentrations, the available sites for adsorption becomes fewer as illustrated by Balakrishnan *et al*. (2010).

4.6.3.3 Effect of initial concentration on adsorption of Zn (II) ions

The effect of initial concentration on percentage removal of Zn (II) ions (range 20 – 200 mg/L) is shown in figure.4.29.

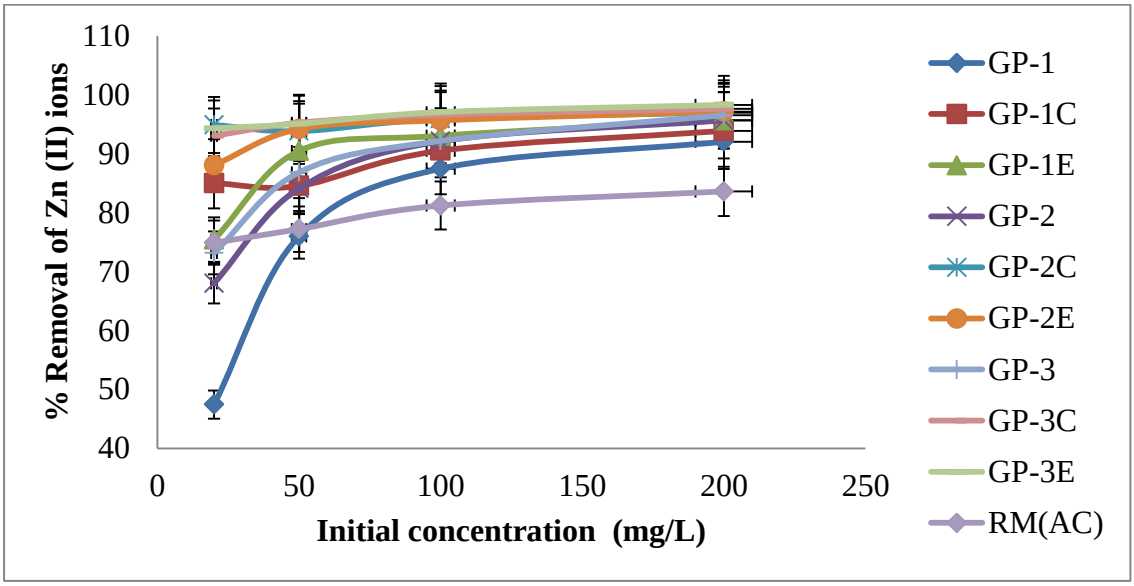

Figure.4.29: Effect of metal ion concentration on Zn (II) ions removal onto geopolymer materials (Contact time = 60 minutes, adsorbent dose = 0.1 g/50 mL, shaking speed = 120 rpm, pH = 5.0, temperature = 25 °C, RM (AC) = reference material activated carbon and error bars indicate the average deviation from the mean).

The adsorption of Zn (II) ions by reference material (AC) recorded similar trend to the geopolymers. Contrary to what was observed for Pb (II) and Cd (II), the percentage adsorption increased with increase in initial concentration up to a certain amount, and then it leveled. Mean percentage removal increased from 47.43 ± 0.41, 84.99 ± 0.18, 75.44 ± 0.68, 68.01 ± 0.63, 94.88 ± 0.08, 88.05 ± 0.09, 73.17 ± 0.39, 93.03 ± 0.13 and 94.30 % ± 0.49 to 92.03 ± 0.01, 93.87 ± 0.10, 95.66 ± 0.02, 95.66 ± 0.03, 96.99 ± 0.01, 97.14 ± 0.31, 96.53 ± 0.07, 97.59 ± 0.09 and 98.28 % ± 0.04 for GP-1, GP-1C, GP-1E, GP-2, GP-2C, GP-2E, GP-3, GP-3C and GP-3E respectively as shown by appendices 3M, 3N and 3O.

At low initial concentration the ratio of number of metal ions to the number of available adsorption sites was small and consequently the adsorption was independent of initial ion concentration, but as the concentration of metal ion increased, the situation changed and the competition for adsorption sites became less (Freundlich, 1906). This may also be as a result of increase in collisions between the reactants, leading to the observed increase in reaction rate and capacity according to the Collision Theory (Zendelska *et al*., 2014). A higher initial concentration provides an important driving force to overcome all mass transfer resistances of the pollutant between the aqueous and solid phases, thus increases the uptake (Senthil Kumar *et al*., 2010).

4.6.4 Effect of shaking speed on adsorption process

The shaking speed is also a significant parameter, which is required to elucidate the exact mechanism of metal ion sorption on the surface of adsorbent (Mishra *et al*., 2012). Increase in agitation rate increases the chances of interaction between metal ions and adsorbents.

4.6.4.1 Effect of shaking speed on adsorption of Pb (II) ions

The effect of shaking speed on adsorption of Pb (II) illustrated in figure 4.30, shows that the adsorption efficiency of geopolymers increased from 76.65 ± 0.26, 83.08 ± 0.68, 65.22 ± 0.04, 82.26 ± 0.42, 72.96 ± 0.26, 88.59 ± 0.03, 76.51 ± 0.26, 93.29 ± 0.11 and 92.39 % ± 0.27 to 98.72 ± 0.02, 99.78 ± 0.01, 89.58 ± 0.02, 85.99 ± 0.33, 99.50 ± 0.07, 94.11 ± 0.07, 86.36 ± 0.25, 99.78 ± 0.02 and 96.06 % ± 0.09 for GP-1, GP-1C, GP-1E, GP-2, GP-2C, GP-2E, GP-3, GP-3Cand GP-3E respectively when the shaking rate increased from 120 to 240 rpm as shown in appendices 1K, 1L and 1M.

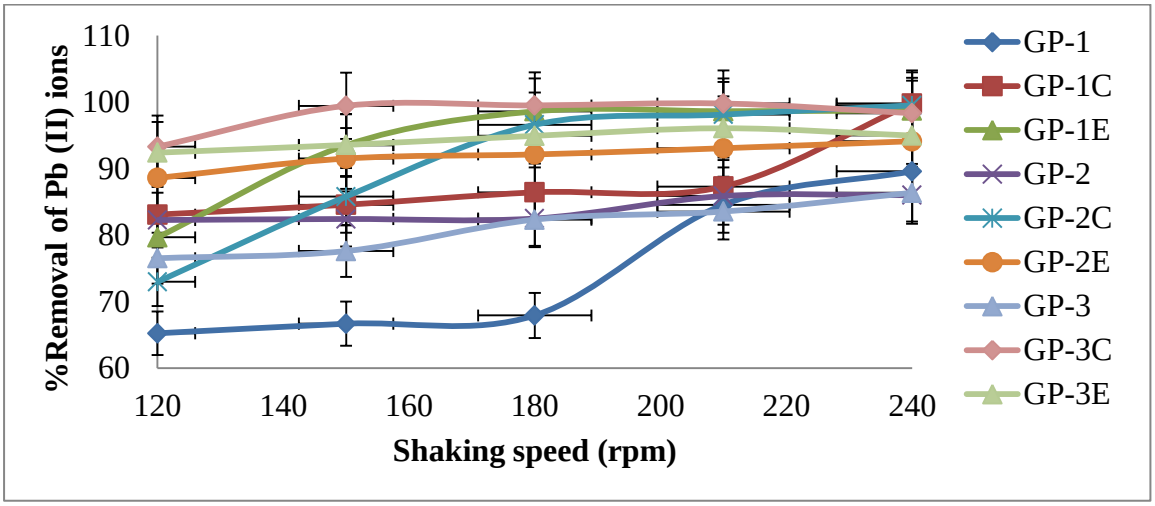

Figure.4.30: Effect of shaking speed on Pb (II) ions removal onto geopolymer materials (Contact time = 60 minutes, adsorbent dose = 0.1 g/50 mL, pH = 4.0 and temperature = 25 °C).

Increase in shaking speed increases the convective mass transfer of solute from the bulk solution, and it also decreases the thickness of the boundary film close to adsorbent surfaces (Murithi *et al*., 2014). According to the research carried out by Nomanbhay and Palanisamy (2005), increase in shaking rate improved the diffusion of metal ions towards the adsorbent surface and the same outcome was observed in this study. Therefore, the constant value of the Pb (II) ions adsorbed by geopolymer GP-2E and GP-3C after 150 rpm and GP- 1E, GP-2C, GP-3, and GP-3E, after 180 rpm was as a result of too vigorous

shaking rate, which caused attainment of equilibrium. Similar results have been reported by Bernard *et al*. (2013) on adsorption of heavy metals from industrial wastewater by activated carbon prepared from coconut shell.

4.6.4.2 Effect of shaking speed on adsorption of Cd (II) ions

The effect of batch shaking speed on Cd (II) ions adsorption onto geopolymers is depicted in figure 4.31.

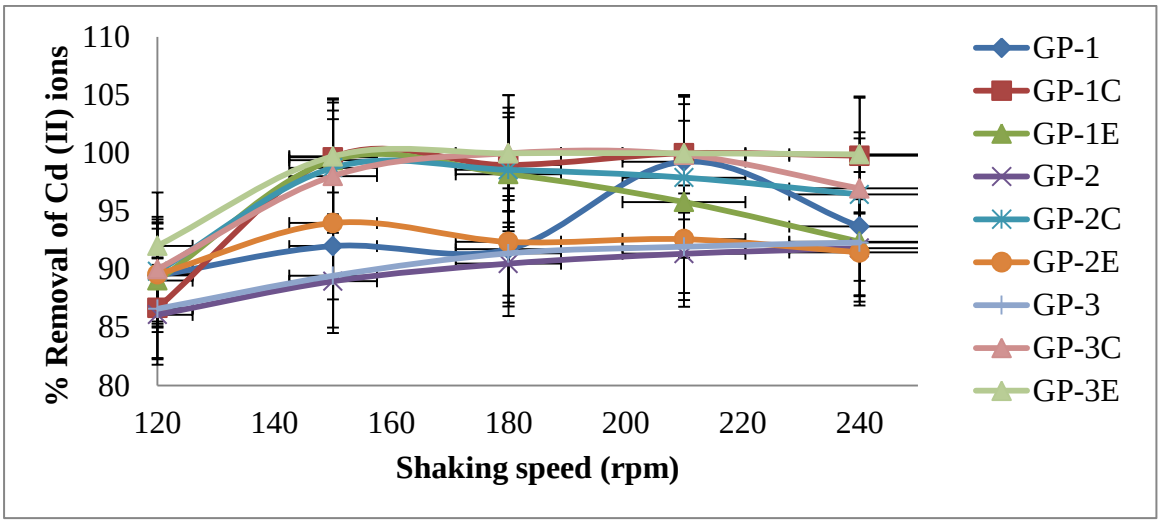

Figure 4.31: Effect of shaking speed on Cd (II) ions removal onto geopolymer materials (Contact time = 60 minutes, adsorbent dose = 0.1 g/50 mL, pH = 5.0, temperature = 25 °C and error bars indicate the average deviation from the mean).

The amount of the metal ions adsorbed increased with increasing agitation speed, and maximum adsorption occurred at 175 rpm. Mean percentage uptake increased from 89.46 ± 0.50, 86.68 ± 0.02, 89.04 ± 0.04, 86.08 ± 0.15, 89.80 ± 0.05, 89.57 ± 0.10, 86.59 ± 0.14, 90.01 ± 0.03 and 92.02 % ± 0.04 to 99.26 ± 0.00, 99.98 ± 0.02, 99.39 ± 0.00, 91.82 ± 0.01, 98.73 ± 0.07, 93.98 ± 0.02, 92.30 ± 0.06, 99.98 ± 0.02 and 99.98 % ± 0.01 for GP-1, GP-1C, GP-1E, GP-2, GP-2C, GP-2E, GP-3, GP-3C and GP-3E respectively as is expounded in appendices 2J, 2K and 2L.

At slow speed, the sorbent settles down and buries many active sites under its top layers. So, only the top layer takes part in adsorption process because the layers buried under do not have contact with metal ions (Raza *et al*., 2015). The external film mass transfer and the sorption rate increased with shaking. Under conditions of optimized agitation, surface reactions or intraparticle diffusion would be rate-limiting (McKay, 1982).

4.6.4.3 Effect of shaking speed on adsorption of Zn (II) ions

The effect of varying shaking speed on the percentage removal of Zn (II) ions is presented in the graph shown in figure 4.32.

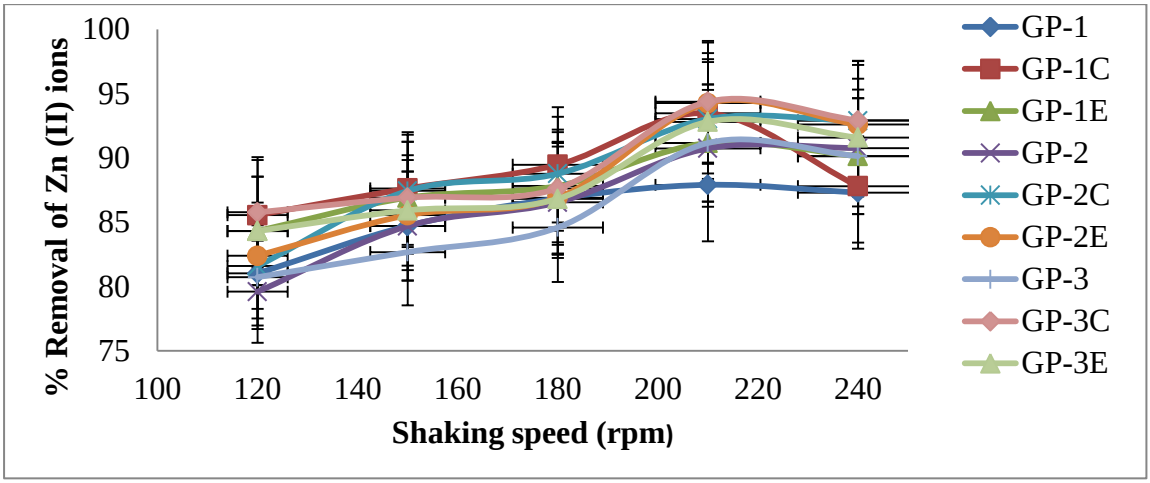

Figure.4.32: Effect of shaking speed on Zn (II) ions removal onto geopolymer materials (Contact time = 60 minutes, adsorbent dose = 0.1 g/50 mL, pH = 5.0, temperature = 25 $^{\circ}$C and error bars indicate the average deviation from the mean).

The percentage removal increased from 81.03 ± 0.05, 85.56 ± 0.12, 84.32 ± 0.04, 79.60 ± 0.01, 81.59 ± 0.08, 82.40 ± 0.29, 80.73 ± 0.23, 85.77 ± 0.06 and 84.32 % ± 0.04 to 87.91 ± 0.10, 93.48 ± 0.70, 91.16 ± 0.10, 90.77 ± 0.12, 93.03 ± 0.07, 94.26 ± 0.10, 91.16 ± 0.10, 94.37 ± 0.37 and 92.81 % ± 0.17 as construed in appendices 3J, 3K and 3L when shaking speed was varied from 120 to 210 rpm and then dropped to 87.31, 87.81, 90.14, 92.89, 92.59, 90.14, 92.92 and 91.59 % with further increase in shaking speed to 240 rpm for

adsorbents GP-1, GP-1C GP-1E, GP-2, GP-2C, GP-2E, GP-3, GP-3C and GP-3E respectively. Shaking speed increases the sorption process because it raises the chances of interaction between ions and geopolymers (Raza *et al*., 2015).

Decrease in adsorption after shaking speed of 210 rpm was observed for all geopolymers. This was due to increase in random collisions between particles (adsorbate- adsorbate, adsorbent-adsorbate, and adsorbent-adsorbent) hence enough time was not provided for heavy metal ions to bind with the surface of the adsorbent. The results follow a similar trend reported by Anwar *et al*. (2010) who observed that low speed accumulates the adsorbent at the bottom, instead of spreading it in the solution, which results in burial of various active sites under the layers of adsorbent. Since adsorption is a surface phenomenon, layers buried under do not play their role in metal uptake (Opeolu and Fatoki, 2016).

4.6.5 Effect of adsorbent dose on the adsorption process

Adsorbent dosage is another important parameter in adsorption processes because it determines the capacity of an adsorbent for a given initial concentration of the adsorbate under a given set of operating conditions (Ghassabzadeh *et al*., 2010). To achieve this, a series of batch experiments were conducted with the adsorbent dose of 0.1, 0.2, 0.3, 0.4, and 0.5 g per 50 mL of test solution.

4.6.5.1 Effect of adsorbent dose on adsorption of Pb (II) ions

The percentage removal and uptake level of Pb (II) ions from solutions by geopolymer adsorbents are shown in figure 4.33.

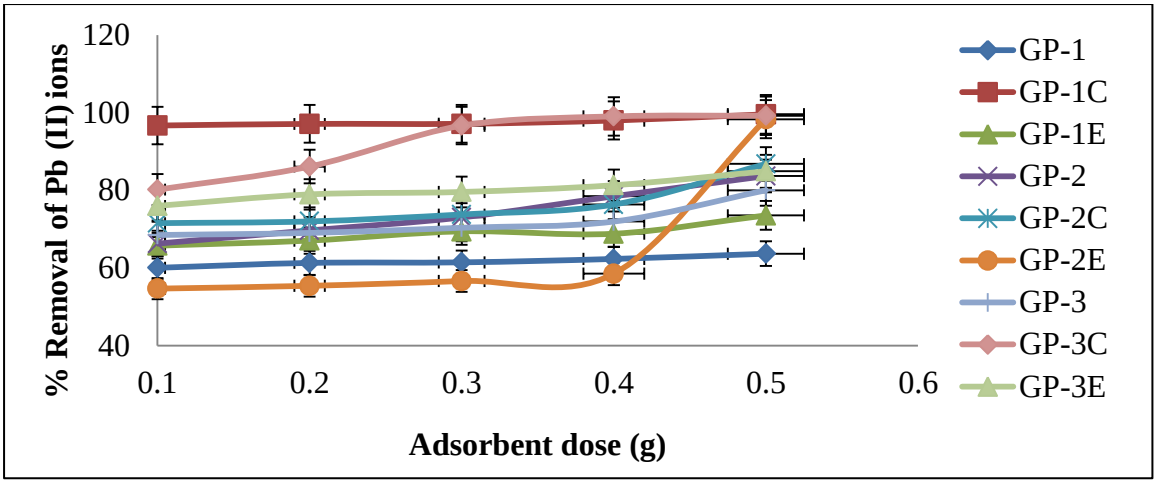

Figure.4.33: Effect of adsorbent dose on Pb (II) ions removal onto geopolymer materials (Contact time = 60 minutes, shaking speed of 120 rpm, pH = 4.0 and temperature = 25 °C).

It was observed that with a general increase in the adsorbent dose from 0.1 g - 0.5 g, there was a corresponding increase in uptake level. There was a slight increase in the mean percent removal from 60.05 ± 0.45, 97.15 ± 0.05, 65.75 ± 0.06, 66.28 ± 0.25, 71.56 ± 0.56, 54.69 ± 1.02, 68.50 ± 0.88, 80.19 ± 0.26 and 76.01 % ± 0.32 to 63.68 ± 1.07, 99.61 ± 0.40, 73.56 ± 0.31, 83.70 ± 0.26, 86.81 ± 0.17, 98.35 ± 0.07, 80.03 ± 0.39, 99.24 ± 0.01 and 84.91 % ± 0.16 for GP-1, GP-1C, GP-1E, GP-2, GP-2C, GP-2E, GP-3, GP-3C and GP-3E respectively. This was due to increase in the available binding sites in the adsorbent. The trend could be explained in terms of progressive increase in the electrostatic interaction between the adsorbent and metal ions (Rotimi and Okeoghene, 2014). Moreover, more adsorption sites were being covered as the dose of the adsorbent increased (Igwe and Abia, 2007).

Increasing adsorbent dosage provided greater surface area available for adsorption due to increased active sites on the geopolymers as demonstrated in appendices 1D, 1E and 1F. Similarly, increasing adsorption with adsorbent weight can be attributed to increased number of unsaturated active sites as well as high accessibility of metals to the binding

sites (Opeolu and Fatoki, 2016). Similar results have been reported in literature (Addour *et al*., 1999; Amir *et al*., 2005).

4.6.5.2 Effect of adsorbent dose on adsorption of Cd (II) ions

Figure 4.34 shows the effect of adsorbent dosage on the adsorption of Cd (II) ions.

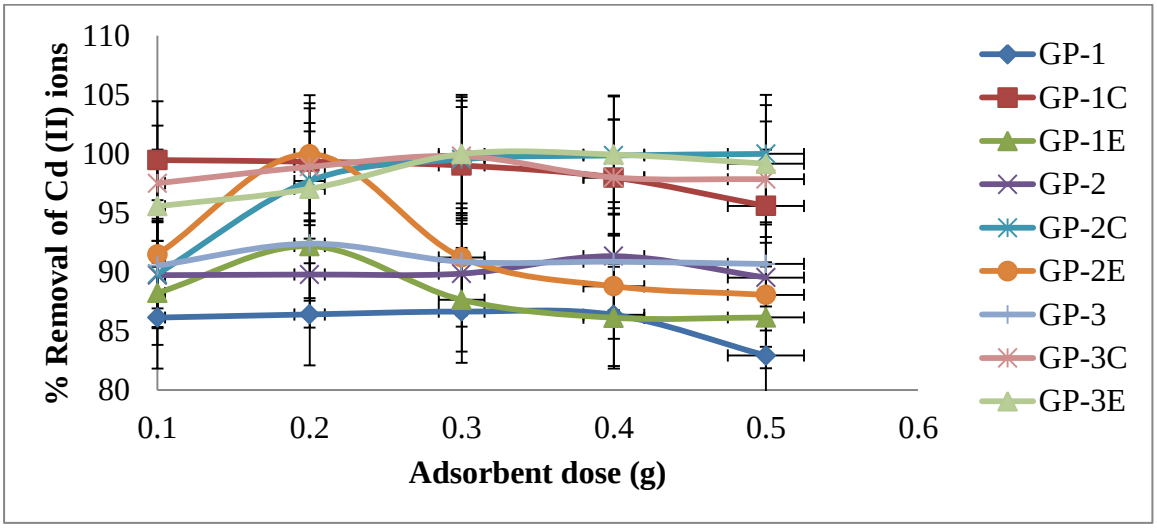

Figure.4.34: Effect of adsorbent dose on Cd (II) ions removal onto geopolymer materials (Contact time = 60 minutes, shaking speed of 120 rpm, pH = 5.0 and temperature = 25 °C).

The mean adsorption percentage increased with increasing sorbent dose from 86.14 ± 0.13, 88.23 ± 0.01, 89.73 ± 0.03, 89.83 ± 0.47, 91.49 ± 0.08, 90.54 ± 0.07, 97.51 ± 0.07 and 95.57 % ± 0.05 to an optimum uptake of 86.65 ± 0.09, 92.18 ± 0.03, 91.34 ± 0.07, 99.99 ± 0.06, 99.98 ± 0.01, 92.40 ± 0.06, 99.80 ± 0.00 and 99.98 % ± 0.01 for geopolymers 1, 1E, 2, 2C, 2E, 3, 3C and 3E respectively. The uptake then decreased as presented in the appendices 2D, 2E and 2F.

The increase in the adsorption percentage with increase in adsorbent dose was due to an increase in active sites on the adsorbent, thus facilitating the penetration of metal ions to the sorption sites. It is plausible that with higher dosage of adsorbent there would be

greater availability of exchangeable sites for metal ions (Babel and Kurniawan, 2004). According to Garg *et al*. (2003), decrease in percent removal after adsorption equilibrium could be attributed by the overlapping of the adsorption sites as a result of overcrowding of adsorbent particles. Moreover, the high adsorbent dosage could impose a screening effect of the dense outer layer of the cells, thereby shielding the binding sites from metal ions (Pons and Fusté, 1993). This trend is similar to one observed by Sari *et al*. (2007).

4.6.5.3 Effect of adsorbent dose on adsorption of Zn (II) ions

The effect of varying adsorbent dose on the percentage removal of Zn (II) ions is presented in figure 4.35.

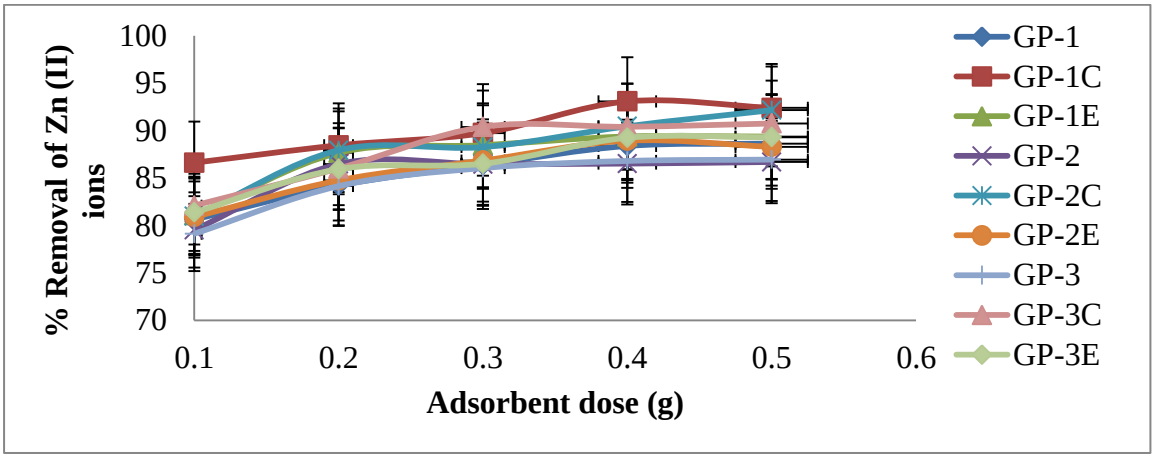

Figure.4.35: Effect of adsorbent dose on Zn (II) ions removal onto geopolymer materials (Contact time = 60 minutes, shaking speed of 120 rpm, pH = 5.0 and temperature = 25 °C).

The mean percentage removal increased from 80.63 ± 0.18, 79.52 ± 0.04, 80.98 ± 0.04, 79.13 ± 0.07, 82.10 ± 0.05 and 81.37 % ± 0.15 to 88.63 ± 0.14, 86.69 ± 0.01, 92.16 ± 0.16, 86.95 ± 0.05, 90.75 ± 0.05 and 89.30 % ± 0.06 as adsorbent dose was varied from 0.1 to 0.5 g for adsorbents GP-1, GP-2, GP-2C, GP-3, GP-3C and GP-3E respectively as shown in the appendices 3D, 3E and 3F. The increase in adsorption may be due to more surfaces and functional groups being available on the adsorbent. In adsorption using GP-

1C, GP-1E and GP-2E, the percentage removal increased from 86.62 ± 0.12, 81.08 ± 0.03 and 80.89 ± 0.16 to 93.09 ± 0.52, 89.38 ± 0.12 and 88.94 % ± 0.06 on varying adsorbent dose from 0.1 to 0.4 g then dropped slightly to 92.40 ± 0.62, 89.37 ± 0.15 and 88.29 % ± 0.06 when the dose was increased to 0.5 g respectively.

These results show that optimal removal was attained at adsorbent dose of 0.4 g and thereafter the metal uptake decreased. This may be attributed to the overlapping of the adsorption sites as a result of overcrowding adsorbent particles (Rajesh *et al*., 2010). Another consequence may be the reduction of active sites at the surface of the adsorbents and also the rate of transfer of Zn (II) at the surface of the adsorbents, meaning that the quantity adsorbed per unit mass of adsorbent has its limit with the adsorbent dosage (Murithi *et al.*, 2014).

4.6.6 Effect of temperature on the adsorption process

Temperature is a crucial parameter in adsorption reactions. Higher temperature increases adsorbate motion allowing the uptake of metal ions into the pores, causing adsorption to increase. Temperature also affects the adsorption rate by altering the molecular interaction and the solubility of the adsorbate (Singh *et al*., 2001). Adsorption studies were carried out at varying temperatures (293 to 328 K) and the results presented as % removal of the metal ions versus temperature as illustrated in figures 4.36, 4.37 and 4.38.

4.6.6.1 Effect of temperature on adsorption of Pb (II) ions

Figure 4.36 shows the effect of percentage removal of Pb (II) against temperature.

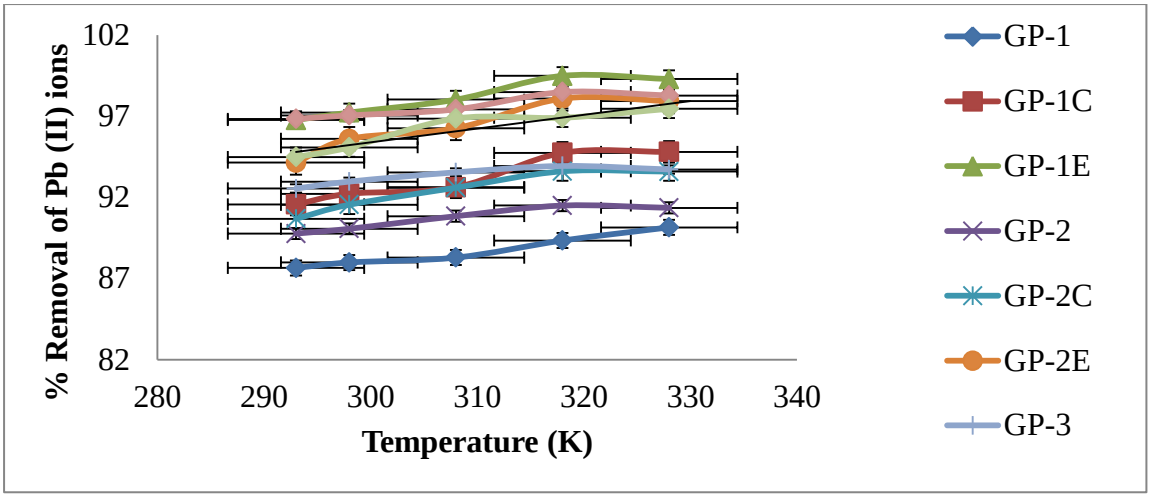

Figure.4.36: Effect of temperature on Pb (II) ions removal onto geopolymer materials (Contact time = 60 minutes, shaking speed of 120 rpm, pH = 4.0 and adsorbent dose = 0.1g/50mL).

The percentage removal increased from 87.65 ± 0.30, 91.57 ± 0.19 and 94.49 % ± 0.09 to 90.15 ± 0.11, 94.81 ± 0.21 and 97.46 % ± 0.10 when the temperature was varied from 293 to 328 K for adsorbents GP-1, GP-1C and GP-3E respectively. The mean percentage removal increased from 96.76 ± 0.24, 89.77 ± 0.11, 90.68 ± 0.06, 94.14 ± 0.20, 92.55 ± 0.08 and 96.84 % ± 0.11 to 99.49 ± 0.02, 91.5 ± 0.02, 93.61 ± 0.02, 98.09 ± 0.02, 93.94 ± 0.05 and 98.49 % ± 0.01 when the temperature was adjusted from 293 to 318 K and then dropped to 99.29, 91.35, 93.59, 97.94, 93.72 and 98.28 % for adsorbents GP-1E GP-2, GP-2C, GP-2E, GP-3 and GP-3C respectively as shown in appendices 1Q, 1R and 1S. According to Nassar and Magdy (1997), increase in adsorption at equilibrium with increase in temperature is due to the acceleration of some originally slow adsorption steps or to the creation of some active sites on the adsorbent surface. Adsorption with ion exchange is an endothermic reaction, whereas adsorption with nonionic exchange is an exothermic reaction (Cheng *et al*., 2012).

Therefore, increasing temperature increased the sorption rate suggesting that Pb (II) ions and Na ions underwent an ionic exchange to achieve heavy metal removal by the

geopolymer. At temperature above 318 K, the thickness of the boundary layer decreased due to the increased tendency of the metal ions to escape from most of the geopolymers surface to the bulk of solution. This leads to decrease in adsorption as temperature increases (Aksu and Kutsal, 1991). Al-Zboon *et al*. (2011) studied the effects of temperature on the adsorption of Pb (II) ions from aqueous solution by fly ash-based geopolymer, which showed a similar pattern.

4.6.6.2 Effect of temperature on the adsorption of Cd (II) ions

Figure 4.37 represents the change in extent of adsorption of Cd (II) ions with respect to temperature.

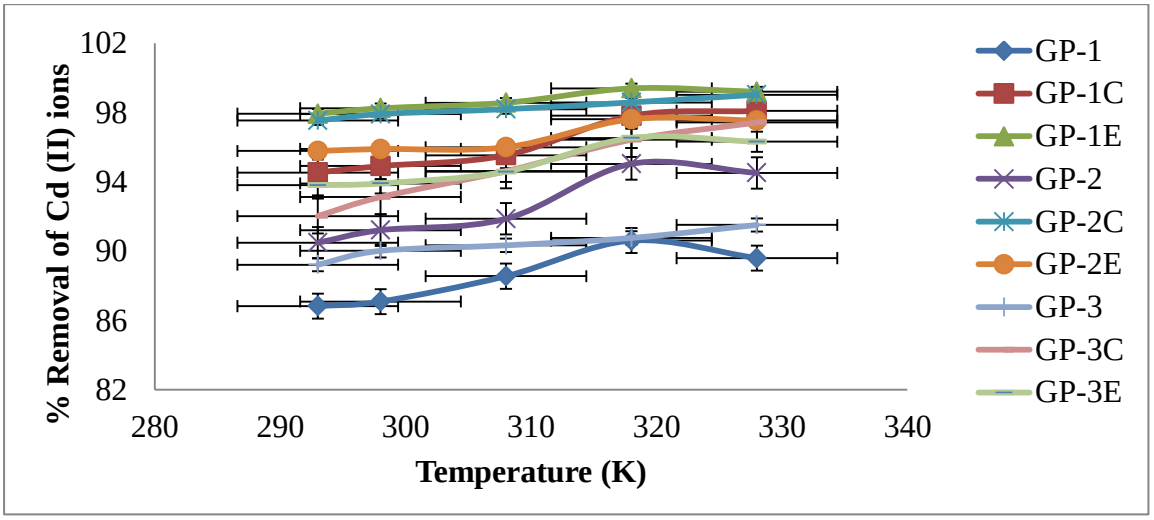

Figure.4.37: Effect of temperature on Cd (II) ions removal onto geopolymer materials (Contact time = 60 minutes, shaking speed of 120 rpm, pH = 5.0 and adsorbent dose = 0.1g/50mL).

The mean percent removal increased from 89.22 ± 0.19, 94.54 ± 0.14, 97.54 ± 0.08, and 92.03 % ± 0.06 to 91.52 ± 0.48, 98.10 ± 0.03, 99.03 ± 0.04, and 97.43 % ± 0.11 when temperature was adjusted from 293 to 328 K for adsorbents GP-2, GP-1C, GP-2C, and GP-3C respectively. The retention of metal ions increased with increasing temperature, which may be attributed to the activation of geopolymer at increased temperatures

(Vengris *et al*., 2001). This suggests monolayer coverage of the surface of geopolymers by the metal ions which may be followed by r extra layers of molecules which may be physically adsorbed (Martins *et al*., 2010).

For adsorbents GP-1, GP-1E, GP-2E, GP-3 and GP-3E, the metal uptake rate increased from 86.83 ± 0.11, 97.94 ± 0.14 , 95.78 ± 0.15, 90.49 ± 0.03 and 93.81 % ± 0.18 to 90.61 ± 0.07, 99.40 ± 0.03, 97.62 ± 0.04, 95.04 ± 0.02and 96.54 % ± 0.08 when temperature was varied from 293 to 318 K and then decreased to 89.60, 99.21, 97.55, 94.52, and 96.32 % as construed in appendices 2P, 2Q and 2R, when temperature was raised to 328 K respectively. Similar trends were also observed by other researchers for aqueous phase adsorption (Bhattacharya *et al*., 2008; Mahmoud *et al*., 2013).

4.6.6.3 Effect of temperature on the adsorption of Zn (II) ions

The effect of varying temperature on the percentage removal of Zn (II) ions is presented in a graph as shown in figure 4.38 and statistical data is presented in appendices 3P, 3Q and 3R.

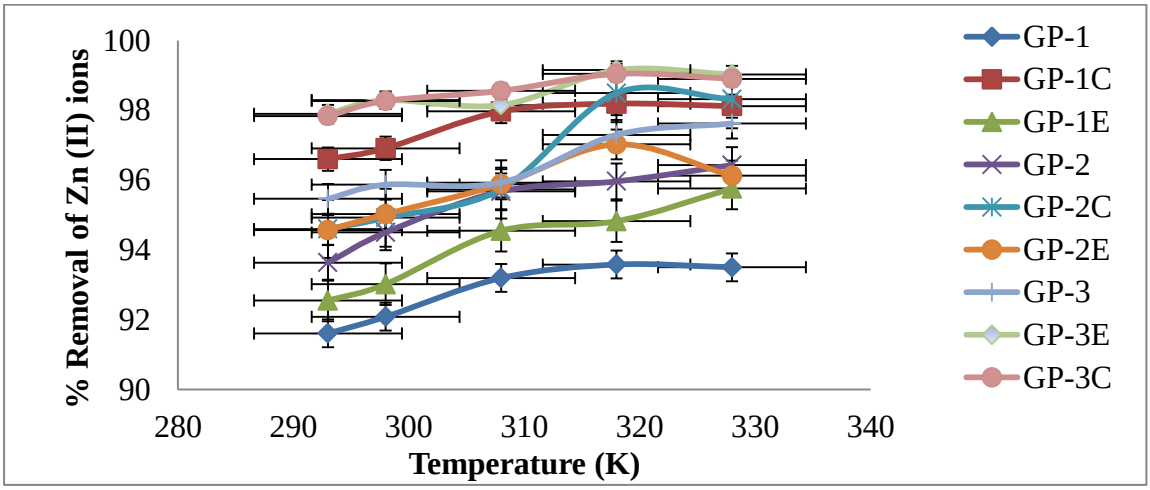

Figure.4.38: Effect of temperature on Zn (II) ions removal onto geopolymer materials (Contact time = 60 minutes, shaking speed of 120 rpm, pH = 5.0 and adsorbent dose = 0.1g/50mL).

The percentage removal increased from 92.56 ± 0.09, 93.64 ± 0.06 and 95.46 % ± 0.10 to 95.76 ± 0.13, 96.43 ± 0.20 and 97.62 % ± 0.03 when the temperature was varied from 293 to 328 K for geopolymers GP-1E, GP-2 and GP-3 respectively. For geopolymer adsorbent GP-1, GP-1C, GP-2C, GP-2E, GP-3C and GP-3E, the metal uptake increased from 91.61 ± 0.02, 96.60 ± 0.10, 94.60 ± 0.03, 94.57 ± 0.22, 97.84 ± 0.23 and 97.90 % ± 0.05 to 93.58 ± 0.10, 98.19 ± 0.02, 98.49 ± 0.01, 97.02 ± 0.06, 99.04 ± 0.07 and 99.15 % ± 0.06 when the temperature was changed from 293 to 318 K and then reduced to 93.50 ± 0.06, 98.12 ± 0.02, 98.32 ± 0.01, 96.13 ± 0.11, 98.90 ± 0.04 and 99.03 % ± 0.04 when the temperature was adjusted to 328 K respectively.

The increase in the adsorption uptake of metal ions with temperature may be attributed to either change in pore size of the adsorbent, improving intraparticle diffusion within the pores or enhancement in the chemical affinity of Zn (II) ions on the surface of the adsorbent. The decrease in percentage of adsorption at temperatures higher than 318 K may be due to desorption caused by an increase of the thermal energy that may induce higher mobility of the adsorbate causing desorption (Baral *et al*.,2006).

4.7 Column adsorption studies of Pb (II), Cd (II) and Zn (II) ions

In order to improve the adsorption processes with conditions closer to a real life water treatment system, continuous processes are adopted. A packed column bed is considered as an effective process for continuous wastewater treatment for a number of reasons; it makes the best use of the concentration difference known to be a driving force for heavy metal adsorption; it allows more effective utilization of adsorption capacity, and results in better quality of effluent (Thilagan *et al*., 2015).

4.7.1 Column adsorption studies of Pb (II) onto geopolymers

From figure 4.39 percentage Pb (II) ion uptake increased on functionalization from 80.54 ± 0.94 to 85.02 ± 0.76 and 84.26 % ± 0.34 for GP-1C and GP-1E respectively.

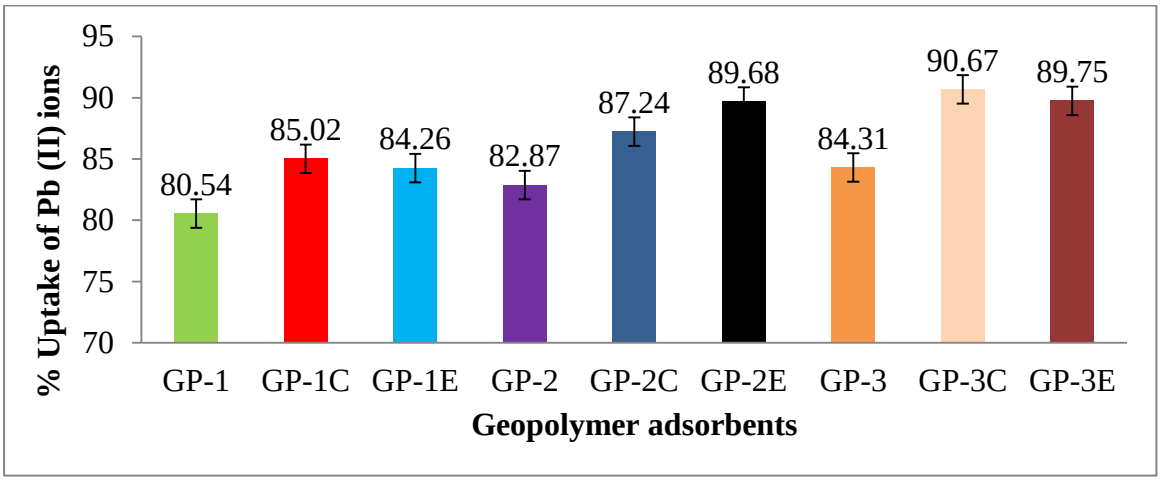

Figure.4.39: Effect of gravitational column adsorption of Pb (II) ions onto geopolymer materials (Volume of effluent = 50 mL, pH = 4.0 and adsorbent dose = 0.50g).

For GP–2, the mean percentage removal increased from 82.87 ± 0.26 to 87.24 ± 0.30 and 89.68 % ± 0.95 upon functionalization using citric acid and EDTA respectively. The mean uptake increased from 84.31 ± 0.74 to 90.67 ± 0.41 and 89.75 % ± 0.13 when GP-3 was tethered with citric acid and EDTA respectively. There was no significant difference in metal ion removal for citric acid and EDTA functionalized geopolymers of GP-1 and GP-3 but there was significant difference in Pb (II) ions removal between GP-2C and GP-2E as demonstrated by statistical data presented in appendix 6A. Improved Pb (II) uptake upon functionalization of the geopolymers could be attributed to the fact that new functional groups such as -OH were anchored on the surface of geopolymers. Percentage removal of Pb (II) increased with change of adsorbent from GP-1 to GP-3. Increase in SiO_2/Al_2O_3 ratio from GP-1 to GP-3 increased electrostatic attraction between the positively charged sorbate ions and the adsorbent.

4.7.2 Column adsorption of Cd (II) onto geopolymers

Figure 4.40 presents the results of gravitational column adsorption of Cd (II).

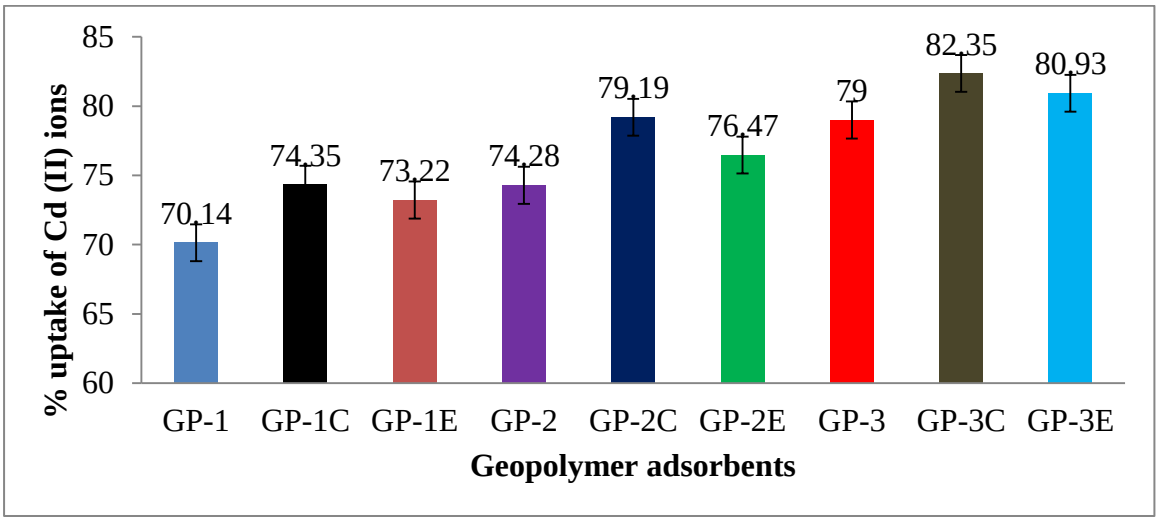

Figure.4.40: Effect of gravitational column adsorption of Cd (II) ions onto geopolymer materials (Volume of effluent= 50 mL, pH = 5.0 and adsorbent dose = 0.50g).

Percentage Cd (II) ions uptake increased from 70.14 ± 0.49 to 74.35 ± 0.25 and 73.22 % ± 0.38 upon functionalization of GP-1 with citric acid and EDTA respectively. Percentage removal changed from 74.28 ± 0.60 to 79.19 ± 0.60 and 76.47 % ± 0.11 for GP-2 to GP-2C and GP-2E respectively. With the use of GP–3, the mean percentage removal increased from 79.00 ± 0.64 to 82.35 ± 0.24 and 80.93 % ± 0.13 upon functionalization using citric acid and EDTA respectively. There was a significant difference in Cd (II) ion removal using all citric acid and EDTA functionalized geopolymers as shown by the statistical data presented in appendix 6B. Improved Cd (II) ion removal upon functionalization of the geopolymers could be attributed to the fact that new active sites such as -OH and $–COO^-$ are tethered on the surface of geopolymers. Percentage removal of Cd (II) ions increased with increase in Si: Al ratio from GP-1 to GP-3 due to similar reasons as explained in adsorption of Pb (II) ions.

4.7.3 Column adsorption of Zn (II) onto geopolymers

Figure 4.41 shows the percentage removal of Zn (II) ions from synthetic wastewaters using geopolymer adsorbents.

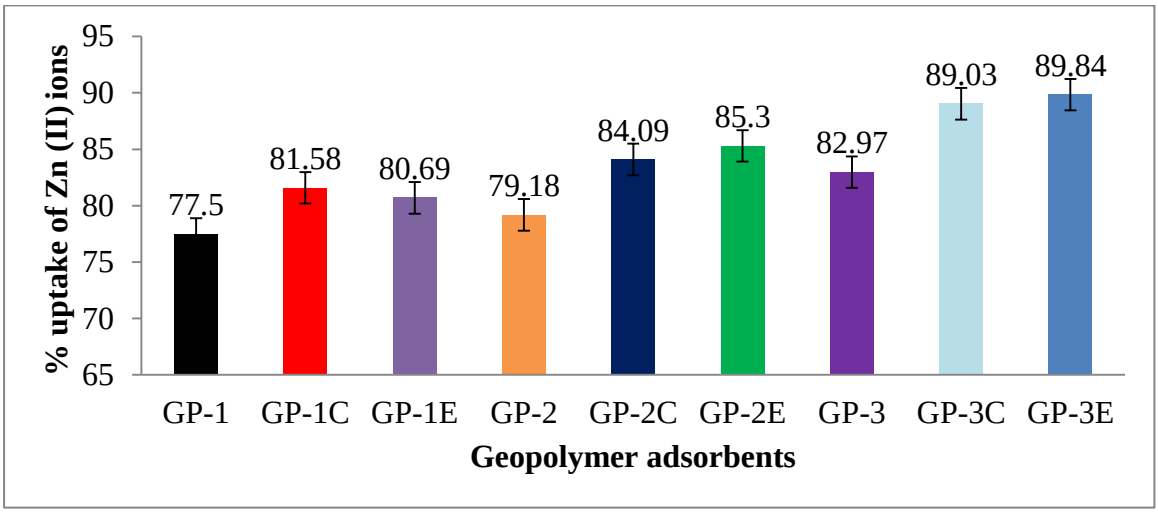

Figure.4.41: Effect of gravitational column adsorption of Zn (II) ions onto geopolymer materials (Volume of effluent= 50 mL, pH = 5.0 and adsorbent dose = 0.50g).

The uptake increased from 77.50 ± 0.16 to 81.58 % ± 0.14 when GP-1 was anchored with citric acid and 80.69 % ± 0.27 with EDTA respectively. There was significant difference in metal ion uptake upon functionalization as indicated in appendix 6C. The mean percentage removal of Zn (II) using GP-2 and GP-3 increased from 79.18 ± 0.78 and 82.97 ± 0.26 to 84.09 ± 0.28 and 89.03 % ± 0.56 when tethered with citric acid and to 85.30 ± 0.38 and 89.84 % ± 0.38 when functionalized with EDTA as shown in appendix 6C. The column studies registered lower metal ion uptake in comparison with the batch mode. This difference could be explained by the fact that equilibrium between the solution phase metals and adsorbed phase metals had not been reached in the column study (Sounthararajah *et al*., 2015). However, the column study is closer to the real full-scale treatment system and consequently the results from this study are more applicable to real practical conditions (Sounthararajah *et al*., 2015).

4.8 Equilibrium studies using adsorption isotherms

This study employed Langmuir, Freundlich and Langmuir Freundlich and Temkin isotherms in fitting of experimental data obtained when initial metal ion concentrations were varied from 20 - 500 mg/L. The Langmuir isotherm (Langmuir, 1916) assumes a monolayer adsorption in which adsorbates are adsorbed to a finite number of definite localized sites that are identical and equivalent with no lateral interaction (Foo and Hameed, 2010). The Freundlich model applies multilayer adsorption over the heterogeneous surface (Foo and Hameed, 2010). The Langmuir Freundlich isotherm, also known as Sip's model, is a versatile isotherm expression that simulate both Langmuir and Freundlich behaviors (Sips, 1948; Nahm *et al*., 1977). Equilibrium constants obtained from this study on adsorption of Pb (II), Cd (II) and Zn (II) are as shown in tables 4.3, 4.4 and 4.5 respectively.

4.8.1 Adsorption isotherms of Pb (II) ions

The adsorption data for Pb (II) ions on the adsorbents were fitted onto Langmuir, Freundlich, and Sips isotherms and their equilibrium constants are presented in tables 4.3. The adsorption data for all the adsorbents best fitted into the modified Langmuir Freundlich isotherm.

Table 4.3: Isotherm model constants and correlation coefficients for adsorption of Pb (II) ions on geopolymers

Freundlich				Langmuir			Langmuir Freundlich			
Sorbent	1/n	K_F (mg/g)	R^2	K_L L/mg	Q_{max} (mg/g)	R^2	Q_{max} (mg/g)	K_{LF}	1/n	R^2
GP-1	1.33	0.76	0.995	-1.00	0.006	0.423	27.0	$1.0x10^{1}$	0.72	0.996
GP-1C	1.48	0.33	0.992	-3.35	0.005	0.764	50.61	$1.0x10^{-3}$	0.64	0.995
GP-1E	1.54	0.07	0.967	-4.46	0.007	0.512	60.71	$1.3x10^{-5}$	0.61	0.997
GP-2	1.33	0.75	0.983	-0.99	0.007	0.522	57.96	$1.5x10^{-4}$	0.68	0.999
GP-2C	2.30	0.08	0.839	-7.48	0.008	0.605	58.97	$1.0x10^{-1}$	0.44	0.920
GP-2E	1.55	0.06	0.978	-3.94	0.006	0.654	79.58	$1.7x10^{-5}$	0.62	0.997
GP-3	1.44	0.41	0.962	-2.68	0.006	0.610	209.9	5.85	0.62	0.982
GP-3C	1.69	0.27	0.915	-3.15	0.007	0.682	221.1	$1.1x10^{-5}$	0.50	0.964
GP-3E	1.67	0.05	0.983	-3.55	0.007	0.745	326.5	$2.3x10^{-5}$	0.58	0.985

C and E- Geopolymer functionalized with citric acid and EDTA respectively, 1/n = heterogeneity index, K_F =Freundlich constant, R^2= correlation coefficient, Q_{max}= adsorption capacity, K_L = Langmuir constant and K_{LF}= Modified Langmuir –Freundlich constant.

The variables estimation was done using the Microsoft excel solver with a non-negativity constraint restriction for K_{LF} values. Isotherm fitting's R^2 values of 0.996, 0.995, 0.997 0.999, 0.920, 0.997, 0.982, 0.964 and 0.985 for GP-1, GP- 1C, GP-1E, GP-2, GP-2C, GP-2E, GP-3, GP-3C and GP-3E were obtained respectively. These results show that the modified Langmuir Freundlich isotherm was best suited to describe metal ion dependent adsorption effects. Consequently, it implies that cooperative adsorption occurred between the heterogeneous surface and homogenous surface of the adsorbent. The index of heterogeneity, 1/n were 0.72, 0.64, 0.61, 0.68, 0.44, 0.62, 0.62, 0.50 and 0.58 for GP-1, GP- 1C, GP-1E, GP-2, GP-2C, GP-2E, GP-3, GP-3C and GP-3E respectively.

These values decreased with functionalization and we can infer that the process increases the favourability of adsorption of Pb (II) ions. According to Rushton *et al*. (2005),

approach of heterogeneity index to unity indicates change of adsorbent surface to homogenous and when the index decreases approaching zero, it indicates change of surface to heterogeneous. The values obtained in this study show functionalization of geopolymers favoured change of surface to heterogeneous. Increase in Si/Al ratio caused by use of different clays increased the isomorphous replacement of Si^{4+} by Al^{3+} hence producing more negative charges in the geopolymer lattice (Shaheen *et al*., 2012). The negative charges are balanced by Na^{+} which is exchangeable with heavy metal ions increasing adsorption capacities (Erdem *et al*., 2004). Adsorption capacities obtained using Sips isotherms are recorded in table 4.3. Günay *et al*. (2007) also stated that three-parameter isotherm models resulted in better performance than two-parameter models.

4.8.2 Adsorption isotherms of Cd (II) ions

Equilibrium constants obtained are presented in table 4.4.

Table 4.4: Isotherm model constants and correlation coefficients on adsorption of Cd (II) ions on geopolymers

Freundlich				**Langmuir**			**Langmuir Freundlich**			
		K_F		K_L						
sorbent	1/n	mg/g	R^2	L/mg	Q_{max}	R^2	Q_{max}	K_{LF}	1/n	R^2
GP-1	1.25	0.14	0.982	-3.80	0.003	0.927	6.04	0.63	0.79	0.984
GP-1C	1.59	0.03	0.976	-5.97	0.005	0.828	24.2	0.009	0.69	0.993
GP-1E	1.32	0.13	0.967	-4.11	0.006	0.368	51.4	$2.5x10^{-5}$	0.64	0.998
GP-2	1.15	0.34	0.728	-22.02	0.017	0.108	45.2	0.111	0.67	0.939
GP-2C	2.36	0.001	0.919	-6.91	0.005	0.841	91.5	$4.5x10^{-4}$	0.57	0.991
GP-2E	1.31	0.13	0.994	-3.37	0.004	0.662	160.5	$1.1x10^{-4}$	0.72	0.997
GP-3	1.29	0.14	0.939	-3.52	0.004	0.776	136.2	$2.1x10^{-2}$	0.96	0.989
GP-3C	2.55	0.004	0.890	-8.09	0.006	0.731	162.6	$4.6x10^{-5}$	0.46	0.971
GP-3E	1.44	0.063	0.930	-4.72	0.004	0.781	175.5	$1.7x10^{-3}$	0.69	0.987

C and E- Geopolymer functionalized with citric acid and EDTA respectively, 1/n = heterogeneity index, K_F =Freundlich constant, R^2= correlation coefficient, Q_{max}= adsorption capacity, K_L = Langmuir constant and K_{LF}= Modified Langmuir –Freundlich constant.

The R^2 show that the data fitted best in modified Langmuir Freundlich isotherm (Sips) for all adsorbents. The R^2 values were 0.984, 0.993, 0.998, 0.939, 0.991, 0.997, 0.989, 0.971 and 0.987 for adsorbents GP-1, GP-1C, GP-1E, GP-2, GP-2C, GP-2E, GP-3, GP-3C and GP-3E respectively showing a good data fit. These adsorption capacities obtained were, 6.04, 24.2, 51.4, 45.2, 91.5, 160.5, 136.2, 162.6 and 175.5 mg/g for GP-1, GP-1C, GP-1E, GP-2, GP-2C, GP-2E, GP-3, GP-3C and GP-3E respectively. The adsorption capacities increased with functionalization. Since the value of 1/n obtained in Freundlich isotherm was greater than 1, then the adsorption coefficient increased with increasing concentration of the solution leading to an increase in hydrophobic surface characteristics after monolapisan (Ghazi *et al*., 2013).

4.8.3 Adsorption isotherms of Zn (II) ions

Table 4.5 shows the equilibrium constants for adsorption of Zn (II) ions.

Table 4.5: Isotherm model constants and correlation coefficients on adsorption of Zn (II) ions on geopolymers

Freundlich				**Langmuir**			**Langmuir Freundlich**			
		K_F		K_L						
sorbent	1/n	mg/g	R^2	L/mg	Q_{max}	R^2	Q_{max}	K_{LF}	1/n	R^2
GP-1	13.4	7.78	0.917	0.18	0.35	0.497	10.1	$7.6x10^{-2}$	0.16	0.970
GP-1C	1.49	1.67	0.823	-1.75	-0.04	0.789	14.8	$1.9x10^{-3}$	0.42	0.824
GP-1E	5.15	2.76	0.887	-0.80	-0.15	0.525	21.1	$1.1x10^{-1}$	5.15	0.938
GP-2	7.22	5.14	0.695	-0.36	-0.30	0.724	64.7	$6.0x10^{-2}$	0.12	0.936
GP-2C	1.24	0.32	0.915	-6.67	-0.01	0.775	62.1	$4.6x10^{-3}$	0.64	0.935
GP-2E	3.37	0.93	0.973	-2.92	-0.45	0.636	175.3	$1.8x10^{-1}$	0.40	0.980
GP-3	7.70	4.33	0.309	-0.45	-0.25	0.730	72.4	$1.4x10^{-1}$	0.13	0.823
GP-3C	1.92	0.45	0.979	-0.613	-0.02	0.820	130	$3.3x10^{-2}$	0.52	0.983
GP-3E	1.90	0.40	0.948	-6.77	-0.02	0.658	169.9	$1.5x10^{-2}$	0.51	0.964

C and E- Geopolymer functionalized with citric acid and EDTA respectively, 1/n = heterogeneity index, K_F =Freundlich constant, R^2= correlation coefficient, Q_{max}= adsorption capacity, K_L = Langmuir constant and K_{LF}= Modified Langmuir –Freundlich constant.

From these data, it is evident that the experimental data fitted best in modified Langmuir Freundlich isotherm (Sips) for most of the adsorbents. The R^2 values for GP-1, GP-1C, GP-1E, GP-2, GP-2C, GP-2E, GP-3, GP-3C and GP-3E were 0.970, 0.824, 0.938, 0.936, 0.935, 0.980, 0.823, 0.983 and 0.964 respectively and their adsorption capacities 10.1, 14.8, 21.1, 64.7, 62.1, 175.5, 72.4, 130, and 169.9 mg/g respectively. Increase in adsorption capacities was observed to increase with Si/Al ratio and subsequent functionalization.

4.8.4 Equilibrium studies of Zn (II), Pb (II) and Cd (II) using Temkin adsorption isotherm

The Temkin adsorption isotherm model was chosen to evaluate the adsorption potentials of the adsorbent for adsorbate (Shahmohammadi-Kalalagh and Babazadeh, 2014). The isotherm parameters are given in table 4.6.

Table 4.6: Temkin adsorption isotherm constants of Pb (II), Cd (II) and Zn (II) onto geopolymers

	Pb (II)			Cd (II)			Zn (II)		
Geopolymer	B_T	A_T	R^2	B_T	A_T	R^2	B_T	A_T	R^2
GP-1	33.24	9.91	0.773	23.11	3.30	0.889	2.89	11.08	0.900
GP-1C	30.13	3.03	0.789	30.02	1.69	0.809	10.00	3.77	0.445
GP-1E	32.97	2.68	0.714	27.06	3.21	0.715	4.29	4.86	0.759
GP-2	38.72	8.85	0.764	23.52	5.46	0.703	2.85	6.91	0.811
GP-2C	55.44	1.93	0.619	52.41	4.85	0.618	11.57	1.49	0.638
GP-2E	32.67	2.65	0.761	25.56	3.43	0.786	6.20	2.64	0.853
GP-3	31.79	3.99	0.751	24.61	3.48	0.834	2.65	5.72	0.634
GP-3C	39.90	2.62	0.729	60.03	8.07	0.561	8.14	1.75	0.803
GP-3E	37.32	2.63	0.783	27.54	2.38	0.809	8.19	1.51	0.802

C and E- geopolymer functionalized with citric acid and EDTA respectively, A_T = Temkin equilibrium binding constant (L/g), $B_{T=}$ Temkin constant related to heat of adsorption (J/mole) and R^2= correlation coefficient.

The B_T values obtained for adsorption of Zn (II), Pb (II) and Cd (II) ions with the heat of sorption indicating a physical adsorption process (Dada *et al*., 2012), did not show a specific trend with increase in Si/Al ratio and also upon functionalization. This is an indication that increases in Si/Al ratio and functionalization did not have verifiable effects on heat of adsorption. B_T values calculated were 33.24, 38.72 and 31.79 J/mole when using GP-1, GP-2 and GP-3 for adsorption of Pb (II). The increasing values indicated a strong interaction between the adsorbate and the adsorbent (Abechi *et al*., 2013).

Temkin values for cadmium sorption showed an increase in B_T values. These values are 23.11, 23.52 and 24.61 for GP-1, GP-2 and GP-3 representing an increase in Si/Al ratio (Table 4.6). The heat of adsorption of Cd (II) ions was directly related to coverage of the ions onto geopolymers due to adsorbent-adsorbate interaction (Erhayem *et al*., 2015). For adsorption of Zn (II) the values decreased with increase in Si/Al ratio in geopolymers. GP-1 recorded B_T value of 2.89; GP-2 gave a value of 2.85 while GP-3 obtained 2.65 J/mole. According to Erhayem *et al*. (2015), decreased heat of adsorption of Cd (II) ions onto the surface of geopolymers implies the sorption process was exothermic. The correlation coefficients of Temkin obtained were lower than those of Langmuir, Freundlich and Langmuir Freundlich. By comparing the correlation coefficients (R^2) obtained from the four isotherms plots (Table 4.3, 4.4, 4.5 and 4.6), it can be concluded that Sips (Langmuir Freundlich) model can be applied successfully to Cd (II) and Zn (II) and Pb (II) ions.

4.9 Thermodynamic studies of Zn (II), Pb (II) and Cd (II) ions

In an environment, the concept of energy and entropy must be calculated for the occurrence of spontaneity of an adsorption reaction (Chand and Pakade, 2013). Analysis

of thermodynamics of equilibrium adsorption data can give more important information on the adsorption process (Ghomri *et al*., 2013). The thermodynamic parameters standard free energy (ΔG°), enthalpy change (ΔH°), and entropy change (ΔS°) were estimated to evaluate the feasibility and exothermic nature of the adsorption process. Thermodynamic studies of Pb (II), Cd (II) and Zn (II) were done when varying the adsorption temperatures from 293 – 328 K. Tables 4.7, 4.8 and 4.9 present thermodynamic parameters ΔG°, ΔH° and ΔS° for the adsorption processes.

4.9.1 Thermodynamic studies of Pb (II) ions onto geopolymers

The ΔH°, ΔG and ΔS° values obtained by plotting ln K_c versus 1/T are presented in table 4.7.

Table 4.7: Thermodynamic parameters on adsorption of Pb (II) ions computed from the linearized plot of ln K_c versus 1/T and n=3.

			ΔG°(kJ/mol)			
	ΔH°	ΔS°	293K	298K	308K	318K
GP	kJ/mol)	(J/mol/K)	Mean±SD	Mean±SD	Mean±SD	Mean±SD
1	2.49	15.51	-4.78 ± 0.07^{d}	-4.93 ± 0.02^{c}	-5.17 ± 0.02^{b}	-5.62 ±0.01^{a}
1C	5.63	27.76	-5.81 ± 0.06^{d}	-6.13 ± 0.01^{c}	-6.48 ± 0.03^{b}	-7.65 ± 0.01^{a}
1E	18.67	75.75	-8.28 ± 0.16^{d}	-8.82 ± 0.04^{c}	-10.00 ±0.08^{b}	-13.95 ±0.11^{a}
2	2.08	14.99	-5.29 ± 0.03^{c}	-5.46 ± 0.02^{c}	-5.88 ± 0.15^{b}	-6.282 ±0.01^{a}
2C	4.24	22.81	-5.54 ± 0.02^{d}	-5.90 ± 0.00^{c}	-6.47 ±0.031^{b}	-7.10 ± 0.01^{a}
2E	11.57	49.70	-6.77 ± 0.09^{d}	-7.63 ± 0.00^{c}	-8.32 ± 0.17^{b}	-10.42 ±0.03^{a}
3	1.99	15.99	-6.14 ± 0.03^{d}	-6.40 ± 0.04^{c}	-6.85 ± 0.03^{b}	-7.25 ± 0.02^{a}
3C	7.46	37.75	-8.34 ± 0.09^{d}	-8.66 ± 0.10^{c}	-9.31 ± 0.01^{b}	-11.05 ±0.02^{a}
3E	8.02	37.78	-6.92 ± 0.04^{d}	-7.34 ± 0.01^{c}	-8.78 ± 0.05^{b}	-9.11 ± 0.06^{a}

Mean in a row without a common superscript letter differ ($P < 0.05$), as analyzed by one-way ANOVA, SD= standard deviation, GP= geopolymer, ΔH° = standard enthalpy change, ΔS° = standard entropy change, n= no of replicates and ΔG°= standard free energy change.

From the table 4.7, decrease in the value of ΔG° with increase in temperature shows that the reaction was more spontaneous, which indicates that adsorption was favoured by increase in temperature (Mustafa *et al*., 2008). All ΔG° values calculated were between 0 and -20 kJ/mole corresponding to spontaneous physisorption (Mahmoud *et al*., 2013). The positive values of ΔH° obtained indicated the endothermic nature of adsorption and governs the possibility of physical adsorption (Ghosh and Bhattacharyya, 2002). The low ΔH° values also depict that the metal ion was physisorbed onto the adsorbent (Gong *et al*., 2005; Bueno *et al*., 2008). The negative values of ΔG° (Table 4.7) stipulate that the adsorption was highly favourable for Pb (II) ions.

Additionally, the positive values of ΔS° confirmed the increased randomness at the solid-solute interface during the adsorption process, which shows the solution system tends towards stability when the adsorption of Pb (II) ions on the surface of adsorbent occurs according to the second law of thermodynamics (Liu *et al*., 2012). The result on ΔH° shows that functionalization increased the endothermic nature of adsorption. More heat was required to bind the metal ions on the surface of adsorbent. This indicated that adsorption increased with increase in temperature after functionalization.

4.9.2 Thermodynamic studies of Cd (II) onto geopolymers

Table 4.8 shows the thermodynamic parameters of Cd (II) adsorption on the geopolymers at different temperatures. The ΔG° obtained was negative for all temperatures studied. This indicates spontaneity of process according to Andrabi (2011) and the values became significantly more negative as temperatures rose due to increase in spontaneity of the adsorption with increase in temperatures (Deosarkar, 2012). Entropy change was positive demonstrating structural changes at active sites of the geopolymers during adsorption process. The values of ΔG decreased with increased temperature, showing that the

reaction was spontaneous and more favourable at higher temperature (Ghomri *et al*., 2013). For the metal ions to be adsorbed, they have to lose part of their hydration sheath. This energy of dehydration supersedes the exothermicity of the ions getting attached to the surface (Naseem and Tahir, 2001).

Table 4.8: Thermodynamic parameters of adsorption of Cd (II) ions computed from the linearized plot of ln K_c versus 1/T and n=3

			ΔG°(kJ/mol)			
	ΔH°	ΔS°	293K	298K	308K	318K
GP	kJ/mol)	(J/mol/K)	Mean±SD	Mean±SD	Mean±SD	Mean±SD
1	5.37	36.04	-4.60 ± 0.02^{d}	-4.73 ± 0.01^{c}	-5.24 ± 0.05^{b}	-6.00 ± 0.02^{a}
1C	27.42	116.49	-6.95 ± 0.07^{d}	-7.25 ± 0.03^{c}	-7.85 ± 0.06^{b}	-10.06 ±0.03^{a}
1E	26.84	123.70	-9.41 ± 0.17^{d}	-9.98 ± 0.08^{c}	-10.84 ± 0.06^{b}	-13.52 ±0.15^{a}
2	7.96	42.87	-5.49 ± 0.01^{d}	-5.80 ± 0.01^{c}	-6.21 ± 0.08^{b}	-7.81 ± 0.01^{a}
2C	15.12	77.03	-8.97 ± 0.08^{d}	-9.54 ± 0.05^{c}	-10.25 ± 0.10^{b}	-11.23 ±0.03^{a}
2E	20.31	99.78	-7.61 ± 0.09^{d}	-7.81 ± 0.05^{c}	-8.14 ± 0.04^{b}	-9.82 ± 0.04^{a}
3	16.07	73.43	-5.15 ± 0.05^{c}	-5.45 ± 0.01^{bc}	5.73 ± 0.09^{ab} -	-6.06 ± 0.37^{a}
3C	27.25	113.04	-5.96 ± 0.02^{d}	-6.46 ± 0.02^{c}	-7.35 ± 0.04^{b}	-8.72 ± 0.04^{a}
3E	15.13	73.84	-6.62 ± 0.08^{d}	-6.78 ± 0.02^{c}	-7.33 ± 0.04^{b}	-8.80 ± 0.06^{a}

Means in a row with the same letter are not significantly different from each other (Tukey–Kramer test, P>0.05), SD= standard deviation, GP= geopolymer, ΔH° = standard enthalpy change, ΔS° = standard entropy change, n= no of replicates and ΔG°= standard free energy change.

4.9.3 Thermodynamic studies of Zn (II) onto geopolymers

The negative value of ΔG° obtained in adsorption of Zn (II) ions signals the feasibility and spontaneous nature of the adsorption process and the more negative it is indicates the adsorption process becoming more spontaneous with rise in temperature, which favours the adsorption process (Kumar and Gayathri, 2009; Sharma *et al.*, 2010). The ΔG° values obtained in this study for the Zn (II) ions were < 20 kJ/mole, indicating physical adsorption was the predominant mechanism in the sorption process. This is similar to the results obtained by Abdel Ghani and Elchaghaby (2007). The positive value of ΔS° reflected the affinity of the adsorbent for particular heavy metal ions and confirms the

increased randomness at the solid–solution interface during adsorption (Hameed *et al*, 2009; Kumar and Gayathri, 2009). These results also support the suggestion that the adsorption capacity of adsorbent increases with increasing temperature (Thajeel, 2013).

Table 4.9: Thermodynamic parameters on adsorption of Zn (II) ions computed from the linearized plot of ln K_c versus 1/T and n=3

			ΔG° (kJ/mol)			
	ΔH°	ΔS°	293K	298K	308K	318K
GP	kJ/mol)	(J/mol/K)	Mean±SD	Mean±SD	Mean±SD	Mean±SD
1	6.83	43.45	-5.82 ± 0.01^{d}	-6.08 ± 0.05^{c}	-6.70 ± 0.01^{b}	-7.09 ± 0.04^{a}
1C	15.51	81.23	-8.16 ± 0.07^{d}	-8.54 ± 0.04^{c}	-9.93 ± 0.02^{b}	-10.56 ± 0.04^{a}
1E	13.20	66.67	-6.14 ± 0.03^{d}	-6.42 ± 0.02^{c}	-7.31 ± 0.10^{b}	-7.69 ± 0.08^{a}
2	32.85	135.02	-6.98 ± 0.02^{d}	-7.26 ± 0.03^{c}	-7.97 ± 0.12^{b}	-11.05 ± 0.03^{a}
2C	13.47	68.77	-6.55 ± 0.02^{d}	-7.05 ± 0.01^{c}	-7.93 ± 0.02^{b}	-8.38 ± 0.03^{a}
2E	10.95	61.53	-6.96 ± 0.10^{d}	-7.31 ± 0.03^{c}	-8.06 ± 0.06^{b}	-9.21 ± 0.06^{a}
3	15.83	79.02	-7.42 ± 0.05^{d}	-7.79 ± 0.09^{c}	-8.10 ± 0.17^{b}	-9.47 ± 0.03^{a}
3C	17.31	91.41	-9.30 ± 0.27^{d}	-10.01 ± 0.07^{c}	-10.82 ±0.02^{b}	-12.27 ± 0.19)^{a}
3E	20.13	100.60	-9.37 ± 0.06^{c}	-10.04 ± 0.10^{b}	-10.17 ±0.02^{b}	-12.59 ± 0.18^{a}

Mean percentages with same letters in the same row are not significantly different at 95 % confidence level SD= standard deviation, GP= geopolymer, ΔH° = standard enthalpy change, ΔS° = standard entropy change, n= no of replicates and ΔG°= standard free energy change.

4.10 Adsorption kinetic modeling

Adsorption kinetics, which indicates the adsorption rate, is an important characteristic of adsorbents (Wu *et al*., 2016). The transient behavior of the Pb (II), Cd (II) and Zn (II) ions adsorption process was analyzed using three adsorption kinetic models; pseudo- first and pseudo-second order rate models and intraparticle diffusion models. The rate constant of adsorption was determined from the pseudo-first order rate model and pseudo-second order model (Sen and Sarzali, 2008) based on equilibrium adsorption. Tables 4.10, 4.11 and 4.12 represent the descriptive kinetic data for Pb (II), Cd (II) and Zn (II) ions obtained from this study respectively.

4.10.1 Kinetic modeling on adsorption of Pb (II) ions

The slopes and intercepts of plots of log ($q_e - q_t$) versus t were used to determine the first order rate constant k_1 and equilibrium adsorption density q_e. However, the experimental data deviated considerably from the calculated data as shown in table 4.10. A comparison of the results with the correlation coefficients is shown in table 4.10.

Table 4.10: Descriptive data on rate constants of Pb (II) adsorption on geopolymers as estimated from pseudo-first and second order kinetic models

Pseudo-first order							**Pseudo-second order**			
GP	q_e(exp)	SD	q_e(cal)	SD	k_1	R^2	q_e(cal)	SD	k_2	R^2
1	36.34	0.05	15.91	1.34	0.034	0.939	39.95	0.09	$2.5x10^{-3}$	0.996
1C	46.67	0.16	56.43	2.69	0.044	0.779	62.37	0.23	$5.2x10^{-4}$	0.957
1E	40.51	0.11	58.20	13.36	0.053	0.898	48.70	0.36	$1.0x10^{-3}$	0.981
2	39.82	0.04	21.82	0.65	0.033	0.887	43.54	0.11	$2.0x10^{-3}$	0.991
2C	49.25	0.00	92.59	3.97	0.054	0.978	68.49	0.00	$4.07x10^{-4}$	0.987
2E	41.30	0.00	28.32	0.04	0.030	0.733	46.95	0.00	$1.31x10^{-3}$	0.959
3	45.12	0.01	62.78	0.51	0.054	0.773	57.47	0.00	$7.05x10^{-4}$	0.968
3C	49.66	0.01	116.09	2.11	0.073	0.908	64.94	0.00	$5.86x10^{-4}$	0.975
3E	42.27	0.03	28.84	0.33	0.029	0.584	53.95	0.17	$1.07x10^{-3}$	0.970

GP= geopolymer adsorbents, C = citric acid functionalized, E = EDTA functionalized, SD = standard deviation, q_e (exp) (mg/g) = q_e obtained from adsorption experiment, q_e (cal) (mg/g) = q_e calculated from the pseudo graphs, $k_1(min^{-1})$ = rate constant for pseudo –first order reaction, k_2(g/mg.min) = rate constant for pseudo –second order reaction, h = is the initial sorption rate (mg/ g min) and R^2 = correlation coefficients, initial metal ion concentration = 100mg/L and residence time varied (20 - 100 minutes).

The correlation coefficients for the pseudo- first order kinetic obtained at the studied concentration were low compared to those of pseudo- second order kinetic. Also the theoretical q_e values found from the pseudo-first order kinetic did not give values closer to the experimental values. This suggests that the adsorption system of Pb (II) ions was not a first order reaction. The correlation coefficients for the second order kinetic obtained were greater than 0.95.

The equilibrium adsorption capacities obtained with pseudo-second order model were slightly more reasonable than those of the pseudo-first order when comparing predicted results with experimental data. Moreover, the values of R^2 also indicated that this model produced better results. These indicate that the adsorption system studied belongs to the Pseudo-second order kinetic model that presupposes that Pb (II) ions adsorption on geopolymer adsorbents may occur through a chemical process involving the valence forces or exchanged electrons (Al-Ghouti *et al*., 2005). Similar phenomena were also observed in adsorption of Cu (II) ions and Pb (II) ions on tea waste (Amarasinghe and Williams, 2007).

4.10.2 Kinetic modeling on adsorption of Cd (II) ions

Different kinetic parameters calculated by linear regression for Cd (II) are summarized in table 4.11. The correlation coefficients (R^2) obtained from the plots of pseudo- second order kinetics were larger ($R^2 > 0.997$) than those of the pseudo-first order model. It is deduced that, the initial adsorption rates ($h_\circ$) obtained were 42.37 to 54.07 and 72.37 mg /g min as the SiO_2/Al_2O_3 ratio of geopolymer increased from 4.16 to 8.28 (Table 4.2) for adsorbents GP-1, GP-2 and GP-3 respectively. This may have attributed the increased driving force between the liquid and solid phase (Liu *et al*., 2012).

Table 4.11: Descriptive data on rate constants of Cd (II) adsorption onto geopolymers as estimated from pseudo- first and second order kinetic models

Pseudo-first order							**Pseudo-second order**			
GP	q_e(exp)	SD	q_e(cal)	SD	k_1	R^2	q_e(cal)	SD	h_o	R^2
1	43.23	0.07	2.46	0.53	0.013	0.729	43.48	0.20	42.37	1.0
1C	46.17	0.04	8.64	0.35	0.040	0.828	47.17	0.00	20.33	0.999
1E	44.91	0.13	5.80	0.74	0.021	0.931	45.52	0.24	18.05	0.999
2	43.14	0.05	1.79	0.27	0.025	0.509	43.23	0.11	54.07	1.0
2C	45.16	0.05	3.25	1.02	0.021	0.917	45.66	0.36	23.31	0.999
2E	44.80	0.12	4.75	0.18	0.016	0.834	44.91	0.12	19.96	0.998
3	44.73	0.04	4.65	0.14	0.019	0.991	45.18	0.12	72.37	0.999
3C	44.97	0.09	9.27	1.40	0.034	0.840	47.02	0.13	19.46	1.0
3E	49.85	0.01	23.96	0.25	0.046	0.944	52.63	0.00	9.61	0.997

GP= geopolymer adsorbents, C = citric acid functionalized, E = EDTA functionalized SD = standard deviation, q_e (exp) (mg/g) = q_e obtained from adsorption experiment, q_e (cal) (mg/g) = q_e calculated from the pseudo graphs, $k_1(min^{-1})$ = rate constant for pseudo –first order reaction, h_o= is the initial sorption rate (mg/ g min) and R^2= correlation coefficients, initial metal ion concentration = 100mg/L and residence time varied (20 - 100 minutes).

4.10.3 Kinetic modeling on adsorption of Zn (II) ions

The pseudo-first order kinetic predicted much different values of the equilibrium adsorption capacities than the experimental values and hence gave inapplicability of this model. The pseudo-second order kinetic model fitted very well with high regression coefficients ($R^2 \geq 0.996$) shown in table 4.12. Higher correlation coefficients (R^2) with respect to the fitted pseudo-second order model suggested that adsorption of metal ions on geopolymers followed this order.

Table 4.12: Descriptive data on rate constants of Zn (II) ions adsorption onto geopolymers as estimated by pseudo-first and second order kinetic models

	Pseudo-first order						Pseudo-second order			
GP	q_e(exp)	SD	q_e(cal)	SD	k_1	R^2	q_e(cal)	SD	k_2	R^2
1	40.30	0.04	1.47	0.15	0.015	0.222	40.53	0.08	$3.0x10^{-2}$	1.0
1C	46.78	0.03	5.27	0.84	0.027	0.257	47.47	0.13	$1.4x10^{-2}$	1.0
1E	41.79	0.03	14.71	3.95	0.042	0.782	43.04	0.10	$6.80x10^{-3}$	0.999
2	41.78	0.06	6.69	0.43	0.030	0.858	42.49	0.10	$1.0x10^{-2}$	0.999
2C	43.77	0.08	9.37	0.06	0.027	0.848	44.64	0.00	$6.81x10^{-3}$	0.998
2E	42.70	0.16	25.17	10.61	0.044	0.732	44.18	0.23	$5.16x10^{-3}$	0.996
3	41.53	0.07	3.17	0.17	0.012	0.839	41.90	0.10	$8.83x10^{-3}$	0.998
3C	45.20	0.11	24.82	8.70	0.044	0.888	47.39	0.23	$4.22x10^{-3}$	0.999
3E	42.77	0.13	2.21	0.32	0.007	0.086	41.55	0.36	$8.5x10^{-2}$	0.996

GP= geopolymer adsorbents, C = citric acid functionalized, E = EDTA functionalized SD = standard deviation, q_e (exp) (mg/g) = q_e obtained from adsorption experiment, q_e (cal) (mg/g) = q_e calculated from the pseudo graphs, $K_L(min^{-1})$= rate constant for Pseudo –first order reaction, k_2(g/mg.min) = rate constant for pseudo –second order reaction and R^2 = correlation coefficients, initial metal ion concentration = 100mg/L and residence time varied (20 - 100 minutes).

The low values of rate constant (k_2) shown in table 4.12, suggested that the adsorption rate decreased with the increase of the phase contact time and the adsorption rate was proportional to the number of unoccupied sites (Krukowska *et al*., 2017). Ding *et al*. (2014) obtained similar results studying the adsorption of Pb (II) ions on the bagasse biochar.

4.10.4 Intra-particle diffusion models

The time dependent data from this study was further used to investigate whether intra-particle diffusion also played significant roles in the adsorption of Pb (II), Cd (II) and Zn (II) ions from their aqueous solutions. Their intra-particle diffusion kinetic plots of q_t against $t^{1/2}$ were taken and presented in figures 4.42, 4.43 and 4.44 respectively. According to this model, a plot of q_t versus $t^{0.5}$ should be linear if intra-particle diffusion

is involved in the adsorption process and if the plot passes through the origin then intraparticle diffusion is the sole rate-limiting step. It has also been suggested that in instances when qt versus $t^{1/2}$ is multilinear, two or more steps govern the adsorption process (Wu *et al.*, 2005; Unuabonah *et al.*, 2007).

4.10.4.1 Intra-particle diffusion models of Pb (II), Cd (II) and Zn (II) ions uptake onto geopolymers

Intra-particle diffusion plots for adsorption of Pb (II) ions is shown in figure 4.42.

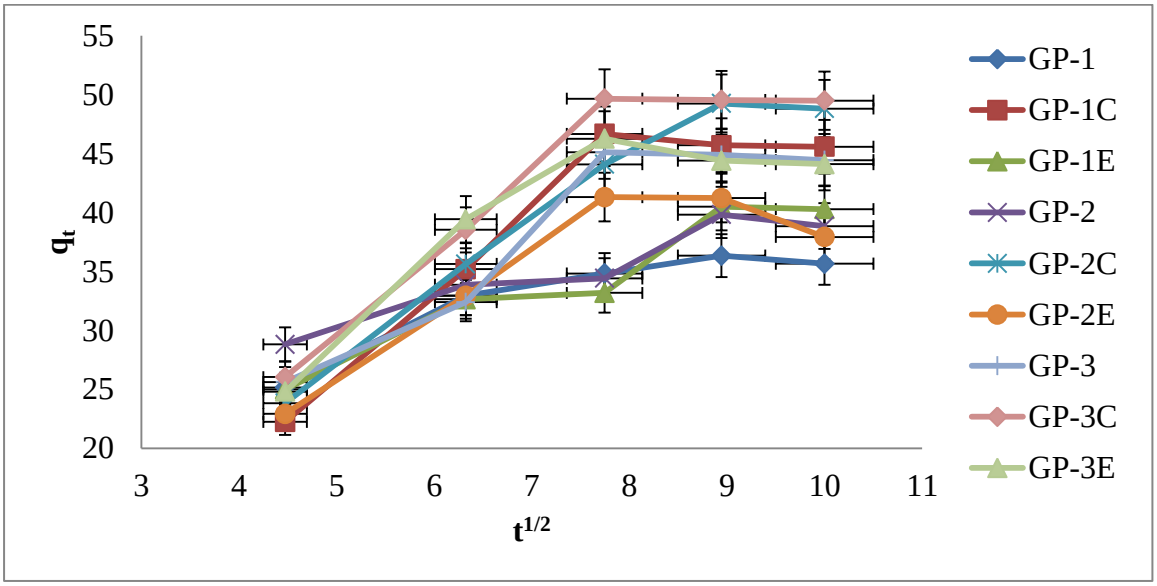

Figure 4.42: Intra-particle diffusion plot for the adsorption process of Pb (II) ions (geopolymer dosage = 2g/L, time 20-100 minutes, [Pb (II)] = 100mg/L, T = 298 K, pH 4.0, V = 0.050 L and error bars indicate the average deviation from the mean).

From the intra-particle diffusion plots shown in figure 4.42, it was evident that the adsorption processes followed two steps. The first linear portion followed the boundary layer diffusion followed by another linear portion, which represented the intra-particle diffusion (Nethaji *et al.*,2013). The adsorption processes were not only by intra-particle diffusion, but film diffusion also played a role in the observed processes (Kumar *et al.*, 2005). As the plot did not pass through the origin, intraparticle diffusion was not the only rate-limiting step (Nethaji *et al.*, 2013). Given the multilinearity of this plot for adsorption

of Pb (II) on geopolymer particles, it is proposed that adsorption occurred in two phases (Fig 4.42). The initial steeper section represented surface or film diffusion, the second linear section a gradual adsorption stage where intra-particle or pore diffusion was rate-limiting. Figure 4.43 shows the intraparticle plots of Cd (II) ions.

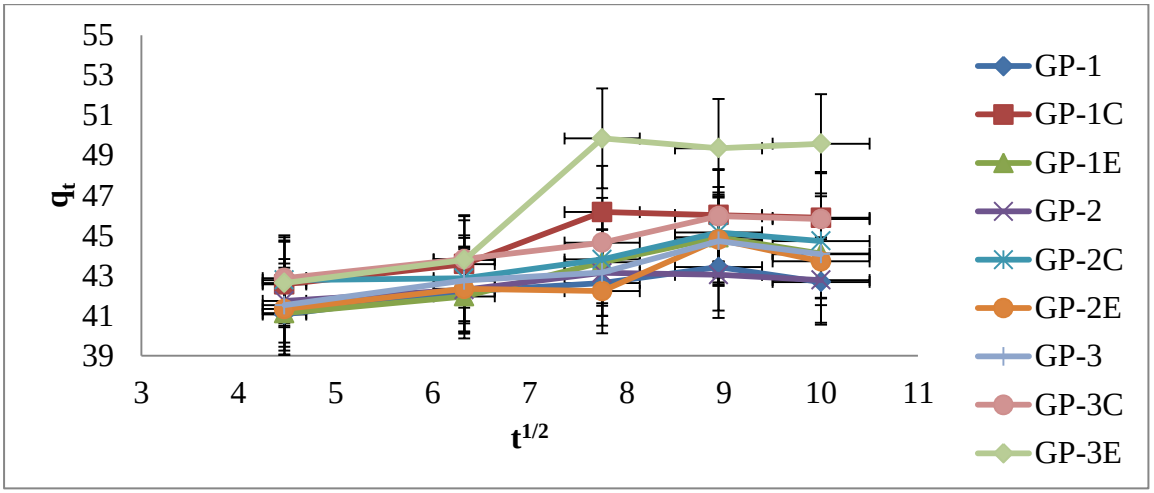

Figure 4.43: Intra-particle diffusion plot for the adsorption process of Cd (II) ions (geopolymer dosage = 2g/L, time 20-100 minutes, [Cd (II)] = 100mg/L, T = 298 K, pH 5.0, V = 0.050 L and error bars indicate the average deviation from the mean).

The data obtained exhibits multi linear plots revealing that the adsorption process was governed by two or more steps. The first linear part conceivably attributed to immediate utilization of most readily available sorbing sites on the sorbent surface. The second portion may be attributed to very slow diffusion of Cd (II) from the geopolymer surface site into the inner pores (Mahmoud *et al*., 2013). Figure 4.44 shows the intra-particle plots of Zn (II) ions.

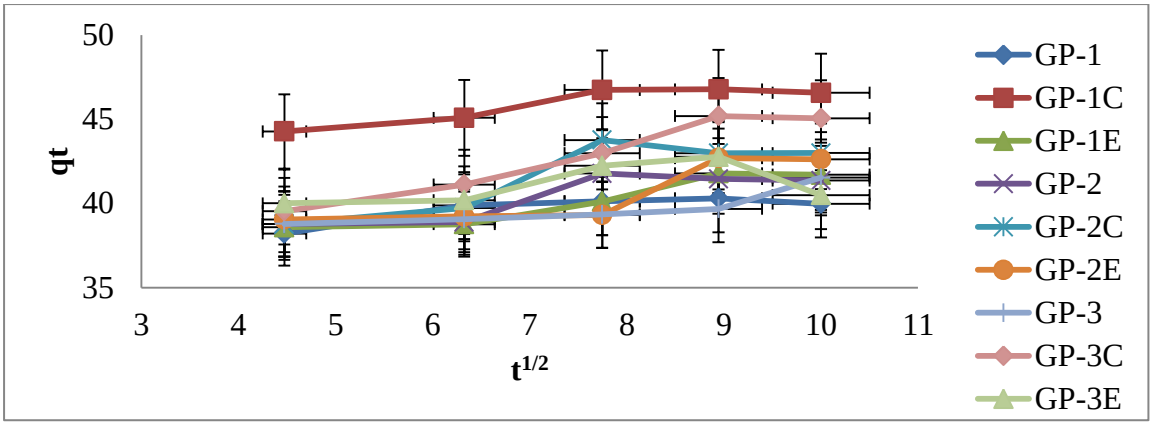

Figure 4.44: Intra-particle diffusion plot for the adsorption process of Zn (II) ions (geopolymer dosage = 2g/L, time 20-100 minutes, [Zn (II)] = 100mg/L, T = 298 K, pH 5.0 and V = 0.050 L).

The figure shows deviation from linearity thus other surface phenomena are involved in adsorption mechanism (Nwagbara *et al.*, 2010). The adsorption mechanism of metal ions onto the adsorbent followed film diffusion, pore diffusion and intra-particle transport (Singh and Pant, 2004) visible from the three evident phases in figure 4.43 and 4.44.

4.10.4.2 Deduction of k_{id} in terms of % sorption of Pb (II), Cd (II) and Zn (II) ions

Figure 4.45, presents plots of log R vs. log t of adsorption of Pb (II).

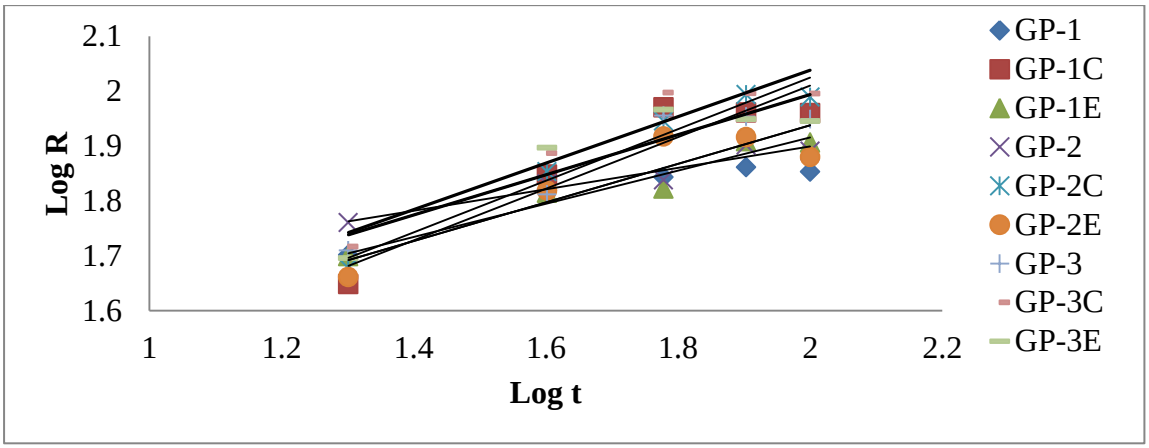

Figure 4.45: Analysis for intra-particle diffusion study (based on % adsorbed per unit time) of Pb (II) uptake onto geopolymer adsorbent.

The k_{id} values obtained from this plots are tabulated in appendix 7A. These values are 11.74, 27.11, 20.49, 12.15, 32.26, 17.21, 15.61, 16.58 and 18.34 for GP-1, GP-1C, GP-1E, GP-2, GP-2C, GP-2E, GP-3, GP-3C and GP-3E respectively. The 'a' values which according to Mahmoud *et al*. (2013) delineate the adsorption mechanism were 0.223, 0.470, 0.302, 0.196, 0.470, 0.351, 0.382, 0.422 and 0.365 for GP-1, GP-1C, GP-1E, GP-2, GP-2C, GP-2E, GP-3, GP-3C and GP-3E respectively. Increased values of "a" with functionalization insinuates increase in adsorption mechanism due to increased number of active sites upon functionalization. Figure 4.46 presents the plots for intra particle diffusion of Cd (II) ions.

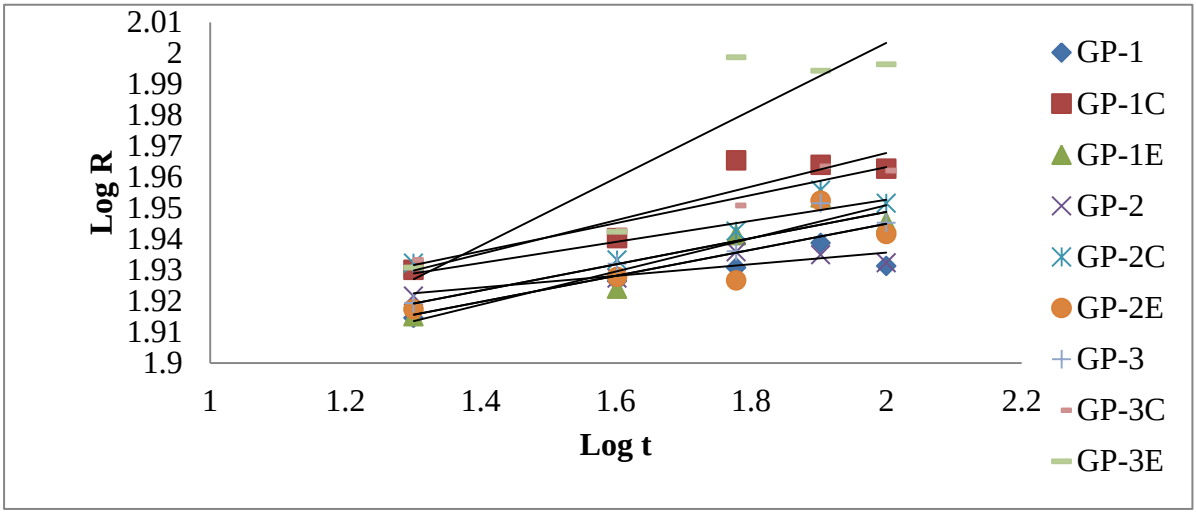

Figure 4.46: Analysis of intra-particle diffusion study (based on % adsorbed per unit time) of Cd (II) ions uptake onto geopolymer adsorbent.

The k_{id} values obtained for intra-particle diffusion studies of Cd (II) as presented in appendix 7B are 69.79, 72.31, 75.53, 72.61, 79.09, 76.67, 60.97, 74.59 and 73.13 for GP-1, GP-1C, GP-1E, GP-2, GP-2C, GP-2E, GP-3, GP-3C and GP-3E respectively. Notably there was increased value of k_{id} with functionalization of geopolymers. The values 'a' obtained from the isotherms were 0.029, 0.054, 0.054, 0.019, 0.034, 0.042, 0.042, 0.045 and 0.109 for GP-1 to GP-3E.

Figure 4.47 shows the intra-particle diffusion plots of adsorption of Zn (II) ions.

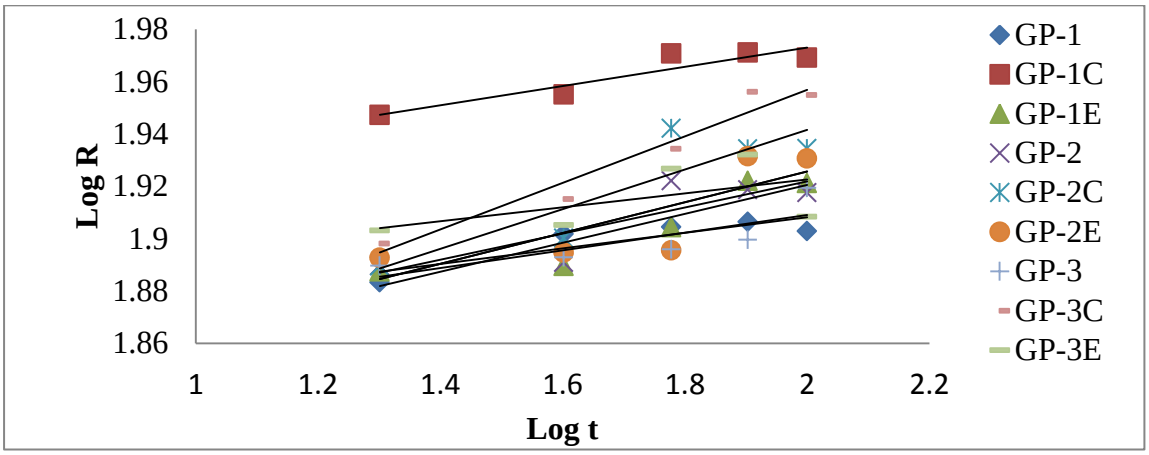

Figure 4.47: Analysis of intra-particle diffusion study (based on % adsorbed per unit time) of Zn (II) ions uptake onto geopolymer adsorbent.

The k_{id} values obtained for intra-particle diffusion studies of Zn (II) ions as presented in appendix 7C are 64.60, 79.34, 70.60, 61.70, 66.42, 64.28, 60.10, 69.44 and 74.05 for GP-1, GP-1C, GP-1E, GP-2, GP-2C, GP-2E, GP-3, GP-3C and GP-3E respectively. There was notable increase in the value of k_{id} with functionalization of geopolymers. The values 'a' obtained from the isotherms were 0.03, 0.037, 0.055, 0.05, 0.076, 0.059, 0.033, 0.089 and 0.027 for GP-1, GP-1C, GP-1E, GP-2, GP-2C, GP-2E, GP-3, GP-3C and GP-3E respectively.

Increase in values of k_{id} with functionalization observed for the three metal ions illustrated an enhancement in the rate of adsorption, whereas larger k_{id} values illustrate a better adsorption mechanism, which is related to an improved bonding between pollutant and the geopolymer particles (Itodo *et al*., 2010).

4.11 Desorption studies

Desorption studies help to describe the behavior of adsorption, the recovery of metal ions from aqueous solutions, the recycling of the adsorbent and practical applications of the treatment of industrial effluents (Moheb, 2015). Desorption of analyte ions adsorbed onto geopolymers was studied using HNO_3 at a concentration of 0.1 M.

4.11.1 Desorption studies of Pb (II) ions

The plot of the mean percentage of Pb (II) ions desorbed against the sorption time employed is shown in figure 4.48.

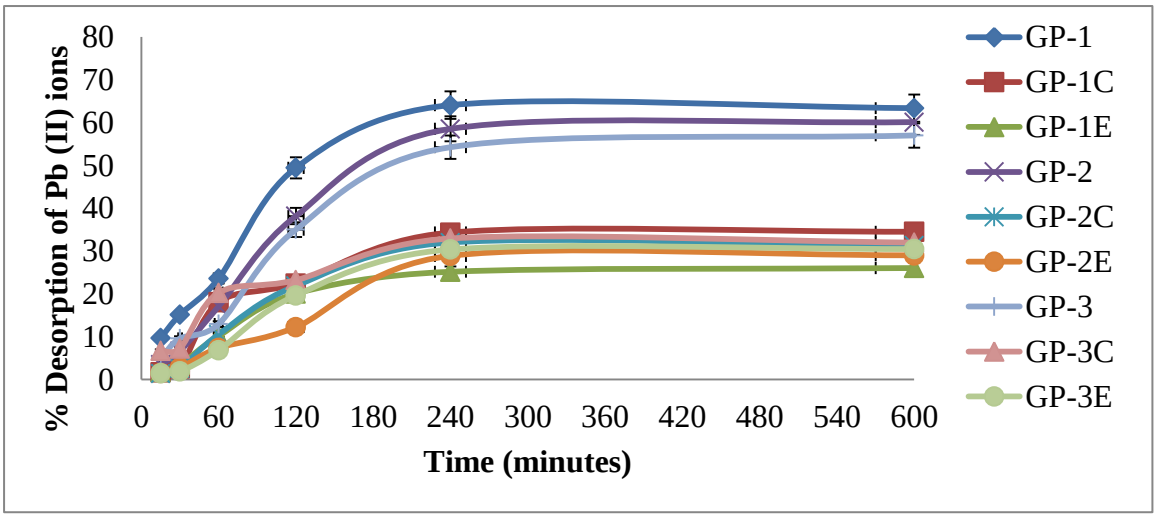

Figure.4.48: Effect of contact time on desorption of Pb (II) ions from geopolymer materials (Adsorbent dose=1.0 g/200 mL, shaking speed = 120 rpm, and temperature = 25 °C).

The figure reveals that the amounts of metal ions desorbed increased with increase in the sorption time. The mean desorption efficiency as shown in appendices 4A, 4B and 4C increased from 1.67 ± 0.02, 1.75 ± 0.01, 3.49 ± 0.01, 1.56 ± 0.01, 5.02 ± 0.02, 1.50 % ± 0.02 to 34.50 ± 0.02, 26.03 ± 0.00, 60.11 ± 0.02, 29.00 ± 0.06, 56.99 ± 0.01, 30.46 % ± 0.01, when contact time was varied from 15 to 600 minutes with adsorbent dose of 0.1 g/50 mL for geopolymers GP-1C, GP-1E, GP-2, GP-2E, GP-3 and GP-3E respectively.

For GP-1, GP-2C and GP-3C, the mean desorption percentage increased from 9.72 ± 0.02, 1.38 ± 0.01 and 6.67 ± 0.03 to 64.07 ± 0.07, 32.00 ± 0.03 and 32.93 % ± 0.00 when contact time was varied from 15 to 240 minutes and then dropped to 63.37 ± 0.12, 31.27 ± 0.03 and 31.97 % ± 0.02 respectively. This perhaps was due to the fact that in the process of desorption, after the acid was added, numerous hydrogen ions were immediately introduced.

As the concentration of hydrogen ions became drastically higher than that of the heavy metal ions, the surface groups of the adsorbent were occupied by hydrogen ions or hydroxonium ions and accordingly desorption of the Pb (II) ions occurred (Hu *et al*., 2016). Desorption efficiencies of the unfunctionalized geopolymers were higher than those of functionalized as shown in appendices 4A, 4B and 4C. This could be attributed to the fact that adsorption of metal ions by functionalized geopolymers could have had chelation effect that shielded the metal ions from acid protons during desorption process.

4.11.2 Desorption studies of Cd (II) ions

Results contained in appendices 4D, 4E and 4F generated the figure 4.49 showing the effects of varying contact time on the percentage desorption of Cd (II) ions.

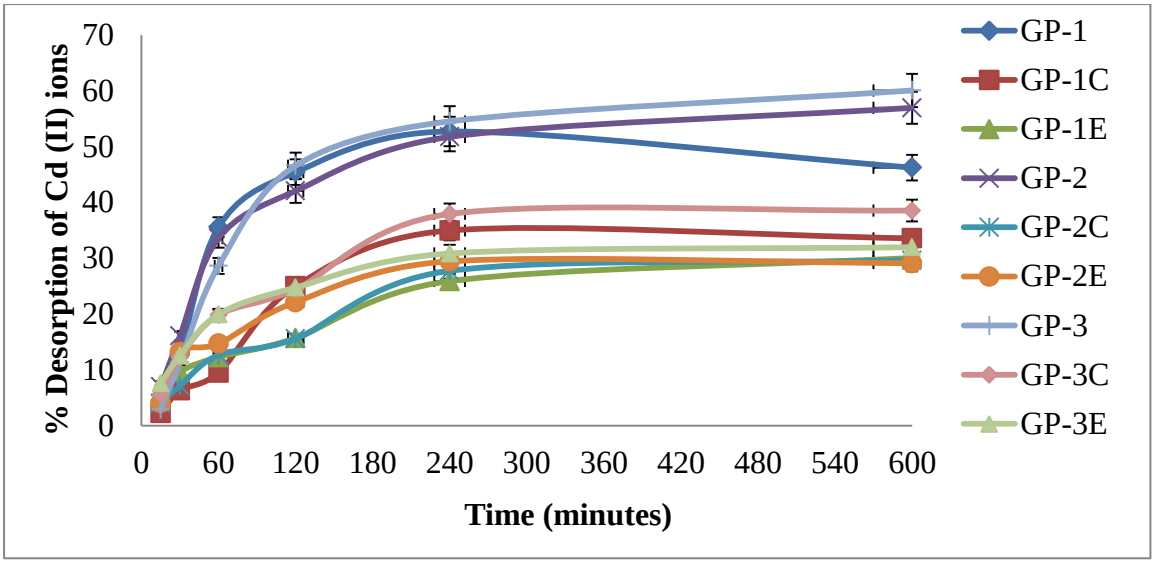

Figure.4.49: Effect of contact time on desorption Cd (II) ions from geopolymer materials (Adsorbent dose=1.0 g/200 mL, shaking speed = 120 rpm, and temperature = 25 $^{\circ}$C).

The mean percentage desorption increased from 4.29 ± 0.05, 6.94 ± 0.03, 4.02 ± 0.02, 2.91 ± 0.01, 5.54 ± 0.01 and 7.60 % ± 0.01 to 26.50 ± 0.01, 56.97 ± 0.02, 29.64 ± 0.01, 60.08 ± 0.01, 38.56 ± 0.01 and 31.98 % ± 0.01 when contact time was varied from 15 to 600 minutes for geopolymers GP-1E, GP-2, GP-2C, GP-3, GP-3C and GP-3E respectively. For geopolymer adsorbents GP-1, GP-1C and GP-2E the metal desorption increased from 4.52 ± 0.02, 2.27 ± 0.02 and 4.04 % ± 0.01 to 52.73 ± 0.023, 34.98 ± 0.00 and 29.45 % ± 0.03 when the contact time was changed from 15 to 240 minutes and then reduced to 46.26 ± 0.07, 33.57 ± 0.01 and 29.12 % ± 0.02 when residential time was adjusted to 600 minutes respectively.

The results (Fig 4.49) showed that as the contact time attributed to the reutilization of the geopolymer was enhanced, the amount of Cd (II) ions desorbed increased. The resultant desorption phenomenon observed in HNO_3 might be attributed to ion exchange type interaction rather than chemical sorption (Venkata *et al*., 2002).

4.11.3 Desorption studies of Zn (II) ions

The results on effects of varying contact time on the mean percentage desorption of Zn (II) ions are presented in a graph shown in figure 4.50. The figure was generated from the results raw data contained in appendices 4G, 4H and 4I.

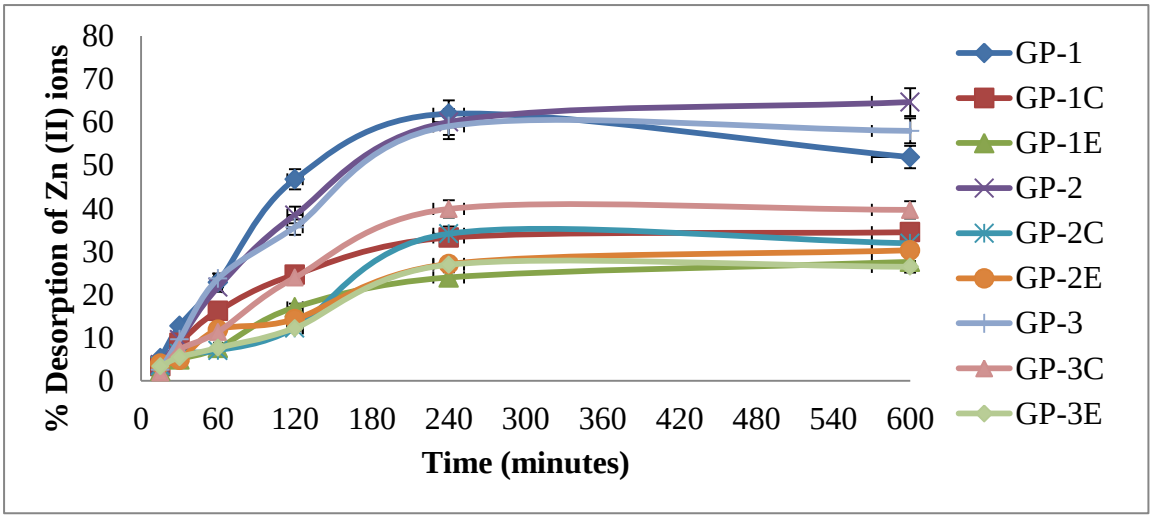

Figure.4.50: Effect of contact time on Zn (II) desorption from geopolymer materials (Adsorbent dose=1.0 g/200 mL, shaking speed = 120 rpm, and temperature = 25 $^{\circ}$C).

As shown, the percentage desorption increased from 3.42 ± 0.01, 2.29 ± 0.02, 3.77 ± 0.01 and 3.98 % ± 0.01 to 34.47 ± 0.01, 27.60 ± 0.01, 64.68 ± 0.01 and 30.30 % ± 0.01 when contact time was varied from 15 to 600 minutes for GP-1C, GP-1E, GP-2 and GP-2E respectively. For GP-1, GP-2C, GP-3, GP-3C and GP-3E regeneration rate increased from 5.25 ± 0.01, 3.50 ± 0.01, 2.55 ± 0.02, 1.87 ± 0.01 and 3.36 % ± 0.01 to 61.96 ± 0.01, 34.12 ± 0.02, 59.05 ± 0.06, 39.87 ± 0.01 and 26.93 % ± 0.05 when residence time was adjusted from 15 to 240 minutes then dropped to 51.90 ± 0.02, 31.90 ± 0.03, 57.98 ± 0.02, 39.66 ± 0.02 and 26.45 % ± 0.04 as construed in appendices 4G, 4H and 4I, when time was increased to 600 minutes respectively.

The results show similar trend to that of desorption Pb (II) and Cd (II). The desorption of metal ion by mineral acids medium indicates that the Zn (II) ions were adsorbed onto the geopolymers through physisorption mechanism (Balakrishnan *et al.*, 2010). Geopolymers functionalized with citric acid and EDTA recorded low rates of percentage regeneration. This could be as a result of strong complexing abilities of EDTA and citric acid functional groups with metal ions (Saleem and Bhatti, 2011).

4.12 Adsorption studies of methylene blue

4.12.1 Point of zero charge (pHpzc) studies and the effect of pH on MB adsorption

The point of zero charge (pHpzc) is an important factor that determines the linear range of pH sensitivity and then indicates the type of surface active centers and the adsorption ability of the surface (Poghossian, 1997). Cationic dye adsorption is favoured at pH ≥ pHpzc where the surface becomes negatively charged (Yagub *et al.*, 2014). The graph of pH final vs. pH initial was plotted as shown in figure.4.51.

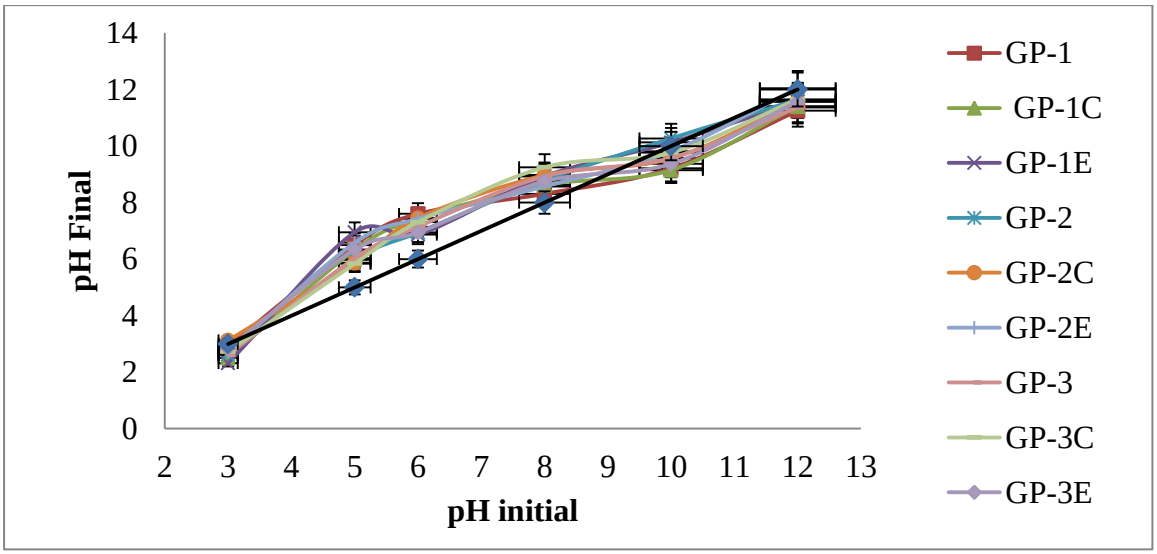

Figure 4.51: A graph of pH final of geopolymer adsorbent against pH initial (Adsorbent dose = 0.10 g, volume of distilled water= 100 m/L, room temperature 25 ± 2 °C and shaking speed of 120 rpm).

The intersections of the curves with the straight line are known as the end points of the pHpzc, and these values were 8.7, 9.4, 9.4, 10.2, 9.7, 9.5, 9.7, 9.7 and 9.3 for geopolymers GP-1, GP-1C, GP-1E, GP-2, GP-2C, GP-2E, GP-3, GP-3C and GP-3E respectively. At higher solution pH (pH ≥ pHpzc), the geopolymers became negatively charged and enhanced adsorption of the positively charged dye cations through electrostatic forces of attraction (Ebrahimian Pirbazari *et al*., 2014).

The calibration curve of MB is shown in appendix 5A. The pH of aqueous solutions is a key factor in the adsorption process which is a function of hydrogen and hydroxyl ions concentrations (Hassan, 2013). The effects of solution pH on MB adsorption onto geopolymer were investigated and the results are illustrated in figure 4.52, which shows that the elevations of pH lead to increasing percentage uptake of MB onto geopolymer.

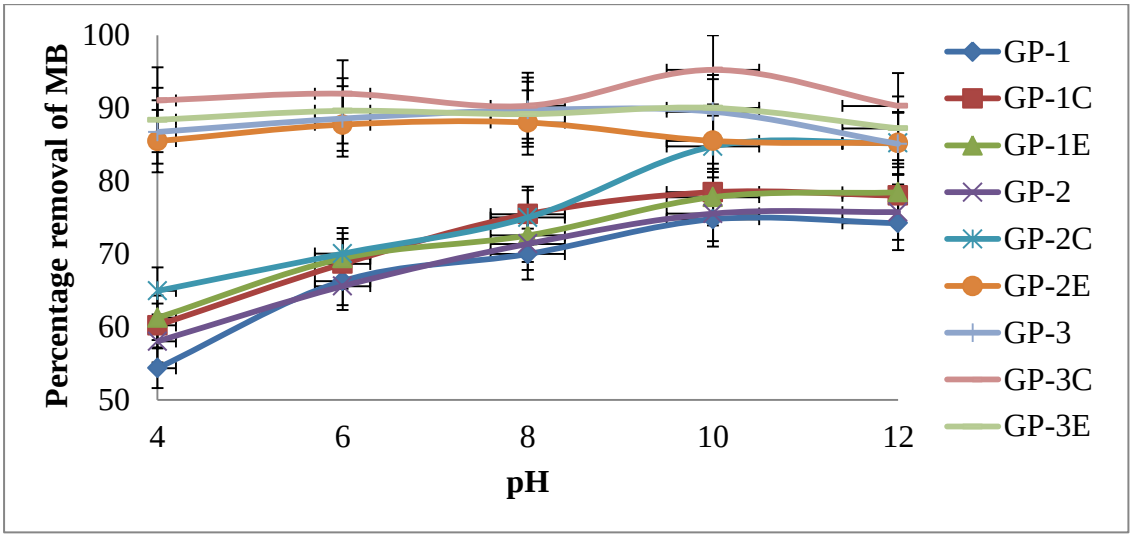

Figure 4.52: Effect of pH on adsorption of MB onto geopolymer (Contact time=60 minutes, shaking speed of 120 rpm, pH = 10.0, adsorbent dose = 0.1 g/25 mL and initial concentration of MB= 25 mg/L).

When the pH of the aqueous solution increased from 4 to 12, percentage uptake increased from 54.34 ± 0.11, 60.21 ± 0.41, 91.06 ± 0.36 and 88.40 % ± 0.17 to 74.77 ± 0.10, 78.48 ± 0.23, 95.26 ± 0.10 and 90.04 % ± 0.15 when the pH was increased from 4 to 10 and

then dropped when pH was adjusted to 12 for GP-1, GP-1C, GP-3C and GP-3E respectively. For GP-1E, GP-2 and GP-2C, the removal of MB increased from 61.25 ± 0.17, 58.02 ± 0.26 and 64.94 % ± 0.23 to 78.45 ± 0.37, 75.75 ± 0.29 and 85.21 % ± 0.20 respectively. Similarly, higher removal percentages of MB from solution were observed (88.03 ± 0.12 and 89.74 % ± 0.12) at pH (8) and then dropped for GP-2E and GP-3 respectively. Statistical data to this effect can be obtained from appendices 5B, 5C and 5D. Lower adsorption of MB at acidic pH (pH ≤ pHpzc) was due to the presence of excess H^+ ions competing with the cation groups on the dye for adsorption sites (Ebrahimian Pirbazari *et al*., 2014).

The functionalized geopolymers contained carboxylic functional groups which were electrons rich and therefore increased the attraction of the electrophilic sites in the ionized dye. According to Said *et al*. (2014) methylene blue is adsorbed in basic conditions. Literature reports indicate that increased pH should result in increase in adsorption for cationic dyes due to increase in number of negatively charged surface sites on the adsorbent resulting in electrostatic attraction (Senthil Kumar *et al*., 2010). Similar results were reported in literature on adsorption of dyes (Kavitha and Namasivayam, 2007; Demirbas, 2009).

4.12.2 Effect of contact time on adsorption of MB

Figure 4.53 shows the graph of percentage removal of MB against contact time. Experimental data contained in appendices 5H, 5I and 5J was used in plotting figure 4.53. The mean percentage removal increased from 58.51 ± 0.37, 63.41 ± 0.47, 89.35 ± 0.01 and 89.43 % ± 0.00.to 85.03 ± 0.31, 86.41 ± 0.11, 99.60 ± 0.01 and 99.58 % ± 0.01 for adsorbents GP-1, GP-1C, GP-3 and GP-3C respectively when contact time was varied

from 20 to 60 minutes and thereafter dropped slightly on increase of contact time to 80 minutes. For adsorbents GP-1E, GP-2, GP-2C, GP-2E and GP-3E, the MB uptake increased from 69.17 ± 0.35, 62.27 ± 0.30, 79.68 ± 0.40, 73.67 ± 0.32 and 89.33 % ± 0.01 to 87.95 ± 0.12, 86.49 ± 0.29, 88.36 ± 0.06, 89.44 ± 0.27 and 99.64 % ± 0.01 respectively for contact time between 20 and 80 minutes.

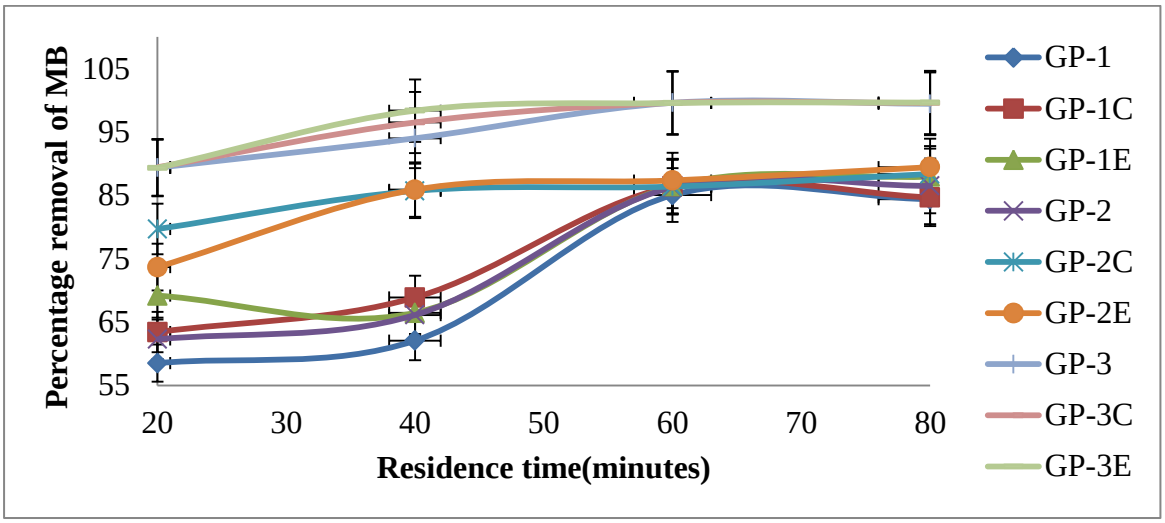

Figure 4.53: Effect of residence time on adsorption of MB onto geopolymer (shaking speed of 120 rpm, pH = 10.0 and concentration of MB = 25 mg/L).

The results suggest that, adsorption took place rapidly at the initial stage on the external surface of the adsorbent followed by a slower internal diffusion process, which may be the rate determining step (Koumanova and Allen, 2005; Gialamouidis *et al*., 2010). In addition, the fast adsorption at the initial stage may be due to the fact that a large number of surface sites are available for adsorption, but after a lapse of time, the remaining surface sites are difficult to be occupied (Idris *et al*., 2011). This agrees with the report of other investigators in literature (Kannan and Meenakshisundaram, 2002; Garg *et al*., 2003).

4.12.3 Effect of adsorbent dose on adsorption of MB

The effect of varying adsorbent dose on the percentage removal of MB studied at room temperature (25 °C ± 2) by varying the adsorbent amounts from 0.1 to 0.5 g is presented in the graph shown in figure 4.54. The raw experimental data is presented in appendices 5K, 5L and 5M.

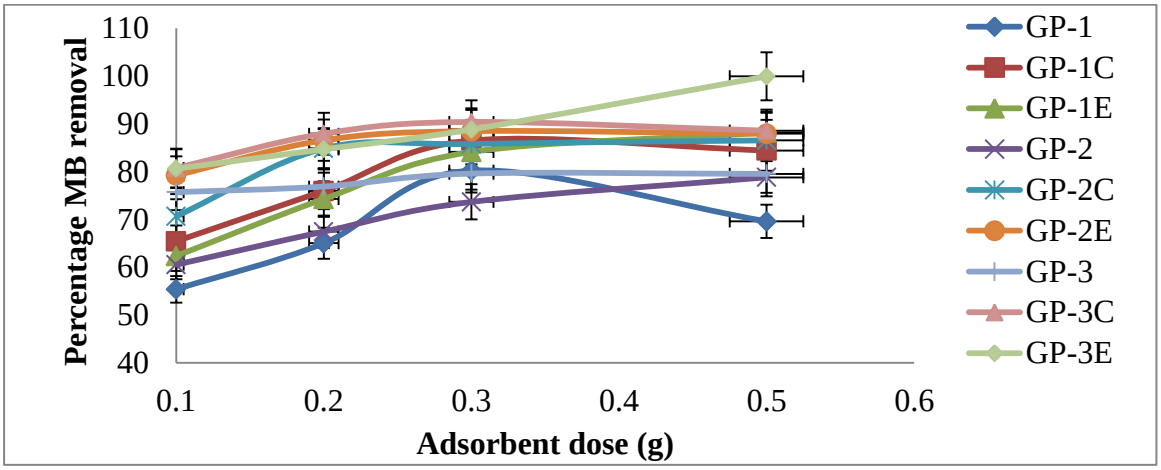

Figure 4.54: Effect of adsorbent dose on adsorption of MB onto geopolymer (Contact time = 60 minutes, shaking speed of 120 rpm, pH = 10.0 and concentration of MB = 25 mg/L).

The mean percentage removal increased from 55.42 ± 0.15, 65.38 ± 0.19, 79.30 ± 0.08, 84.58 ± 0.31 and 80.86 % ± 0.43 to 80.37 ± 0.35, 86.44 ± 0.08, 88.47 ± 0.21, 90.41 ± 0.13 and 90.16 % ± 0.25 as adsorbent dose was varied from 0.1 to 0.3 g for adsorbents GP-1, GP-1C, GP-2E, GP-3 and GP-3C respectively and then dropped on further increase in adsorbent dose. The percentage removal increased for adsorbent GP-1E, GP-2, GP-2C and GP-3E from 62.36 ± 0.22, 60.45 ± 0.45, 70.57 ± 0.55 and 80.50 % ± 0.32 to 88.08 ± 0.11, 78.69 ± 0.16, 86.36 ± 0.19 and 99.68 % ± 0.29 as dose was varied from 0.1 to 0.5 g respectively.

At constant initial dye concentration, increasing the geopolymer dosage provides a greater surface area and larger number of active sites which enhances of dye uptake (Bello and

Ahmad, 2011). More adsorption sites remained unsaturated during the adsorption process since increasing the adsorbent dose lead to an increase in the number of sites available for adsorption (Khattri and Singh, 2009). A similar trend on effect of adsorbent dose on adsorption of MB was reported by (Amuda *et al*., 2014).

4.12.4 Effect of temperature on adsorption of MB

The effect of temperature on the adsorption rate of MB on geopolymers was investigated at four different temperatures (298, 308, 318 and 328 K) using initial concentration of 25 mg/L. Figure 4.55 shows the effect of temperature on adsorption of MB.

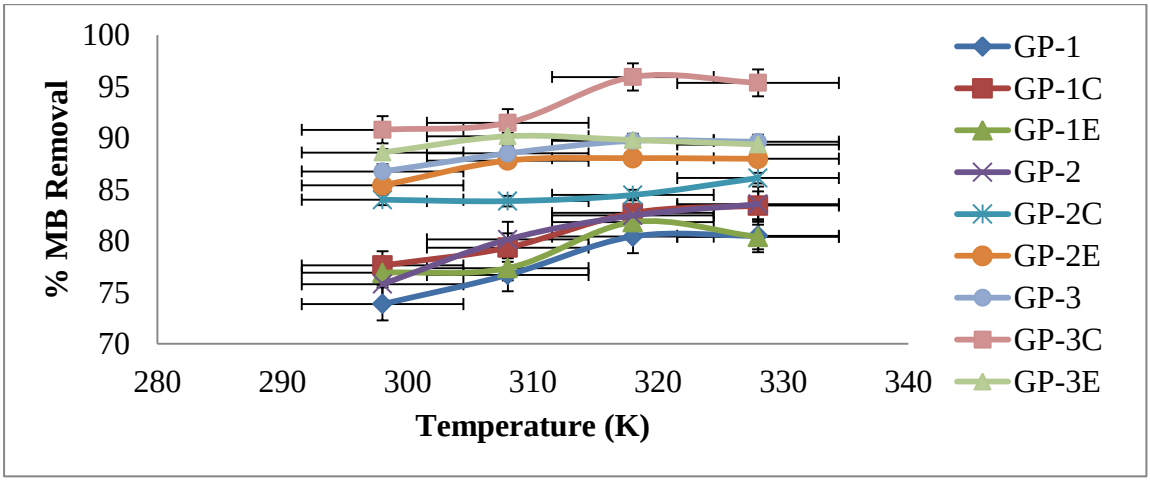

Figure 4.55: Effect of temperature on adsorption of MB onto geopolymer (Contact time = 60 minutes, shaking speed of 120 rpm, pH = 10.0, adsorbent dose = 0.1 g/25 mL and initial concentration of MB= 25 mg/L).

From figure 4.55, the mean percentage removal as presented in appendices 5N, 5O and 5P, increased from 77.64 ± 0.48, 76.15 ± 0.31, 83.75 ± 0.28 and 86.72 % ± 0.09 to 83.44 ± 0.14, 84.02 ± 0.41, 86.40 ± 0.28 and 89.76 % ± 0.39 with increased temperature from 298 to 328 K for GP-1C, GP-2, GP-2C and GP-3 respectively. For GP-1, GP-1E, GP-2E, GP-3C and GP-3E, the percentage removal increased from 73.75 ± 0.14, 76.82 ± 0.12, 85.25 ± 0.13, 90.75 ± 0.27 and 88.58 % ± 0.09 to 80.29 ± 0.15, 82.07 ± 0.25, 88.26 ±

0.21, 95.95 ± 0.19 and 89.79 % ± 0.07 respectively when temperature was adjusted from 298 to 318 K and then dropped on further increase in temperature.

Increase in temperature increased the rate of diffusion of the MB molecules within the internal pores of the adsorbent and the external boundary layer and, due to decrease in the viscosity of the solution (Ghasemi and Asadpour, 2007). This may also be due to the mobility of molecules, which increases generally with a rise in temperature, thereby facilitating the formation of surface monolayers (Dogan, 2003). The drop recorded after maximum adsorption with increase in temperature could be attributed to the fact that higher temperatures induce higher mobility of the adsorbate causing desorption (Pandey *et al*., 2010).

4.12.5 Effect of initial dye concentration on adsorption of MB

The effect of the initial dye concentration on adsorption of MB depends on the immediate relation between the dye concentration and the available active sites on an adsorbent lattice (Salleh *et al*., 2011). Figure 4.56 shows the effect of initial dye concentration.

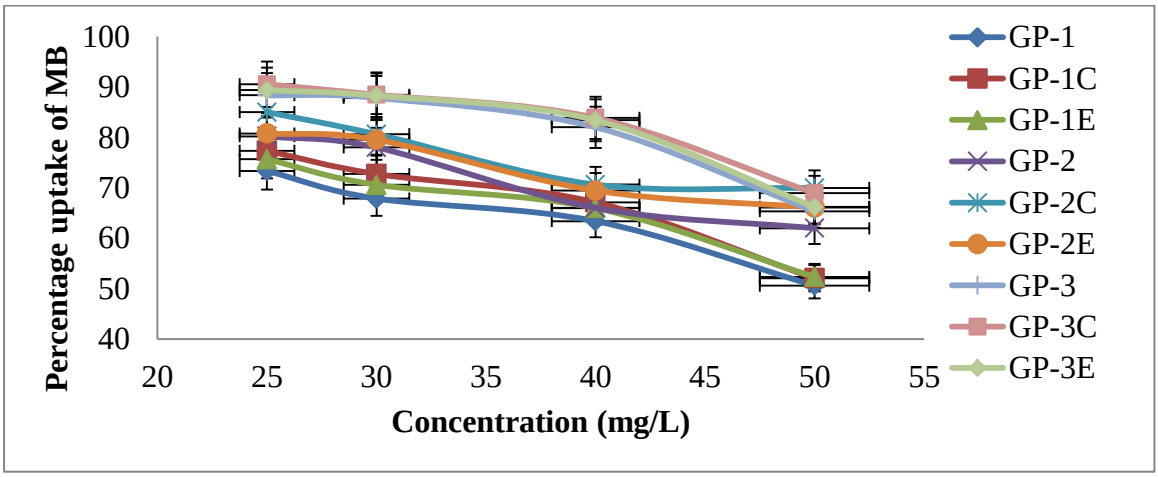

Figure 4.56: Effect of initial concentration on adsorption of MB onto geopolymer (Contact time = 60 minutes, shaking speed of 150 rpm, pH = 10.0 and adsorbent dose = 0.1 g/25 mL).

The percentage of uptake of MB as indicated in appendices 5E, 5F and 5G, decreased from 73.68 ± 0.73, 77.35 ± 0.24, 75.75 ± 0.55, 80.31 ± 0.11, 85.15 ± 0.15, 80.77 ± 0.12, 88.19 ± 0.15, 90.47 ± 0.25 and 89.29 % ± 0.25 to 50.49 ± 0.77, 52.07 ± 0.24, 52.39 ± 0.21, 61.79 ± 0.24, 69.95 ± 0.31, 66.17 ± 0.32, 65.49 ± 0.40, 69.09 ± 0.16 and 66.18 % ± 0.71 when concentration of MB was varied from 25 to 50mg/L for GP-1,GP-1C, GP-1E,GP-2,GP-2C,GP-2E,GP-3,GP-3C and GP-3E respectively.

The percentage of dye removal decreased with an increase in initial dye concentration, which may be due to the saturation of adsorption sites on the adsorbent surface (Eren and Acar, 2006). There will be unoccupied active sites on the adsorbent surface at low concentration. When the initial dye concentration is increased, the active sites required for adsorption of the dye molecules will disappear (Kannan and Sundaram, 2001). However, there will be an increase in the loading capacity of the adsorbent caused by increase in the initial MB concentration and this may be due to the high mass driving force (Bulut and Aydin, 2006). A similar trend on effect of initial dye concentration on adsorption of MB has been reported by Amuda *et al*. (2014).

4.12.6 The effect of shaking speed on MB uptake onto geopolymers

The effect of stirring speed was evaluated by varying the speed of agitation that is; (150-240 rpm) at an initial dye concentration of 25 mg/L and contact time of 60 minutes. As shown in figure 4.57, the sorption of MB on geopolymers increased with increase of stirring speeds.

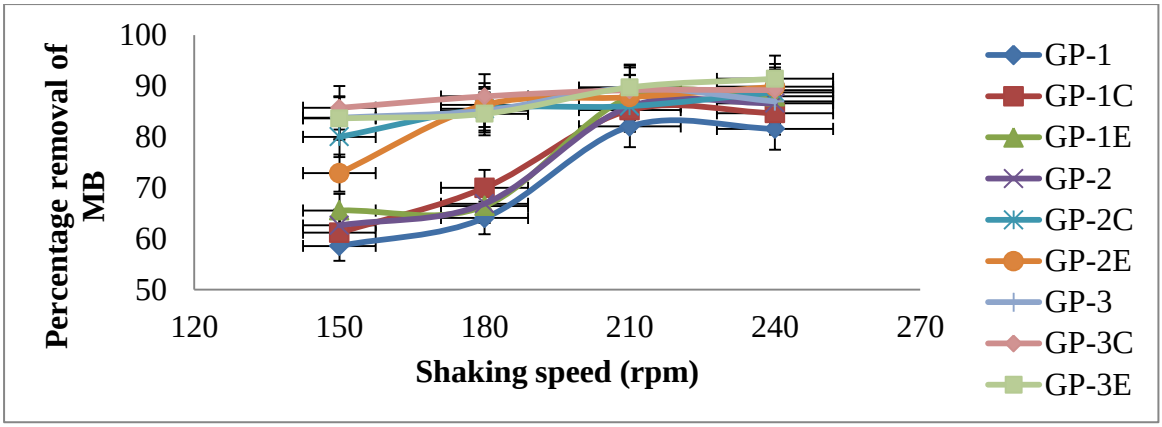

Figure 4.57: Effect of shaking speed (rpm) on adsorption of MB onto geopolymer (Contact time = 60 minutes, pH = 10.0, initial MB concentration = 25 mg/L and adsorbent dose = 0.1 g/25 mL)

The mean MB uptake using the adsorbents is tabulated in appendices 5Q, 5R and 5P increased from 58.58 ± 1.78, 61.18 ± 1.01 and 83.78 % ± 0.54 to 82.07 ± 0.95, 85.27 ± 0.45 and 89.57 % ± 1.63 for GP-1, GP-1C and GP-3 respectively when shaking speed was adjusted from 150 to 210rpm. Then uptake decreased to 81.59 ± 1.01, 84.66 ± 1.27 and 86.97 % ± 0.11. This may be explained by the fact that when the stirring speed increases, all particles are kept in suspension, the contact surface solid/liquid increases, and the transfer of dye molecules to the surface of adsorbent will be favourable (Amrhar *et al*., 2015). The drop recorded could be attributed to the fact that high shaking speed provided sufficient additional energy to break newly formed bonds between the MB and the adsorbent surface (Bernard *et al.*, 2013).

For GP-1E, GP-2, GP-2C, GP-2E, GP-3C and GP-3E, the uptake increased on increasing shaking speed from 150 to 240 rpm from 65.54 ± 0.83, 62.62 ± 0.44, 80.01 ± 0.14, 72.89 ± 0.41, 85.71 ± 1.06 and 83.64 ± 1.17 % to 87.96 ± 0.93, 86.63 ± 0.02, 88.77 ± 0.40, 89.85 ± 2.01, 89.19 ± 1.50 and 91.42 ± 1.16 % respectively. This effect can probably be attributed to the decrease in boundary layer thickness around the adsorbent particles that results from increasing the degree of mixing (Wood *et al*., 2014). Shaking the mixture

conveyed the adsorbent to move hastily in the solution, and this increased the concentration of MB near the surface of the geopolymers (Bernard *et al*., 2013).

4.12.7 Adsorption isotherms

For solid–liquid adsorption system, the adsorption isotherm is an important model in the description of adsorption behavior. Upon the adsorption reaction reaching the equilibrium state, the adsorption isotherm can be used to provide the distribution of dye molecules between the solid phase and the liquid phase (Tan *et al*., 2008). It is significant to understand the adsorption behavior and identify the most appropriate adsorption isotherm model. In this study, Langmuir, Freundlich, Temkin and Sips isotherm were employed to investigate the adsorption behaviour. Adsorption isotherms were studied at four different concentrations of 25, 30, 40 and 50 g.

4.12.7.1 Freundlich isotherm of adsorption of methylene blue

The Freundlich model yielded a good fit with a correlation coefficient value of 0.96. The values of 1/n, which are a function of the strength of adsorption in the adsorption process obtained in adsorption of methylene blue, are presented in table 4.13.

Table 4.13: Equilibrium parameters of adsorption of MB using various studied adsorption models

Sorbents		GP-1	GP-1C	GP-1E	GP-2	GP-2C	GP-2E	GP-3	GP-3C	GP-3E
	1/n	1.61	1.82	1.76	2.54	3.47	2.85	3.52	4.14	3.7
Freundlich	K_F	2.97	5.21	4.44	40.85	618.59	102.47	672.98	422.78	113.4
	R^2	0.979	0.976	0.978	0.994	0.992	0.996	0.976	0.969	0.976
Langmuir	K_L	0.62	0.79	0.74	1.62	3.02	2.04	3.15	4.31	3.51
	R_L	0.057	0.046	0.049	0.024	0.013	0.019	0.012	0.009	0.011
	Q	0.11	0.1	0.1	0.08	0.07	0.07	0.07	0.07	0.07
	R^2	0.97	0.991	0.991	0.998	0.996	0.995	0.997	0.997	0.997
Sips	Q	15.95	16.83	16.54	17.89	19.14	18.49	20.22	20.74	20.45
	K_S	10.95	13.57	21.17	15.95	5.74	27.22	29.67	31.7	27.12
	n_s	0.35	0.29	0.3	0.33	0.28	0.31	0.30	0.29	0.295
	R^2	0.999	0.998	0.999	0.998	1	0.998	0.999	1	0.999
Temkin	B_T	115.7	126.09	122.66	154.8	195.55	167.52	203.75	232.42	211.9
	K_T	196.0	225.68	216.07	358.6	728.42	449.67	794	1351.5	915.3
	R^2	0.991	0.989	0.99	0.997	0.995	0.998	0.984	0.978	0.983

C and E- geopolymer functionalized with citric acid and EDTA respectively, 1/n = heterogeneity index, K_F =Freundlich constant, R^2= correlation coefficient, Q_{max} (mg/g) = adsorption capacity, K_L = Langmuir constant and n_s= Sips constant, A_T = Temkin adsorption potential, B_T = Temkin constant related to heat of adsorption (J/Mole).

The heterogeneity index of the geopolymers ranges from 1.61 to 4.14 as shown in table 4.13. These values are greater than one suggesting cooperative adsorption (Mohan and Karthikeyan, 1997). Generally, $1<1/n<10$ is characteristic of cooperative adsorption and indicative of a favourable adsorption process as reported in literature (Hameed *et al*., 2007; Shabudeen *et al*., 2007). In cooperative adsorption, the formation of a second layer is ruled out as there is no obvious phase change (Kippling, 1965).

4.12.7.2 Langmuir isotherm of adsorption of methylene blue

The Langmuir isotherm parameters are presented in table 4.13. The essential features of the Langmuir isotherm expressed in terms of equilibrium parameter R_L, which is a

dimensionless constant referred to as separation factor or equilibrium parameter, for geopolymers GP-1, GP-1C, GP-1E, GP-2, GP-2C, GP-2E, GP-3, GP-3C and GP-3E are 0.057, 0.046, 0.049, 0.024, 0.013, 0.019, 0.012, 0.009 and 0.011 respectively indicating that the equilibrium sorption was favourable ($R_L < 1$) and the R^2 value was ≥ 0.97 proving that the sorption data fitted well to this model. The values of K_L for GP-1, GP-1C, GP-1E, GP-2, GP-2C, GP-2E, GP-3, GP-3C and GP-3E were 0.62, 0.79, 0.74, 1.62, 3.02, 2.04, 3.15, 4.31 and 3.51 respectively. These values were found to increase upon increase in Si/Al ratios of the geopolymers and also on functionalization. The increase in K_L values with increase in Si/Al ratio and functionalization indicates that adsorption was accompanied by higher heat of adsorption (Zhang *et al*., 2010).

4.12.7.3 Temkin isotherm on adsorption of methylene blue

The Temkin isotherm model assumes that the heat of adsorption of all the molecules in the layer decreases linearly with coverage due to sorbent-sorbate interactions. The adsorption is therefore, characterized by uniform distribution of the binding energy (Hameed *et al*., 2008). The Temkin isotherm parameters for the adsorption of MB from aqueous solution onto the geopolymers are shown in table 4.13. The high correlation coefficient (> 0.98), characterized by the plots obtained indicates a good fit into the model. The high values indicated strong interaction between the adsorbate and the adsorbent.

The Temkin isotherm constant (Table 4.13) shows that the value of B_T, which is related to heat of adsorption were 115.67, 126.09, 122.09, 154.76, 195.55, 167.52, 203.75, 232.42 and 211.94 kJ/mole for GP-1, GP-1C, GP-1E, GP-2, GP-2C, GP-2E, GP-3, GP-3C and GP-3E respectively. These values are indicative of physiosorption (Dada *et al*., 2012).

Increase in B_T value suggests increase in heat of sorption for the methylene ion onto geopolymers and this agrees well with what was obtained in Langmuir model. The Temkin adsorption potentials, K_T of the adsorbent were 196.03, 225.68, 216.07, 358.55, 728.42, 449.67, 794, 1351.5 and 915.3 (dm^3/g).

4.12.7.4 Sips isotherm on adsorption of methylene blue

The Sips isotherm is a combination of the Langmuir and Freundlich isotherms and can be derived using either equilibrium or thermodynamic approach (Repo *et al*., 2011). The n_s values as shown in table 4.13 obtained are 0.35, 0.29, 0.30, 0.33, 0.28, 0.31, 0.30, 0.29 and 0.295 for GP-1, GP-1C, GP-1E, GP-2, GP-2C, GP-2E, GP-3, GP-3C and GP-3E respectively.

There was a slight decrease in value of n_s from GP-1 to GP-3. This implies that increase in SiO_2/Al_2O_3 ratio in geopolymers increased deviation of adsorption from homogeneous to heterogeneous (Nethaji *et al*., 2013). The Sips isotherm gave the highest correlation coefficients compared to the other models as shown in table 4.13 implying it has the best fit for the experimental data. The adsorption capacities obtained were 15.95, 16.83, 16.54, 17.89, 19.14, 18.49, 20.22, 20.74 and 20.45 mg/g for GP-1, GP-1C, GP-1E, GP-2, GP-2C, GP-2E, GP-3, GP-3C and GP-3E respectively. Increase in adsorption capacities was noted on increase in Si/Al ratio and also upon functionalization. This could be attributed to increase in the number of active sites. Table 4.14 shows some of the reported adsorption capacities of MB using different adsorbents.

Table 4.14: Comparison of adsorption capacities, Q_o of MB by various adsorbents

Adsorbent	Adsorption capacities (mg/g)	References
Banana peel	20.8	Annadurai *et al*. (2002)
Walnut bark	15.10	Bushra *et al*. (2010)
Rice husk	40.6	Vadivelan andVasanth Kumar (2005)
Sugarcane bagasse	34.20	Consolin *et al*.(2007)
Lantana camera stem	19.84	Amuda *et al*.(2014)
GP-3	20.22	
GP-3C	20.74	
GP-3E	20.45	

4.12.8 Adsorption kinetics

It is important to be able to predict the rate at which contaminants are removed from aqueous solutions in order to design an adsorption treatment plant (Elass *et al*., 2010). In order to investigate the mechanism of adsorption and potential rate controlling steps such as mass transfer and chemical reaction, the kinetics of MB sorption onto geopolymers was investigated using different models (Amuda *et al*., 2014). Figure 4.58 shows the pseudo- second order kinetic model plots for adsorption of MB at various contact time at room temperature. From the relationship k_d and q_e were determined from the intercept and slope of the plot.

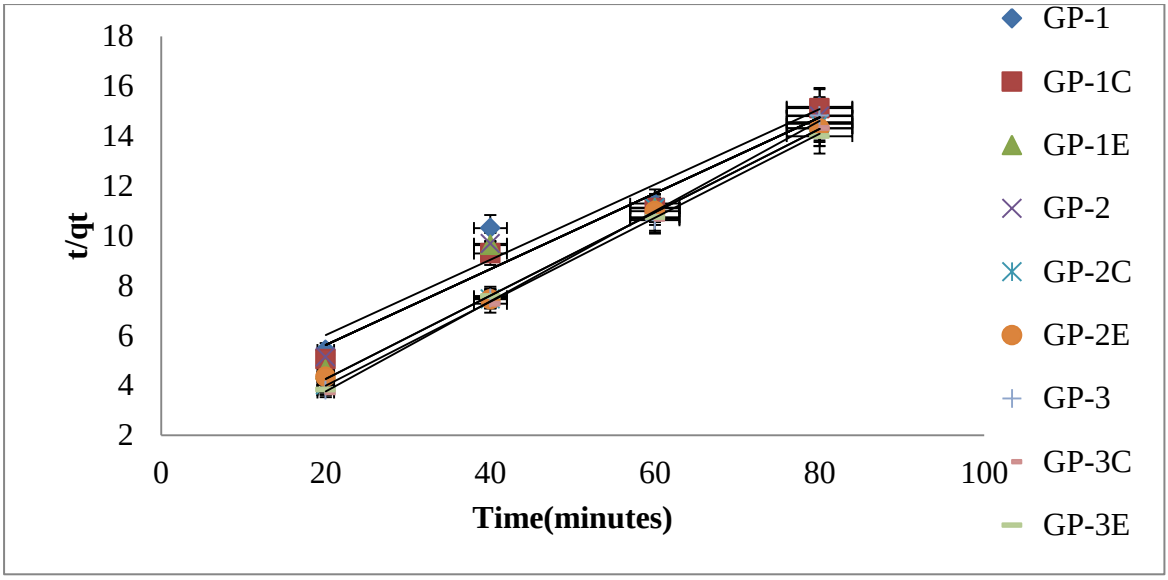

Figure 4.58: Pseudo - second order kinetic model for adsorption of MB by geopolymers

The R^2 values obtained for the pseudo-first order kinetic model were lower than that of the second order kinetic model and the experimental q_e values did not agree with the calculated values obtained from the linear plots as shown in table 4.15.

Table 4.15: Descriptive data on parameters of kinetic models for the adsorption of MB onto geopolymers at 298K

Pseudo-first order							Pseudo-second order			
sorbents	q_e(ex)	SD	q_e(cal)	SD	K_{ad}	R^2	q_e(cal)	SD	1/h	R^2
GP-1	5.30	0.02	8.64	1.18	0.08	0.851	6.64	0.05	2.99	0.947
GP-1C	5.39	0.01	4.66	0.33	0.05	0.717	6.25	0.02	2.13	0.979
GP-1E	5.48	0.01	6.91	1.06	0.07	0.103	6.41	0.03	2.17	0.958
GP-2	5.39	0.02	36.1	30.5	0.08	0.107	6.60	0.03	2.58	0.966
GP-2C	5.51	0.00	1.10	0.07	0.008	0.041	5.69	0.01	0.507	0.999
GP-2E	5.58	0.02	2.34	0.14	0.002	0.004	5.98	0.04	0.913	0.999
GP-3	5.64	0.01	2.24	0.19	0.001	0.002	5.52	0.04	0.145	0.997
GP-3C	5.61	0.01	2.08	0.26	0.02	0.131	5.67	0.02	0.199	0.999
GP-3E	5.71	0.02	1.17	0.07	0.005	0.020	5.94	0.02	0.623	0.999

GP= geopolymer adsorbents, q_e (exp) (mg/g) = q_e obtained from adsorption experiment, q_e (cal) = q_e calculated from the pseudo graphs, SD= standard deviation, K_{ad}= rate constant for pseudo –first order reaction, 1/h= is the initial sorption rate (mg/ g min) and R^2= correlation coefficients.

This suggests that the adsorption of MB onto geopolymers did not follow Pseudo-first order kinetics. Similar results were reported for the adsorption of MB ions on various adsorbents by several authors (Bulut and Aydin, 2006; Postai *et al.*, 2016). Pseudo-second order rate constants k_2 (calculated from the intercept and slope) as well as linear regression correlation coefficients R^2 are summarized in table 4.15. These result shows that correlation coefficients R^2 for the pseudo- second order kinetics are greater than those for pseudo- first order, indicating good agreement with the experimental data. It can be inferred that the pseudo- second order equation fits the adsorption data better than the pseudo- first order model.

4.12.8.1 Deduction from the shape of the intra-particle diffusion plot

A non-regression coefficient plot by fitting experimental data to equation 4.1

$q_t = k_{id}\, t^{(1/2)} + C_i$. …………………………………………………………… 4.1

gave the 3 phased plot of type in figure 4.59.

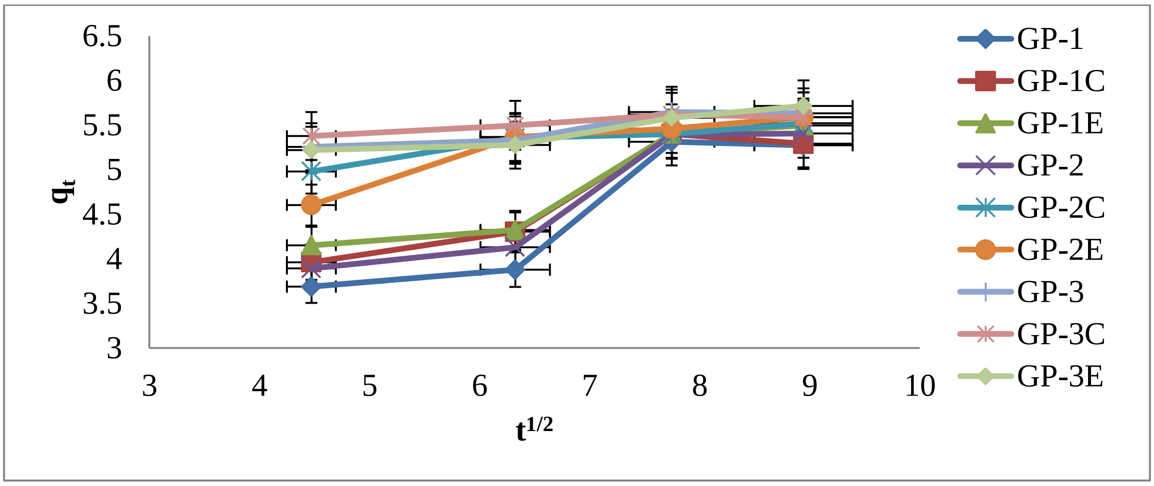

Figure 4.59: Intra-particle diffusion plot for the adsorption process (Geopolymer dosage = 4 g/L, Time 20 - 80 minutes, [MB] = 25 mg/L, T = 298 K, pH 10 and V = 0.025 L).

Explanation of these phases was based on reports earlier presented by Ji *et al*. (2009). The plot in this study revealed a linear step, corresponding to fast uptake of sorbate. The line in the initial stage does not pass through the origin. The MB removal was dominated by film diffusion more than it does for the intra-particle diffusion process. Sorbate adsorption speeds up in the second stage reflecting nonconsecutive diffusion of molecules into the micro pores with wider pore width within the sorbent (Ji *et al*., 2009). Diffusion remained fairly constant in the third phase when the pore volume was exhausted. Generally, adsorption controlled by means of the intra-particle model is due to the preferential adsorption of sorbate into the micro pores (Ji *et al*., 2009).

4.12.8.2. Deduction of k_{id} in terms of percentage sorption

The intra-particle diffusion parameters obtained are tabulated in table 4.16.

Table 4.16: Intra-particle diffusion parameters for the sorption of MB onto geopolymers

Geopolymer	K_{id}	a	R^2
GP-1	23.6	0.293	0.813
GP-1C	30.63	0.237	0.867
GP-1E	36.37	0.197	0.658
GP-2	27.25	0.265	0.845
GP-2C	64.61	0.072	0.943
GP-2E	49.46	0.139	0.908
GP-3	76.3	0.033	0.413
GP-3C	78.45	0.031	0.906
GP-3E	67.53	0.067	0.854

k_{id}= is diffusion rate constant, 'a'= diffusion mechanism

The values of 'a' depict the adsorption mechanism. K_{id} is the intra-particle rate constant ($time^{-1}$). It is taken as rate factor i.e. percent of sorbate adsorbed per unit time ($mgg^{-1}min^{-1}$). The K_{id} values obtained were 23.6, 30.63, 36.37, 27.25, 64.61, 49.46, 76.3, 78.45 and 67.53 $mgg^{-1}min^{-1}$ for GP-1, GP-1C, GP-1E, GP-2, GP-2C, GP-2E, GP-3, GP-3C and GP-

3E respectively. The K_{id} values increased with increase in Si/Al ratio and upon functionalization as observed in table 4.16. Larger k_{id} values expound higher adsorption which is related to improved bonding among sorbate and sorbent particles (Demirbas *et al*., 2004). Also higher value of k_{id} illustrate an enhanced rate of adsorption (Itodo *et al*., 2010).

4.12.8.3 Intra-particulate diffusivities of sorbate on sorbents

The fractional attainment at equilibrium is the ratio of the amounts of sorbate removed from solution after a certain time to that removed when sorption equilibrium is attained (Itodo *et al*., 2010). It would definitely be expected that factors such as the number of reactive sites on the substrate and the bulkiness of the substrate would affect the rate of sorption of MB. However, a great deal of information is obtained from the fractional attainment of equilibrium. The rate of attainment of equilibrium may be either film diffusion controlled or particle-diffusion controlled, even though this two different mechanisms cannot be sharply demarcated (Okieimen and Okundia, 1991). The fractional attainment at equilibrium α was calculated from the relationship in equation 4.2.

$$\alpha_e = q_t / q_e \quad \ldots\ldots 4.2$$

Where q_t is the amount of sorbate at any time t and q_e is the amount at infinity (That is. equilibrium) with units in mg/g. The plot of α_e against time is shown in figure 4.60.

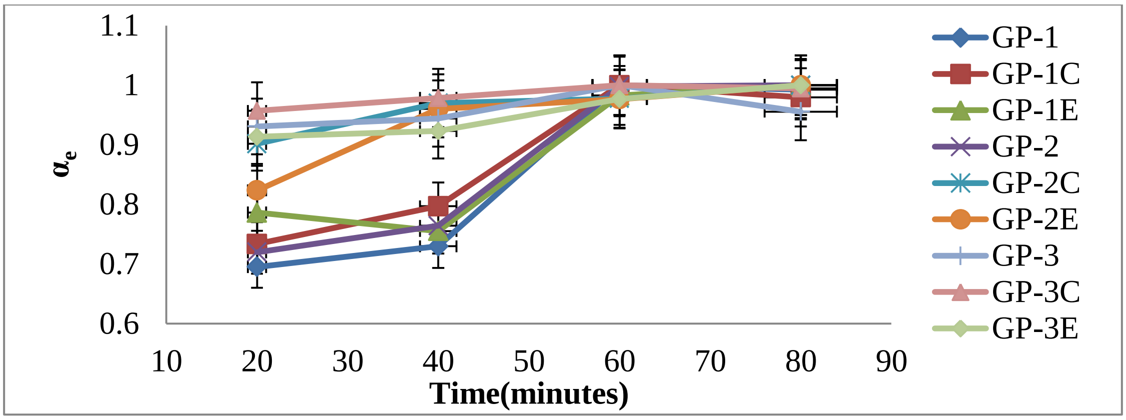

Figure 4.60: Fractional attainment at equilibrium(α) against time for MB uptake by geopolymer sorbents (Temp= 25 ± 2 ºC, pH=10, shaking speed of 120 rpm and MB concentration =25 mg/L).

It is observed that the value of α_e with change in time increased from about 0.695, 0.734, 0.931 and 0.957 to 1.00 at 60 min for GP-1, GP-1C, GP-3 and GP-3C respectively while for GP-1E, GP-2, GP-2C, and GP-2E and GP-3E, the αe value changed from 0.786, 0.720, 0.902, 0.824 and 0.914 and converge to one at 80 min respectively. These values of α_e at 60 and 80 minutes showed that MB was adsorbed most, followed by 40 minutes and least at 20 minutes. This means that the rate of adsorption at 60 and 80 minutes was faster (Itodo *et al*., 2010).

Equation 4.3 shows the relationship for particle-diffusion controlled sorption processes as a driving force developed using linear regression (Okieimen and Okundia, 1991).

In $(1-\alpha_e) = -k_p t$ …………………………………………………………….…..… 4.3

α_e is the fractional attainment of equilibrium, it thus implies that equilibrium time for this analysis was 60 minutes for GP-1, GP-1C, GP-3 and GP-3C while that of GP-1E, GP-2, GP-2C, and GP-2E and GP-3E was 80 minutes. k_p is the rate coefficient for particle diffusion controlled process corresponding to particle size of the sorbent. k_p values were

estimated as the rate of diffusion "t" was time and In (1- α_e) was a measure of the intraparticulate diffusivity with negative values as shown in appendix 8. In this analysis, linear plots with correlation coefficient values of R^2=0.910, 0.945, 0.710, 0.777, 0.893, 0.929, 0.975, 1 and 0.816 were obtained (Figure 4.61). It thus follows that the sorption process is particle- diffusion controlled (Itodo *et al*., 2010).

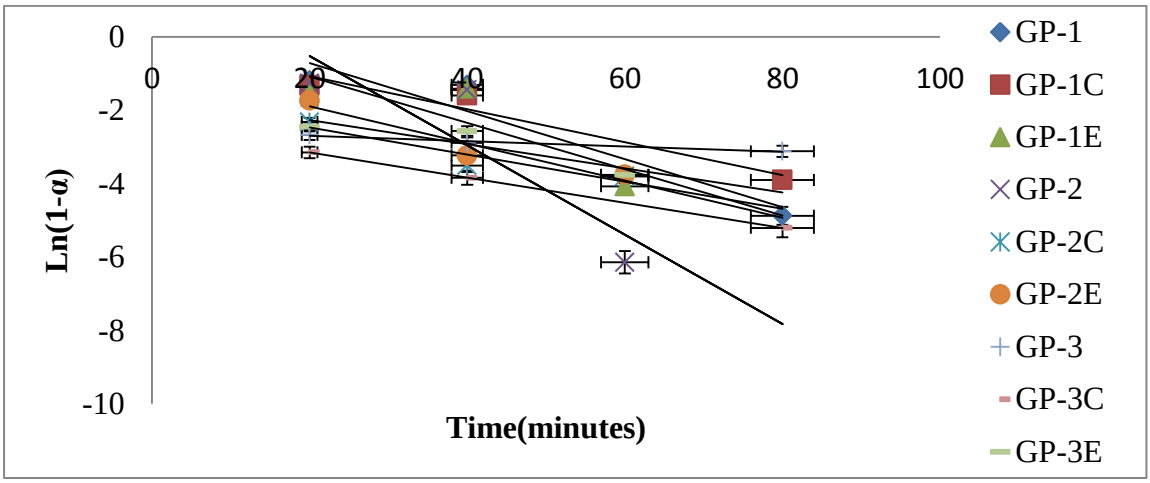

Figure 4.61: Particle diffusion controlled sorption for MB uptake by geopolymer sorbents (Temp = 25 °C ± 2, pH=10, shaking speed of 150 rpm and MB concentration = 25 mg/L).

4.12.9 Thermodynamic parameters

Thermodynamic parameters were investigated to determine whether the adsorption phenomenon was favourable or not. ΔG°, ΔH°, and ΔS° were obtained from the experimental studies at different temperatures of 298, 308, 318 and 328 K by applying equations 3.4 and 3.5 in the previous chapter and plots are shown in appendix 10. Thermodynamic parameters obtained are shown in table 4.17

Table 4.17: Thermodynamic parameters for the adsorption of MB onto geopolymers

			ΔG° (kJ/mol)			
	ΔH°	ΔS°	298K	308K	318K	328K
GP	(kJ/mol)	(J/mol/K)	Mean±SD	Mean±SD	Mean±SD	Mean±SD
1	4.4	18.59	-2.56 ± 0.02^{a}	-3.05 ± 0.04^{b}	-3.71 ± 0.02^{c}	-3.75 ± 0.10^{c}
1C	4.73	20.34	-3.09 ± 0.07^{a}	-3.45 ± 0.06^{b}	-4.14 ± 0.04^{c}	-4.41 ± 0.03^{d}
1E	3.15	14.94	-2.97 ± 0.02^{a}	3.21 ± 0.08^{b}	-4.02 ± 0.04^{d}	-3.83 ± 0.02^{c}
2	5.85	23.93	-2.88 ± 0.04^{a}	-3.61 ± 0.05^{b}	-4.13 ± 0.03^{c}	-4.53 ± 0.08^{d}
2C	2.34	13.70	-4.06 ± 0.05^{a}	-4.31 ± 0.08^{b}	-4.57 ± 0.08^{c}	-5.04 ± 0.07^{d}
2E	2.66	15.50	-4.35 ± 0.03^{a}	-5.06 ± 0.03^{b}	-5.33 c± 0.05^{c}	-5.39 ± 0.04^{d}
3	3.61	19.01	-4.65 ± 0.02^{a}	-5.27 ± 0.05^{b}	-5.73 ± 0.05^{c}	-5.92 ± 0.12^{d}
3C	10.30	42.77	-5.66 ± 0.08^{a}	-6.17 ± 0.08^{b}	-8.37 ± 0.13^{c}	-8.16 ± 0.10^{c}
3E	0.85	10.47	-5.07 ± 0.02^{a}	-5.68 ± 0.04^{b}	-5.75 ± 0.02^{c}	-5.82 ± 0.02^{d}

Means in a row with the same letter are not significantly different from each other (Tukey–Kramer test, P>0.05), SD= standard deviation, GP= geopolymer, ΔH° = standard enthalpy change, ΔS° = standard entropy change and ΔG° = standard free energy change).

The ΔG° values changed from -2.56 ± 0.02, -3.09 ± 0.07, -2.97 ± 0.02, -2.88 ± 0.04, -4.06 ± 0.05, -4.35 ± 0.03, -4.65 ± 0.02, -5.66 ± 0.08 and -5.07 ± 0.02 to -3.75 ± 0.10, -4.41 ± 0.03, -3.83 ± 0.02, -4.53 ± 0.08, -5.04 ± 0.07, -5.39 ± 0.04, -5.92 ± 0.12, -8.16 ± 0.10 and -5.82 ± 0.02 while the temperatures varied from 298 to 328 K for GP-1, GP-1C, GP-1E, GP-2, GP-2C, GP-2E, GP-3, GP-3C and GP-3E respectively. These negative values indicate that dye adsorption reaction was spontaneous in nature at all the studied temperatures. The decrease in ΔG° values with increasing temperature was an indication that MB adsorption on geopolymer was more favourable (Selçuk, 2017).

It was evident from table 4.17, that the adsorption of methylene blue was endothermic since the values of ΔH° were positive. Similar results for endothermic adsorption were observed on bentonite, activated carbon prepared from deoiled soya (Önal *et al*.,2006), activated carbon prepared from Tuncbilek lignite and hen feathers. Also noted was that

increase in Si/Al ratio and functionalization decreased ΔG° values an indication of increased favourability of adsorption process. The values of ΔG° were between 0 and 20 kJ/mole which is consistent with electrostatic interaction between adsorption sites and the adsorbing ions (physical adsorption) (Al-Othman *et al*., 2013). The positive value of ΔS° showed the increased randomness of the adsorbate molecules on the solid surfaces than in the solution for methylene blue dye.

CHAPTER FIVE

CONCLUSIONS AND RECOMMENDATIONS

5.1 Conclusions

This study was carried out to investigate suitability for use of common clay in geopolymer synthesis for adsorption application and whether tethering them with EDTA and citric acid functional groups would enhance their adsorption efficiencies. The results have shown that:

i. Common clays from Molo, Kuresoi and Kakamega contained silica and alumina as their main chemical components, with all the three types containing over 65 % weight (SiO_2 + Al_2O_3) as shown by the EDX analysis results. Rice husk ash was found to contain a high percentage of silica.

ii. Calcined common clays from Molo, Kuresoi and Kakamega were a potential source of aluminosilicate and when blended with rice husk ash became potential raw materials for geopolymer synthesis. This was shown by XRD analysis which indicated presence of an amorphous hump between 18 – 36° (2θ) as reported by other researchers (Guo *et al*., 2010). The FTIR indicated presence of stretching vibrations of bonds of Al-O and Si-O, which are finger prints of geopolymerization. SEM coupled with EDS analysis confirmed geopolymerization occurred with the former images showing presence of dense concrete shaped structures and the later indicating presence of phases containing Na- Si- Al in bulk regions suggesting presence of silicate - activated gel by polymerization (Silva *et al*., 2007).

iii. Functionalization of geopolymers with EDTA and citric acid was achieved. This was proven by presence of –COO- functional groups identified by FTIR and which were missing in the original geopolymers. SEM images also showed change in the microstructures upon functionalization.

iv. Percentage uptake of Pb (II), Cd (II), Zn (II) and MB was found to be dependent on pH, contact time, shaking speed, temperature, sorbent dose, initial pollutant concentrations and Si/Al ratio in geopolymers. GP-3 gave higher mean percentage removals of the pollutants. Functionalization increased the pollutants uptake. Geopolymers with higher SiO_2/Al_2O_3 ratios are better adsorbents since they contains higher negative environment that boosts adsorption of positively charged pollutants. Functionalization increased the uptakes and therefore GP-3C and GP-3E were the best adsorbents of the four water pollutants studied.

v. Experimental data was fitted in various equilibrium models. Based on their correlation coefficients (R^2), the data was found to fit best in Sips model and hence the model was used to predict the adsorption capacities of the geopolymer adsorbents. From the adsorption capacities obtained of the four pollutants, it is apparent that citric acid functionalized geopolymer synthesized from Molo clay was the best adsorbent of the Pb (II), Cd (II), Zn (II) ions and cationic MB.

vi. Regeneration of the used adsorbents showed that the adsorbent materials synthesized can easily be recovered hence reducing the effects of secondary pollution that may emanate from their uses. Over 60 % recovery was attained on unfunctionalized geopolymers. Although functionalized geopolymers have very

high pollutant removal efficiencies, they have more negative environmental impact due to their low levels of regeneration compared to unfunctionalized ones.

vii. Transient behaviour of adsorption of Pb (II), Zn (II), Cd (II) and methylene blue was done using pseudo-first order, pseudo-second order and intra-particle diffusion models. Based on correlation coefficients, the data was found to follow pseudo- second order kinetics and the adsorption process of the four studied pollutants utilized valence forces and exchangeable electrons between the adsorbents and adsorbate. Chemisorption was more pronounced in the rate determining step hence drawing a conclusion that the process was mainly physiosorption.

5.2 Recommendations

5.2.1 Recommendations from this study

i. The use of common clays as a source of aluminosilicate and rice husk ash as a source of silica be enhanced in the synthesis of geopolymers for adsorption applications that will go a long way in solving the problem of presence of heavy metals and dyes in our water systems.

ii. Tethering of geopolymers using citric acid is encouraged to enhance adsorption efficiency.

iii. Industries that use heavy metals as raw materials or produce products of heavy metals and dyes be encouraged to embrace geopolymer filters before allowing their industrial effluents to the water systems.

5.2.2 Recommendation for further studies

i. Clays from other areas should be studied on their effectiveness as raw materials for geopolymer synthesis.

ii. Geopolymer synthesis parameters such as temperature, concentration of stabilizers among others to be studied on their effect on adsorption efficiencies of geopolymers.

iii. Functionalization using other agents with different functional groups be studied to check their effectiveness.

iv. Further research need to be done on synergistic effects of other components contained in the raw materials on adsorption properties of geopolymers.

v. Adsorption studies of the geopolymers using industrial wastewaters and effects of interfering ions are carried out studied.

vi. Adsorption of anionic pollutants using geopolymers be studied.

REFFERENCES

Abdelghani, N. T., and Elchaghaby, G. A. (2007). Influence of operating conditions on the removal of Cu, Zn, Cd and Pb ions from waste water by adsorption. *International Journal of Environtal Science and Technology*, **4,** 451–456.

Abdelghhani, N. T., Hefny, M., and Elchaghaby, G. A. F. (2007). Removal of lead from aqueous solution using low cost abundantly available adsorbents. *International Journal of Environmental Science and Technology*, **4,** 67–73.

Abechi, S. E., Gimba, C. E., and Uzairu, A., O. J. (2013). Equilibrium Adsorption Studies Of Methylene Blue Onto Palm Kernel Shell-Based Activated Carbon. *International Refereed Journal of Engineering and Science*, **2,** 38–45.

Abou-Arab, A. A. K., Ayesh, A. M., Amra, H. A., and Naguib, K. (1996). Characteristic levels of some pesticides and heavy metals in imported fish. *Food Chemistry*, **57,** 487–492.

Acar, F. N., and Eren, Z. (2006). Removal of Cu(II) ions by activated poplar sawdust (Samsun Clone) from aqueous solutions. *Journal of Hazardous Materials*, **137,** 909–914.

Adam, F., Balakrishnan, S., and Wong, P. L. (2006). Rice Husk Ash Silica As a Support Material for Ruthenium Based Heterogenous Catalyst. *Journal of Physical Science*, **17,** 1–13.

Addour, L., Belhocine, D., Boudries, N., Comeau, Y., Pauss, A., and Mameri, N. (1999). Zinc uptake by Streptomyces rimosus biomass using a packed-bed column. *Journal of Chemical Technology and Biotechnology*, **74,** 1089–1095.

Aeisyah, A., Ismail, M. H. S., Lias, K., and Izhar, S. (2014). Adsorption process of heavy metals by low-cost adsorbent: A review. *Research Journal of Chemistry and Environment*, **18,** 91–102.

Agbozu, I. E., and Emoruwa, F. O. (2014). Batch adsorption of heavy metals (Cu, Pb, Fe, Cr and Cd) from aqueous solutions using coconut husk. *African Journal of Environmental Science and Technology*, **8,** 239–246.

Akpomie, K. G., Dawodu, F. A., and Adebowale, K. O. (2015). Mechanism on the sorption of heavy metals from binary-solution by a low cost montmorillonite and its desorption potential. *Alexandria Engineering Journal*, **54,** 757–767.

Akpor, O. B. (2014). Heavy Metal Pollutants in Wastewater Effluents: Sources, Effects and Remediation. *Advances in Bioscience and Bioengineering*, **2,** 37- 48.

Aksu, Z., and Kutsal, T. (1991). A bioseparation process for removing lead (II) ions from waste water by using Chlorella vulgaris. *Journal of Chemical Technology and Biotechnology*, **52,** 109–118.

Al-Anber, Z. A., and Al-Anber, M. A. S. (2008). Thermodynamics and kinetic studies of iron(iii) adsorption by olive cake in a batch system. *Journal of the Mexican Chemical Society*, **52,** 108–115.

Al-Anber, Z. A., and Matouq, M. A. D. (2008). Batch adsorption of cadmium ions from aqueous solution by means of olive cake. *Journal of Hazardous Materials*, **151,** 194–201.

Al bakri Abdullah, M. M., Hussin, K., Bnhussain, M., Ismail, K. N., Yahya, Z., and Razak, R. A. (2012). Fly ash-based geopolymer lightweight concrete using foaming agent. *International Journal of Molecular Sciences*, ***13,*** 7186–7198.

Al-Ghouti, M., Khraisheh, M. A. M., Ahmad, M. N. M., and Allen, S. (2005). Thermodynamic behavior and the effect of temperature on the removal of dyes from aqueous solution using modified diatomite: A kinetic study. *Section Title: Surface Chemistry and Colloids*, **287,** 6–13.

Ali, W. N. N. W., Sufian, S., and Abdullah, M. Z. (2016). Green Functionalization: Comparison of Different Carbonaceous Materials. *Procedia Engineering*, **148,** 795–805.

Al-Othman, Z. A., Habila, M. A., Ali, R., and Hassouna, I and Mohamed Salah el-Din. (2013). Kinetic and Thermodynamic Studies for Methylene Blue Adsorption using Activated Carbon Prepared from Agricultural and Municipal Solid Wastes. *Asian Journal of Chemistry*, **25,** 8301–8306.

Al-Zboon, K., Al-Harahsheh, M. S., and Hani, F. B. (2011). Fly ash-based geopolymer for Pb removal from aqueous solution. *Journal of Hazardous Materials*, **188,** 414–421.

Alexander, B. H., Checkoway, H., van Netten, C., Muller, C. H., Ewers, T. G., Kaufman, J. D., and Faustman, E. M. (1996). Semen quality of men employed at a lead smelter. *Occupational and Environmental Medicine*, **53,** 411–416.

Alonso, S., and Palomo, A. (2001). Alkaline activation of metakaolin and calcium hydroxide mixtures: Influence of temperature, activator concentration and solids ratio. *Materials Letters*, **47,** 55–62.

Alyüz, B., and Veli, S. (2009). Kinetics and equilibrium studies for the removal of nickel and zinc from aqueous solutions by ion exchange resins. *Journal of Hazardous Materials*, **167,** 482–488.

Alzaydien, A. S. (2009). Adsorption of methylene blue from aqueous solution onto a low-cost natural Jordanian Tripoli. *American Journal of Applied Sciences*, **6,** 1047–1058.

Amarasinghe, B. M. W. P. K., and Williams, R. A. (2007). Tea waste as a low cost adsorbent for the removal of Cu and Pb from wastewater. *Chemical Engineering Journal*, **132,** 299–309.

Amer, M. W., Khalili, F. I., and Awwad, A. M. (2010). Adsorption of lead , zinc and cadmium ions on polyphosphate-modified kaolinite clay. *Environmental Chemistry*, **2,** 001–008.

Amir, H., Mahvi, D., Naghipour, and Forugh Vaezi, S. N. (2005). Teawaste as An Adsorbent for Heavy Metal Removal from Industrial Wastewaters. *American Journal of Applied Sciences*, **2,** 372–375.

Amrhar, O., Nassali, H., and Elyoubi, M. S. (2015). Adsorption of a cationic dye, Methylene

Blue, onto Moroccan Illitic Clay. *Journal of Material and Environment Science*, **6,** 3054–3065.

Amuda, O. S., Olayiwola, A. O., and Alade, A. O. (2014). Adsorption of Methylene Blue from Aqueous Solution Using Steam-Activated Carbon Produced from Lantana camara Stem. *Journal of Environmental Protection*, **1,** 1352–1363.

Andrabi, S. M. A. (2011). Sawdust of lam tree (Cordia africana) as a low-cost, sustainable and easily available adsorbent for the removal of toxic metals like Pb(II) and Ni(II) from aqueous solution. *European Journal of Wood and Wood Products*, **69,** 75–83.

Andreoli, M., Luca, G. T., and Miyamaru Seo, E. S. (2000). Characteristics of rice husks for chlorination reaction. *Materials Letters*, **44,** 294–298.

Annadurai, G., Juang, R. S., and Lee, D. J. (2002). Use of cellulose-based wastes for adsorption of dyes from aqueous solutions. *Journal of Hazardous Materials*, **92,** 263–274.

Anwar, J., Shafique, U., Waheed-uz-Zaman, Salman, M., Dar, A., and Anwar, S. (2010). Removal of Pb(II) and Cd(II) from water by adsorption on peels of banana. *Bioresource Technology*, **101,** 1752–1755.

Aranberri, I., and Bismarck, A. (2007). Caracterización Superficial de Minrales Arcillosos Presentes en los Depósitos de Crudo. *Anales de Quimica*, **103,** 23–27.

Arias, F., and Sen, T. K. (2009). Removal of zinc metal ion (Zn^{2+}) from its aqueous solution by kaolin clay mineral: A kinetic and equilibrium study. *Colloids and Surfaces A: Physicochemical and Engineering Aspects*, **348,** 100–108.

Arshadi, M., Amiri, M. J., and Mousavi, S. (2014). Kinetic, equilibrium and thermodynamic investigations of Ni(II), Cd(II), Cu(II) and Co(II) adsorption on barley straw ash. *Water Resources and Industry*, **6,** 1–17.

Aruldhas, M. M., Subramanian, S., Sekar, P., Vengatesh, G., Chandrahasan, G., Govindarajulu, P., and Akbarsha, M. A. (2005). Chronic chromium exposure-induced changes in testicular histoarchitecture are associated with oxidative stress: Study in a non-human primate (Macaca radiata Geoffroy). *Human Reproduction*, **20,** 2801–2813.

Aziz, H. A., Adlan, M. N., and Ariffin, K. S. (2008). Heavy metals (Cd, Pb, Zn, Ni, Cu and Cr(III)) removal from water in Malaysia: post treatment by high quality limestone. *Bioresource Technology*, **99,** 1578–1583.

Aziz, H. A., Yusoff, M. S., Adlan, M. N., Adnan, N. H., and Alias, S. (2004). Physico-chemical removal of iron from semi-aerobic landfill leachate by limestone filter. *Waste Management*, **24,** 353–358.

Babel, S., and Kurniawan, T. A. (2003). Low-cost adsorbents for heavy metals uptake from contaminated water: a review. *Journal of Hazardous Materials*, **97,** 219–243.

Babel, S., and Kurniawan, T. A. (2004). Cr(VI) removal from synthetic wastewater using

coconut shell charcoal and commercial activated carbon modified with oxidizing agents and/or chitosan. *Chemosphere*, **54,** 951–967.

Baker, C. (2017). Quantitative research designs: Experimental, quasi-experimental, and descriptive. *Jones and Bartlett Learning,* pp.155–183.

Balakrishnan, V., Arivoli, S., Begum, A. S., Ahamed, A. J., and Nadu, T. (2010). *Journal of Chemical and Pharmaceutical Research,* **2,** 176–190.

Banat, F. A., Al-Bashir, B., Al-Asheh, S., and Hayajneh, O. (2000). Adsorption of phenol by bentonite. *Environmental Pollution*, **107,** 391–398.

Barakat, M. A. (2011). New trends in removing heavy metals from industrial wastewater. *Arabian Journal of Chemistry*, **4,** 361–377.

Baranauskas, A., Jasaitis, D., and Kareiva, A. (2002). Characterization of sol-gel process in the Y-Ba-Cu-O acetate-tartrate system using IR spectroscopy. *Vibrational Spectroscopy,* **28,** 263–275.

Baral, S. S., Das, S. N., and Rath, P. (2006). Hexavalent chromium removal from aqueous solution by adsorption on treated sawdust. *Biochemical Engineering Journal*, **31,** 216–222.

Barbosa, V. F. F., and MacKenzie, J. D. (2003). Synthesis and thermal behaviour of potassium sialate geopolymers. *Materials Letters,* **57,** 1477–1482.

Barrer, R. M., and Mainwaring, D. E. (1972). Chemistry of soil minerals. Part XI. Hydrothermal transformations of metakaolinite in potassium hydroxide. *Journal of the Chemical Society, Dalton Transactions*, **12,** 1254- 1263.

Beagle, E. C. (1978). Rice-husk, conversion to energy FAO agricultural services bulletin; 31, Food and Agriculture Organization of the United Nations, Rome.

Bello, O. S., and Ahmad, M. A. (2011). Adsorptive removal of a synthetic textile dye using cocoa pod husks. *Toxicological and Environmental Chemistry*, **93,** 1298–1308.

Berhe, S., Ayele, D., Tadesse, A., and Mulu, A. (2015). Adsorption Efficiency of Coffee Husk for Removal of Lead (II) from Industrial Effluents : *Equilibrium,* **5,** 1–8.

Bernard, E., Jimoh, A, and Odigure, J. O. (2013). Heavy Metals Removal from Industrial Wastewater by Activated Carbon Prepared from Coconut Shell. *Research Journal of Chemical Sciences*, **3,** 3–9.

Beyer, H. (2002). Dealumination techniques for zeolites. *Post-Synthesis Modification I,* **3,** 203–255.

Bhattacharya, A. K., Mandal, S. N., and Das, S. K. (2006). Adsorption of Zn(II) from aqueous solution by using different adsorbents. *Chemical Engineering Journal*, **123,** 43–51.

Bhattacharya, A. K., Naiya, T. K., Mandal, S. N., and Das, S. K. (2008). Adsorption, kinetics

and equilibrium studies on removal of Cr(VI) from aqueous solutions using different low-cost adsorbents. *Chemical Engineering Journal*, **137,** 529–541.

Bhattacharya, S. C., Arul Joe, M., Kandhekar, Z., Abdul Salam, P., and Shrestha, R. M. (1999). Greenhouse-gas emission mitigation from the use of agricultural residues: The case of ricehusk. *Energy*, **24,** 43–59.

Biswas, S., and Mishra, U. (2015). Continuous Fixed-Bed Column Study and Adsorption Modeling: Removal of Lead Ion from Aqueous Solution by Charcoal Originated from Chemical Carbonization of Rubber Wood Sawdust. *Journal of Chemistry, 2015*. https://doi.org/10.1155/2015/907379.

Blum, A.,and Lasaga, A. (1988). Role of surface speciation in the low temperature dissoltion of minerals. *Nature*, **331,** 431–433.

Buchwald, A., Zellmann, H. D., and Kaps, C. (2011). Condensation of aluminosilicate gels-model system for geopolymer binders. *Journal of Non-Crystalline Solids*, **357,** 1376–1382.

Bueno, B. Y. M., Torem, M. L., Molina, F., and de Mesquita, L. M. S. (2008). Biosorption of lead(II), chromium(III) and copper(II) by R. opacus: Equilibrium and kinetic studies. *Minerals Engineering*, **21,** 65–75.

Bulut, Y., and Aydin, H. (2006). A kinetics and thermodynamics study of methylene blue adsorption on wheat shells. *Desalination*, **194,** 259–267.

Bundy, W. M. (1993). The diverse industrial applications of kaolin. Kaolin Genesis and Utilization (Murray, H. H., Bundy, W. and Harvey, C., eds.). *Clay Mineral Society*, **1,** 43–47.

Bushra, K., Azra, Y., Muhammed, F., Lubna, L. and Benish, I. (2010). Study of Colour Measurements of Leather Dyed with Walnut Bark Natural Dye. *Journal of Industrial Resources*, **53,** 252–257.

Castro-González, M. I., and Méndez-Armenta, M. (2008). Heavy metals: Implications associated to fish consumption. *Environmental Toxicology and Pharmacology*, **26,** 263-271.

Chand, P., and Pakade, Y. B. (2013). Removal of Pb from water by adsorption on apple pomace: Equilibrium, kinetics, and thermodynamics studies. *Journal of Chemistry*. https://doi.org/10.1155/2013/164575

Chen, G. (2004). Electrochemical technologies in wastewater treatment. *Separation and Purification Technology*, **38,** 11–41.

Chen, H. L., and Burns, L. D. (2006). Environmental Analysis of Textile Products. *Clothing and Textiles Research Journal*, **24,** 248–261.

Cheng, T. W., Lee, M. L., Ko, M. S., Ueng, T. H., and Yang, S. F. (2012). The heavy metal adsorption characteristics on metakaolin-based geopolymer. *Applied Clay Science*, **56,**

90–96.

Chiem, L. T., Huynh, L., Ralston, J., and Beattie, D. A. (2006). An insitu ATR-FTIR study of polyacrylamide adsorption at the talc surface. *Journal of Colloid and Interface Science*, **297,** 54–61.

Cols, N., Roepstorff, K., Gonzàlez-Duarte, R., and Atrian, S. (2001). Secretion of mouse-metallothionein by engineered E. coli cells in metal-enriched culture media. *Journal of Molecular Microbiology and Biotechnology*, **3,** 507–512.

Connors, K. A. (1990). Uses of chemical kinetics. In Chemical Kinetics: The Study of Reaction Rates in Solution pp. 2-4.

Consolin, F. N., Venancio, E. C., Barriquello, M. F., Hechenleitner, A. A. W., and Pineda, E. A. G. (2007). Methylene blue adsorption onto modified lignin from sugar cane bagasse. *Ecletica Quimica*, **32,** 63–70.

Crea, F., Aiello, R., Nastro, A., and Nagy, J. B. (1991). Synthesis of ZSM-5 zeolite from very dense systems: Formation of pelleted ZSM-5 zeolite from (Na, Li, TPA, Si, Al) hydrogels. *Zeolites*, **11,** 521–527.

Cullum, B. M., and Vo-dinh, T. (2014). Preparation of Liquid and Solid Samples. *Handbook of Spectroscopy*, **1,** 3–14.

Dada, A., Olalekan, A., Olatunya, A., and Dada, O. (2012). Langmuir , Freundlich , Temkin and Dubinin – Radushkevich Isotherms Studies of Equilibrium Sorption of Zn^{2+} Unto Phosphoric Acid Modified Rice Husk. *IOSR Journal of Applied Chemistry*, **3,** 38–45.

Davidovits, J. (1989). Geopolymers and geopolymeric materials. *Journal of Thermal Analysis*, **35,** 429–441.

Davidovits, J. (1991). Geopolymers - Inorganic polymeric new materials. *Journal of Thermal Analysis*, **37,** 1633–1656.

Davidovits, J. (1998). Geopolymer chemistry and properties. *1st European Conference on Soft Mineralurgy, Compiegne, France*, **1,** 25–48.

Davidovits, J., Douglas C. Comrie, John H., and Paterson, D. J. R. (1990). Geopolymeric concrete for environmental protection. *Concrete International*, **12,** 30–40.

Dehghani, M. H., Mesdaghinia, A. R., Nasseri, S., Mahvi, A. H., and Azam, K. (2008). Application of SCR technology for degradation of reactive yellow dye in aqueous solution. *Water Quality Resource Journal of Canada*, **43,** 1–10.

Della, V. P., Kühn, I., and Hotza, D. (2002). Rice husk ash as an alternate source for active silica production. *Materials Letters*, **57,** 818–821.

Demirbas, E., Kobya, M., Senturk, E., and Ozkan, T. (2004). Adsorption kinetics for the removal of chromium (VI) from aqueous solutions on the activated carbons prepared from agricultural wastes. *Water SA*, **30,** 533–539.

Deosarkar, S. D. (2012). Thermodynamics of adsorption of Pb (II) and Cd (II) metal ions from aqueous solution by Punica granatum L . husk. *Journal of Hazardous Materials*, **4,** 3319–3323.

Derakhshan, Z., and Baghapour, M. (2013). Adsorption of Methylene Blue Dye from Aqueous Solutions by Modified Pumice Stone: Kinetics and Equilibrium Studies. *Health Scope*, **2,** 136–144.

Dermont, G., Bergeron, M., Mercier, G., and Richer-Laflèche, M. (2008). Metal-Contaminated Soils: Remediation Practices and Treatment Technologies. *Practice Periodical of Hazardous, Toxic and Radioactive Waste Management*, **12,** 188–209.

Ding, W., Dong, X., Ime, I. M., Gao, B., and Ma, L. Q. (2014). Pyrolytic temperatures impact lead sorption mechanisms by bagasse biochars. *Chemosphere*, **105,** 68–74. .

Dogan, M. A. (2003). Adsorptionkineticsofmethylvioletontoperlite. *Chemosphere*, ***50,*** 517–528.

Dubey, A., and Shiwani, S. (2012). Adsorption of lead using a new green material obtained from Portulaca plant. *International Journal of Environmental Science and Technology*, **9,** 15–20.

Duruibe, J. O., Ogwuegbu, M. O. C., and Egwurugwu, J. N. (2007). Heavy metal pollution and human biotoxic effects. *International Journal of Physical Sciences*, **2,** 112–118.

Duxson, P., Fernández-Jiménez, A., Provis, J. L., Lukey, G. C., Palomo, A., and Van Deventer, J. S. J. (2007). Geopolymer technology: The current state of the art. *Journal of Materials Science*, **42,** 2917–2933.

Duxson, P., Lukey, G. C., and Van Deventer, J. S. J. (2007). Physical evolution of Na-geopolymer derived from metakaolin up to 1000 °C. *Journal of Materials Science*, **42,** 3044–3054.

Duxson, P., Provis, J. L., Lukey, G. C., Mallicoat, S. W., Kriven, W. M., and Van Deventer, J. S. J. (2005). Understanding the relationship between geopolymer composition, microstructure and mechanical properties. *Colloids and Surfaces A: Physicochemical and Engineering Aspects*, **269,** 47–58.

Duxson, P., Provis, J. L., Lukey, G. C., Mallicoat, S. W., Kriven, W. M., and Van Deventer, J. S. J. (2005). Understanding the relationship between geopolymer composition, microstructure and mechanical properties. *Colloids and Surfaces A: Physicochemical and Engineering Aspects*, **269,** 1–3.

Ebrahimian Pirbazari, A., Saberikhah, E., Badrouh, M., and Emami, M. S. (2014). Alkali treated Foumanat tea waste as an efficient adsorbent for methylene blue adsorption from aqueous solution. *Water Resources and Industry*, ***6,*** 64–80.

Eccles, H. (1999). Treatment of metal-contaminated wastes: Why select a biological process? *Trends in Biotechnology*, **17,** 462–465.

Edokpayi, J. N., Odiyo, J. O., Msagati, T. A. M., and Popoola, E. O. (2015). A Novel Approach for the Removal of Lead(II) Ion from Wastewater Using Mucilaginous Leaves of Diceriocaryum eriocarpum Plant, (Ii), pp,14026–14041.

El-Ashtoukhy, E. S. Z., Amin, N. K., and Abdelwahab, O. (2008). Removal of lead (II) and copper (II) from aqueous solution using pomegranate peel as a new adsorbent. *Desalination*, **223,** 162–173.

Elass, K., Laachach, A., Alaoui, A., and Azzi, M. (2010). Removal of methylene blue from aqueous solution using ghassoul, a low-cost adsorbent. *Applied Ecology and Environmental Research*, **8**, 153–163.

Elmorsi, T. M., Mohamed, Z. H., Shopak, W., and Ismaiel, A. M. (2014). Kinetic and Equilibrium Isotherms Studies of Adsorption of Pb (II) from Water onto Natural Adsorbent. *Journal of Environmental Protection*, **5,** 1667–1681.

El-Sayed, G. O. (2011). Removal of methylene blue and crystal violet from aqueous solutions by palm kernel fiber. *Desalination*, ***272,*** 225–232.

Erdem, E., Karapinar, N., and Donat, R. (2004). The removal of heavy metal cations by natural zeolites. *Journal of Colloid and Interface Science*, **280,** 309–314.

Eren, Z., and Acar, F. N. (2006). Adsorption of Reactive Black 5 from an aqueous solution: equilibrium and kinetic studies. *Desalination*, **194**, 1–10.

Erhayem, M., Al-tohami, F., Mohamed, R., and Ahmida, K. (2015). Isotherm , Kinetic and Thermodynamic Studies for the Sorption of Mercury (II) onto Activated Carbon from Rosmarinus officinalis Leaves. *American Journal of Analytical Chemistry*, **6,** 1–10.

Esrey, S. A., Feachem, R. G., and Hughes, J. M. (1985). Interventions for the control of diarrhoeal diseases among young children: Improving water supplies and excreta disposal facilities. *Bulletin of the World Health Organization*, **63,** 757–772.

Esrey, S. A, Potash, J. B., Roberts, L., and Shiff, C. (1991). Effects of improved water supply and sanitation on ascariasis, diarrhoea, dracunculiasis, hookworm infection, schistosomiasis, and trachoma. *Bulletin of the World Health Organization*, **69,** 609–621.

European Commission DG ENV. (2002). Heavy Metals in Waste. Department for Environment, Food and Rural Affairs.

Fahim, M. A., Nemmar, A., Dhanasekaran, S., Singh, S., Shafiullah, M., Yasin, J., and Hasan, M. Y. (2012). Acute cadmium exposure causes systemic and thromboembolic events in mice. *Physiological Research*, **61,** 73–80.

Faimon, J. (1996). Oscillatory silicon and aluminum aqueous concentrations during experimental aluminosilicate weathering. *Geochimica et Cosmochimica Acta*, **60,** 2901-2907.

Fatiha, M., and Belkacem, B. (2016). Adsorption of methylene blue from aqueous solutions using natural clay. *Journal of Materials and Environmental Science*, **7,** 285–292.

Fernández-Jiménez, A., and Palomo, A. (2005). Mid-infrared spectroscopic studies of alkali-activated fly ash structure. *Microporous and Mesoporous Materials*, **86,** 207–214.

Fernandez-Leborans, G., and Herrero, Y. O. (2000). Toxicity and bioaccumulation of lead and cadmium in marine protozoan communities. *Ecotoxicology and Environmental Safety*, **47,** 266–276.

Ferone, C., Colangelo, F., Roviello, G., Asprone, D., Menna, C., Balsamo, A., and Manfredi, G. (2013). Application-oriented chemical optimization of a metakaolin based geopolymer. *Materials*, **6,** 1920–1939.

Foo, K. Y., and Hameed, B. H. (2010). Insights into the modeling of adsorption isotherm systems. *Chemical Engineering Journal*, **156,** 2-10.

Fosmire, G. J. (1990). Zinc toxicity. *American Journal of Clinical Nutrition*, **51,** 225–227.

Fraga, C. G. (2005). Relevance, essentiality and toxicity of trace elements in human health. *Molecular Aspects of Medicine*, **26,** 235-244.

Freundlich, H. M. F. (1906). over the adsorption in solutions. *Journal of Physical Chemistry*, **57,** 385–471.

Fu, F., and Wang, Q. (2011). Removal of heavy metal ions from wastewaters : A review. *Journal of Environmental Management*, **92,** 407–418.

Garg, V. K., Gupta, R., Yadav, A. B., and Kumar, R. (2003). Dye removal from aqueous solution by adsorption on treated sawdust. *Bioresource Technology*, **89,** 121–124.

Ghassabzadeh, H., Ahmadi, S. J., and Taheri, H. (2010). Removal of cadmium and nickel from aqueous solution using expanded perlite. *Journal Brazilian Chemical Engineering*, **27,** 299–308.

Ghasemi, J., and Asadpour, S. (2007). Thermodynamics' study of the adsorption process of methylene blue on activated carbon at different ionic strengths. *Journal of Chemical Thermodynamics*, **39,** 967–971.

Ghazi Bin Ismail, M., Ngai Weng, C., Abdul Rahman, H., and Azazi Zakaria, N. (2013). Freundlich Isotherm Equilibrium Equastions in Determining Effectiveness a Low Cost Absorbent to Heavy Metal Removal In Wastewater (Leachate) At Teluk Kitang Landfill. *Journal of Geography and Earth Science*, **1,** 1–8.

Ghomri, F., Lahsini, A., Laajeb, A., and Addaou, A. (2013). The removal of heavy metal ions (copper , zinc , nickel and cobalt) by natural bentonite, pp. 37–54.

Ghosh, D., and Bhattacharyya, K. G. (2002). Adsorption of methylene blue on kaolinite. *Applied Clay Science*, **20,** 295–300.

Gialamouidis, D., Mitrakas, M., and Liakopoulou-Kyriakides, M. (2010). Equilibrium, thermodynamic and kinetic studies on biosorption of Mn(II) from aqueous solution by Pseudomonas sp., Staphylococcus xylosus and Blakeslea trispora cells. *Journal of*

Hazardous Materials, **182,** 672–680.

Glukhovsky, V. D. (1959). Soil silicates. Gosstroyizdat, Kiev, pp.154.

Goldberg, S. (2005). Equations and models describing adsorption processes in soils. Soil Science Society of America Book Series Number 8, pp. 489.

Gong, R., Li, M., Yang, C., Sun, Y., and Chen, J. (2005). Removal of cationic dyes from aqueous solution by adsorption on peanut hull. *Journal of Hazardous Materials*, **121,** 247–250.

Goretta, K. C., Gutierrez-Mora, F., Singh, D., Routbort, J. L., Lukey, G. C., and Van Deventer, J. S. J. (2007). Erosion of geopolymers made from industrial waste. *Journal of Materials Science*, **42,** 3066–3072.

Goyer, R. A., Diwan, B. A., Ward, J. M., and Devor, D. E. (1995). Renal Tubular Tumors and Atypical Hyperplasias in B6C3F1 Mice Exposed to Lead Acetate during Gestation and Lactation Occur with Minimal Chronic Nephropathy. *Cancer Research*, **55,** 5265–5271.

Granizo, M. L., Alonso, S., Blanco-Varela, M. T., and Palomo, A. (2002). Alkaline Activation of Metakaolin : Effect of Calcium Hydroxide in the Products of Reaction. *Journal of American Ceramc Society*, **85,** 225–231.

Grant, W. M. (1986).Toxicology of the Eye, Third Edition, Springfield, Illinois: C.C. Thomas, pp. 374- 375.

Grim, R. E. (1981). Technology of Clay. *Journal of American Ceramic Society*, **64,** 90- 99.

Grimshaw, R. W. (1971). The Chemistry and Physics of Clays and Allied Ceramic Materials. Ernest Benn Ltd, 4th Ed 1971, pp. 1–29.

Gunatilake, S. K. (2015). Methods of Removing Heavy Metals from Industrial Wastewater. *Journal of Multidisciplinary Engineering Science Studies*, **1,** 12–18.

Günay, A., Arslankaya, E., and Tosun, I. (2007). Lead removal from aqueous solution by natural and pretreated clinoptilolite: Adsorption equilibrium and kinetics. *Journal of Hazardous Materials*, **146,** 362–371.

Guo, X. L, Shi, H. S, and Dick, W. A. (2010). Compressive strength and microstructural characteristics of class C fly ash geopolymer. *Cement and Concrete Composites*, **32,** 142–147.

Hajimohammadi, A., Provis, J. L., and Van Deventer, J. S. J. (2011). The effect of silica availability on the mechanism of geopolymerisation. *Cement and Concrete Research*, **41,** 210–216.

Halder, J. N., and Islam, M. N. (2015). Water Pollution and its Impact on the Human Health, *Journal of Environmen*t and *Human*, **2,** 36–46.

Hameed, B. H., Ahmad, A. A., and Aziz, N. (2009). Adsorption of reactive dye on palm-oil

industry waste: Equilibrium, kinetic and thermodynamic studies. *Desalination*, **247,** 551–560.

Hameed, B. H., Din, A. T. M., and Ahmad, A. L. (2007). Adsorption of methylene blue onto bamboo-based activated carbon: Kinetics and equilibrium studies. *Journal of Hazardous Materials*, **141,** 819–825.

Hameed, B. H., Mahmoud, D. K., and Ahmad, A. L. (2008). Equilibrium modeling and kinetic studies on the adsorption of basic dye by a low-cost adsorbent: Coconut (Cocos nucifera) bunch waste. *Journal of Hazardous Materials*, ***158,*** 65–72.

Hassan, Z. A S. (2013). Methylene Blue Removal from Aqueous Solution by Adsorption on Eggshell Bed. *Euphrates Journal of Agriculture Science*, **5,** 11–23.

He, J. (2012). Synthesis and characterization of geopolymers for infrastrucral applications. PhD Dissertation, (August). https://doi.org/10.1007/s13398-014-0173-7.2

He, J., Hong, S., Zhang, L., Gan, F., and Ho, Y. (2010). Equilibrium and Thermodynamic Parameters of. *Fresenius Environmental Bulletin*, **19,** 2651–2656.

Heath, J. (2015). Energy Dispersive Spectroscopy. Essential Knowledge Briefings, Second Edition, pp. 32.

Hon, Y. M., Lin, S. P., Fung, K. Z., and Hon, M. H. (2002). Synthesis and characterization of nano-$LiMn_2O_4$ powder by tartaric acid gel process. *Journal of the European Ceramic Society*, **22,** 653–660.

Hsu, P. C., Liu, M. Y., Hsu, C. C., Chen, L. Y., and Leon Guo, Y. (1997). Lead exposure causes generation of reactive oxygen species and functional impairment in rat sperm. *Toxicology*, **122,** 133–143.

Hui, K. S., Chao, C. Y. H., and Kot, S. C. (2005). Removal of mixed heavy metal ions in wastewater by zeolite 4A and residual products from recycled coal fly ash. *Journal of Hazardous Materials*, **127,** 89–101.

Hutton, M., and Symon, C. (1986). The quantities of cadmium, lead, mercury and arsenic entering the U.K. environment from human activities. *Science of the Total Environment*, **57,** 129–150.

Idris, M. N., Ahmad, Z. A. and Ahmad, M. (2011). Adsorption Equilibrium of Malachite Green Dye onto Rubber Seed Coat Based Activated Carbon. *International Journal of Basic and Applied Sciences*, **11,** 305–311.

Igwe, J. C., and Abia, A. A. (2007). Adsorption isotherm studies of Cd (II), Pb (II) and Zn (II) ions bioremediation from aqueous solution using unmodified and EDTA-modified maize cob. *Ecletica Quimica*, **32,** 33–42.

Ii, P. Z., Ii, C., Mn, D., Daripada, I. I., Akueus, L., Penjerapan, M., and Jagung, P. T. (2011). Removal of Zn (II), Cd (II) and Mn (II) from aqueous solutions by adsorption on maize stalks. *The Malaysian Journal of Analytical Sciences*, **15,** 8–21.

Ischia, G., Wenk, H. R., Lutterotti, L., and Berberich, F. (2005). Quantitative Rietveld texture analysis of zirconium from single synchrotron diffraction images. *Journal of Applied Crystallography*, **38,** 377–380.

Itodo, A., Abdulrahman, F., Hassan, L., Maigandi, S. A., and Itodo, H. (2010). Intraparticle diffusion and intraparticulate diffusivities of herbicide on derived activated carbon. *Researcher*, **2,** 74–86.

IUPAC. (2000). Guidelines for Single-Laboratory Validation of Analytical Methods for Trace-Level Concentrations of Organic Chemicals. In: Principles and Practices of Method Validation. Edited by A. Fajgelj and A. Ambrus Royal Society of Chemistry, Cambridge.

Ivanova, I. I., Aiello, R., Nagy, J. B., Crea, F., Derouane, E. G., Dumont, N.,and Testa, F. (1994). Influence of cations on the physicochemical and structural properties of aluminosilicate gel precursors. II. Multinuclear magnetic resonance characterization. *Microporous Materials*, **3,** 245–257.

Jain, A. K., Sharma, S. K. and Singh, D. (1996). Reaction Kinetics of Paddy Husk Thermal Decomposition: *Proceedings 31th Intersociety of Energy Conversion Engineering Conference*, **4,** 2274–2279.

Jalali, R., Ghafourian, H., Asef, Y., Davarpanah, S. J., and Sepehr, S. (2002). Removal and recovery of lead using nonliving biomass of marine algae. *Journal of Hazardous Materials*, **92,** 253–262.

Jarup, L. (2003). Hazards of heavy metal contamination. *British Medical Bulletin*, **68,** 167–182.

Jeppu, G. P., and Clement, T. P. (2012). A modified Langmuir-Freundlich isotherm model for simulating pH-dependent adsorption effects. *Journal of Contaminant Hydrology*, **129,** 46–53.

Ji, B., Shao, F., Hu, G., Zheng, S., Zhang, Q., and Xu, Z. (2009). Adsorption of methyl tert-butyl ether (MTBE) from aqueous solution by porous polymeric adsorbents. *Journal of Hazardous Materials*, **161,** 81–87.

Jnr, M. H., and Harcourt, P. (2004). Studies on the effect of pH on the sorption of Pb^{2+} and Cd^{2+} ions from aqueous solutions by Caladium bicolor (Wild Cocoyam) biomass. *Electronic Journal of Biotechnology*, **7,** 313–323.

Jnr, M. H., and Spiff, A. I. (2005). Effect of metal ion concentration on the biosorption of Pb^{2+} and Cd^{2+} by Caladium bicolor (wild cocoyam). *African Journal of Biotechnology*, **4**, 191–196

Juberg, D. R., Kleiman, C. F., and Kwon, S. C. (1997). Position paper of the American Council on Science and Health: lead and human health. *Ecotoxicology and Environmental Safety*, **38,** 162–80.

Kang, S. Y., Lee, J. U., Moon, S. H., and Kim, K. W. (2004). Competitive adsorption characteristics of Co^{2+}, Ni^{2+}, and Cr^{3+} by IRN-77 cation exchange resin in synthesized

wastewater. *Chemosphere*, **56,** 141–147.

Kannan, N., and Meenakshisundaram, M. (2002). Adsorption of Congo Red on various activated carbons. *Water, Air, and Soil Pollution*, **138,** 289–305.

Kannan, N., and Sundaram, M. M. (2001). Kinetics and mechanism of removal of methylene blue by adsorption on various carbons a comparative study. *Dyes and Pigments*, **51,** 25–40.

Kavitha, D., and Namasivayam, C. (2007). Experimental and kinetic studies on methylene blue adsorption by coir pith carbon. *Bioresource Technology*, **98**, 14–21.

Khattri, S. D., and Singh, M. K. (2009). Removal of malachite green from dye wastewater using neem sawdust by adsorption. *Journal of Hazardous Materials*, **167,** 1089–1094.

Kippling, J. (1965). Adsorption from solutions of non-electrolytes. Academic Press inc. (London) Limited, pp. 131.

Kobya, M., Demirbas, E., Senturk, E., and Ince, M. (2005). Adsorption of heavy metal ions from aqueous solutions by activated carbon prepared from apricot stone. *Bioresource Technology*, **96,** 1518–1521.

Kong, D. L. Y., Sanjayan, J. G., and Sagoe-Crentsil, K. (2007). Comparative performance of geopolymers made with metakaolin and fly ash after exposure to elevated temperatures. *Cement and Concrete Research*, **37,** 1583–1589.

Koumanova, B., and Allen, S. J. (2005). Decolourisation of Water / Wastewater Using Adsorption (Review). *Journal of the University of Chemical Technology and Metallurgy*, **40,** 175–192.

Kounou, G. N., Nsami, J. N., Belibi, D. P. B., Kouotou, D., Tagne, G. M., Joh, D., and Mbadcam, J. K. (2015). Adsorption of Zinc (II) ions from aqueous solution onto Kaolinite and Metakaolinite. *Der Pharma Chemica*, **7,** 51–58.

Krika, F., Azzouz, N., and Ncibi, M. C. (2016). Adsorptive removal of cadmium from aqueous solution by cork biomass: Equilibrium, dynamic and thermodynamic studies. *Arabian Journal of Chemistry*, **9,** S1077–S1083.

Krishnarao, R. V., Subrahmanyam, J., and Jagadish Kumar, T. (2001). Studies on the formation of black particles in rice husk silica ash. *Journal of the European Ceramic Society*, **21,** 99–104.

Krukowska, J., Thomas, P., and Kołodyn, D. (2017). Comparison of sorption and desorption studies of heavy metal ions from biochar and commercial active carbon, **307,** 353–363.

Ku, Y., and Jung, I. L. (2001). Photocatalytic reduction of Cr(VI) in aqueous solutions by UV irradiation with the presence of titanium dioxide. *Water Research*, **35,** 135–142.

Kumar, K. V., Ramamurthi, V., and Sivanesan, S. (2005). Modeling the mechanism involved during the sorption of methylene blue onto fly ash. *Journal of Colloid and Interface*

Science, **284,** 14–21.

Kumar, P. S. (2013). Adsorption of Lead(II) Ions from Simulated Wastewater Using Natural Waste: A Kinetic, Thermodynamic and Equilibrium Study," Environmental Progress and Sustainable Energy, pp. 1–10.

Kumar, P. S., and Gayathri, R. (2009). Adsorption of Pb^{2+} ions from aqueous solutions onto bael tree leaf powder : isotherms , kinetics and thermodynamics study. *Journal of Engineering Science and Technology*, **4,** 381–399.

Küpper, H., Lombi, E., Zhao, F. J., and McGrath, S. P. (2000). Cellular compartmentation of cadmium and zinc in relation to other elements in the hyperaccumulator Arabidopsis halleri. *Planta*, **212,** 75–84.

Kurniawan, T. A., Chan, G. Y. S., Lo, W. H., and Babel, S. (2006). Physico-chemical treatment techniques for wastewater laden with heavy metals. *Chemical Engineering Journal*, **118,** 83–98.

Lagergren, S. (1898). Zur theorie der sogenannten adsorption geloster stoffe. *Kungliga Svenska Vetenskaps*, **24,** 1- 10.

Langmuir, I. (1916). the Constitution and Fundamental Properties of Solids and Liquids. Part I. Solids. *Journal of the American Chemical Society*, **252,** 2221–2295.

Laxmipriya, P., Swagat, S. R., Danda, S. R., Binod, B. N., Bisweswar, D., and Pramila, K. M. (2018). Thorough understanding of the kinetics and mechanism of heavy metal adsorption onto a pyrophyllite mine waste based geopolymer. *Journal of Molecular Liquids,* **263,** 428–441.

Lee, W. K. W., and Van Deventer, J. S. J. (2002a). Structural reorganisation of class F fly ash in alkaline silicate solutions. *Colloids and Surfaces A: Physicochemical and Engineering Aspects*, **211,** 49–66.

Lee, W. K. W., and Van Deventer, J. S. J. (2002b). The effect of ionic contaminants on the early-age properties of alkali-activated fly ash-based cements. *Cement and Concrete Research*, **32,** 577–584.

Lenga, R.E. (1988). The Sigma-Aldrich library of chemical safety data, edition II. Milwaukee, Wisconsin. Sigma-Aldrich Corp.

Li, Z. and Liu, S. (2007). Influence of slag as additive on compressive strength of fly ash-based geopolymer. *Journal of Materials in Civil Engineering*, **19,** 470–474.

Li, X., Ma, X., Zhang, S.,and Zheng, E. (2013). Mechanical Properties and Microstructure of Class C Fly Ash-Based Geopolymer Paste and Mortar, pp. 1485–1495.

Liu, L. E., Liu, J., Li, H., Zhang, H., Liu, J., and Zhang, H. (2012). Equilibrium, kinetic, and thermodynamic studies of lead (II) biosorption on sesame leaf. *BioResources*, **7,** 3555–3572.

Lloyd, R. R., Provis, J. L., and Van Deventer, J. S. J. (2009). Microscopy and microanalysis of inorganic polymer cements. 1: Remnant fly ash particles. *Journal of Materials Science*, **44,** 608–619.

López, F. J., Sugita, S., Tagaya, M., and Kobayashi, T. (2014a). Geopolymers Using Rice Husk Silica and Metakaolin Derivatives; Preparation and Their Characteristics. *Journal of Materials Science and Chemical Engineering*, **2,** 35–43.

López, F. J., Sugita, S., Tagaya, M., and Kobayashi, T. (2014b). Metakaolin-Based Geopolymers for Targeted Adsorbents to Heavy Metal Ion Separation, pp. 16–27.

Mahmoud, M., El-Latif, A., Ibrahim, A. M., Showman, M. S., and Hamide, R. R. A. (2013). Alumina/Iron Oxide Nano Composite for Cadmium Ions Removal from Aqueous Solutions. *International Journal of Nonferrous Metallurgy*, **2,** 47–62.

Malakootian, M., Khodashenas Limoni, Z., and Malakootian, M. (2016). The efficiency of lead biosorption from industrial wastewater by micro-alga spirulina platensis. *International Journal of Environmental Research*, **10,** 357–366.

Maleki, A., Mahvi, A. H., Ebrahimi, R., and Zandsalimi, Y. (2010). Study of photochemical and sonochemical processes efficiency for degradation of dyes in aqueous solution. *Korean Journal of Chemical Engineering*, **27,** 1805-1810.

Malferrari, D., Brigatti, M. F., Laurora, A., Pini, S., and Medici, L. (2007). Sorption kinetics and chemical forms of Cd (II) sorbed by thiol-functionalized 2:1 clay minerals. *Journal of Hazardous Materials*, **143,** 73–81.

Mann, U. S., Dhingra, A., and Singh, J. (2014). Water Pollution : Causes , Effects and Remedies, *International Journal of Advanced Technology in Engineering and Science*, **2,** 70–74.

Martins, R. J. E., Vilar, V. J. P., and Boaventura, R. A. R. (2010). Removal of Pb(II) from wastewaters by Fontinalis antipyretica biomass: Experimental study and modelling. *Desalination and Water Treatment*, **20,** 179–188.

McKay, G. (1982). Adsorption of dyestuffs from aqueous solutions with activated carbon I: Equilibrium and batch contact-time studies. *Journal of Chemical Technology and Biotechnology*, **32,** 759–772.

Mehdizadeh, S., Sadjadi, S., Ahmadi, S. J., and Outokesh, M. (2014). Environmental health Removal of heavy metals from aqueous solution using platinum nanopartcles / Zeolite-4A. *Journal of Environmental Health Science and Engineering*, **12,** 1–7.

Mehta, P. K., and Pitt, N. (1976). Energy and industrial materials from crop residues. *Resource Recovery and Conservation*, **2,** 23–38.

Mishra, V., Balomajumder, C., and Agarwal, V. K. (2012). Kinetics, Mechanistic and Thermodynamics of Zn(II) Ion Sorption: A Modeling Approach. *Clean - Soil, Air, Water*, **40,** 718–727.

Mohan, D., and Singh, K. P. (2002). Single- and multi-component adsorption of cadmium and zinc using activated carbon derived from bagasse an agricultural waste. *Water Research*, **36,** 2304–2318.

Mohan, S. V., and Karthikeyan, J. (1997). Removal of lignin and tannin colour from aqueous solution by adsorption onto activated charcoal. *Environmental Pollution*, **97,** 183–187.

Mohd, N. I., and Zainal, M. A. A. (2011). Adsorption equilibrium of malachite green dye onto rubber seed coat based activated carbon. *International Journal Basic and Applied Science*, ***11,*** 38–43.

Moheb, E. C. E. A. A. (2015). Adsorption of cadmium ions from aqueous solutions using sesame as a low-cost biosorbent : kinetics and equilibrium studies. *International Journal of Environmental Science and Technology*, **12,** 2579–2592.

Mona, K., Ahmad, K., Hanafy, H., Zakia., O. (2014). Heavy Metals Removal Using Activated Carbon, Silica and Silica Activated Carbon Composite. *Energy Procedia* **50**: 113 – 120.

Moosavirad, S. M., Sarikhani, R., Shahsavani, E., and Mohammadi, S. Z. (2015). Removal of some heavy metals from inorganic industrial wastewaters by ion exchange method. *Journal of Water Chemistry and Technology*, **37,** 191–199.

Moreno-piraján, J. C., and Giraldo, L. (2012). Heavy Metal Ions Adsorption from Wastewater Using Activated Carbon from Orange Peel, *European Journal of Chemistry*, **9,** 926–937.

Moyo, M., and Chikazaza, L. (2013). Bioremediation of Lead (II) from Polluted Wastewaters Employing Sulphuric Acid Treated Maize Tassel Biomass, pp. 689–695.

Moyo, M., Chikazaza, L., Nyamunda, B. C., and Guyo, U. (2013). Adsorption Batch Studies on the Removal of Pb (II) Using Maize Tassel Based Activated Carbon Adsorption Batch Studies on the Removal of Pb (II). *Journal of Chemistry*, **17,** 3–8.

Mu, M. N., Zeliæ, J., and Joziæ, D. (2012). Microstructural Characteristics of Geopolymers Based on Alkali-Activated Fly Ash, *Chemical and Biochemical Engineering*, **26,** 89–95.

Muriithi, N. T., K. K. B. and G. A. N. (2012). Chemical and mineral analyses of Mwea clays. *International Journal of Physical Sciences*, **7,** 5865–5869.

Murithi, G., Onindo, C. O., Wambu, E. W., and Muthakia, G. K. (2014). Removal of Cadmium(II) Ions from Water by Adsorption using Water Hyacinth (Eichhornia crassipes) Biomass. *Bioresources*, **9,** 3613–3631.

Murray, H. H. (1991). Overview - clay mineral applications. *Applied Clay Science*, **5,** 379–395.

Murray, H. H. (2006). Applied Clay Mineralogy - Occurrences, Processing and Application of Kaolins, Bentonites, Palygorskite-Sepiolite, and Common Clays. Developments in Clay Scienc*e* (Vol. 2). https://doi.org/10.1016/S1572-4352(06)02001-0.

Murthy, N. S. (2004). Recent developments in polymer characterization using x-ray diffraction, *The Rigaku Journal*, **21,** 15–24.

Mustafa, S., Zaman, M. I., Gul, R., and Khan, S. (2008). Effect of Ni^{2+} loading on the mechanism of phosphate anion sorption by iron hydroxide. *Separation and Purification Technology*, **59,** 108–114.

Muthadhi, A., Anitha, R., and Kothandaraman, S. (2007). Rice Husk Ash -Properties and its Uses : A Review. *Journal of the Institution of Engineers India. Civil Engineering Division*, **88,** 50–56.

Nahm, M. H., Herzenberg, L. A., Little, K., and Little, J. R. (1977). A new method of applying the Sips equation. *Journal of Immunology*, **119,** 301–305.

Nandi, B. K., Goswami, A., and Purkait, M. K. (2009). Adsorption characteristics of brilliant green dye on kaolin. *Journal of Hazardous Materials*, **161,** 387–395.

Naseem, R., and Tahir, S. S. (2001). Removal of Pb(II) from aqueous/acidic solutions by using bentonite as an adsorbent. *Water Research*, **35,** 3982–3986.

Nassar, M. M., and Magdy, Y. H. (1997). Removal of different basic dyes from aqueous solutions by adsorption on palm-fruit bunch particles. *Chemical Engineering Journal*, **66,** 223–226.

Nayak, P. S., and Singh, B. K. (2007). Instrumental characterization of clay by XRF, XRD and FTIR. *Bulletin of Materials Science*, **30,** 235–238.

Nethaji, S., Sivasamy, A., and Mandal, A. B. (2013). Adsorption isotherms, kinetics and mechanism for the adsorption of cationic and anionic dyes onto carbonaceous particles prepared from Juglans regia shell biomass. *International Journal of Environmental Science and Technology*, **10,** 231–242.

Nmiri, A., Hamdi, N., Duc, M., and Srasra, E. (2017). Synthesis and characterization of kaolinite-based geopolymer : Alkaline activation effect on calcined kaolinitic clay at different temperatures, *Journal of Materials and Environmental Sciences*, **8,** 276–290.

Nogueira, C. A., and Margarido, F. (2012). Production and Characterisation of Amorphous Silica. *4th International Conference on Engineering for Waste and Biomass Valorisation*, pp. 1817-1821.

Nomanbhay, S. M., and Palanisamy, K. (2005). Removal of heavy metal from industrial wastewater using chitosan coated oil palm shell charcoal. *Electronic Journal of Biotechnology*, **8,** 43–53.

Nriagu, J. O., and Pacyna, J. M. (1988). Quantitative assessment of worldwide contamination of air, water and soils by trace metals. *Nature*, **333,** 134–139.

Nwagbara, K, G., Bassey, N. K., , Ape, N. A., Abuh, D. I., and Akpomie M. A. (2010). Kinetic Rate Equations Application on the Removal of Copper (II) and Zinc (II) by Unmodified Lignocellulosic Fibrous Layer of Palm Tree Trunk - Single Component

System Studies, *International Journal of Engineering Science Invention*, **6,** 800–809.

Oelkers, E. H. (2001). General kinetic description of multioxide silicate mineral and glass dissolution. *Geochimica et Cosmochimica Acta*, **65,** 3703–3719.

Ogoyi, D. O., Mwita, C. J., Nguu, E. K., and Shiundu, P. M. (2011). Determination of Heavy Metal Content in Water, Sediment and Microalgae from Lake Victoria, East Africa. *The Open Environmental Engineering Journal*, **4,** 156–161.

Okewale, A., Babayemi, K., and Olalekan, A. (2013). Adsorption Isotherms and Kinetics Models of Starchy Adsorbents on Uptake of Water from Ethanol – Water Systems. *International Journal of Applied Science and Technology*, **3,** 35–42.

Okieimen, F. E., Okundia, E. U. O. DE. (1991). Sorption of cadmium and lead ions on modified groundnut (Arachis hypogea) husks. *Journal of Chemical Technology and Biotechnology*, **51,** 97–103.

Önal, Y., Akmil-Başar, C., Eren, D., Sarici-Özdemir, Ç., and Depci, T. (2006). Adsorption kinetics of malachite green onto activated carbon prepared from Tunbilek lignite. *Journal of Hazardous Materials*, **128,** 150–157.

Opeolu, B., and Fatoki, O. (2016). Dynamics of zinc sorption from aqueous matrices using plantain (Musa sp.) peel biomass. *African Journal of Biotechnology*, **11,** 13194–13201.

Owa, F. D. (2013). Water Pollution: Sources, Effects, Control and Management. *Mediterranean Journal of Social Sciences*, **4,** 65–68.

Ozacar, M., and Sengil, I. A. (2005). Adsorption of metal complex dyes from aqueous solutions by pine sawdust. *Bioresource Technology*, **96,** 791–795.

Ozdemir, C., Karatas, M., Dursun, S., Argun, M. E., and Dogan, S. (2005). Effect of $MnSO_4$ on the chromium removal from the leather industry wastewater. *Environmental Technology*, **26,** 397–400.

Özer, D., Dursun, G., and Özer, A. (2007). Methylene blue adsorption from aqueous solution by dehydrated peanut hull. *Journal of Hazardous Materials*, **144,** 171–179.

Palomo, A., Blanco-Varela, M. T., Granizo, M. L., Puertas, F., Vazquez, T., and Grutzeck, M. W. (1999). Chemical stability of cementitious materials based on metakaolin - Isothermal conduction calorimetry study. *Cement and Concrete Research*, **29,** 997–1004.

Pamukoglu, M. Y., and Kargi, F. (2008). Biological treatment of Cu (II) containing synthetic wastewater in an activated sludge unit: Copper (II) ion toxicity. *Environmental Engineering Science* DOI 10.1089/ees.2007.0113.

Pandey, P. K., Sharma, S. K., and Sambi, S. S. (2010). Kinetics and equilibrium study of chromium adsorption on zeoliteNaX, *International Journal of Environmental Science and Technology*, **7,** 395–404.

Parmar, M., and Thakur, L. S. (2013). Heavy metal Cu , Ni and Zn : Toxicity , health hazards

and their removal techniques by low cost adsorbents : a short overview. *International Journal of Plant, Animal and Environmental Sciences*, **3,** 143–157.

Pehlivan, E., and Altun, T. (2006). The study of various parameters affecting the ion exchange of Cu^{2+}, Zn^{2+}, Ni^{2+}, Cd^{2+}, and Pb^{2+} from aqueous solution on Dowex 50W synthetic resin. *Journal of Hazardous Materials*, **134,** 149–156.

Peleckis, G., Tõnsuaadu, K., Baubonyte, T., and Kareiva, A. (2002). Sol-gel chemistry approach in the preparation of precursors for the substituted superconducting oxides. *Journal of Non-Crystalline Solids*, **311,** 250–258.

Peter, O., and Olalekan, O. (2014). Comparative assessment of lead and zinc in the Coastal Areas of Niger Delta, pp**.** 39–45.

Phair, J. W., and Van Deventer, J. S. J. (2002). Effect of the silicate activator pH on the microstructural characteristics of waste-based geopolymers. *International Journal of Mineral Processing*, **66,** 121–143.

Pons, M. P., and Fusté, M. C. (1993). Uranium uptake by immobilized cells of Pseudomonas strain EPS 5028. *Applied Microbiology and Biotechnology*, **39,** 661–665.

Poghossian, A. A. (1997). Determination of the pHpzc of insulators surface from capacitance–voltage characteristics of MIS and EIS structures. *Sensor and Actuator B: Chemical*, **44,** 551–553.

Postai, D. L., Demarchi, C. A., Zanatta, F., Melo, D. C. C., and Rodrigues, C. A. (2016). Adsorption of rhodamine B and methylene blue dyes using waste of seeds of Aleurites Moluccana, a low cost adsorbent. *Alexandria Engineering Journal*, **55,** 1713–1723.

Provis, J. L., Lukey, G. C., and Van Deventer, J. S. J. (2005). Do geopolymers actually contain nanocrystalline zeolites? a reexamination of existing results. *Chemistry of Materials*, **17,** 3075–3085.

Rahier, H., Wastiels, J., Biesemans, M., Willlem, R., Van Assche, G., and Van Mele, B. (2007). Reaction mechanism, kinetics and high temperature transformations of geopolymers. *Journal of Materials Science*, **42,** 2982–2996.

Rahimi, M., and Vadi, M. (2014). Langmuir, Freundlich and Temkin Adsorption Isotherms of Propranolol on Multi-Wall Carbon Nanotube. *Journal of of Modern Drug Discovery And Drug Delivery Research*, **1,** 1–3.

Rajesh, K. R., Rajasimman, M., Rajamohan, N., and Sivaprakash, B. (2010). Equilibrium and kinetic studies on sorption of malachite green using Hydrilla Verticillata biomass. *International Journal of Environmental Research*, **4,** 817–824.

Rama, R. G. V., Surya Narayana, D. S., Varadaraju, U. V., Rao, G. V. N., and Venkadesan, S. (1995). Synthesis of $YBa_2Cu_3O_7$ through different gel routes. *Journal of Alloys and Compounds*, **217,** 200–208.

Raza, M. H., Sadiq, A., Farooq, U., Athar, M., Hussain, T., Mujahid, A., and Salman, M. (2015). Phragmites karka as a Biosorbent for the Removal of Mercury Metal Ions from Aqueous Solution : Effect of Modification, *Journal of Chemistry*, **15,** 1-12.

Rees, C. A, Provis, J. L., Lukey, G. C., and van Deventer, J. S. J. (2007). Attenuated total reflectance fourier transform infrared analysis of fly ash geopolymer gel aging. Langmuir : The ACS Journal of Surfaces and Colloids, **23,** 8170–8179.

Reichle, R. A., McCurdy, K. G., and Hepler, L. G. (1975). Zinc Hydroxide: Solubility Product and Hydroxy-complex Stability Constants from 12.5–75°C. *Canadian Journal of Chemistry*, **53,** 3841–3845.

Repo, E., Malinen, L., Koivula, R., Harjula, R., and Sillanp, M. (2011). Capture of Co(II) from its aqueous EDTA-chelate by DTPA-modified silica gel and chitosan. *Journal of Hazardous Materials*, **187**, 122–132.

Rezaei, H. (2016). Biosorption of chromium by using Spirulina sp. *Arabian Journal of Chemistry*, **9,** 846–853.

Richer, R. (1998). Direct synthesis of functionalized mesoporous silica by non-ionic alkylpolyethyleneoxide surfactant assembly. *Chemical Communications*, **16,** 1775–1777.

Rotimi, A., and Okeoghene, G. (2014). Sorption and Desorption Studies on Toxic Metals From Brewery Effluent Using Eggshell as Adsorbent. *Advances in Natural Science*, **7,** 15–24.

Rushton, G. T., Karns, C. L., and Shimizu, K. D. (2005). A critical examination of the use of the Freundlich isotherm in characterizing molecularly imprinted polymers (MIPs). *Analytica Chimica Acta*, **528,** 107–113.

Ryan, J., Estefan, G., and Rashid, A. (2001). Soil and Plant analysis Laboratory Manual, (2 nd ed.), International Center for Agricult ural Research in the Dry Areas, Aleppo, Syeria, pp. 5–141.

Said, A., Hakim, M. S., and Rohyami, Y. (2014). The Effect of Contact Time and pH on Methylene Blue Removal by Volcanic Ash, pp. 13–15.

Saleem, N., and Bhatti, H. N. (2011). Adsorptive removal and recovery of U(VI) by citrus waste biomass. *Bioresources*, **6,** 2522–2538.

Salleh, M. A. M., Mahmoud, D. K., Karim, W. A. W. A., and Idris, A. (2011). Cationic and anionic dye adsorption by agricultural solid wastes: A comprehensive review. *Desalination*, **280,** 1-13.

Santhi, T., Manonmani, S., and Smitha, T D. S. (2009). Uptake of Cationic ous Solution by Bioadsorption onto Granular Cucumis Sativa. *Journal of Applied Sciences in Environmental Sanitation*, **4,** 29–35.

Sari, A., Tuzen, M., Citak, D., and Soylak, M. (2007a). Adsorption characteristics of Cu(II) and Pb(II) onto expanded perlite from aqueous solution. *Journal of Hazardous Materials*,

148, 387–394.

Sari, A., Tuzen, M., Citak, D., and Soylak, M. (2007b). Equilibrium, kinetic and thermodynamic studies of adsorption of Pb (II) from aqueous solution onto Turkish kaolinite clay. *Journal of Hazardous Materials*, **149,** 283–291.

Sarioglu, M., and Atay, U. A. (2006). Removal of methylene blue by using biosolid. *Global N Environmental Sscience Technology Journal*, **8,** 113–120.

Sato, M., and Takizawa, Y. (1982). Cadmium-binding proteins in human organs. *Toxicology Letters*, **11,** 269–273.

Selçuk, N. Ç. (2017). Kinetics and Thermodynamic Studies of Adsorption of Methylene Blue from Aqueous Solutions onto Paliurus spina-christi Mill. Frutis and Seeds. *IOSR Journal of Applied Chemistry*, **10,** 53–63.

Sen, T. K., and Khoo, C. (2013). Adsorption Characteristics of Zinc (Zn^{2+}) from Aqueous Solution by Natural Bentonite and Kaolin Clay Minerals: A Comparative Study. *Computational Water, Energy, and Environmental Engineering*, **2,** 1–6.

Sen, T. K., and Sarzali, M. V. (2008). Removal of cadmium metal ion (Cd^{2+}) from its aqueous solution by aluminium oxide (Al_2O_3): A kinetic and equilibrium study. *Chemical Engineering Journal*, **142,** 256–262.

Sen Gupta, S., and Bhattacharyya, K. G. (2008). Immobilization of Pb(II), Cd(II) and Ni(II) ions on kaolinite and montmorillonite surfaces from aqueous medium. *Journal of Environmental Management*, **87,** 46–58.

Senthil Kumar, P., and Gayathri, R. (2009). Adsorption of Pb^{2+} ions from aqueous solutions onto bael tree leaf powder: Isotherms, kinetics and thermodynamics study. *Journal of Engineering Science and Technology*, **4,** 381–399.

Senthil Kumar, P., Ramalingam, S., Senthamarai, C., Niranjanaa, M., Vijayalakshmi, P., and Sivanesan, S. (2010). Adsorption of dye from aqueous solution by cashew nut shell: Studies on equilibrium isotherm, kinetics and thermodynamics of interactions. *Desalination*, **261,** 52–60.

Shabudeen, P. S. S., Venckatesh, R., Kadirvelu, K., Madhavakrishnan, S., and Pattabhi, S. (2007). Removal of reactive dye from aqueous solution by using Kapok Hull activated carbon. *Pollution Research*, **26,** 233–242.

Shah, B. A, Shah, A V, and Singh, R. R. (2009). Sorption isotherms and kinetics of chromium uptake from wastewater using natural sorbent material. *International Journal of Environmental Science and Technology*, **6,** 77–90.

Shaheen, S. M., Derbalah, A. S., and Moghanm, F. S. (2012). Removal of Heavy Metals from Aqueous Solution by Zeolite in Competitive Sorption System. *International Journal of Environmental Science and Development*, **3,** 362–367.

Shahmohammadi-Kalalagh, S., and Babazadeh, H. (2014). Isotherms for the sorption of zinc

and copper onto kaolinite: Comparison of various error functions. *International Journal of Environmental Science and Technology*, **11,** 111 .

Sharma, P., Kaur, R., Baskar, C., and Chung, W. J. (2010). Removal of methylene blue from aqueous waste using rice husk and rice husk ash. *Desalination*, **259,** 249–257.

Shichi, T., and Takagi, K. (2000). Clay minerals as photochemical reaction fields. *Journal of Photochemistry and Photobiology C: Photochemistry Reviews*, **1,** 113–130.

Silva, P. De, Sagoe-Crenstil, K., and Sirivivatnanon, V. (2007). Kinetics of geopolymerization: Role of Al_2O_3 and SiO_2. *Cement and Concrete Research*, **37,** 512–518.

Simeonov, L., Kochubovski, M., Simeonova, B., Draghici, C., Chirila, E., and Canfield, R. (2011). *Environmental Heavy Metal Pollution and Effects on Child Mental Development*. *NATO Science for Peace and Security Series C: Environmental Security* (Vol. 1). https://doi.org/10.1007/978-94-007-0253-0.

Sindhunata, Van Deventer, J. S. J., Lukey, G. C., and Xu, H. (2006). Effect of curing temperature and silicate concentration on fly-ash-based geopolymerization. *Industrial and Engineering Chemistry Research*, **45,** 3559–3568.

Singh, S. P., Ma, L. Q. and Harris, W. . (2001). Heavy metal interaction with phosphatic clay: sorption and desorption behavior. *Journal Environmental Quaility*, **30**, 1961–1968.

Singh, J., and Singh, H. (2015). A Review on Utilization of Rice Husk Ash in, *International Journal of Innovations in Engineering Research and Technology*, **2,** 1–7.

Singh, T. S., and Pant, K. K. (2004). Equilibrium , kinetics and thermodynamic studies for adsorption of As (III) on activated alumina. *Separation and Purification Technology*, **36,** 139–147.

Sips, R. (1948). On the Structure of a Catalyst Surface. *The Journal of Chemical Physics*, **16,** 490.

Sobhanardakani, S., Zandipak, R., and Javad, M. (2016). Removal of Ni (II) and Zn (II) from Aqueous Solutions Using Chitosan, *Archives of Hygiene Science*, **5,** 47–55.

Sokol, R. Z., Wang, S., Wan, Y. J. Y., Stanczyk, F. Z., Gentzschein, E., and Chapin, R. E. (2002). Long-term, low-dose lead exposure alters the gonadotropin-releasing hormone system in the male rat. *Environmental Health Perspectives*, **110,** 871–874.

Sounthararajah, D., Loganathan, P., Kandasamy, J., and Vigneswaran, S. (2015). Effects of Humic Acid and Suspended Solids on the Removal of Heavy Metals from Water by Adsorption onto Granular Activated Carbon. *International Journal of Environmental Research and Public Health*, **12,** 10475–10489.

Sposito, G. (2008). The Chemistry of Soils. Sposito, G. 2008. The Chemistry of Soils. 2nd Ed. Oxford University Press, New York. (Vol. 53), pp. 330.

Stohs, S. J., Bagchi, D., Hassoun, E., and Bagchi, M. (2000). Oxidative mechanisms in the toxicity of chromium and cadmium ions. *Journal Environmental, Pathology, Toxicology and Oncology*, **19,** 201–213.

Suryadi, I., Felycia, E., and Aning, A. (2015). clay materials for environmental remediation, pp. 5-37.

Svoboda, L., Zimmermannová, K., and Kalač, P. (2000). Concentrations of mercury, cadmium, lead and copper in fruiting bodies of edible mushrooms in an emission area of a copper smelter and a mercury smelter. *Science of the Total Environment*, **246,** 61–67.

Swaddle, T. W. (2001). Silicate complexes of aluminum(III) in aqueous systems. *Coordination Chemistry Reviews*, pp. 674.

Swaddle, T. W., Salerno, J., and Tregloan, P. A. (1994). Aqueous aluminates, silicates, and aluminosilicates. *Chemical Society Reviews*, **23,** 319- 327.

Swanepoel, J. C., and Strydom, C. A. (2002). Utilisation of fly ash in a geopolymeric material. *Applied Geochemistry*, **17,** 1143–1148).

Tan, I. A. W., Ahmad, A. L., and Hameed, B. H. (2008). Preparation of activated carbon from coconut husk: Optimization study on removal of 2,4,6-trichlorophenol using response surface methodology. *Journal of Hazardous Materials*, **153,** 709–717.

Tan, I. A. W., and Hameed, B. H. (2010). Adsorption isotherms, kinetics, thermodynamics and desorption studies of basic dye on activated carbon derived from oil palm empty fruit bunch. *Journal of Applied Sciences*, **10,** 2565–2571.

Taylor, P., Brozni, D., and Milin, Č. (2012). Journal of Environmental Science and Health , Part B : Effects of temperature on sorption-desorption processes of imidacloprid in soils of Croatian coastal regions Effects of temperature on sorption-desorption processes of imidacloprid in soils of Croatia, pp. 37–41.

Temkin, M. J., and Pyzhev, V. (1940). Recent modifications to Langmuir isotherms. *Acta Physiochim. URSS*, **12,** 217–222.

Thajeel, A. S. (2013). Isotherm , Kinetic and Thermodynamic of Adsorption of Heavy Metal Ions onto Local Activated Carbon, *Aquatic Science and Technology*, **1,** 53–77.

Theodore, L., and Ricci, F. (2010). Mass Transfer Operations for the Practicing Engineer. New Jersey: John Wiley and Sons, Inc.

Thienes, C. H., and Haley, T. J. (1972). Clinical Toxicology, Fifth Edition. Philadelphia: Lea and Febiger, pp. 237-239.

Thilagan, J., Kumar, A. V., Rajasekaran, K., and Raja, C. (2015). Continuous Fixed Bed Column Adsorption of Copper (II) Ions from Aqueous Solution by Calcium Carbonate, pp. 413–418.

Treacy, M. M. J., and Higgins, J. B. (2001). Collection of simulated XRD powder patterns for

zeolites. *Elsevier*, pp. 13.

Tripathi, A., and Rawat Ranjan, M. (2015). Heavy Metal Removal from Wastewater Using Low Cost Adsorbents. *Journal of Bioremediation and Biodegradation*, **6,** 1–5.

Turiel, E., Perez-Conde, C., and Martin-Esteban, A. (2003). Assessment of the crossreactivity and binding sites characterisation of a propazine-imprinted polymer using the Langmuir-Freundlich isotherm. *The Analyst*, **128,** 137–141.

UNESCO. (2009). The United Nations World Water Development Report 3: Water in a Changing World. World Water. Ecological, pp. 1-429.

Unuabonah, E. I., Adebowale, K. O., and Olu-Owolabi, B. I. (2007). Kinetic and thermodynamic studies of the adsorption of lead (II) ions onto phosphate-modified kaolinite clay. *Journal of Hazardous Materials*, **144,** 386–395.

Vadivelan, V., and Vasanth Kumar, K. (2005). Equilibrium, kinetics, mechanism, and process design for the sorption of methylene blue onto rice husk. *Journal of Colloid and Interface Science*, **286,** 90–100.

Vaishnav, V., Chandra, S., and Daga, K. (2011). Adsorption Studies of Zn (II) Ions from wastewater using Calotrop is procera as an adsorbent, *Research Journal of Recent Sciences* **2,** 1–6.

Valls, M., De Lorenzo, V., Gonzàlez-Duarte, R., and Atrian, S. (2000). Engineering outer-membrane proteins in Pseudomonas putida for enhanced heavy-metal bioadsorption. *Journal of Inorganic Biochemistry*, **79,** 219–223.

Van Jaarsveld, J. G. S., Van Deventer, J. S. J., Lorenzen, L. L., Jaarsveld, J. G. S., Deventer, J. S. J., and Lorenzen, L. L. (1998). Factors affecting the immobilization of metals in geopolymerized flyash. *Metallurgical and Materials Transactions*, **29,** 283–291.

Vandevivere, P. C., Bianchi, R., and Verstraete, W. (1998). Treatment and reuse of wastewater from the textile wet-processing industry: Review of emerging technologies. *Journal of Chemical Technology and Biotechnology*, **72,** 289-302.

Vengris, T., Binkiene, R., and Sveikauskaite, A. (2001). Nickel, copper and zinc removal from waste water by a modified clay sorbent. *Applied Clay Science*, **18,** 183–190.

Venkata, M. S., Chandrasekhar Rao, N., and Karthikeyan, J. (2002). Adsorptive removal of direct azo dye from aqueous phase onto coal based sorbents: A kinetic and mechanistic study. *Journal of Hazardous Materials*, **90,** 189–204.

Verma, R., and Dwivedi, P. (2013). Heavy metal water pollution- A case study. *Recent Research in Science and Technology*, **5,** 98–99.

Vigneswaran, R., Aitchison, S. J., McDonald, H. M., Khong, T. Y., and Hiller, J. E. (2004). Cerebral palsy and placental infection: a case-cohort study. *Pregnancy and Childbirth*, **4,** 1-12.

Vijayakumar, G., Tamilarasan, R., and Dharmendirakumar, M. (2012). Adsorption, kinetic, equilibrium and thermodynamic studies on the removal of basic dye Rhodamine-B from aqueous solution by the use of natural adsorbent perlite. *Journal of Materials and Environmental Science*, **3,** 157–170.

Vijayakumaran, V., Arivoli, S., and Ramuthai, S. (2009). Adsorption of Nickel Ion by Low Cost Carbon- Kinetic , Thermodynamic and Equilibrium Studies. *European Journal of Chemistry*, **6,** S347–S357.

Wang, D.A. Vaccari, Y., and Li, N. K. S. (2004). Physiochemical Treatment Processes. *Humana Press*, **3,** 141–198.

Weber, T. W., and Chakravorti, R. K. (1974). Pore and solid diffusion models for fixed bed adsorbers. *American Institute of Chemical Engineers Journal*, **20,** 228–238.

Weber, W. J., and Morris, J. C. (1963). Kinetics of Adsorption on Carbon from Solution. *Journal of the Sanitary Engineering Division*, **89,** 31–60.

Weng, C.-H., and Huang, C. P. (2004). Adsorption characteristics of Zn (II) from dilute aqueous solution by fly ash. *Colloids and Surfaces A: Physicochemical and Engineering Aspects*, **247,** 137–143.

WHO. (2008). Guidelines for Drinking-water Quality. Third edition incorporating the first and second addenda. *World Health Organisation*, **1,** 1–668.

Wood, M., Al-riyami, H. H., Jahan, S., and Dwivedi, P. B. (2014). Treatment of Battery Waste Water Using. *International Conference on Advances in Agricultural, Biological & Environmental Sciences*, **15,** 22–27.

Wu, C. H., Kuo, C. Y., and Guan, S. S. (2016). Adsorption kinetics of lead and zinc ions by coffee residues. *Polish Journal of Environmental Studies*, **24,** 761–767.

Wu, F., Tseng, R., and Juang, R. (2005). Comparisons of porous and adsorption properties of carbons activated by steam and KOH. *Journal of Harzadous Materials*, **283,** 49–56.

Xu, H., and van Deventer, J. S. J. (2000). Geopolymerisation of alumino-silicate minerals. *International Journal of Mineral Processing*, **59,** 247–266.

Xu, J., Xin, N., Li, J., and Yang, L. (2013). The acid treatments of the Hß zeolite as the catalyst in the synthesis of ethyl tertiary butyl ether antiknock additive. *Research and Technology*, **2,** 9–17.

Yagub, M. T., Sen, T. K., Afroze, S., and Ang, H. M. (2014). Dye and its removal from aqueous solution by adsorption: A review. *Advances in Colloid and Interface Science*, **209,** 172-184.

Yan, Z., Gittins, D. I., Skuse, D., Cosgrove, T., and Van Duijneveldt, J. S. (2007). Nonaqueous suspensions of surface-modified kaolin. *Langmuir*, **23,** 3424–3431.

Yao, Y., Xu, F., Chen, M., Xu, Z., and Zhu, Z. (2010). Adsorption behavior of methylene blue

on carbon nanotubes. *Bioresource Technology*, **101,** 3040–3046.

Yip, C. K., Lukey, G. C., and Van Deventer, J. S. J. (2003). Effect of blast furnace slag addition on microstructure and properties of metakaolinite geopolymeric materials. *Advances in Ceramic Matrix Composites IX*, **153,** 187–209 347.

Yip, C. K., and Van Deventer, J. S. J. (2003). Microanalysis of calcium silicate hydrate gel formed within a geopolymeric binder. *Journal of Materials Science*, **38,** 3851–3860.

Yu, H. N., Shen, S. R., and Yin, J. J. (2007). Effects of Metal Ions, Catechins, and Their Interactions on Prostate Cancer. *Critical Reviews in Food Science and Nutrition*, **47,** 711–719.

Yu, M. H. (2005). biological and health effects of pollutants. Environmental toxicology 2nd Edition , pp. 185-214.

Zendelska, A., Golomeova, M., Blazev, K., and Krstev, B. (2014). Kinetic studies of zinc ions removal from aqueous. *International Journal of Science, Environment*, **3,** 1303–1318.

Zhang, G., He, J., and Gambrell, R. (2010). Synthesis, Characterization, and Mechanical Properties of Red Mud-Based Geopolymers. *Transportation Research Record: Journal of the Transportation Research Board*, ***2167,*** 1–9.

Zhang, Y., jun, Chen, J., Rong, and Yan, X. yang. (2008). Equilibrium and kinetics studies on adsorption of Zn(II) from aqueous solutions onto a graft copolymer of cross-linked starch/acrylonitrile (CLSAGCP). *Colloids and Surfaces A: Physicochemical and Engineering Aspects*, **316,** 190–193.

Zhao, Y. E., Cai, C. Y., Luo, Y. Y., and He, Z. H. (2004). FTIR Spectra of the M(EDTA)n-Complexes in the Process of Sol-Gel Technique. *Journal of Superconductivity*, **17,** 383–387.

APPENDICES

Appendix 1A
Effect of pH on Pb (II) ions uptake using GP-1, GP-1C and GP-1E adsorbent

	GP-1	**GP-1C**	**GP-1E**
PH	Mean ± SD	Mean ± SD	Mean ± SD
2	58.62 ± 0.39^{d}	44.48 ± 0.67^{e}	49.99 ± 0.60^{d}
3	66.34 ± 0.40^{c}	70.39 ± 0.44^{d}	81.02 ± 0.42^{a}
4	69.82 ± 0.54^{b}	93.34 ± 0.06^{a}	70.91 ± 0.22^{b}
5	72.54 ± 0.43^{a}	72.16 ± 0.18^{c}	65.27 ± 0.05^{c}
6	72.25 ± 0.25^{a}	74.74 ± 0.20^{b}	66.34 ± 0.57^{c}

SD stands for standard deviation
Mean in a row without a common superscript letter differ ($P < 0.05$), as analyzed by one-way ANOVA

Appendix 1B
Effect of pH on Pb (II) ions uptake using GP-2, GP-2C and GP-2E adsorbent

	GP-2	**GP-2C**	**GP-2E**
PH	Mean ± SD	Mean ± SD	Mean ± SD
2	50.31 ± 0.44^{e}	47.01 ± 0.56^{e}	45.84 ± 0.03^{e}
3	65.90 ± 0.44^{d}	70.25 ± 0.20^{d}	65.88 ± 0.45^{d}
4	79.65 ± 0.27^{a}	89.77 ± 0.17^{c}	88.61 ± 0.07^{a}
5	77.68 ± 0.35^{b}	98.90 ± 0.06^{a}	75.85 ± 0.97^{c}
6	71.32 ± 0.05^{c}	97.24 ± 0.03^{b}	82.45 ± 0.02^{b}

Mean in a row with a common superscript letter differ ($P < 0.05$), as analyzed by one-way ANOVA

Appendix 1C
Effect of pH on Pb (II) ions uptake using GP-3, GP-3C and GP-3E adsorbent

	GP-3	**GP-3C**	**GP-3E**
PH	Mean ± SD	Mean ± SD	Mean ± SD
2	51.24 ± 0.14^{d}	52.07 ± 4.60^{c}	49.62 ± 0.46^{d}
3	64.79 ± 0.20^{c}	77.06 ± 0.51^{b}	78.86 ± 0.65^{c}
4	90.23 ± 0.04^{a}	99.32 ± 0.04^{a}	92.53 ± 0.08^{a}
5	80.68 ± 1.04^{b}	99.09 ± 0.01^{a}	88.80 ± 0.36^{b}
6	81.90 ± 0.65^{b}	98.99 ± 0.03^{a}	88.20 ± 0.05^{b}

Mean in a row without a common superscript letter differ ($P < 0.05$), as analyzed by one-way ANOVA

Appendix 1D

Effect of adsorbent dose on Pb (II) ions uptake using GP-1, GP-1C and GP-1E adsorbent

	GP-1	**GP-1C**	**GP-1E**
Dose(g)	Mean ± SD	Mean ± SD	Mean ± SD
0.1	60.05 ± 0.45^{c}	97.15 ± 0.05^{d}	65.75 ± 0.60^{c}
0.2	62.33 ± 0.35^{ab}	96.71 ± 0.10^{c}	67.06 ± 0.06^{c}
0.3	61.31 ± 0.01^{bc}	97.13 ± 0.07^{c}	69.44 ± 1.18^{b}
0.4	61.45 ± 0.42^{bc}	98.00 ± 0.03^{b}	68.83 ± 0.09^{b}
0.5	63.68 ± 1.07^{a}	99.61 ± 0.04^{a}	73.56 ± 0.31^{a}

Mean in a row without a common superscript letter differ ($P < 0.05$), as analyzed by one-way ANOVA

Appendix 1E

Effect of dose on Pb (II) ions uptake using GP-2, GP-2C and GP-2E adsorbent

	GP-2	**GP-2C**	**GP-2E**
Dose(g)	Mean ± SD	Mean ± SD	Mean ± SD
0.1	66.28 ± 0.25^{e}	71.56 ± 0.56^{e}	54.69 ± 1.02^{d}
0.2	69.68 ± 0.33^{d}	72 ± 0.06^{a}	55.41 ± 0.52^{cd}
0.3	73.03 ± 0.07^{c}	73.79 ± 0.22^{d}	56.65 ± 0.86^{c}
0.4	78.48 ± 0.58^{b}	76.36 ± 0.09^{c}	58.54 ± 0.46^{b}
0.5	83.70 ± 0.26^{a}	86.81 ± 0.17^{b}	98.35 ± 0.07^{a}

Mean in a row without a common superscript letter differ ($P < 0.05$), as analyzed by one-way ANOVA

Appendix 1F

Effect of dose on Pb (II) ions uptake using GP-3, GP-3C and GP-3E adsorbent

	GP-3	**GP-3C**	**GP-3E**
Dose(g)	Mean ± SD	Mean ± SD	Mean ± SD
0.1	68.50 ± 0.88^{d}	80.19 ± 0.26^{d}	76.01 ± 0.32^{d}
0.2	69.04 ± 0.08^{cd}	86.14 ± 0.09^{c}	78.97 ± 0.08^{c}
0.3	70.37 ± 0.61^{c}	96.67 ± 0.06^{b}	79.59 ± 0.46^{c}
0.4	71.97 ± 0.07^{b}	99.06 ± 0.02^{a}	81.33 ± 0.38^{b}
0.5	80.03 ± 0.39^{a}	99.24 ± 0.01^{a}	84.91 ± 0.16^{a}

Mean in a row without a common superscript letter differ ($P < 0.05$), as analyzed by one-way ANOVA

Appendix 1G

Effect of time on Pb (II) ions uptake using GP-1, GP-1C and GP-1E adsorbent

	GP-1	**GP-1C**	**GP-1E**
Time(min)	Mean ± SD	Mean ± SD	Mean ± SD
20	72.99 ± 0.90^{d}	99.72 ± 0.01^{c}	67.43 ± 1.01^{a}
40	74.75 ± 0.24^{c}	99.65 ± 0.01^{d}	73.83 ± 0.19^{b}
60	79.50 ± 0.45^{b}	99.41 ± 0.01^{e}	78.25 ± 0.34^{c}
80	82.11 ± 0.05^{a}	99.86 ± 0.00^{b}	93.54 ± 0.12^{e}
100	83.18 ± 0.08^{a}	99.97 ± 0.01^{a}	90.43 ± 0.53^{d}

Mean in a row with a different superscript letter differ ($P < 0.05$), as analyzed by one-way ANOVA

Appendix 1H

Effect of time on Pb (II) ions uptake using GP-2, GP-2C and GP-2E adsorbent

	GP-2	**GP-2C**	**GP-2E**
Time(min)	Mean ± SD	Mean ± SD	Mean ± SD
20	72.33 ± 0.24^{e}	65.37 ± 0.36^{c}	88.60 ± 0.05^{d}
40	78.76 ± 0.26^{d}	69.49 ± 0.76^{b}	90.42 ± 0.23^{c}
60	81.28 ± 0.08^{c}	98.79 ± 0.05^{a}	91.39 ± 0.06^{b}
80	93.42 ± 0.03^{b}	98.61 ± 0.53^{a}	91.88 ± 0.08^{a}
100	97.88 ± 0.07^{a}	98.34 ± 0.31^{a}	91.96 ± 0.10^{a}

Mean in a row with a different superscript letter differ ($P < 0.05$), as analyzed by one-way ANOVA

Appendix II

Effect of time on Pb (II) ions uptake using GP-3, GP-3C and GP-3E adsorbent

	GP-3	**GP-3C**	**GP-3E**
Time(min)	Mean ± SD	Mean ± SD	Mean ± SD
20	67.43 ± 0.51^{a}	90.21 ± 0.02^{a}	90.86 ± 0.11^{c}
40	69.22 ± 0.17^{b}	98.32 ± 0.05^{b}	92.45 ± 0.06^{b}
60	99.32 ± 0.03^{d}	98.42 ± 0.05^{c}	92.28 ± 0.23^{b}
80	99.23 ± 0.06^{c}	98.98 ± 0.07^{e}	98.12 ± 0.05^{a}
100	99.25 ± 0.05^{c}	98.60 ± 0.03^{d}	98.42 ± 0.21^{a}

Mean in a row with a different superscript letter differ ($P < 0.05$), as analyzed by one-way ANOVA

Appendix IK

Effect of shaking speed on Pb (II) ions uptake using GP-1, GP-1C and GP-1E adsorbent

	GP-1	**GP-1C**	**GP-1E**
Shaking(rpm)	Mean ± SD	Mean ± SD	Mean ± SD
120	65.22 ± 0.04^{e}	83.08 ± 0.68^{e}	79.65 ± 0.26^{c}
150	66.67 ± 0.30^{d}	84.56 ± 0.06^{d}	93.50 ± 0.34^{b}
180	67.91 ± 0.08^{c}	86.43 ± 0.10^{c}	98.60 ± 0.00^{a}
210	84.56 ± 0.06^{b}	87.30 ± 0.06^{b}	98.62 ± 0.01^{a}
240	89.58 ± 0.02^{a}	99.78 ± 0.01^{a}	98.72 ± 0.02^{a}

Mean in a row without a common superscript letter differ ($P < 0.05$), as analyzed by one-way ANOVA

Appendix IL

Effect of shaking speed on Pb (II) ions uptake using GP-2, GP-2C and GP-2E adsorbent

	GP-2	**GP-2C**	**GP-2E**
Shaking(rpm)	Mean ± SD	Mean ± SD	Mean ± SD
120	82.26 ± 0.42^{b}	72.96 ± 0.26^{e}	88.59 ± 0.03^{d}
150	82.41 ± 0.28^{b}	85.79 ± 0.17^{d}	91.50 ± 0.06^{c}
180	82.48 ± 0.08^{b}	96.58 ± 0.49^{c}	92.12 ± 0.63^{c}
210	85.86 ± 0.21^{a}	98.12 ± 0.04^{b}	93.05 ± 0.08^{b}
240	85.99 ± 0.33^{a}	99.50 ± 0.07^{a}	94.11 ± 0.07^{a}

Mean in a row without a common superscript letter differ ($P < 0.05$), as analyzed by one-way ANOVA

Appendix 1M

Effect of shaking speed on Pb (II) ions uptake using GP-3, GP-3C and GP-3E adsorbent

	GP-3	**GP-3C**	**GP-3E**
Shaking(rpm)	Mean ± SD	Mean ± SD	Mean ± SD
120	76.51 ± 0.26^{e}	93.29 ± 0.11^{d}	92.39 ± 0.27^{d}
150	77.60 ± 0.17^{d}	99.43 ± 0.06^{b}	93.55 ± 0.10^{c}
180	82.32 ± 0.28^{c}	99.49 ± 0.01^{b}	94.92 ± 0.14^{b}
210	83.53 ± 0.26^{b}	99.78 ± 0.02^{a}	96.06 ± 0.09^{a}
240	86.36 ± 0.25^{a}	98.32 ± 0.09^{c}	94.96 ± 0.05^{b}

Mean in a row without a common superscript letter differ ($P < 0.05$), as analyzed by one-way ANOVA

Appendix 1N

Effect of initial concentration of Pb (II) ions on uptake using GP-1, GP-1C and GP-1E adsorbent

	GP–1	**GP-1C**	**GP-1E**
Metal ions (mg/L)	Mean ± SD	Mean ± SD	Mean ± SD
20	89.33 ± 1.12[a]	90.79 ± 0.03[a]	91.81 ± 0.24[a]
50	82.72 ± 0.85[b]	84.80 ± 0.34[b]	86.94 ± 0.97[b]
100	71.27 ± 0.61[c]	79.79 ± 0.03[c]	72.79 ± 0.06c
200	69.31 ± 0.04[d]	74.42 ± 0.10[d]	71.87 ± 0.29[cd]

Mean in a row without a common superscript letter differ (P < 0.05), as analyzed by one-way ANOVA

Appendix 1O

Effect of initial concentration of Pb (II) ions on uptake using GP-2, GP-2C and GP-2E adsorbent

	GP-2	**GP-2C**	**GP-2E**
Metal ions (mg/L)	Mean ± SD	Mean ± SD	Mean ± SD
20	95.82 ± 0.51[a]	98.72 ± 0.09[a]	91.26 ± 0.61[a]
50	76.96 ± 0.93[b]	92.64 ± 0.07[b]	88.63 ± 0.10[b]
100	70.44 ± 0.60[c]	72.44 ± 0.14[c]	75.26 ± 0.05[c]
200	65.77 ± 0.04[d]	69.10 ± 0.08[d]	73.14 ± 0.03[d]

Mean in a row without a common superscript letter differ (P < 0.05), as analyzed by one-way ANOVA

Appendix 1P

Effect of initial concentration of Pb (II) ions on uptake using GP-3, GP-3C and GP-3E adsorbent

	GP-3	**GP-3C**	**GP-3E**	**RM (AC)** (Mona *et al*., 2014)
Metal ions (mg/L)	Mean ± SD	Mean ± SD	Mean ± SD	Mean
20	88.15 ± 2.44[a]	92.64 ± 0.32[a]	91.35 ± 0.92[a]	83.00
50	77.49 ± 1.14[b]	77.64 ± 0.33[b]	84.25 ± 0.12[b]	74.00
100	76.15 ± 0.40[b]	78.07 ± 0.20[b]	81.31 ± 0.56[c]	73.00
200	66.02 ± 0.04[c]	62.79 ± 0.11[c]	64.30 ± 0.00[d]	69.00

Mean in a row without a common superscript letter differ (P < 0.05), as analyzed by one-way ANOVA, RM(AC)= refference material activated carbon.

Appendix 1Q

Effect of temperature on Pb (II) ions on uptake using GP-1, GP-1C and GP-1E adsorbent

	GP-1	**GP-1C**	**GP-1E**
Temperature (K)	Mean ± SD	Mean ± SD	Mean ± SD
293	87.65 ± 0.30^{d}	91.57 ± 0.19^{d}	96.76 ± 0.21^{d}
298	87.99 ± 0.07^{cd}	92.22 ± 0.04^{c}	97.23 ± 0.04^{c}
308	88.29 ± 0.06^{c}	92.63 ± 0.07^{b}	98.03 ± 0.06^{b}
318	89.34 ± 0.03^{b}	94.74 ± 0.01^{a}	99.49 ± 0.02^{a}
328	90.15 ± 0.11^{a}	94.81 ± 0.21^{a}	99.29 ± 0.02^{a}

Mean in a row without a common superscript letter differ ($P < 0.05$), as analyzed by one-way ANOVA

Appendix 1R

Effect of temperature on Pb (II) ions on uptake using GP-2, GP-2C and GP-2E adsorbent

	GP-2	**GP-2C**	**GP-2E**
Temperature (K)	Mean ± SD	Mean ± SD	Mean ± SD
293	89.77 ± 0.11^{c}	90.68 ± 0.06^{d}	94.14 ± 0.20^{d}
298	90.06 ± 0.08^{c}	91.55 ± 0.02^{c}	95.61 ± 0.01^{c}
308	90.84 ± 0.47^{b}	92.60 ± 0.08^{b}	96.26 ± 0.23^{b}
318	91.50 ± 0.02^{ab}	93.61 ± 0.02^{a}	98.09 ± 0.02^{a}
328	91.35 ± 0.12^{a}	93.59 ± 0.10^{a}	97.94 ± 0.07^{a}

Mean in a row without a common superscript letter differ ($P < 0.05$), as analyzed by one-way ANOVA

Appendix 1S

Effect of temperature on Pb (II) ions on uptake using GP-3, GP-3C and GP-3E adsorbent

	GP-3	**GP-3C**	**GP-3E**
Temperature (K)	Mean ± SD	Mean ± SD	Mean ± SD
293	92.55 ± 0.08^{d}	96.84 ± 0.11^{e}	94.49 ± 0.09^{d}
298	92.97 ± 0.11^{c}	97.05 ± 0.12^{d}	95.08 ± 0.02^{c}
308	93.54 ± 0.08^{b}	97.43 ± 0.08^{c}	96.86 ± 0.06^{b}
318	93.94 ± 0.05^{ab}	98.49 ± 0.01^{b}	96.91 ± 0.07^{b}
328	93.72 ± 0.10^{a}	98.28 ± 0.03^{a}	97.46 ± 0.10^{a}

Mean in a row without a common superscript letter differ ($P < 0.05$), as analyzed by one-way ANOVA

Appendix 2A

Effect of pH on Cd (II) ions uptake using GP-1, GP-1C and GP-1E adsorbent

	GP-1	**GP-1C**	**GP-1E**
pH	Mean ± SD	Mean ± SD	Mean ± SD
2	82.85 ± 0.20^{d}	83.69 ± 0.32^{d}	82.35 ± 0.35^{d}
3	84.48 ± 0.23^{b}	86.31 ± 0.14^{c}	83.66 ± 0.09^{c}
4	85.78 ± 0.15^{a}	87.12 ± 0.27^{b}	87.34 ± 0.10^{b}
5	86.16 ± 0.31^{a}	92.05 ± 0.10^{a}	88.55 ± 0.19^{a}
6	84.35 ± 0.15^{c}	91.77 ± 0.09^{a}	87.63 ± 0.06^{b}

Mean percentages with the same letters in the same row are not significantly different at 95% confidence level

Appendix 2B

Effect of pH on Cd (II) ions uptake using GP-2, GP-2C and GP-2E adsorbent

	GP-2	**GP-2C**	**GP-2E**
PH	Mean ± SD	Mean ± SD	Mean ± SD
2	82.93 ± 0.13^{bc}	84.71 ± 0.13^{c}	81.66 ± 0.09^{e}
3	84.58 ± 0.04^{d}	85.75 ± 0.13^{d}	83.67 ± 0.08^{d}
4	86.34 ± 0.26^{a}	87.61 ± 0.04^{c}	84.46 ± 0.09^{c}
5	86.71 ± 0.11^{ab}	89.79 ± 0.05^{a}	89.78 ± 0.07^{a}
6	85.56 ± 0.12^{c}	88.14 ± 0.11^{b}	86.35 ± 0.27^{b}

Mean percentages with the same letters in the same row are not significantly different at 95% confidence level

Appendix 2C

Effect of pH on Cd (II) ions uptake using GP-3, GP-3C and GP-3E adsorbent

	GP-3	**GP-3C**	**GP-3E**
PH	Mean ± SD	Mean ± SD	Mean ± SD
2	85.41 ± 0.11^{d}	85.84 ± 0.20^{d}	85.20 ± 0.05^{d}
3	85.82 ± 0.24^{c}	86.47 ± 0.23^{c}	86.57 ± 0.30^{c}
4	87.36 ± 0.07^{b}	88.32 ± 0.05^{b}	98.99 ± 0.07^{b}
5	89.63 ± 0.18^{a}	90.05 ± 0.10^{a}	99.74 ± 0.01^{a}
6	84.84 ± 0.07^{c}	85.71 ± 0.07^{a}	99.17 ± 0.01^{b}

Mean percentages with the same letters in the same row are not significantly different at 95% confidence level

Appendix 2D

Effect of adsorbent dose on Cd (II) ions uptake using GP-1, GP-1C and GP-1E adsorbent

	GP-1	**GP-1C**	**GP-1E**
Dose(g)	Mean ± SD	Mean ± SD	Mean ± SD
0.1	86.14 ± 0.13^{c}	99.47 ± 0.00^{a}	88.23 ± 0.01^{b}
0.2	86.41 ± 0.04^{ab}	99.33 ± 0.02^{a}	92.18 ± 0.03^{a}
0.3	86.65 ± 0.09^{a}	99.01 ± 0.04^{b}	87.65 ± 0.11^{c}
0.4	86.37 ± 0.12^{bc}	97.99 ± 0.02^{c}	86.12 ± 0.26^{d}
0.5	82.93 ± 0.08^{d}	95.59 ± 0.13^{d}	86.15 ± 0.07^{d}

Mean percentages with the same letters in the same row are not significantly different at 95% confidence level

Appendix 2E

Effect of adsorbent dose on Cd (II) ions on uptake using GP-2, GP-2C and GP-2E adsorbent

	GP-2	**GP-2C**	**GP-2E**
Dose(g)	Mean ± SD	Mean ± SD	Mean ± SD
0.1	89.73 ± 0.27^{b}	89.83 ± 0.47^{c}	91.49 ± 0.08^{b}
0.2	89.79 ± 0.02^{b}	97.71 ± 0.13^{b}	99.98 ± 0.01^{a}
0.3	89.86 ± 0.04^{b}	99.54 ± 0.01^{a}	91.23 ± 0.03^{b}
0.4	91.34 ± 0.07^{a}	99.86 ± 0.01^{a}	88.79 ± 0.22^{c}
0.5	89.53 ± 0.05^{b}	99.99 ± 0.06^{a}	88.07 ± 0.10^{d}

Mean percentages with the same letters in the same row are not significantly different at 95% confidence level

Appendix 2F

Effect of adsorbent dose on Cd (II) ions on uptake using GP-3, GP-3C and GP-3E adsorbent

	GP-3	**GP-3C**	**GP-3E**
Dose(g)	Mean ± SD	Mean ± SD	Mean ± SD
0.1	90.54 ± 0.07^{d}	97.51 ± 0.07^{d}	95.57 ± 0.05^{d}
0.2	92.40 ± 0.06^{a}	98.90 ± 0.06^{b}	97.04 ± 0.05^{c}
0.3	90.86 ± 0.01^{b}	99.80 ± 0.00^{a}	99.98 ± 0.01^{a}
0.4	90.87 ± 0.03^{b}	98.00 ± 0.06^{c}	99.94 ± 0.01^{a}
0.5	90.68 ± 0.05^{c}	97.85 ± 0.09^{c}	99.16 ± 0.09^{b}

Mean percentages with the same letters in the same row are not significantly different at 95% confidence level

Appendix 2G

Effect of time on Cd (II) ions on uptake using GP-1, GP-1C and GP-1E adsorbent

	GP-1	**GP-1C**	**GP-1E**
Time(min)	Mean ± SD	Mean ± SD	Mean ± SD
20	89.13 ± 0.01^{b}	98.20 ± 0.01^{d}	91.94 ± 0.13^{e}
40	89.35 ± 0.25^{b}	99.61 ± 0.01^{c}	92.45 ± 0.10^{d}
60	89.49 ± 0.01^{b}	99.58 ± 0.01^{c}	93.58 ± 0.10^{c}
80	89.64 ± 0.12^{b}	99.68 ± 0.05^{b}	98.48 ± 0.02^{b}
100	90.46 ± 0.48^{a}	99.87 ± 0.00^{a}	99.20 ± 0.01^{a}

Mean percentages with the same letters in the same row are not significantly different at 95% confidence level

Appendix 2H

Effect of time on Cd (II) ions uptake using GP-2, GP-2C and GP-2E adsorbent

	GP-2	**GP-2C**	**GP-2E**
Time(min)	Mean ± SD	Mean ± SD	Mean ± SD
20	89.69 ± 0.03^{c}	92.28 ± 0.05^{d}	90.97 ± 0.30^{b}
40	89.79 ± 0.04^{bc}	93.54 ± 0.05^{c}	89.56 ± 0.43^{c}
60	89.95 ± 0.11^{b}	93.57 ± 0.15^{c}	90.86 ± 0.09^{b}
80	90.34 ± 0.12^{a}	94.50 ± 0.08^{b}	92.35 ± 0.08^{a}
100	88.97 ± 0.03^{a}	97.89 ± 0.07^{a}	91.50 ± 0.02^{b}

Mean percentages with same letters in the same row are not significantly different at 95% confidence level

Appendix 2I

Effect of time on Cd (II) ions uptake using GP-3, GP-3C and GP-3E adsorbent

	GP-3	**GP-3C**	**GP-3E**
Time(min)	Mean% ± SD	Mean% ± SD	Mean% ± SD
20	90.27 ± 0.10^{b}	91.63 ± 0.11^{d}	99.63 ± 0.05^{c}
40	90.25 ± 0.05^{b}	92.39 ± 0.03^{c}	99.78 ± 0.01^{b}
60	90.39 ± 0.14^{b}	97.69 ± 0.02^{b}	99.82 ± 0.05^{b}
80	90.85 ± 0.06^{a}	99.99 ± 0.00^{a}	99.94 ± 0.05^{a}
100	89.95 ± 0.12^{c}	99.98 ± 0.01^{a}	99.98 ± 0.00^{a}

Mean percentages with same letters in the same row are not significantly different at 95% confidence level

Appendix 2J

Effect of shaking speed on Cd (II) ions uptake using GP-1, GP-1C and GP-1E adsorbent

	GP-1	**GP-1C**	**GP-1E**
Shaking (rpm)	Mean ± SD	Mean ± SD	Mean ± SD
120	89.46 ± 0.50^{d}	86.68 ± 0.02^{c}	89.04 ± 0.04^{e}
150	92.00 ± 0.01^{c}	99.63 ± 0.56^{ab}	99.39 ± 0.00^{a}
180	91.72 ± 0.00^{c}	98.97 ± 0.02^{b}	98.18 ± 0.04^{b}
210	99.26 ± 0.00^{a}	99.98 ± 0.02^{a}	95.79 ± 0.17^{c}
240	93.68 ± 0.08^{b}	99.77 ± 0.01^{a}	92.37 ± 0.08^{d}

Appendix 2K

Effect of shaking speed on Cd (II) ions uptake using GP-2, GP-2C and GP-2E adsorbent

	GP-2	**GP-2C**	**GP-2E**
Shaking (rpm)	Mean ± SD	Mean ± SD	Mean ± SD
120	86.08 ± 0.15^{d}	89.80 ± 0.05^{d}	89.57 ± 0.10^{d}
150	88.97 ± 0.25^{c}	98.73 ± 0.07^{a}	93.98 ± 0.02^{a}
180	90.49 ± 0.45^{b}	98.55 ± 0.04^{a}	92.36 ± 0.11^{b}
210	91.33 ± 0.15^{a}	97.89 ± 0.07^{b}	92.59 ± 0.09^{b}
240	91.82 ± 0.01^{a}	96.44 ± 0.09^{c}	91.45 ± 0.13^{c}

Mean percentages with same letters in the same row are not significantly different at 95% confidence level

Appendix 2L

Effect of shaking speed on Cd (II) ions uptake using GP-3, GP-3C and GP-3E adsorbent

	GP-3	**GP-3C**	**GP-3E**
Shaking (rpm)	Mean ± SD	Mean ± SD	Mean ± SD
120	86.59 ± 0.14^{e}	90.01 ± 0.03^{d}	92.02 ± 0.04^{d}
150	89.44 ± 0.04^{d}	98.02 ± 0.06^{b}	99.72 ± 0.03^{c}
180	91.37 ± 0.21^{c}	99.98 ± 0.02^{a}	99.98 ± 0.01^{a}
210	91.94 ± 0.08^{b}	99.86 ± 0.01^{a}	99.98 ± 0.01^{a}
240	92.30 ± 0.06^{a}	96.95 ± 0.14^{c}	99.89 ± 0.02^{b}

Mean percentages with same letters in the same row are not significantly different at 95% confidence level

Appendix 2M

Effect of concentration of Cd (II) ions uptake using GP-1, GP-1C and GP-1E adsorbent

	GP-1	**GP-1C**	**GP-1E**
Metal ions(mg/L)	Mean ± SD	Mean ± SD	Mean ± SD
20	88.01 ± 0.82^{ab}	94.42 ± 0.31^{a}	91.44 ± 0.81^{a}
50	87.12 ± 0.21^{b}	92.92 ± 0.17^{b}	80.75 ± 0.13^{b}
100	88.57 ± 0.04^{a}	86.36 ± 0.15^{c}	78.36 ± 0.15^{c}
200	82.14 ± 0.21^{c}	81.30 ± 0.01^{d}	78.19 ± 0.04^{cd}

Mean percentages with same letters in the same row are not significantly different at 95% confidence level

Appendix 2N

Effect of concentration of Cd (II) ions uptake using GP-2, GP-2C and GP-2E adsorbent

	GP-2	**GP-2C**	**GP-2E**
Metal ions(mg/L)	Mean ± SD	Mean ± SD	Mean ± SD
20	81.80 ± 2.64^{ab}	96.49 ± 0.09^{a}	89.49 ± 0.15^{a}
50	82.92 ± 0.79^{a}	93.22 ± 0.02^{b}	85.11 ± 0.28^{b}
100	79.02 ± 0.41^{bc}	86.58 ± 0.18^{c}	79.81 ± 0.00^{c}
200	78.59 ± 0.06^{bc}	84.32 ± 0.05^{d}	79.23 ± 0.05^{d}

Mean percentages with same letters in the same row are not significantly different at 95% confidence level

Appendix 2O

Effect of concentration of Cd (II) ions uptake using GP-3, GP-3C and GP-3E adsorbent

	GP-3	**GP-3C**	**GP-3E**	**RM (AC)** (Mona *et al*., 2014)
Metal ions (mg/L)	Mean ± SD	Mean ± SD	Mean ± SD	Mean
20	88.26 ± 2.25^{a}	98.00 ± 0.03^{a}	92.77 ± 0.55^{a}	86.00
50	85.02 ± 0.27^{b}	92.80 ± 0.07^{b}	86.86 ± 0.44^{b}	84.00
100	86.45 ± 0.42^{ab}	86.62 ± 0.10^{c}	88.45 ± 0.16^{c}	70.00
200	77.66 ± 0.41^{c}	79.85 ± 0.07^{d}	79.11 ± 0.06^{d}	66.10

Appendix 2P

Effect of temperature onCd (II) ions uptake using GP-1, GP-1C and GP-1E adsorbent

	GP–1	**GP-1C**	**GP-1E**
Temperature (K)	Mean ± SD	Mean ± SD	Mean ± SD
293	86.83 ± 0.11^{d}	94.54 ± 0.14^{e}	97.94 ± 0.14^{d}
298	87.10 ± 0.03^{d}	94.92 ± 0.05^{d}	98.25 ± 0.06^{c}
308	88.56 ± 0.21^{c}	95.54 ± 0.10^{c}	98.57 ± 0.04^{b}
318	90.61 ± 0.07^{a}	97.82 ± 0.02^{b}	99.40 ± 0.03^{a}
328	89.60 ± 0.06^{b}	98.10 ± 0.03^{a}	99.21 ± 0.05^{a}

Appendix 2Q

Effect of temperature onCd (II) ions uptake using GP-2, GP-2C and GP-2E adsorbent

	GP–2	**GP-2C**	**GP-2E**
Temperature (K)	Mean ± SD	Mean ± SD	Mean ± SD
293	89.22 ± 0.19^{b}	97.54 ± 0.08^{e}	95.78 ± 0.15^{b}
298	90.02 ± 0.04^{ab}	97.92 ± 0.04^{d}	95.90 ± 0.07^{b}
308	90.34 ± 0.31^{ab}	98.20 ± 0.07^{c}	96.00 ± 0.05^{b}
318	90.77 ± 1.13^{a}	98.59 ± 0.02^{b}	97.62 ± 0.04^{a}
328	91.52 ± 0.48^{a}	99.03 ± 0.04^{a}	97.55 ± 0.09^{a}

Appendix 2R
Effect of temperature onCd (II) ions uptake using GP-3, GP-3C and GP-3E adsorbent

	GP-3	**GP-3C**	**GP-3E**
Temperature (K)	Mean ± SD	Mean ± SD	Mean ± SD
293	90.49 ± 0.03^{e}	92.03 ± 0.06^{e}	93.81 ± 0.18^{c}
298	91.21 ± 0.04^{d}	93.13 ± 0.06^{d}	93.92 ± 0.04^{c}
308	91.87 ± 0.24^{c}	94.63 ± 0.09^{c}	94.59 ± 0.08^{b}
318	95.04 ± 0.02^{a}	96.43 ± 0.05^{b}	96.54 ± 0.08^{a}
328	94.52 ± 0.14^{b}	97.43 ± 0.11^{a}	96.32 ± 0.11^{a}

Appendix 3A
Effect of pH on Zn (II) ions uptake using GP-1, GP-1C and GP-1E adsorbent

	GP-1	**GP-1C**	**GP-1E**
PH	Mean ± SD	Mean ± SD	Mean ± SD
2	78.04 ± 0.56^{b}	89.22 ± 0.38^{d}	78.06 ± 0.07^{d}
3	78.74 ± 0.09^{b}	91.23 ± 0.35^{c}	78.36 ± 0.09^{d}
4	80.19 ± 0.07^{a}	92.36 ± 0.21^{b}	79.54 ± 0.24^{c}
5	80.26 ± 0.10^{a}	93.56 ± 0.07^{a}	81.19 ± 0.06^{a}
6	79.97 ± 0.06^{a}	93.18 ± 0.05^{a}	80.41 ± 0.15^{b}

Appendix 3B
Effect of pH on Zn (II) ions uptake using GP-2, GP-2C and GP-2E adsorbent

	GP-2	**GP-2C**	**GP-2E**
PH	Mean ± SD	Mean ± SD	Mean ± SD
2	77.23 ± 0.14^{d}	77.58 ± 0.04^{d}	78.03 ± 0.10^{d}
3	77.78 ± 0.07^{c}	79.47 ± 0.19^{c}	78.44 ± 0.08^{c}
4	78.51 ± 0.06^{b}	79.69 ± 0.30^{c}	78.94 ± 0.10^{b}
5	79.29 ± 0.13^{a}	81.39 ± 0.16^{a}	81.16 ± 0.08^{a}
6	79.04 ± 0.06^{a}	80.47 ± 0.07^{b}	79.19 ± 0.19^{b}

Appendix 3C
Effect of pH on Zn (II) ions uptake using GP-3, GP-3C and GP-3E adsorbent

	GP-3	**GP-3C**	**GP-3E**
PH	Mean ± SD	Mean ± SD	Mean ± SD
2	77.67 ± 0.06^{d}	78.21 ± 0.45^{e}	79.94 ± 0.10^{d}
3	78.32 ± 0.21^{c}	82.90 ± 0.16^{d}	80.25 ± 0.12^{cd}
4	78.69 ± 0.25^{c}	85.90 ± 0.09^{c}	80.61 ± 0.19^{c}
5	79.36 ± 0.06^{b}	91.33 ± 0.06^{a}	81.83 ± 0.05^{a}
6	80.07 ± 0.13^{a}	88.45 ± 0.11^{b}	81.06 ± 0.16^{b}

Appendix 3D
Effect of dose on Zn (II) ions uptake using GP-1, GP-1C and GP-1E adsorbent

	GP-1	**GP-1C**	**GP-1E**
Dose(g)	Mean ± SD	Mean ± SD	Mean ± SD
0.1	80.63 ± 0.18^{d}	86.62 ± 0.12^{d}	81.08 ± 0.03^{d}
0.2	84.22 ± 0.16^{c}	88.45 ± 0.08^{c}	87.67 ± 0.07^{c}
0.3	86.38 ± 0.12^{b}	89.74 ± 0.08^{b}	88.46 ± 0.10^{b}
0.4	88.39 ± 0.09^{a}	93.09 ± 0.52^{a}	89.38 ± 0.12^{a}
0.5	88.63 ± 0.14^{a}	92.40 ± 0.62^{a}	89.37 ± 0.15^{a}

Appendix 3E
Effect of dose on Zn (II) ions uptake using GP-2, GP-2C and GP-2E adsorbent

	GP-2	**GP-2C**	**GP-2E**
Dose(g)	Mean ± SD	Mean ± SD	Mean ± SD
0.1	79.52 ± 0.04^{b}	80.98 ± 0.04^{d}	80.89 ± 0.16^{e}
0.2	86.47 ± 0.12^{a}	87.94 ± 0.07^{c}	84.75 ± 0.08^{d}
0.3	86.46 ± 0.18^{a}	88.26 ± 0.21^{c}	86.84 ± 0.02^{c}
0.4	86.52 ± 0.11^{a}	90.46 ± 0.12^{b}	88.94 ± 0.06^{a}
0.5	86.69 ± 0.01^{a}	92.16 ± 0.16^{a}	88.29 ± 0.06^{b}

Appendix 3F
Effect of dose on Zn (II) ions uptake using GP-3, GP-3C and GP-3E adsorbent

	GP-3	**GP-3C**	**GP-3E**
Dose(g)	Mean ± SD	Mean ± SD	Mean ± SD
0.1	79.13 ± 0.07^{d}	82.10 ± 0.05^{d}	81.37 ± 0.15^{d}
0.2	84.15 ± 0.11^{c}	86.01 ± 0.02^{c}	85.94 ± 0.09^{c}
0.3	86.05 ± 0.10^{b}	90.40 ± 0.16^{b}	86.51 ± 0.06^{b}
0.4	86.80 ± 0.06^{a}	90.41 ± 0.06^{b}	89.25 ± 0.07^{a}
0.5	86.95 ± 0.05^{a}	90.75 ± 0.05^{a}	89.30 ± 0.06^{a}

Appendix 3G
Effect of time on Zn (II) ions uptake using GP-1, GP-1C and GP-1E adsorbent

	GP-1	**GP-1C**	**GP-1E**
Time(min)	Mean ± SD	Mean ± SD	Mean ± SD
20	80.22 ± 0.12^{c}	82.62 ± 0.08^{c}	81.30 ± 0.25^{b}
40	86.14 ± 0.06^{b}	86.42 ± 0.04^{b}	86.58 ± 0.11^{a}
60	86.45 ± 0.08^{a}	86.72 ± 0.10^{a}	86.68 ± 0.15^{a}
80	86.61 ± 0.10^{a}	86.85 ± 0.07^{a}	86.77 ± 0.03^{a}
100	86.67 ± 0.11^{a}	86.85 ± 0.10^{a}	86.85 ± 0.08^{a}

Appendix 3H
Effect of time on Zn (II) ions uptake using GP-2, GP-2C and GP-2E adsorbent

	GP-2	**GP-2C**	**GP-2E**
Time(min)	Mean ± SD	Mean ± SD	Mean ± SD
20	79.28 ± 0.10^{c}	81.22 ± 0.14^{b}	81.21 ± 0.10^{c}
40	84.39 ± 0.03^{b}	86.37 ± 0.16^{a}	86.14 ± 0.08^{b}
60	84.47 ± 0.11^{ab}	86.46 ± 0.10^{a}	86.27 ± 0.14^{ab}
80	84.56 ± 0.08^{ab}	86.62 ± 0.18^{a}	86.37 ± 0.09^{ab}
100	84.64 ± 0.12^{a}	86.63 ± 0.12^{a}	86.47 ± 0.03^{a}

Appendix 3I
Effect of time on Zn (II) ions uptake using GP-3, GP-3C and GP-3E adsorbent

	GP-3	**GP-3C**	**GP-3E**
Time(min)	Mean ± SD	Mean ± SD	Mean ± SD
20	80.40 ± 0.10^{d}	86.22 ± 0.07^{c}	81.30 ± 0.25^{d}
40	84.68 ± 0.25^{c}	87.48 ± 0.35^{b}	86.44 ± 0.10^{c}
60	88.16 ± 0.12^{a}	91.32 ± 0.23^{a}	88.23 ± 0.20^{b}
80	89.44 ± 0.12^{a}	91.62 ± 0.04^{a}	89.35 ± 0.01^{a}
100	88.34 ± 0.11^{a}	91.64 ± 0.01^{a}	89.67 ± 0.05^{a}

Appendix 3J
Effect of shaking speed on Zn (II) ions uptake using GP-1, GP-1C and GP-1E adsorbent

	GP-1	**GP-1C**	**GP-1E**
Shaking (rpm)	Mean ± SD	Mean ± SD	Mean ± SD
120	81.03 ± 0.05^{e}	85.56 ± 0.12^{d}	84.32 ± 0.04^{e}
150	84.72 ± 0.31^{d}	87.63 ± 0.07^{c}	86.91 ± 0.09^{d}
180	86.86 ± 0.11^{c}	89.47 ± 0.11^{b}	87.83 ± 0.08^{c}
210	87.91 ± 0.10^{a}	93.48 ± 0.70^{a}	91.16 ± 0.10^{a}
240	87.31 ± 0.08^{b}	87.81 ± 0.04^{c}	90.14 ± 0.13^{b}

Appendix 3K
Effect of shaking speed on Zn (II) ions uptake using GP-2, GP-2C and GP-2E adsorbent

	GP-2	**GP-2C**	**GP-2E**
Shaking (rpm)	Mean ± SD	Mean ± SD	Mean ± SD
120	79.60 ± 0.01^{d}	81.59 ± 0.08^{d}	82.40 ± 0.29^{e}
150	84.71 ± 0.16^{c}	87.44 ± 0.25^{c}	85.56 ± 0.14^{d}
180	86.55 ± 0.07^{b}	88.77 ± 0.17^{b}	86.91 ± 0.09^{c}
210	90.75 ± 0.16^{a}	93.03 ± 0.07^{a}	94.26 ± 0.10^{a}
240	90.77 ± 0.12^{a}	92.89 ± 0.01^{a}	92.59 ± 0.01^{b}

Appendix 3L

Effect of shaking speed on Zn (II) ions uptake using GP-3, GP-3C and GP-3E adsorbent

	GP-3	**GP-3C**	**GP-3E**
Shaking (rpm)	Mean ± SD	Mean ± SD	Mean ± SD
120	80.73 ± 0.23^{e}	85.77 ± 0.06^{e}	84.32 ± 0.04^{e}
150	82.68 ± 0.13^{d}	86.91 ± 0.09^{d}	85.93 ± 0.12^{d}
180	84.60 ± 0.07^{c}	87.63 ± 0.08^{c}	86.83 ± 0.08^{c}
210	91.16 ± 0.10^{a}	94.37 ± 0.37^{a}	92.81 ± 0.17^{a}
240	90.14 ± 0.13^{b}	92.92 ± 0.07^{b}	91.59 ± 0.07^{b}

Appendix 3M

Effect of concentration of Zn (II) ions uptake using GP-1, GP-1C and GP-1E adsorbent

	GP-1	**GP-1C**	**GP-1E**
Metal ion (mg/L)	Mean ± SD	Mean ± SD	Mean ± SD
20	47.43 ± 0.41^{e}	84.99 ± 0.18^{e}	75.44 ± 0.68^{e}
50	75.97 ± 1.69^{d}	84.53 ± 0.14^{d}	90.46 ± 0.41^{d}
100	87.46 ± 0.25^{c}	90.51 ± 0.15^{c}	93.05 ± 0.02^{c}
200	92.03 ± 0.01^{b}	93.87 ± 0.10^{b}	95.66 ± 0.02^{b}

Appendix 3N

Effect of concentration of Zn (II) ions uptake using GP-2, GP-2C and GP-2E adsorbent

	GP-2	**GP-2C**	**GP-2E**
Metal ions (mg/L)	Mean ± SD	Mean ± SD	Mean ± SD
20	68.01 ± 0.63^{e}	94.88 ± 0.08^{d}	88.05 ± 0.09^{e}
50	84.09 ± 0.20^{d}	93.82 ± 0.09^{e}	94.19 ± 0.37^{d}
100	92.10 ± 0.05^{c}	95.90 ± 0.08^{c}	95.66 ± 0.12^{c}
200	95.66 ± 0.03^{b}	96.99 ± 0.01^{b}	97.14 ± 0.31^{b}

Appendix 3O

Effect of concentration of Zn (II) ions uptake using GP-3, GP-3C and GP-3E adsorbent

	GP-3	**GP-3C**	**GP-3E**	**RM (AC)** (Mona *et al*., 2014)
Metal ions (mg/L)	Mean ± SD	Mean ± SD	Mean ± SD	Mean
20	73.17 ± 0.39^{e}	93.03 ± 0.13^{e}	94.30 ± 0.49^{d}	74.9
50	86.82 ± 0.43^{d}	95.24 ± 0.15^{d}	95.07 ± 0.20^{c}	77.2
100	92.17 ± 0.01^{c}	96.62 ± 0.06^{c}	97.06 ± 0.01^{b}	81.2
200	96.53 ± 0.07^{b}	97.59 ± 0.09^{b}	98.28 ± 0.04^{a}	83.6

Appendix 3P
Effect temperature on Zn (II) ions uptake using GP-1, GP-1C and GP-1E adsorbent

	GP–1	**GP-1C**	**GP-1E**
Temperature (K)	Mean ± SD	Mean ± SD	Mean ± SD
293	91.61 ± 0.02^{d}	96.60 ± 0.10^{d}	92.56 ± 0.09^{d}
298	92.09 ± 0.14^{c}	96.91 ± 0.05^{c}	93.02 ± 0.04^{c}
308	93.20 ± 0.03^{b}	97.97 ± 0.01^{b}	94.55 ± 0.20^{b}
318	93.58 ± 0.10^{a}	98.19 ± 0.02^{a}	94.82 ± 0.14^{b}
328	93.50 ± 0.06^{a}	98.12 ± 0.02^{a}	95.76 ± 0.13^{a}

Appendix 3Q
Effect temperature on Zn (II) ions uptake using GP-2, GP-2C and GP-2E adsorbent

	GP–2	**GP-2C**	**GP-2E**
Temperature (K)	Mean ± SD	Mean ± SD	Mean ± SD
293	93.64 ± 0.06^{e}	94.60 ± 0.03^{d}	94.57 ± 0.22^{d}
298	94.50 ± 0.02^{d}	94.92 ± 0.06^{c}	95.03 ± 0.05^{c}
308	95.68 ± 0.03^{c}	95.74 ± 0.19^{b}	95.88 ± 0.09^{b}
318	95.96 ± 0.04^{b}	98.49 ± 0.01^{a}	97.02 ± 0.06^{a}
328	96.43 ± 0.20^{a}	98.32 ± 0.01^{a}	96.13 ± 0.11^{b}

Appendix 3R
Effect temperature on Zn (II) ions uptake using GP-3, GP-3C and GP-3E adsorbent

	GP–3	**GP-3C**	**GP-3E**
Temperature (K)	Mean ± SD	Mean ± SD	Mean ± SD
293	95.46 ± 0.10^{c}	97.84 ± 0.23^{c}	97.90 ± 0.05^{d}
298	95.87 ± 0.15^{b}	98.27 ± 0.05^{b}	98.29 ± 0.07^{b}
308	95.93 ± 0.27^{b}	98.56 ± 0.01^{b}	98.15 ± 0.02^{c}
318	97.29 ± 0.03^{a}	99.04 ± 0.07^{a}	99.15 ± 0.06^{a}
328	97.62 ± 0.03^{a}	98.90 ± 0.04^{a}	99.03 ± 0.04^{a}

Appendix 4A
Mean percentage desorption of Pb (II) ions from GP-1, GP-1C and GP-1E adsorbent

	GP-1	**GP-1C**	**GP-1E**
Time (minutes)	Mean ± SD	Mean ± SD	Mean ± SD
15	9.72 ± 0.02^{f}	1.67 ± 0.02^{f}	1.75 ± 0.01^{f}
30	15.16 ± 0.03^{e}	2.62 ± 0.01^{e}	3.42 ± 0.03^{e}
60	23.59 ± 0.03^{d}	18.04 ± 0.01^{d}	10.17 ± 0.15^{d}
120	49.44 ± 0.07^{c}	22.43 ± 0.01^{c}	20.06 ± 0.02^{c}
240	64.07 ± 0.07^{a}	34.31 ± 0.02^{b}	25.16 ± 0.01^{b}
600	63.37 ± 0.12^{b}	34.50 ± 0.02^{a}	26.03 ± 0.00^{a}

Mean percentages with same letters in the same row are not significantly different at 95% confidence level

Appendix 4B

Mean percentage desorption of Pb (II) ions from GP-2, GP-2C and GP-2E adsorbent

	GP-2	**GP-2C**	**GP-2E**
Time (minutes)	Mean ± SD	Mean ± SD	Mean ± SD
15	3.49 ± 0.01^{f}	1.38 ± 0.01^{f}	1.56 ± 0.01^{f}
30	6.64 ± 0.03^{e}	2.61 ± 0.01^{e}	2.73 ± 0.01^{e}
60	17.09 ± 0.04^{d}	10.54 ± 0.01^{d}	7.35 ± 0.01^{d}
120	38.17 ± 0.01^{c}	21.88 ± 0.02^{c}	12.22 ± 0.00^{c}
240	58.53 ± 0.03^{b}	32.00 ± 0.03^{a}	28.88 ± 0.03^{b}
600	60.11 ± 0.02^{a}	31.27 ± 0.03^{b}	29.00 ± 0.06^{a}

Mean percentages with same letters in the same row are not significantly different at 95% confidence level

Appendix 4C

Mean percentage desorption of Pb (II) ions from GP-3, GP-3C and GP-3E adsorbent

	GP-3	**GP-3C**	**GP-3E**
Time (minutes)	Mean ± SD	Mean ± SD	Mean ± SD
15	5.02 ± 0.02^{f}	6.67 ± 0.03^{f}	1.50 ± 0.02^{f}
30	9.60 ± 0.04^{e}	7.26 ± 0.01^{e}	1.92 ± 0.01^{e}
60	12.95 ± 0.02^{d}	20.26 ± 0.05^{d}	6.88 ± 0.01^{d}
120	35.00 ± 0.03^{c}	23.19 ± 0.00^{c}	19.64 ± 0.02^{c}
240	54.25 ± 0.01^{b}	32.93 ± 0.00^{a}	30.36 ± 0.01^{b}
600	56.99 ± 0.01^{a}	31.97 ± 0.02^{b}	30.46 ± 0.01^{a}

Appendix 4D

Mean percentage desorption of Cd (II) ions from GP-1, GP-1C and GP-1E adsorbent

	GP-1	**GP-1C**	**GP-1E**
Time (minutes)	Mean ± SD	Mean ± SD	Mean ± SD
15	4.52 ± 0.04^{f}	2.27 ± 0.02^{f}	4.29 ± 0.05^{f}
30	12.70 ± 0.01^{e}	6.31 ± 0.02^{e}	8.47 ± 0.03^{e}
60	35.59 ± 0.05^{d}	9.51 ± 0.04^{d}	10.82 ± 0.02^{d}
120	45.44 ± 0.08^{c}	24.97 ± 0.07^{c}	13.82 ± 0.02^{c}
240	52.73 ± 0.02^{a}	34.98 ± 0.00^{a}	22.83 ± 0.04^{b}
600	46.26 ± 0.07b	33.57 ± 0.01^{b}	26.50 ± 0.01^{a}

Mean percentages with same letters in the same row are not significantly different at 95% confidence level

Appendix 4E

Mean percentage desorption of Cd (II) ions from GP-2, GP-2C and GP-2E adsorbent

	GP-2	**GP-2C**	**GP-2E**
Time (minutes)	Mean ± SD	Mean ± SD	Mean ± SD
15	6.94 ± 0.03^{f}	4.02 ± 0.02^{f}	4.04 ± 0.01^{f}
30	16.07 ± 0.01^{e}	7.15 ± 0.01^{e}	13.16 ± 0.01^{e}
60	33.58 ± 0.09^{d}	12.66 ± 0.01^{d}	14.69 ± 0.04^{d}
120	42.06 ± 0.02^{c}	15.56 ± 0.03^{c}	22.14 ± 0.01^{c}
240	51.76 ± 0.02^{b}	27.75 ± 0.02^{b}	29.45 ± 0.03^{a}
600	56.97 ± 0.02^{a}	29.64 ± 0.01^{a}	29.12 ± 0.02^{b}

Mean percentages with same letters in the same row are not significantly different at 95% confidence level

Appendix 4F

Mean percentage desorption of Cd (II) ions from GP-3, GP-3C and GP-3E adsorbent

	GP-3	**GP-3C**	**GP-3E**
Time (minutes)	Mean ± SD	Mean ± SD	Mean ± SD
15	2.91 ± 0.01^{f}	5.54 ± 0.01^{f}	7.60 ± 0.01^{f}
30	11.39 ± 0.02^{e}	12.19 ± 0.02^{e}	12.54 ± 0.02^{e}
60	28.64 ± 0.04^{d}	19.83 ± 0.00^{d}	19.95 ± 0.02^{d}
120	46.60 ± 0.01^{c}	24.42 ± 0.05^{c}	24.75 ± 0.03^{c}
240	54.55 ± 0.06^{b}	37.95 ± 0.01^{b}	30.87 ± 0.02^{b}
600	60.08 ± 0.01^{a}	38.56 ± 0.01^{a}	31.98 ± 0.01^{a}

Appendix 4G

Mean percentage desorption of Zn (II) ions from GP-1, GP-1C and GP-1E adsorbent

	GP-1	**GP-1C**	**GP-1E**
Time (minutes)	Mean ± SD	Mean ± SD	Mean ± SD
15	5.25 ± 0.01^{f}	3.42 ± 0.01^{f}	2.29 ± 0.02^{f}
30	12.74 ± 0.01^{e}	8.78 ± 0.01^{e}	4.98 ± 0.06^{e}
60	22.83 ± 0.02^{d}	16.20 ± 0.03^{d}	7.59 ± 0.00^{d}
120	46.77 ± 0.02^{c}	24.63 ± 0.03^{c}	17.04 ± 0.01^{c}
240	61.96 ± 0.01^{a}	33.23 ± 0.03^{b}	23.98 ± 0.01^{b}
600	51.90 ± 0.02^{b}	34.47 ± 0.01^{a}	27.60 ± 0.01^{a}

Mean percentages with same letters in the same row are not significantly different at 95% confidence level

Appendix 4H

Mean percentage desorption of Zn (II) ions from GP-2, GP-2C and GP-2E adsorbent

	GP-2	**GP-2C**	**GP-2E**
Time (minutes)	Mean ± SD	Mean ± SD	Mean ± SD
15	3.77 ± 0.01^{f}	3.50 ± 0.01^{f}	3.98 ± 0.01^{f}
30	9.54 ± 0.02^{e}	6.37 ± 0.01^{e}	4.87 ± 0.00^{e}
60	21.72 ± 0.02^{d}	7.05 ± 0.03^{d}	11.86 ± 0.02^{d}
120	38.46 ± 0.01^{c}	12.19 ± 0.01^{c}	14.29 ± 0.02^{c}
240	60.02 ± 0.01b	34.12 ± 0.02^{a}	27.10 ± 0.02^{b}
600	64.68 ± 0.01^{a}	31.90 ± 0.03^{b}	30.30 ± 0.01^{a}

Mean percentages with same letters in the same row are not significantly different at 95% confidence level

Appendix 4I

Mean percentage desorption of Zn (II) ions from GP-3, GP-3C and GP-3E adsorbent

	GP-3	**GP-3C**	**GP-3E**
Time (minutes)	Mean ± SD	Mean ± SD	Mean ± SD
15	2.55 ± 0.02^{f}	1.87 ± 0.01^{f}	3.36 ± 0.01^{f}
30	9.65 ± 0.01^{e}	7.21 ± 0.00^{e}	5.47 ± 0.01^{e}
60	23.71 ± 0.02^{d}	11.36 ± 0.05^{d}	7.66 ± 0.03^{d}
120	35.64 ± 0.02^{c}	23.94 ± 0.01^{c}	12.25 ± 0.02^{c}
240	59.05 ± 0.06^{a}	39.87 ± 0.01^{a}	26.93 ± 0.05^{a}
600	57.98 ± 0.02^{b}	39.66 ± 0.02^{b}	26.45 ± 0.04^{b}

Appendix 5A

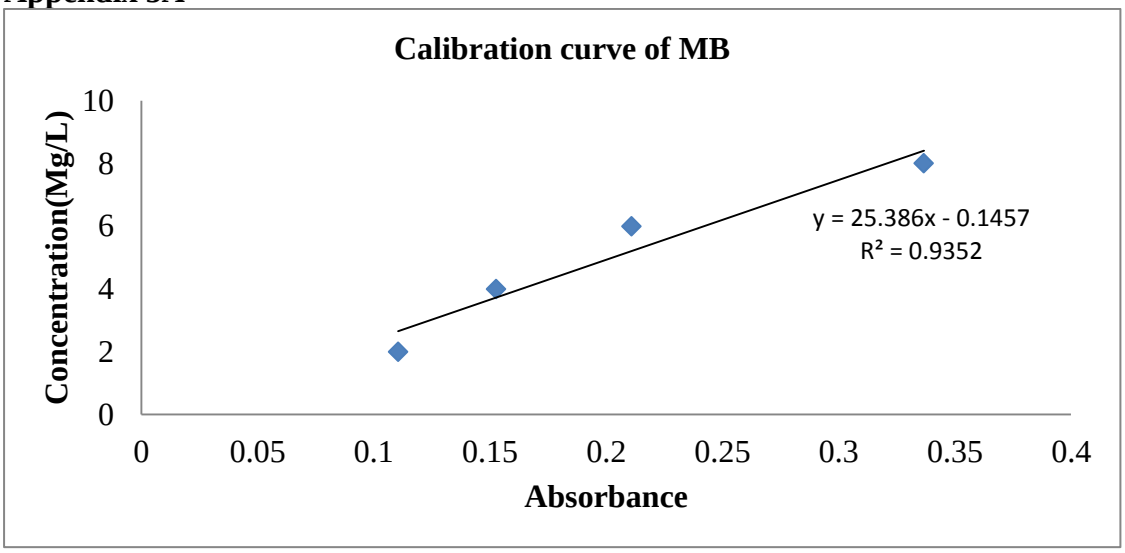

Appendix 5B
Effect of pH on adsorption of MB using GP-1, GP-1C and GP-1E adsorbent

	GP-1	GP-1C	GP-1E
pH	Mean ± SD	Mean ± SD	Mean ± SD
4	54.34 ± 0.11^{d}	60.21 ± 0.41^{d}	61.25 ± 0.17^{d}
6	66.28 ± 0.14^{c}	68.65 ± 0.44^{c}	69.40 ± 0.66^{c}
8	70.00 ± 0.49^{b}	75.46 ± 0.15^{b}	72.54 ± 0.30^{b}
10	74.77 ± 0.10^{a}	78.48 ± 0.23^{a}	77.80 ± 0.27^{a}
12	74.23 ± 0.07^{a}	78.01 ± 0.34^{a}	78.45 ± 0.37^{a}

Mean percentages with same letters in the same row are not significantly different at 95% confidence level

Appendix 5C
Effect of pH on adsorption of MB using GP-2, GP-2C and GP-2E adsorbent

	GP-2	GP-2C	GP-2E
pH	Mean ± SD	Mean ± SD	Mean ± SD
4	58.02 ± 0.26^{d}	64.94 ± 0.23^{d}	85.48 ± 0.29^{a}
6	65.59 ± 0.22^{c}	70.05 ± 0.20^{c}	87.75 ± 0.35^{a}
8	71.39 ± 0.14^{b}	75.00 ± 0.13^{b}	88.03 ± 0.12^{a}
10	75.44 ± 0.61^{a}	84.75 ± 0.33^{a}	85.52 ± 4.52^{a}
12	75.75 ± 0.29^{a}	85.21 ± 0.20^{a}	85.21 ± 0.06^{a}

Mean percentages with same letters in the same row are not significantly different at 95% confidence level

Appendix 5D
Effect of pH on adsorption of MB using GP-3, GP-3C and GP-3E adsorbent

	GP-3	GP-3C	GP-3E
pH	Mean ± SD	Mean ± SD	Mean ± SD
4	86.74 ± 0.07^{c}	91.06 ± 0.36^{a}	88.40 ± 0.17^{d}
6	88.58 ± 0.07^{b}	91.99 ± 0.57^{a}	89.64 ± 0.15^{b}
8	89.74 ± 0.12^{a}	90.33 ± 4.99^{a}	89.19 ± 0.17^{c}
10	89.52 ± 0.12^{a}	95.26 ± 0.10^{a}	90.04 ± 0.15^{a}
12	85.11 ± 0.12^{d}	90.31 ± 0.39^{a}	87.24 ± 0.09^{e}

Mean percentages with same letters in the same row are not significantly different at 95% confidence level

Appendix 5E
Effect of concentration on adsorption of MB using GP-1, GP-1C and GP-1E adsorbent

	GP-1	GP-1C	GP-1E
Concentration (mg/L)	Mean ± SD	Mean ± SD	Mean ± SD
25	73.68 ± 0.73^{a}	77.35 ± 0.24^{a}	75.75 ± 0.55^{a}
30	67.87 ± 0.24^{b}	72.78 ± 0.15^{b}	70.53 ± 0.53^{b}
40	64.38 ± 1.86^{c}	67.09 ± 0.13^{c}	65.89 ± 0.36^{c}
50	50.49 ± 0.77^{d}	52.07 ± 0.24^{d}	52.39 ± 0.21^{d}

Appendix 5F

Effect of concentration on adsorption of MB using GP-2, GP-2C and GP-2E adsorbent

	GP-2	**GP-2C**	**GP-2E**
Concentration (mg/L)	Mean ± SD	Mean ± SD	Mean ± SD
25	80.31 ± 0.11^{a}	85.15 ± 0.15^{a}	80.77 ± 0.12^{a}
30	77.95 ± 0.22^{b}	80.50 ± 0.32^{b}	79.55 ± 0.19^{b}
40	66.01 ± 0.20^{c}	70.38 ± 0.37^{c}	69.54 ± 0.55^{c}
50	61.79 ± 0.24^{d}	69.95 ± 0.31^{c}	66.17 ± 0.32^{d}

Appendix 5G

Effect of concentration on adsorption of MB using GP-3, GP-3C and GP-3E adsorbent

	GP-3	**GP-3C**	**GP-3E**
Concentration (mg/L)	Mean ± SD	Mean ± SD	Mean ± SD
25	88.19 ± 0.15^{a}	90.47 ± 0.25^{a}	89.29 ± 0.25^{a}
30	87.87 ± 0.18^{a}	88.46 ± 0.11^{b}	88.29 ± 0.54^{b}
40	82.01 ± 0.68^{b}	83.71 ± 0.21^{c}	83.65 ± 0.56^{c}
50	65.49 ± 0.40^{c}	69.09 ± 0.16^{d}	66.18 ± 0.71^{d}

Mean percentages with same letters in the same row are not significantly different at 95% confidence level

Appendix 5H

Effect of contact time on adsorption of MB using GP-1, GP-1C and GP-1E adsorbent

	GP-1	**GP-1C**	**GP-1E**
Time (minutes)	Mean ± SD	Mean ± SD	Mean ± SD
20	58.51 ± 0.37^{c}	63.41 ± 0.47^{d}	69.17 ± 0.35^{c}
40	62.06 ± 0.19^{b}	68.87 ± 0.08^{c}	66.45 ± 0.38^{d}
60	85.03 ± 0.31^{a}	86.41 ± 0.11^{b}	86.45 ± 0.31^{b}
80	84.38 ± 0.42^{a}	84.66 ± 0.21^{a}	87.95 ± 0.12^{a}

Appendix 5I

Effect of contact time on adsorption of MB using GP-2, GP-2C and GP-2E adsorbent

	GP-2	**GP-2C**	**GP-2E**
Time (minute)	Mean ± SD	Mean ± SD	Mean ± SD
20	62.27 ± 0.30^{c}	79.68 ± 0.40^{c}	73.67 ± 0.32^{d}
40	66.11 ± 0.38^{b}	85.70 ± 0.16^{b}	85.89 ± 0.19^{c}
60	86.30 ± 0.09^{a}	86.38 ± 0.30^{b}	87.35 ± 0.20^{b}
80	86.49 ± 0.29^{a}	88.36 ± 0.06^{a}	89.44 ± 0.27^{a}

Appendix 5J

Effect of contact time on adsorption of MB using GP-3, GP-3C and GP-3E adsorbent

	GP-3	**GP-3C**	**GP-3E**
Time (minutes)	Mean ± SD	Mean ± SD	Mean ± SD
20	89.35 ± 0.01^{d}	89.43 ± 0.00^{d}	89.33 ± 0.01^{d}
40	94.40 ± 0.01^{c}	96.50 ± 0.01^{c}	98.36 ± 0.01^{c}
60	99.60 ± 0.01^{b}	99.58 ± 0.01^{a}	99.56 ± 0.01^{b}
80	99.44 ± 0.02^{a}	99.56 ± 0.01^{b}	99.64 ± 0.01^{a}

Appendix 5K

Effect of adsorbent dose on adsorption of MB using GP-1, GP-1C and GP-1E adsorbent

	GP-1	**GP-1C**	**GP-1E**
Dose (g)	Mean ± SD	Mean ± SD	Mean ± SD
0.1	55.42 ± 0.15^{d}	65.38 ± 0.19^{d}	62.36 ± 0.22^{d}
0.2	65.08 ± 0.08^{c}	75.95 ± 0.24^{c}	74.21 ± 0.22^{c}
0.3	80.37 ± 0.35^{a}	86.44 ± 0.08^{a}	84.06 ± 0.28^{b}
0.5	70.00 ± 0.46^{b}	84.57 ± 0.19^{b}	88.08 ± 0.11^{a}

Mean percentages with same letters in the same row are not significantly different at 95% confidence level

Appendix 5L

Effect of adsorbent dose on adsorption of MB using GP-2, GP-2C and GP-2E adsorbent

	GP-2	**GP-2C**	**GP-2E**
Dose (g)	Mean ± SD	Mean ± SD	Mean ± SD
0.1	60.45 ± 0.45^{d}	70.57 ± 0.55^{c}	79.30 ± 0.08^{c}
0.2	67.44 ± 0.25^{c}	85.05 ± 0.34^{b}	86.54 ± 0.09^{b}
0.3	73.56 ± 0.25^{b}	85.98 ± 0.18^{a}	88.47 ± 0.21^{a}
0.5	78.69 ± 0.16^{a}	86.36 ± 0.19^{a}	88.27 ± 0.31^{a}

Appendix 5M

Effect of adsorbent dose on adsorption of MB using GP-3, GP-3C and GP-3E adsorbent

	GP-3	**GP-3C**	**GP-3E**
Dose (g)	Mean ± SD	Mean ± SD	Mean ± SD
0.1	84.58 ± 0.31^{c}	80.86 ± 0.43^{d}	80.50 ± 0.32^{d}
0.2	85.00 ± 0.12^{c}	87.92 ± 0.08^{c}	84.62 ± 0.23^{c}
0.3	90.41 ± 0.13^{b}	90.16 ± 0.25^{a}	88.89 ± 0.28^{b}
0.5	86.47 ± 0.52^{a}	88.74 ± 0.16^{b}	99.68 ± 0.29^{a}

Appendix 5N

Effect of temperature on adsorption of MB using GP-1, GP-1C and GP-1E adsorbent

	GP-1	**GP-1C**	**GP-1E**
Temperature (K)	Mean ± SD	Mean ± SD	Mean ± SD
298	73.75 ± 0.14^{c}	77.64 ± 0.48^{c}	76.82 ± 0.12^{d}
308	76.67 ± 0.31^{b}	79.35 ± 0.36^{b}	77.81 ± 0.52^{c}
318	80.29 ± 0.15^{a}	82.74 ± 0.24^{a}	82.07 ± 0.25^{a}
328	79.79 ± 0.61^{a}	83.44 ± 0.14^{a}	80.28 ± 0.12^{b}

Appendix 5O

Effect of temperature on adsorption of MB using GP-2, GP-2C and GP-2E adsorbent

	GP-2	**GP-2C**	**GP-2E**
Temperature (K)	Mean ± SD	Mean ± SD	Mean ± SD
298	76.15 ± 0.31^{d}	83.75 ± 0.28^{c}	85.25 ± 0.13^{c}
308	80.39 ± 0.30^{c}	84.31 ± 0.42^{bc}	87.82 ± 0.12^{b}
318	82.64 ± 0.17^{b}	84.92 ± 0.40^{b}	88.26 ± 0.21^{a}
328	84.02 ± 0.41^{a}	86.40 ± 0.28^{a}	87.81 ± 0.17^{b}

Mean percentages with same letters in the same row are not significantly different at 95% confidence level

Appendix 5P

Effect of temperature on adsorption of MB using GP-3, GP-3C and GP-3E adsorbent

	GP-3	**GP-3C**	**GP-3E**
Temperature (K)	Mean ± SD	Mean ± SD	Mean ± SD
298	86.72 ± 0.09^{c}	90.75 ± 0.27^{d}	88.58 ± 0.09^{d}
308	88.67 ± 0.19^{b}	91.74 ± 0.23^{c}	90.18 ± 0.12^{a}
318	89.72 ± 0.17^{a}	95.95 ± 0.19^{a}	89.79 ± 0.07^{b}
328	89.76 ± 0.39^{a}	95.21 ± 0.17^{b}	89.42 ± 0.06^{c}

Mean percentages with same letters in the same row are not significantly different at 95% confidence level

Appendix 5Q

Effect of shaking speed on adsorption of MB using GP-1, GP-1C and GP-1E adsorbent

	GP-1	**GP-1C**	**GP-1E**
Shaking speed(rpm)	Mean ± SD	Mean ± SD	Mean ± SD
150	58.58 ± 1.78^{c}	61.18 ± 1.01^{c}	65.54 ± 0.83^{b}
180	64.07 ± 0.93^{b}	70.00 ± 0.86^{b}	66.42 ± 0.08^{b}
210	82.07 ± 0.95^{a}	85.27 ± 0.45^{a}	87.77 ± 1.05^{a}
240	81.59 ± 1.01^{a}	84.66 ± 1.27^{a}	87.96 ± 0.93^{a}

Mean percentages with same letters in the same column are not significantly different at 95% confidence level

Appendix 5R

Effect of shaking speed on adsorption of MB using GP-2, GP-2C and GP-2E adsorbent

	GP-2	**GP-2C**	**GP-2E**
Shaking speed(rpm)	Mean ± SD	Mean ± SD	Mean ± SD
150	62.62 ± 0.44^{c}	80.01 ± 0.14^{c}	72.89 ± 0.41^{c}
180	66.88 ± 1.05^{b}	85.52 ± 0.86^{b}	86.26 ± 0.60^{b}
210	85.95 ± 0.06^{a}	86.05 ± 1.75^{b}	87.80 ± 0.92^{ab}
240	86.63 ± 0.02^{a}	88.77 ± 0.40^{a}	89.85 ± 2.01^{a}

Mean percentages with same letters in the same column are not significantly different at 95% confidence level

Appendix 5S

Effect of shaking speed on adsorption of MB using GP-3, GP-3C and GP-3E adsorbent

	GP-3	**GP-3C**	**GP-3E**
Shaking speed(rpm)	Mean ± SD	Mean ± SD	Mean ± SD
150	83.78 ± 0.54^{c}	85.71 ± 1.06^{a}	83.64 ± 1.17^{b}
180	85.16 ± 0.64^{bc}	87.96 ± 9.56^{a}	84.54 ± 0.10^{b}
210	89.57 ± 1.63^{b}	89.18 ± 0.81^{a}	89.73 ± 1.02^{a}
240	86.97 ± 0.11^{a}	89.19 ± 1.50^{a}	91.42 ± 1.16^{a}

Mean percentages with same letters in the same column are not significantly different at 95% confidence level

Appendix 6A: Column adsorption of Pb(II) ions onto geopolymers

Geopolymer	**Mean ±SD**	**Geopolymer**	**Mean ± SD**	**Geopolymer**	**Mean ± SD**
GP-1	80.54 ± 0.94^{b}	GP-2	82.87 ± 0.26^{c}	GP-3	84.31 ± 0.74^{b}
GP-1C	85.02 ± 0.76^{a}	GP-2C	87.24 ± 0.30^{b}	GP-3C	90.67 ± 0.41^{a}
GP-1E	84.26 ± 0.34^{a}	GP-2E	89.68 ± 0.95^{a}	GP-3E	89.75 ± 0.13^{a}

C- Citric acid functionalized geopolymers, E- EDTA functionalized and SD- Standard deviation, Mean in a column without a common superscript letter differ ($P < 0.05$), as analyzed by one-way ANOVA

Appendix 6B: Column adsorption of Cd(II) ions onto geopolymers

Geopolymer	Mean ± SD	Geopolymer	Mean ± SD	Geopolymer	Mean ± SD
GP-1	70.14 ± 0.49^{c}	GP-2	74.28 ± 0.60^{c}	GP-3	79.00 ± 0.64^{c}
GP-1C	74.35 ± 0.25^{a}	GP-2C	79.19 ± 0.60^{a}	GP-3C	82.35 ± 0.24^{a}
GP-1E	73.22 ± 0.38^{b}	GP-2E	76.47 ± 0.11^{b}	GP-3E	80.93 ± 0.13^{b}

C- citric acid functionalized geopolymers, E- EDTA functionalized and SD- standard deviation, Mean in a column without a common superscript letter differ ($P < 0.05$), as analyzed by one-way ANOVA

Appendix 6C: Column adsorption of Zn(II) ions onto geopolymers

Geopolymer	Mean ± SD	Geopolymer	Mean ± SD	Geopolymer	Mean ± SD
GP-1	77.50 ± 0.16^{c}	GP-2	79.18 ± 0.78^{b}	GP-3	82.97 ± 0.26^{b}
GP-1C	81.58 ± 0.14^{a}	GP-2C	84.09 ± 0.28^{a}	GP-3C	89.03 ± 0.56^{a}
GP-1E	80.69 ± 0.27^{b}	GP-2E	85.30 ± 0.38^{a}	GP-3E	89.84 ± 0.38^{a}

Appendix 7A: Intraparticle diffusion experimental data of Pb^{2+} uptake onto geopolymers and functionalized geopolymers

Geopolymer	K_{id}	a	R^2
GP-1	11.74	0.223	0.876
GP-1C	27.11	0.470	0.889
GP-1E	20.49	0.302	0.942
GP-2	12.15	0.196	0.925
GP-2C	32.26	0.470	0.962
GP-2E	17.21	0.351	0.822
GP-3	15.61	0.382	0.901
GP-3C	16.58	0.422	0.907
GP-3E	18.34	0.365	0.811

Appendix 7B: Intraparticle diffusion experimental data of Cd^{2+} uptake onto geopolymers and functionalized geopolymers

Geopolymer	K_{id}	a	R^2
GP-1	69.79	0.029	0.817
GP-1C	72.31	0.054	0.852
GP-1E	75.53	0.054	0.872
GP-2	72.61	0.019	0.764
GP-2C	79.09	0.034	0.788
GP-2E	76.67	0.042	0.704
GP-3	60.97	0.042	0.884
GP-3C	74.59	0.045	0.944
GP-3E	73.13	0.109	0.828

K_{id} is the intraparticle diffusion rate constant ($mgg^{-1}min^{-1(1/2)}$), 'a' depicts the adsorption mechanism

Appendix 7C: Intraparticle diffusion experimental data of Zn^{2+} uptake onto geopolymers and functionalized geopolymers

Geopolymer	K_{id}	a	R^2
GP-1	64.60	0.03	0.763
GP-1C	79.34	0.037	0.867
GP-1E	70.60	0.055	0.841
GP-2	61.70	0.05	0.731
GP-2C	66.42	0.076	0.784
GP-2E	64.28	0.059	0.648
GP-3	60.10	0.033	0.630
GP-3C	69.44	0.089	0.951
GP-3E	74.05	0.027	0.303

K_{id} is the intraparticle diffusion rate constant ($mgg^{-1}min^{-1(1/2)}$), 'a' depicts the adsorption mechan

Appendix 8: Intraparticle diffusivities ln(α-1) constants for adsorption of MB onto geopolymers

Time(min)	GP-1	GP-1C	GP-1E	GP-2	GP-2C	GP-2E	GP-3	GP-3C	GP-3E
20	-1.189	-1.324	-1.544	-1.273	-2.321	-1.736	-2.673	-3.146	-2.448
40	-1.309	-1.594	-1.409	-1.445	-3.504	-3.228	-2.883	-3.840	-2.565
60	-	-	-4.069	-6.141	-3.800	-3.756	-	-	-3.765
80	-4.874	-3.898	-	-	-	-	-3.118	-5.204	-

Appendix 9
SEM- EDX spectrum of geopolymers

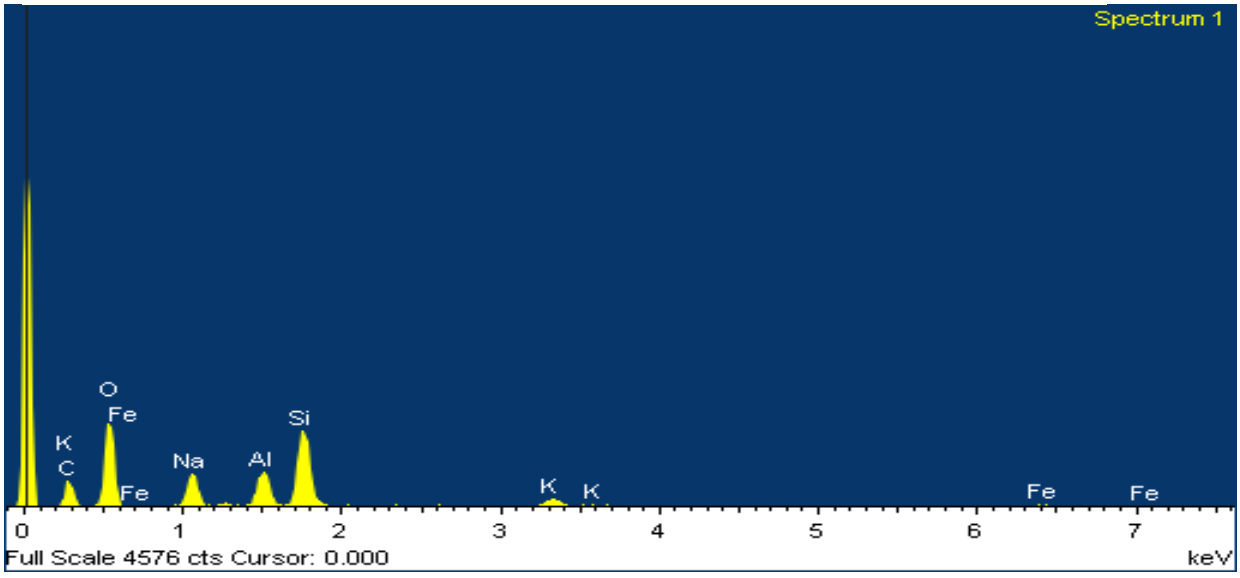

Appendix 10: Plots of thermodynamic studies of geopolymers

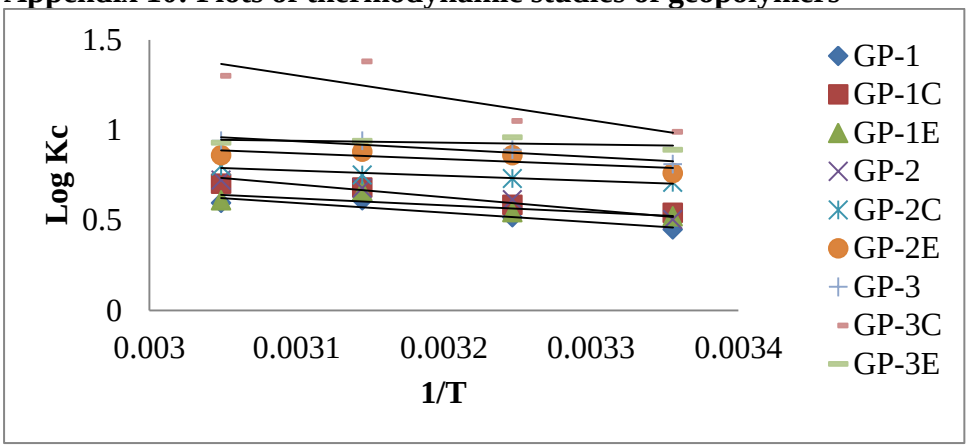

Appendix 11: Calibration curve of Pb (II) ions

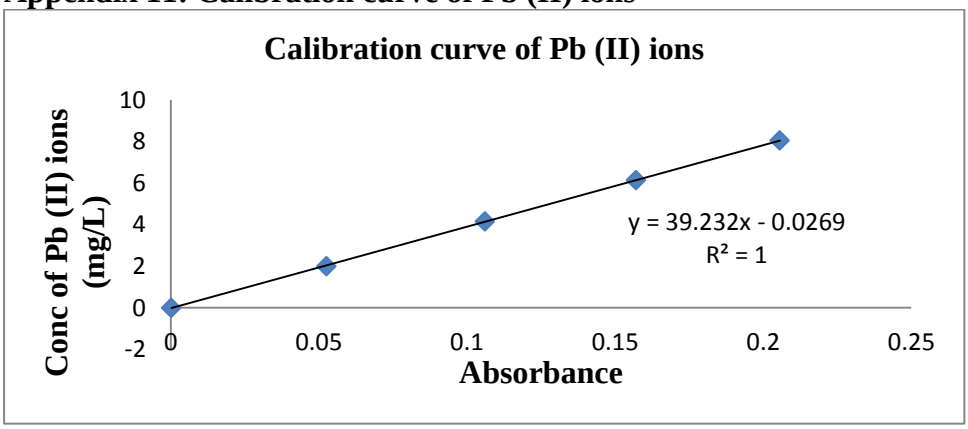

Appendix 12: Calibration curve of Cd (II) and Zn (II) ions